Abstracts from the
2011 EarthScope National Meeting

The following pages contain abstracts for both the oral and poster portions of the meeting sessions.

The abstracts are in alphabetical order by first author. Please be sure to turn on your bookmarks option ⬒ in Acrobat Reader or Acrobat Professional to be able to select and advance to a specific poster from the list.

PyLith: A Finite-Element Code for Modeling Quasi-Static and Dynamic Crustal Deformation

Brad Aagaard, USGS, Menlo Park, *baagaard@usgs.gov*
Charles Williams, GNS Science, *C.Williams@gns.cri.nz*
Matthew Knepley, University of Chicago, *knepley@gmail.com*

We have developed open-source finite-element software for 2-D and 3-D dynamic and quasi-static modeling of crustal deformation. This software, PyLith (current release is 1.5), combines the quasi-static viscoelastic modeling functionality of PyLith 0.8 and its predecessors (LithoMop and Tecton) and the wave propagation modeling functionality of EqSim. The target applications require resolution at spatial scales ranging from tens of meters to hundreds of kilometers and temporal scales for dynamic modeling ranging from milliseconds to minutes or temporal scales for quasi-static modeling ranging from minutes to thousands of years. PyLith development is part of the NSF funded Computational Infrastructure for Geodynamics (CIG) and the software runs on a wide variety of platforms (laptops, workstations, and Beowulf clusters). Binaries (Linux, Darwin, and Windows systems) and source code are available from geodynamics.org. PyLith uses a suite of general, parallel, graph data structures called Sieve for storing and manipulating finite-element meshes. This permits use of a variety of 2-D and 3-D cell types including triangles, quadrilaterals, hexahedra, and tetrahedra.

Current features include prescribed fault ruptures with multiple sequential earthquakes and aseismic creep, spontaneous fault ruptures with a variety of fault constitutive models, time-dependent Dirichlet and Neumann boundary conditions, absorbing boundary conditions, time-dependent point forces, and gravitational body forces. PyLith supports infinitesimal and small strain formulations for linear elastic rheologies, linear and generalized Maxwell viscoelastic rheologies, power-law viscoelastic rheologies, and Drucker-Prager elastoplastic rheologies. Current development focuses on performance improvements and adding additional bulk and fault constitutive models. We also plan to extend PyLith to allow coupling of quasi-static and dynamic simulations to resolve multi-scale deformation across the entire seismic cycle.

PyLith website: http://www.geodynamics.org/cig/software/pylith

2010 San Bernardino Mountains GPS campaign

J.N. Bywater[1], K.K. Chung[2], B.J. Anderson[3], J.C. Duncan[4], M.R. Swift[5], S.F. McGill[5], J.C. Spinler[6], A.D. Hulett[5], and R.A. Bennett[6]

[1]Sonoma State University, [2]Wellesley College, [3]Pasadena City College, [4]Baylor University, [5]California State University- San Bernardino, [6]University of Arizona

Abstract

We conducted a GPS campaign in and around the San Bernardino Mountains, California. Information from these remote sites is filling in a gap where there are little to no recorded velocities. We collected GPS positions from 24 sites over a period of 5 days. Using results from prior years, we calculated velocities for each site, and then used two-dimensional elastic modeling in a spreadsheet to test over a million possible slip rate combinations on 15 faults within a transect that crosses the plate boundary in the vicinity of the San Bernardino Mountains. Using Chi-2 as a criterion, the best-fitting model yielded a slip rate of 5mm/yr for the San Andreas fault and 16 mm/yr for the San Jacinto fault. However, there is a broad range of San Andreas and San Jacinto fault slip rates that fit the GPS velocities reasonably well. Among all of the reasonably fitting models, the combined slip rate on the San Andreas and San Jacinto faults is between 15-26 mm/yr. Because these two faults are so geographically close to each other, we found that it is hard to distinguish exactly how much of this strain each fault contributes. We also found that the Eastern California Shear Zone as a whole contributes 13-17 mm/yr of slip, while faults west of the San Jacinto fault contribute 4.5-13.5 mm/yr. Additionally, models using the published geologic slip rates do not fit the GPS velocities at all. This may be because present-day deformation rates, measured by GPS, differ from the long-term averages recorded by geologic offsets.

Anisotropy within the Bighorn Mountains region, northern Wyoming: Attempts to define cratonic mantle structure

Anderson, M. L.[1], Thayer, D.[1], Hornbuckle, J.[2], Ufret-Alonso, T.[3], Sheehan, A.[4], Yeck, W.[4], Solomon, M.[5], Erslev, E.[6], Siddoway, C.[1], Miller, K.[7]

1. Geology Department, Colorado College, 14 E. Cache La Poudre St., Colorado Springs, CO 80903, Email: megan.anderson@coloradocollege.edu
2. Geology Department, Washington and Lee University
3. Department of Geology, University of Puerto Rico-Mayagüez
4. Geological Sciences, University of Colorado-Boulder
5. Department of Geosciences, Colorado State University
6. Department of Geology and Geophysics, University of Wyoming
7. Department of Geology and Geophysics, Texas A&M University

The Bighorn Mountains within northern Wyoming have been the focus of an intensive Flexible Array experiment from 2009-2010. The experiment included 37 broadband instruments, ~160 short period instruments and ~1600 texans deployed in stages over the course of a little more than a year, which together form the BASE experiment. The target for the network is distinguishing the most likely model among four hypotheses for Laramide-age crustal deformation. However, the data are also useful for determining mantle structure via tomography and shear-wave splitting analysis. These results may influence our interpretations of the involvement of the mantle in deformation and elucidate preexisting lithospheric structure which could have influenced the Laramide-age deformation of the crust. This presentation highlights the preliminary shear-wave splitting results from 26 USArray Transportable stations (TA) that were within the region and the 37 BASE broadband seismometers positioned to densify the TA.

The wave quality, number of recorded events, and raypath orientations for split teleseismic waves under the BASE footprint is extraordinary for a network deployed for just over a year, and rivals some of the densest and longest-running networks worldwide. The range of backazimuths recorded by most stations is up to 355 degrees, with most clustered in a WNW direction over a 120 degree range. Most stations yielded 8-15 good quality results along many different backazimuths. Combined with the density of stations (15-25 km spacing), this is allowing us to perform detailed analysis of the shear wave splitting of a type that is not possible for many past seismic networks. In addition to our goals for understanding Laramide-age deformation of the lithosphere, we are hoping to take a substantial step towards answering more fundamental questions about how shear-wave splitting is interpreted, such as: 1) What layer (crust, mantle, or asthenosphere) dominates the shear wave splitting signature of stable cratonic areas? 2) How much does lateral heterogeneity of anisotropy affect shear wave splitting measurements over the continents?

We are pursuing several different analytical approaches for this dataset. A more standard analysis utilizing a single frequency range and a relatively wide filter,

paired with the computation of station averages allows us to compare our results with older studies that commonly utilized this methodology. The first approach in our expanded investigation computes the variation of regions of data when plotted at different pierce points to estimate the most likely depth of the anisotropy along the near-vertical raypaths. A second analysis examines the highest quality events for frequency-dependent results, with the aim to better constrain potential anisotropic layer thicknesses and depths. Separate analysis of shear wave splitting parameters utilizing waveform modeling at each station will confirm/refute the existence of more than one layer. Finally, petrographic analysis of mantle xenoliths from the Wyoming Province proximal to the Bighorns will constrain likely mantle chemistries and give an indication of potential anisotropic deformational fabrics within the lithospheric mantle.

Results from the wide filter shows heterogeneous, E to NE trending fast directions across the region and lag times averaging 0.7 s. The frequency-dependence investigation indicates a lithospheric source for anisotropy dominating our standard results for many stations, supported by lateral heterogeneity of the measurements across the region & higher wave frequencies affected by anisotropy than for other regions of the world. Lateral heterogeneity within the dataset is dominated by a sharp transition in fast direction and lag time across a boundary that coincides with the eastern range-bounding fault of the Bighorns Arch. Fast directions are dominantly E-trending in the Bighorn Mountains and the Bighorn basin, and fast directions are NE-trending in the Powder River basin (matching North American plate motion direction). This boundary also coincides with a strong change in magnetic anomalies across the region, reflecting structural transitions within the Archean Wyoming Craton, and with a change in lithospheric mantle-depth P-wave velocities within tomographies produced with USArray data. The likeliest depth for anisotropy based on pierce point analysis is approximately 300 km in the western half of the region and 450 km in the Powder River basin. The combination of results indicates a transition in lithospheric structure and thickness at the eastern range front boundary of the Bighorns, and thus a strong suggestion of a causal connection between older lithospheric mantle structure/thickness and the position of the Laramide-age Bighorns uplift boundary.

The EarthScope Plate Boundary Observatory (PBO) High-rate Real-time Cascadia Network

Ken Austin, Adrian A Borsa, Korey Dausz, Karl Feaux, Jason Gerdes, Michael E Jackson, Sara Looney, Emily Seider, Todd B Williams

As part of the 2009 American Recovery and Reinvestment Act (ARRA), NSF is investing in onshore-offshore instrumentation to support geophysical studies of the Cascadia margin. EarthScope's Plate Boundary Observatory (PBO) is contributing to this objective by upgrading 232 of its GPS stations in the Pacific Northwest to high-rate sampling and real-time telemetry to provide streaming data from this large-aperture network to the public. By blanketing the Pacific Northwest with real-time GPS coverage, the NSF is creating a natural laboratory in an area of great scientific interest and high geophysical hazard in order to spur new volcano and earthquake research opportunities. Streaming high-rate GPS data in real-time will enable researchers to routinely analyze for strong ground motion monitoring and earthquake hazards mitigation. As of April, 2011, 199 of the 232 proposed cascadia stations have been equipped with 3G capable modems or high-speed data radios, as well as updated power systems. These stations have been added to PBO's real time network, which is currently providing 1Hz-streaming data from 290 stations in BINEX, RTCM2.3 and RTCM 3.0 formats via the NTrip protocol from servers located at UNAVCO headquarters in Boulder, CO to 385 active connections. All 1Hz streams are also archived and available via FTP. PBO has also been collecting data with the Trimble VRS3Net software for latency comparisons between various cell carriers and radio network configurations. In addition, selected stations have been added to the casters prior to fieldwork in order to provide a baseline data set used to demonstrate improvements in latencies and completeness after upgrades. From the field to the end user, average latencies from cell carriers are typically less than 0.5 seconds, while radio networks are typically in the 1-2 second range, depending on size and configuration. Analysis of this data allows PBO to implement adjustments to the network that will optimize station and data delivery performance.

UNAVCO, Inc
6350 Nautilus Dr
Boulder, CO 80301
(303) 381-7500

EXPLAINING CO-SEISMIC STRAINS ON PBO BOREHOLE STRAINMETERS

ANDREW J. BARBOUR, DUNCAN C. AGNEW

Introduction

We have observed permanent[1] strain offsets occurring at Plate Boundary Observatory (PBO) borehole strainmeters (BSM) as a result of the rapid dynamic-straining from significant earthquakes[2]. Our analyses show these co-seismic offsets are not resultant of pore-fluid pressure changes[3], and cannot be adequately modeled by a point- or distributed-source in an elastic half-space[4]: We observe magnitude discrepancies upwards of 100 times too large, and 20 times too small. Layered models do not improve the fit well enough to account for this apparent anelastic behavior. Consistent trends by station and channel appear absent (Figure 1). There are discrepancies in polarity too: Nearly 3/4 of the observed offsets shown in fig. 1 have the incorrect sign, according to elasticity predictions. Alternative high-sensitivity geodetic observations [i.e. long-baseline laser strainmeters (LSM) and GPS offsets] confirm the lack of agreement between theory and observation.

Assuming the BSM maintains it's high elastic-compliance over all strain rates, these discrepancies suggest the offsets manifest local strain tensor modification by some nearby process, apparently activated or enhanced by rapid strain-rate changes. Our presentation explores the possibility that the combination of tectonic setting and geologic environment of the borehole controls this effect, rather than tectonic strain redistribution and/or pore-fluid pressure perturbation. For example, activation of a nearby joint (with slippage) could theoretically[5] produce enough strain to affect the borehole measurement and remain undetected by other high-resolution instrumentation (i.e. the LSM).

Peak strains, ground velocities, and accelerations

Although the BSMs measure only a horizontal strain tensor, and do not record ambient Earth strain at periods shorter than 1 second[6], we investigate ground motions which produce co-seismic offsets. To do this we compare peak strains from strong earthquakes to peak accelerations and velocities very nearby. In the case of the Anza-cluster instruments, 7/8 boreholes are instrumented with short-period, three-component geophones, sampled

[1] Insofar as the random-walk nature of Earth strain permits such a definition.

[2] cataloged by the National Earthquake Information Center

[3] Observed re-equilibrium timescales for the associated pressure disturbances - at the BSMs - are on the order of days.

[4] Okada, Y. (1992), Internal deformation due to shear and tensile faults in a half-space, *BSSA*, *82*(2), 1018–1040.
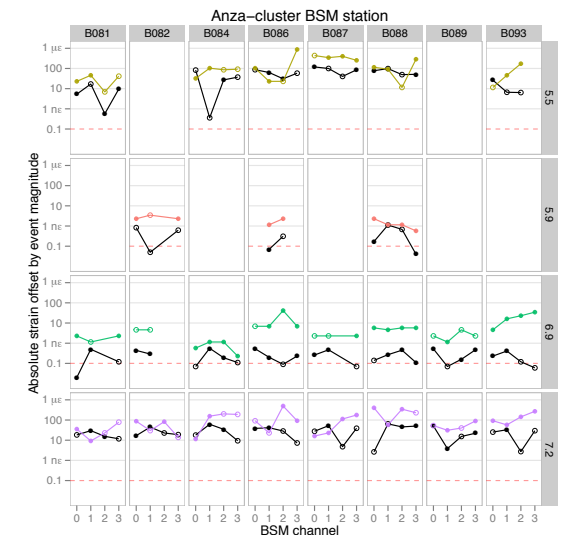

Figure 1: Offsets on Anza-cluster borehole strainmeters (colors) versus model predictions (black) and resolution (dashed). Rows show data for the same earthquake but different stations, with axes representing log-strain; columns show data for the same station but different earthquakes, sorted by channel. Symbols encode polarity. *Predictions are based on moment tensor solutions (NEIC, NCEDC).*

[5] Molnar, P., R. S. Anderson, and S. P. Anderson (2007), Tectonics, fracturing of rock, and erosion, *J. Geophys. Res.*, *112*(F03014).

[6] Barbour, A. J., and D. C. Agnew (2011), Noise Levels on Plate Boundary Observatory Borehole Strainmeters in Southern California, *submitted to Bull. Seismol. Soc. Amer.*.
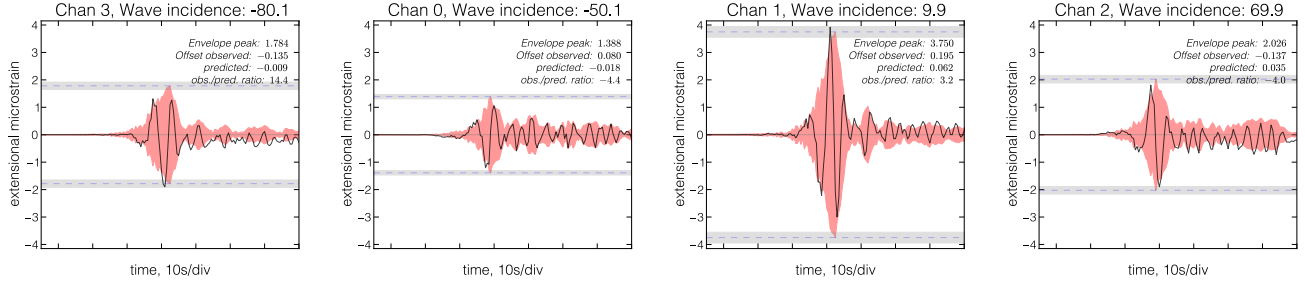
1

Figure 2: Linearized, high-frequency (periods > 2 sec) strain data before and during the Sierra El Mayor/Cucapá mainshock ($M_w = 7.2$) on April 4, 2010, for all channels at B084 at the Piñon Flat Observatory (PFO); the order from left to right is by increasing wave-incidence angle. The strain envelope, calculated using a Hilbert transform on band-limited data (to remove an artifact introduced by the offset), is shown as a red filled-region plotted ±0 strain. As is obvious for channel 1, the offset record exceeds the envelope prior to (or very close to) peak strain; this indicates the permanent offset develops rapidly after first arrivals.

at 100 Hz; and three-component strong-motion accelerometers, sampled at 200 Hz. An example of peak strains from the Sierra El Mayor/Cucapá (EMC) mainshock ($M_w = 7.2$) on April 4, 2010 is shown in Figure 2. The data are from B084 at the Piñon Flat Observatory (see Figure 3), located tens of kilometers northeast from the San Jacinto fault; they show clear permanent offsets and large dynamic strains (max. 3.8 microstrain). Offsets do not occur instantaneously at the P-wave arrival but develop very rapidly after the first arrivals. It's unclear whether they develop discretely, or cumulatively over a series of smaller events initiated by the P-wave. We do not observe similar behavior from teleseismic waves, suggesting the offset is unaffected by long-period surface waves, and controlled primarily by high-frequency body waves.

Groundtruth

We compare our observations of co-seismic strain with independent geodetic measurements, namely InSAR, LSM, and GPS.

Unfortunately, Synthetic Aperture Radar interferograms (InSAR) are too poorly correlated in the Anza region, have coarse temporal resolution, and significant uncertainty from various non-tectonic sources, making it difficult to analyze very small deformations in this context.

At PFO the borehole strainmeter is colocated with three independent LSM, making direct comparisons of high-resolution strain possible. Such a comparison constrains the lower limit of measurable signal at length scales of hundreds of meters, but they must be scrutinized carefully: Strong shaking has a tendency to cause mis-counting of the interference fringes. In Figure 4 we show data from an earthquake on a transform fault in the Gulf of California
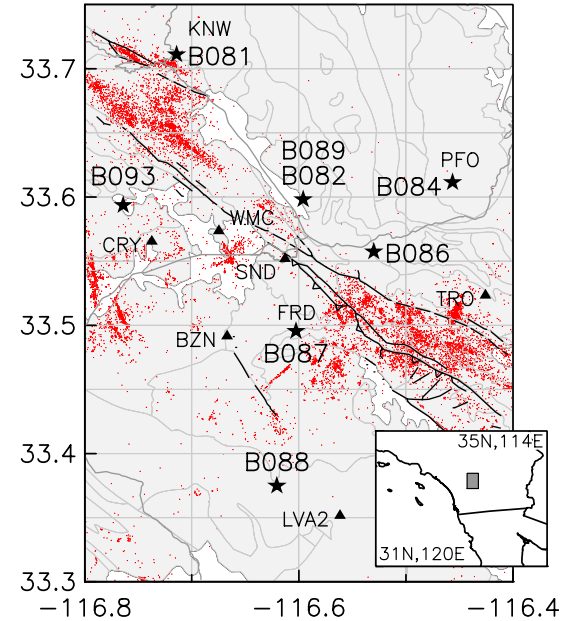

Figure 3: Locations of PBO boreholes (★), Anza broadband seismometers (▲), relocated seismicity (red dot), regions of primarily crystalline surface geology (gray regions), and the San Jacinto fault system (black lines).

(August 3, 2009; M_w=6.9), during which all three LSMs maintain fringe count. Even on a expanded strain scale, no significant off-set shows in the LSM data, while clearly each BSM is offset. The epicenter is 609 km away from PFO along the WGS84 geodesic, whereas the separation between the BSM and LSM is 75 meters or less.

Even with a relatively sparse field of co-seismic GPS displacements and their uncertainties, it is possible to solve for an empirical strain-tensor field[7]. We perform such a computation using the SSPX program and offsets from continuous GPS sites in southern California[8]. We calculate the horizontal field, and the associated uncertainties, using a "nearest neighbor" calculation with distance attenuation[9]. Results for the EMC earthquake are shown in Figures 5–8.
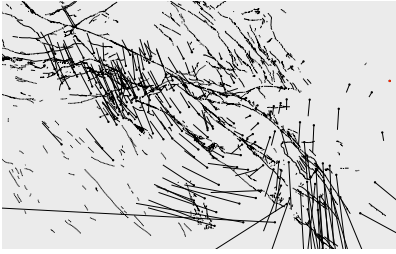

Figure 5: Map of co-seismic displacements (exaggerated) at continuous GPS sites in southern California; secular trends and post-seismic motions are removed.
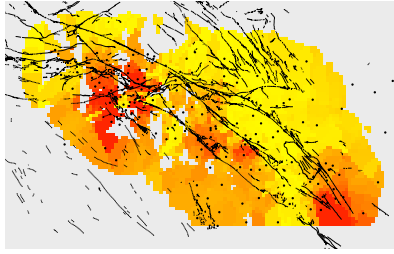

Figure 6: Map of uncertainties in the strain field calculation; linear color scale ranges from BSM instrumental resolution (0.1 nanostrain, yellow) to 100 nanostrain (red).
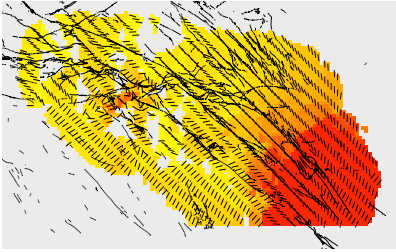

Figure 7: Map of extensional strain with principle directions; linear color scale ranges from BSM instrumental resolution (0.1 nanostrain, yellow) to 1000 nanostrain (red).
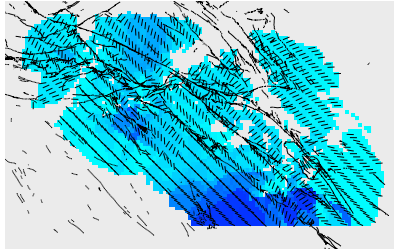

Figure 8: Map of contractional strain, with principle directions; linear color scale ranges from BSM instrumental resolution (-0.1 nanostrain, cyan) to -1000 nanostrain (blue).

The GPS displacements provide valuable upper limits on the magnitude of strain observed over a wide area. At and around the Anza-cluster strainmeters, the GPS solution shows permanent extensional strains of up-to 200 nanostrain and unresolvable contractional offsets; the uncertainty in the solution is at least 20 nanostrain. We compare these groundtruth results in Table 1 for the Anza-region, and the strainmeters installed there.
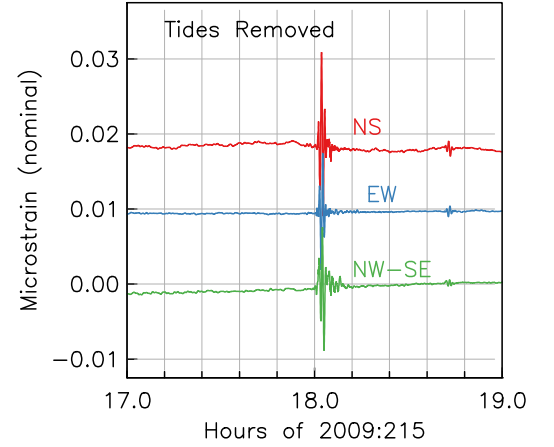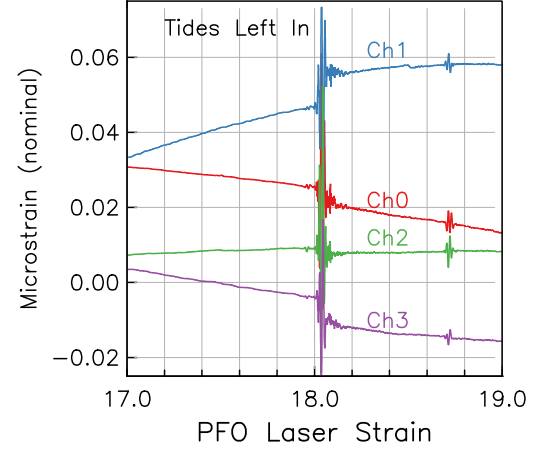
Figure 4: BSM and LSM measurements of the 2009:215 Gulf of California earthquake ($M_w = 6.9$) at PFO. *Note the vertical scale change.*

[7] Cardozo, N., and R. Allmendinger (2009), SSPX: A program to compute strain from displacement/velocity data, *Computers & Geosciences*, *35*(6), 1343 − 1357.

[8] Secular pre-seismic trends, and post-seismic relaxation are removed (B. Crowell, pers. commun., Jan. 2011)

[9] Weighting follows $\exp(-d^2/2\alpha^2)$, where d is the distance to a nearby station, and α is the attenuation factor (70 km in our calculations).

| | Co-seismic offset range in Anza, CA (nanostrain, 10^{-9}) | | | |
| | extension | | contraction | |
	lower	upper	lower	upper
Okada solution	15	94	3	70
GPS solution	50 ± 20	200 ± 20	—	—
BSM observed	9	495	13	230
LSM observed	*unavailable*			

Table 1: Ranges of co-seismic extensional and contractional offsets from the EMC mainshock: Theory (Okada), groundtruth (GPS), and observation (BSM). The "—" marker indicates the value is below the resolution of the BSM (0.1 nanostrain). The LSM comparison is unavailable because of mis-counting.

The Borehole Environment

Instruments in the Anza-cluster are located within tens of kilometers of a proposed slip-gap along the main trace of the San Jacinto fault (SJF) — the "Anza gap". The SJF system accommodates a large proportion of the total slip budget in the region by dextral shear, with the San Andreas fault accommodating the remaining portion.

We have performed preliminary analyses of logging data recorded during the drilling process. Software is being developed to identify features in the acoustic televiewer data, which provides information on lithological structure, fracturing, and stress orientation. We present results from two sites northeast of SJF: B082 (Pathfinder Ranch), located in an alluvial basin; and B084, located in granitic pluton (see Fig. 3). Fracture orientations for these boreholes are shown in Figure 9. Fractures identified for site B082 show trends in strike and dip consistent with shearing on the SJF and regional compression, as well as highly-scattered anisotropy observations[10]; fractures at B084 are not preferentially oriented.
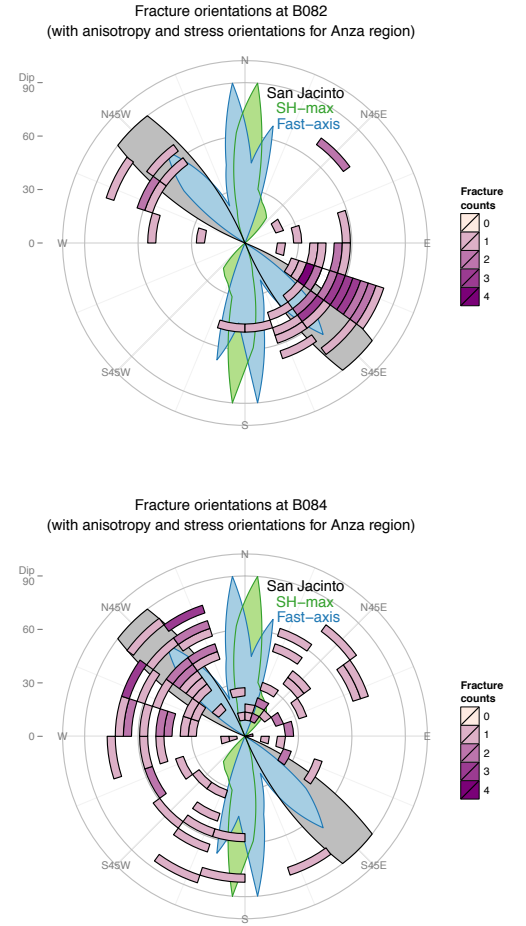

Figure 9: Fracture orientations at B082 (top) and B084, overlain on orientations of the San Jacinto fault, crustal stress (green), and shear-wave splitting fast-axes (blue) in the Anza region.

[10] Yang, Z., A. Sheehan, and P. Shearer (2011), Stress-induced upper crustal anisotropy in southern California, *J. Geophys. Res.*, *116*(B2).

SPACE-TIME RELATIONSHIP OF SLIP AND TREMOR DURING THE 2009 CASCADIA SLOW SLIP EVENT

Noel M Bartlow[1], Shin'ichi Miyazaki[2], Andrew M. Bradley[1], Paul Segall[1]*

1. Department of Geophysics, Stanford University, Stanford, CA, United States.

2. Graduate School of Science, Kyoto University, Sakyo-ku, Kyoto, Japan.

* Presenting author, noelb@stanford.edu

1. ABSTRACT

In the past decade, scientists have recognized slower forms of fault motion, termed slow slip events. These events are found primarily in subduction zones, and occur when the plate interface slips over the course of days to years, often releasing seismic moment equivalent to a large ($M_W > 6$) earthquake [*Peng and Gomberg, 2010, Schwartz and Rokosky, 2007*]. These slow slip events generate surface displacements recorded by GPS networks. Slow slip events are often accompanied by non-impulsive, low- frequency seismic signals, termed non-volcanic or tectonic tremor. The phenomenon of repeating slow slip with accompanying tremor is referred to as episodic tremor and slip (ETS) [*Rogers and Dragert, 2003*]. The precise physical relationship between slip and tremor during ETS has not been established. Multiple hypotheses have been suggested, one of which states that tremor represents slip on small locked asperities within the ETS region driven to instability by creep on the surrounding fault. To test this hypothesis, we invert Plate Boundary Observatory (PBO) GPS data from the August 2009 ETS event in central Cascadia using the Network Inversion Filter. We obtain a history of daily solutions of both slip and slip rate on the plate interface for the duration of the event, and compare to a tremor catalog provided by Aaron Wech. The tremor locations are deteremined using the WECC method [*Wech and Creager, 2008*], and the catalog can be viewed at pnsn.org/tremor [*Wech, 2010*].

For this event, we find that slip is concentrated between 35 and 50 km depth, with a maximum slip of aproximately 5 cm. We find a cumulative moment of 1.65×10^{19} N-m, assuming a shear modulus of 3×10^{10} Pa, which is equivalent to a moment magnitude of 6.8. The final slip distribution and tremor epicenters for the event correlate very well (Figure 1). This inversion fits the data very well, with fits to the static offsets shown in Figure 2 and time dependent fits for selected stations shown in Figure 3. When we examine the slip rate as a function of time, we find an excellent correlation between tremor epicenters and the instantaneous position of high fault slip-rate (Figure 4), consistent with the stated hypothesis. This correlation is especially remarkable given that tremor hypocenters and slip are obtained from completely independent data.

2. References

Peng, Z. & Gomberg, J. An integrated perspective of the continuum between earthquakes and slow-slip phenomena. *Nature Geoscience* **3**, 399-607 (2010)

Schwartz, S. Y. & Rokosky, J. M. Slow slip events and seismic tremor at cricum-Pacific subduction zones. *Rev. Geophys.* **45**, RG3004 (2007)

Rogers, G., & Dragert, H. Episodic tremor and slip on the Cascadia subduction zone: The chatter of slient slip. *Science* **300**, 1942-1943 (2003)

Wech, A.G., & Creager, K. C. Automated detection and location of Cascadia tremor. *Geophys. Res. Lett.* **35**, L20302 (2008)

Wech, A. G. Interactive tremor monitoring. *Seismol. Res. Lett.* **84**, 664-669 (2010)
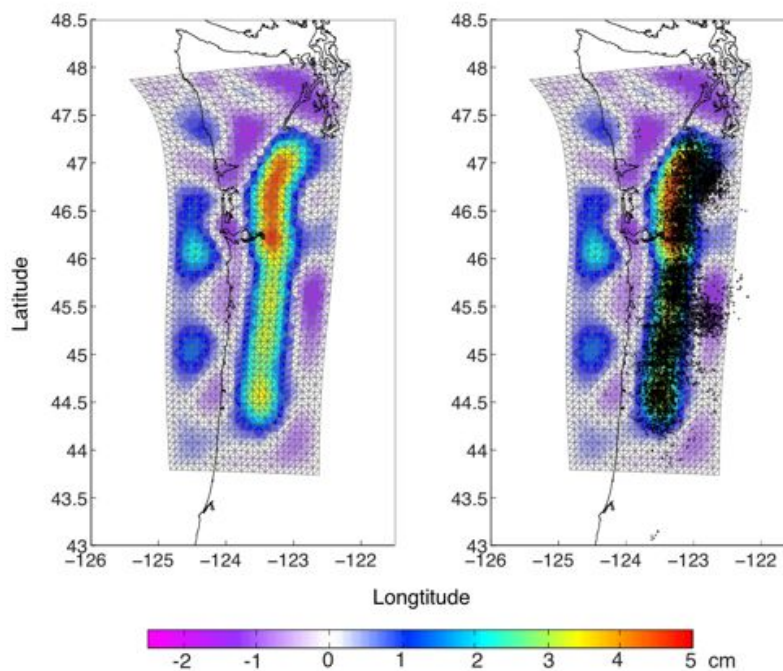
FIGURE 1. Estimated cumulative slip on the plate interface for the August 2009 ETS event. Left panel: Slip at final epoch. Right panel: Same as left, with tremor epicenters for the time interval 08/02/2009 - 09/22/2009 plotted in black.
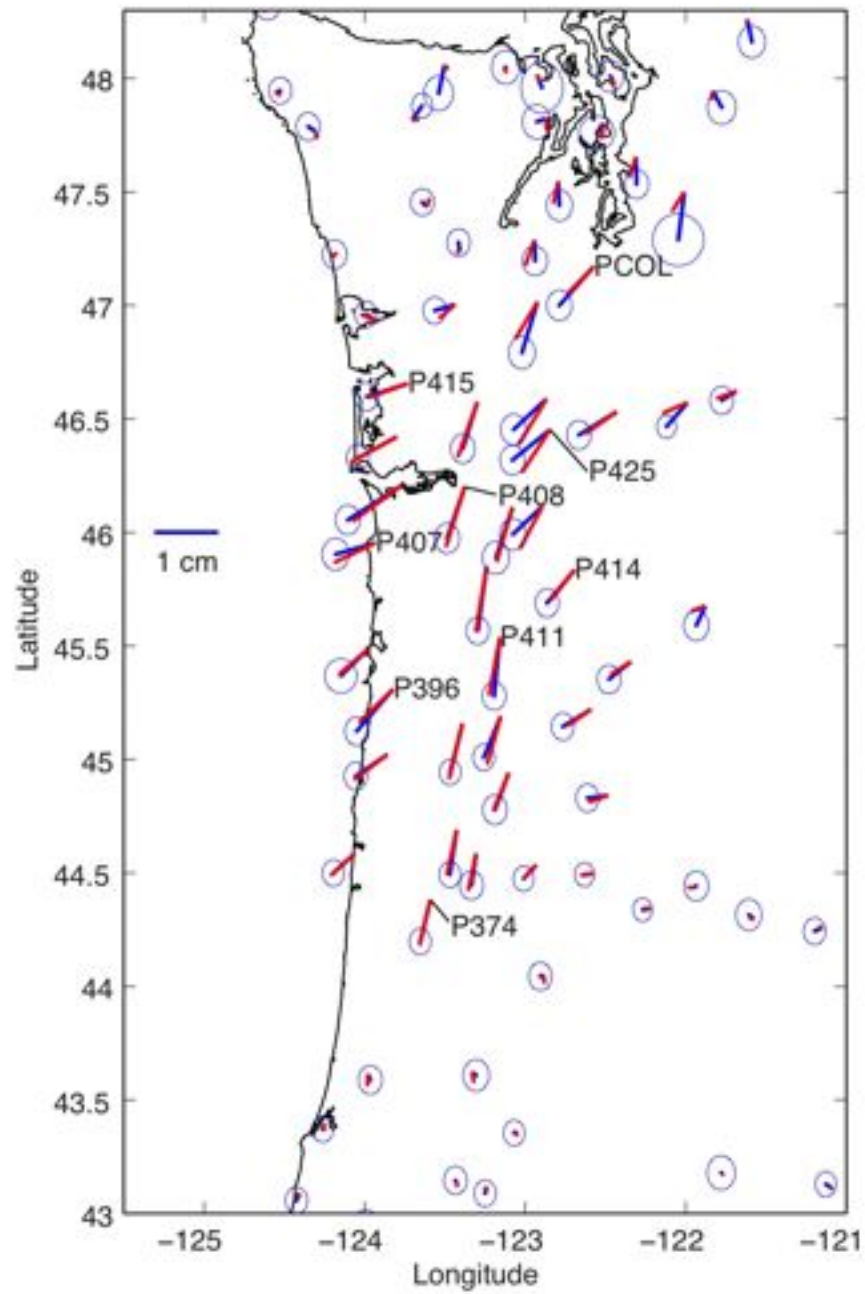
FIGURE 2. Observed and predicted cumulative GPS displacements during the 2009 ETS event. Data and 1σ error ellipses shown in blue; model fit shown in red. Labeled stations refer to time series fits in Figure 3.
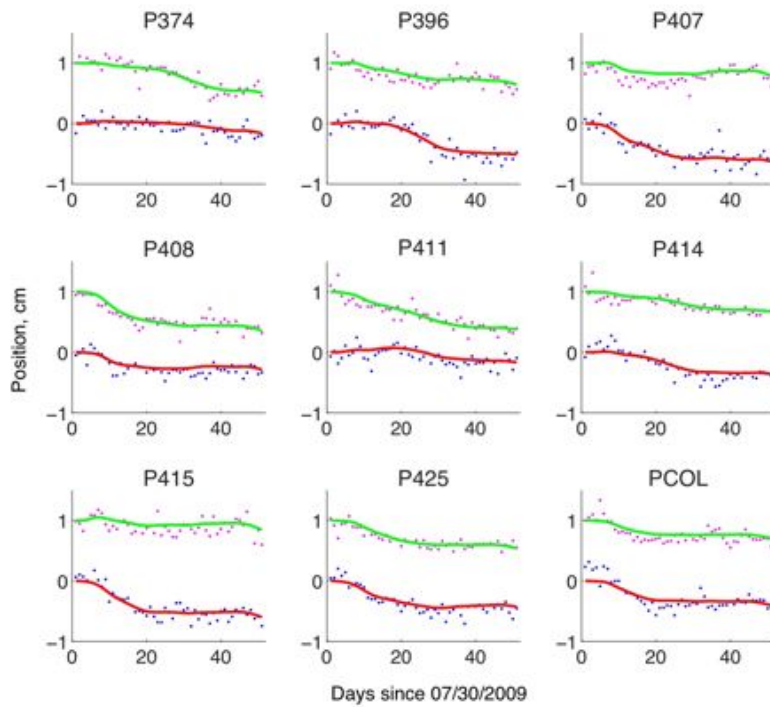
FIGURE 3. Time series fits to GPS data for selected stations (locations shown in Figure 2). Blue dots represent east displacements with model fit in red continuous line; Pink dots represents north displacements with model fit in green. North component offset by 1 cm for clarity.
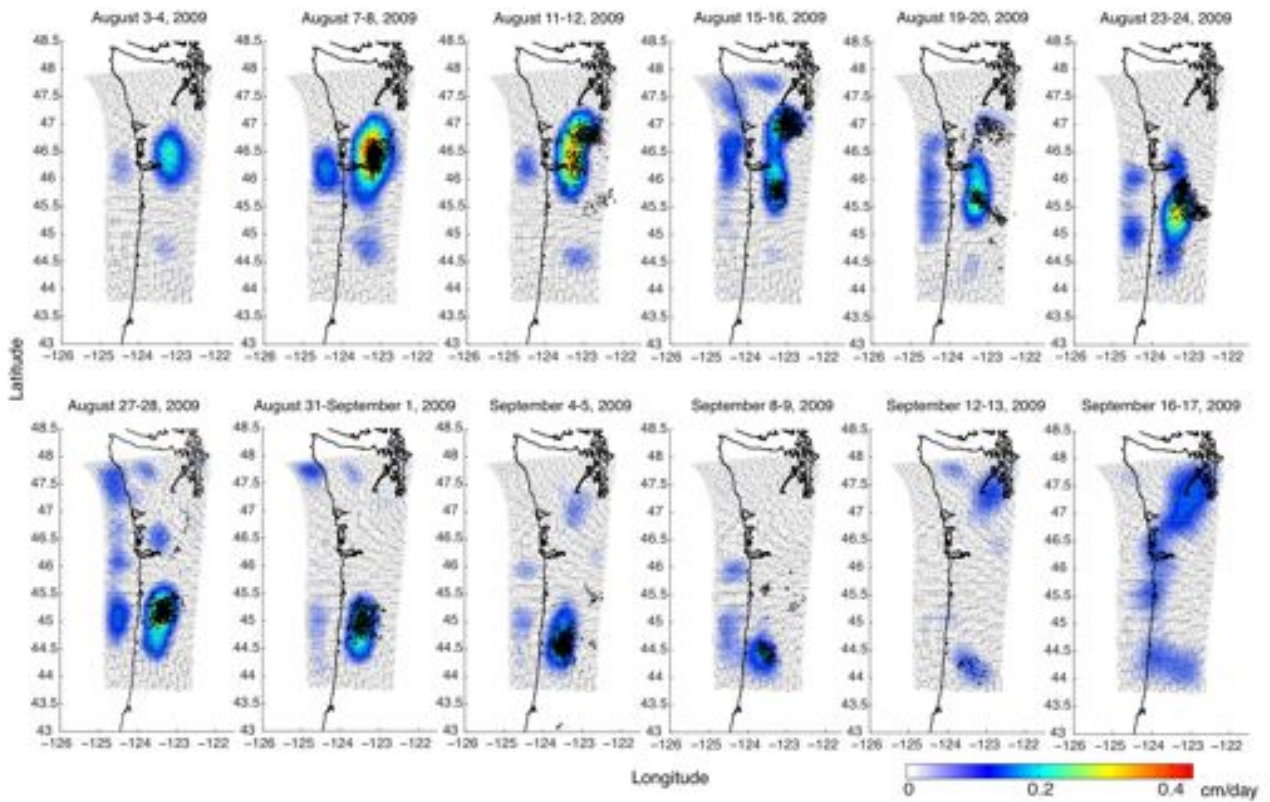
FIGURE 4. Slip rate on the plate interface, averaged over two day intervals. Tremor hypocenters are plotted in black for the same two-day intervals. The plate interface mesh is shown between 10 and 60 km depth. Note that not all of the modeled days are shown.

QUATERNARY GEOLOGIC CONSTRAINTS ON DENALI FAULT STRAIN-PARTITIONING AND IMPLICATIONS FOR INTERIOR ALASKA TECTONICS

Sean P. Bemis* – U.S. Geological Survey and University of Kentucky
Gary A. Carver – Carver Geologic, Inc.
Ray J. Weldon – University of Oregon

The Denali fault system (DFS) is widely recognized as a transpressional system due to the presence of the Denali fault itself, an active, intracontinental right-lateral fault, and sub-parallel late Cenozoic uplift of the Alaska Range. Recent work has identified faults and folds accommodating Quaternary uplift of the Alaska Range and established slip rates on the DFS, but the quantitative interaction between the contractional and translational components of this transpressional system have remained untested. We analyze the style and distribution of active faulting within and adjacent to the Alaska Range to define patterns of strain accommodation and determine how strain is partitioned across the DFS. As the trace of the Denali fault curves by ~70˚ across central Alaska, the mean strike of the thrust system to the north remains sub-parallel to the Denali fault while to the south, the few faults with known or suspected Quaternary offset are oblique to the Denali fault. Therefore, the DFS strongly partitions the NW-directed motion into fault-parallel and fault-perpendicular components which are accommodated predominantly by right-lateral slip on the Denali fault and shortening within the northern Alaska Range. This pattern of strong strain-partitioning across the Denali fault presents fundamental constraints on the active tectonics of interior Alaska. In particular, contrary to the previous model of a broad dextral shear zone driving block rotations and shallow seismicity north of the Denali fault, geologic and seismologic data require a fault-normal principal shortening direction and east-west changes in the observed deformation as the DFS curves through central Alaska.

*email: sean.bemis@uky.edu

University of Alaska Geochronology Facility: Ongoing collaborations on the rock record of Neogene deformation in southern Alaska.

Jeff Benowitz[1], Paul Layer[2], Sean Bemis[3], Sarah Roeske[4]

[1]Department of Geology and Geophysics, University of Alaska, Fairbanks
jbenowitz@alaska.edu
[2]College of Natural Science and Mathematics, University of Alaska, Fairbanks
pwlayer@alaska.edu
[3]Department of Earth and Environmental Sciences, University of Kentucky,
sean.bemis@uky.edu, (presenting author)
[4] Geology Department, University of California, Davis
smroeske@ucdavis.edu

The planned EarthScope deployment of the USArray in Alaska provides exciting opportunities for understanding mantle-crust interactions in a complex convergent margin. An ongoing wide-spread GPS and EarthScope seismic instrument campaign will provide valuable insights into how stress from the ongoing flat-slab subduction of the Yakutat microplate at Alaska's southern margin is distributed inboard. Far-field response to the plate boundary coupling is expressed as both vertical and horizontal tectonics along crustal-scale faults such as the Denali Fault system. Results from this study will have both regional and broad scale tectonic implications. In particular, results from this project will help define what constitutes the boundaries of blocks of Alaska crust, and whether the wide plate boundary zone between the Pacific and North American plates is best characterized by diffuse deformation, block rotation, or both. Results will also have relevance to how surface processes and seasonal hydrological changes affect vertical movement of the upper plate.

The deployments will also present an opportunity to integrate short term observations (e.g. GPS measurements) with Alaska's million year time scale tectonic history preserved in the rock record. The University of Alaska Fairbanks geochronology facility is currently involved in numerous collaborations in southern Alaska using thermochronology and geochronology integrated with micro- and macrostructural analysis to document continental-scale fault movements, block formation, block boundaries and block history, interactions between tectonic and glacial processes, and vertical tectonics. Recent projects have concluded that flat-slab subduction has influenced the tectonics of south-central Alaska for at least ~24 Ma, which is documented in the Neogene formation of the eastern Alaska Range and strike-slip movement along the eastern Denali Fault system. A central focus of our group's research is to investigate if particular regions of Alaska our undergoing diffuse/distributed deformation or are acting more block-like. Continuing and proposed projects along this front relevant to the EarthScope community include, but are not limited too:

a) How do near-field structural irregularities like the Denali Fault restraining bend affect vertical tectonics (e.g. Mount McKinley) and is there a rock record of southern Alaska block movement history along the Denali Fault restraining bend?

b) Why does the slip rate of the Denali fault vary along strike, and do these rates change through time?
c) Does the rock record of the western Alaska Range support the inference of a boundary between the Bering and southern Alaska blocks?
d) In the Talkeetna Mountains, is there a record of south to north Neogene progressive exhumation related to the location of the Yakutat flat slab through time?
e) Do active faults and glacial processes, through an unique feedback system, magnify the effect both processes have on the long-term erosion history of a region?

We look forward to discussing these current projects with the EarthScope community and avenues for integrating the objectives of the USArray with our work. We also look forward to discussing further collaborations integrating the modern and geological record.

2011 EarthScope National Meeting

Title:
Support of EarthScope GPS Campaigns at the UNAVCO Facility

Authors:
Henry Berglund, Frederick Blume, James Normandeau, Abe Morrison
UNAVCO, Boulder, CO 80301-5553
Contact Email: berglund@unavco.org

Abstract:
In order to support portable GPS deployments funded by the NSF's EarthScope Science panel, PBO has purchased 100 campaign GPS systems. Based Topcon GB-1000 equipment, the systems have been designed for stand-alone temporary or semi-permanent deployment that will be used for densifying areas not sufficiently covered by continuous GPS, and responding to volcanic and tectonic crises. UNAVCO provides support for all aspects of these projects, including proposal and budget development, project planning, equipment design, field support, and data archiving. Ten of the 100 systems have been equipped with real-time kinematic (RTK) capability requiring additional radio and data logging equipment. RTK systems can be used to rapidly map fault traces and profile fault escarpments and collect precise position information for GIS based geologic mapping. Each portable self-contained campaign systems include 18 Ah batteries, a regulated 32 watt solar charging system, and a low-power dual frequency GPS receiver and antenna in a waterproof case with security enhancements. The receivers have redundant memory sufficient for storing over a year's worth of data as well as IP and serial communications capabilities for longer-term deployments. Monumentation options are determined on a project-by-project basis, with options including Tech2000 masts, low-profile spike mounts, and traditional tripods and optical tribrachs. Drilled-braced monuments or masts can be installed for "semi- permanent" style occupations. The systems are being used to support several projects, including the University of Nevada Reno's current 34-unit deployment to monitor the motion of the Colorado Plateau and the ongoing Rio Grande Rift experiment, run by the Universities of Colorado, Utah State, and New Mexico, which has seen the construction of 25 permanent monuments in 2006 and 2007 and a 26-site campaign reoccupation in 2008.

A Constantly Growing, Up-To-Date, On-Line, Homogeneous Set of GPS Time Series for Global and Regional Geodetic Studies

Geoffrey Blewitt, Hans-Peter Plag, William C. Hammond, Corné Kreemer

Nevada Bureau of Mines and Geology, University of Nevada, Reno, MS 178, Reno, NV 89557, USA
gblewitt@unr.edu

We routinely collect and analyze all publicly available GPS geodetic data known to us. Time series of station displacements are made available at http://geodesy.unr.edu/networks/stations. Currently, time series for more than 9,000 stations are available in ITRF 2005 (IGS05) and additional references frames including NA09 (ITRF 2005 rotated into a stable North America frame), and GB09 (NA09 but with daily spatial filtering to mitigate common-mode error over the western United States).

The system is based on precise point positioning (PPP) using JPL's GIPSY OASIS II software, coupled with ambiguity resolution and a global network adjustment of 500,000 parameters per day using our newly developed Ambizap3 software. The system is designed to easily and efficiently absorb stations that deliver data very late, by recycling prior computations in the network adjustment, such that the resulting solution is identical to starting from scratch. Thus, it becomes possible to trawl continuously the Internet for late arriving or newly discovered data, and seamlessly update all GPS station time series using the new information content. As new stations are added to the processing archive, automated e-mail requests are made to H.-G. Scherneck's server at Chalmers University to compute ocean loading coefficients used by the station motion model. RINEX file headers are parsed and compared with alias tables in order to infer the correct receiver type and antenna/radome phase calibrations to apply to the data. Strict quality control is implemented at all levels of the system, with the exception that time series analysis is not used to remove outliers, as that could inhibit discovery of unusual site motions.

The web page gives access to station plots, spectra of the time series, and estimates of linear trends and annual and semi-annual constituents. Data quality routines are currently being developed and quality information will be added to the on-line time series. Access to individual stations is available through alphabetical list (global, regional), a clickable map, and a Google map interface.

The time series are available in two different formats: (1) standard topocentric east, north, and vertical (e,n,v) displacements computed relative to coordinates at the start of the time series, (2) coordinates in a new global system we have developed, as a possible candidate for a new standard. The new system defines a unique easting and northing for every longitude and latitude, in a high-precision version of UTM. The vertical coordinate is simply defined as height above the GRS80 ellipsoid. Northing is the geodesic distance from the equator on the GRS80 ellipsoid, computed rapidly according to Vincenty (1975) with ~1 micron accuracy (as we have verified by numerical integration of the elliptic integral). Easting is the meridional distance (along the parallel of latitude) from the nearest reference meridian, defined every 0.1 degrees of longitude. This allows for (e,n,v) coordinates for any stations within each 0.1-degree zone of longitude to be compared directly. The width of this zone ranges from ~11 km at the equator to ~500 meters at HOWE (87.4S), the closest bedrock station to the South Pole. This system has helped to resolve problems with duplicate station names, with RINEX files having the wrong station name, with local relocation of antennas, and with attempts to connect new permanent stations with older campaign stations of a different name. To facilitate plotting of time series, our format breaks each coordinate into integer plus fractional parts. Tectonic velocities computed in this new system agree with those computed using the standard (e,n,v) system to <0.1 mm/yr.

Reference: Vincenty T. (1975). Direct and inverse solutions of geodesics on the ellipsoid with application of nested equations. *Survey Review, Vol. XXIII*(176), 88–93.

Imaging Earthquakes and Plate Tectonic Motion from Japan to Western North America: GPS Total Displacement Waveforms from M9.0 Tohoku-oki Earthquake, GEONET coseismic results, and PBO time series and velocities

Bock, Y.[1]
Crowell, B.[1]
Owen, S.[2]
Melgar, D.[1]
Squibb, M.[1]
Moore, A.[2]
Fang, P.[1]
Dong, D.[2]
Webb, F.[2]
Kedar, S.[2]

1. Cecil H. and Ida M. Green Institute of Geophysics and Planetary Physics, Scripps Institution of Oceanography, La Jolla, CA, USA

2. Jet Propulsion Laboratory, California Institute of Technology, Pasadena, CA, USA

In response to the March 11 Mw 9.0 Tohoku-oki earthquake in Japan, we have generated stacked 1 Hz GPS displacement waveforms from the California Real Time Network (CRTN) that show the dynamic displacements due to the seismic waves as they propagated across the network. We are able to clearly discern the S-wave, Love wave and Rayleigh wave in the horizontal components. Comparisons with seismographs show the arrival of the S-wave at 1400 seconds and the Love wave 2000 after the earthquake onset. Results were archived on the SOPAC archive on the day of the event and later posted on the GPS Explorer portal at http://geoapp03.ucsd.edu/gridsphere/gridsphere.

The large coseismic displacements at Japan's GEONET stations were generated by JPL & Caltech's ARIA team and posted on GPS Explorer's Earthquake page, allowing users to view the displacements in an interactive mapping tool. This mapping tool includes options to display the large horizontal and vertical displacements at different scales, overlay earthquakes, and display the locations of KNet and KikNet accelerometers.

GPS Explorer is the portal for a MEaSUREs-funded project to generate data products for the study of lithospheric deformation in the Western U.S. from PBO and other continuous GPS stations in this region. The project brings together state-of-the art algorithms for generating high quality calibrated and validated time series, velocity fields, transient deformation, and strain maps with advanced IT infrastructure and portal development for accessing these products. The portal, allows users to mine and manipulate these products in a workbench-like environment. We will present some example results of the high-level data products as well as update the community of scientific users on the latest developments in our portal technology.

The Use of Real-time GPS and Accelerometer Data for Earthquake Early Warning and Rapid Response

Yehuda Bock, Scripps Institution of Oceanography

Earthquake early warning (EEW) has been shown to be a practical and effective way to reduce casualties and protect infrastructure during a large event, as evidenced by the successful early warning issued by Japanese authorities for the March 11, 2011 Mw 9.0 Tohoku-oki earthquake. EEW can be considered a form of earthquake prediction. Since radio waves travel much faster than seismic waves, a suitably designed real-time monitoring network can detect the seismic P-wave and issue an alert before the destructive S-wave arrives, for all areas except for a blind zone closest to the epicenter. A warning of even several seconds could be invaluable. In the ShakeOut scenario of a magnitude 7.9 earthquake nucleating at the southern terminus of the San Andreas fault, a warning of 70-90 seconds could be issued for the greater Los Angeles region. Earthquake response in terms of rapid estimates of magnitude and slip is also critical, especially for generating accurate and timely tsunami warnings.

Currently, EEW systems use only traditional seismic instruments, which have limitations in the near field during large earthquakes. Broadband velocity instruments will clip as occurred for the April 4, 2010 Mw 7.2 El Mayor Cucapah earthquake in northern Baja California, while displacements doubly integrated from strong motion instruments (accelerometers) are adversely affected by rotation and tilt. Accelerometer corrections are possible but they are subjective and result in the loss of the static offset. GPS instruments measure both static and dynamic displacements directly but have limited precision compared to inertial instruments, and have poor resolution in the vertical direction. Real-time GPS data are sufficiently precise to detect the S-wave, but that significantly increases the blind zone for EEW although they are quite useful for tsunami warning. Analyzed together using a Kalman smoothing algorithm (*Bock et al*., 2011), GPS displacements and raw accelerometer data at collocated stations provide a true broadband record of displacement across the entire frequency range of surface motion, including the static component at the higher rate sampled by accelerometers (e.g., 100 Hz), and with sufficient timeliness and precision to detect the P-wave. This was convincingly demonstrated for the El Mayor Cucapah earthquake for 12 locations in southern California where a high-rate GPS instrument and accelerometer were within 1.5 km of each other.

There is growing awareness for the need of an effective EEW system in the Western U.S. and that both seismic and geodetic instruments should be used. There are three areas of primary concern in our lifetimes: the Cascadia subduction zone which could experience an M=9 event similar to the March 11 Tohoku-oki earthquake and tsunami, and the southern and northern sections of the San Andreas fault which could experience up to an M=7.9 event. The EarthScope infrastructure in the Western U.S. is well suited to contribute to earthquake and tsunami early warning, including in Alaska, and there is a similar effort in Mexico focused on the Mexican subduction zone. Using EarthScope

infrastructure for EEW requires an accelerated effort to upgrade PBO stations to real-time operations, consideration of adding accelerometers at PBO stations, a concerted effort to be able to estimate integrated displacement seismograms on-the-fly from both geodetic and seismic stations in response to a large earthquake, and coordination with the USGS and earthquake first responders.

Bock, Y., D. Melgar, and B. W. Crowell (2011), Total Displacement Waveforms from Geodetic and Seismic Networks, *BSSA, in review.*

Teleseismic S-Wave Delay Times in the Mid-Continent and the Superior Province Rifting Earthscope Experiment (SPREE)

Trevor Bollmann, Suzan van der Lee, Andrew Frederiksen

A roughly one-billion year old rifting event in the mid-continent left the well known, but not well studied Mid-continent Geophysical Anomaly (MGA). This anomaly includes a dramatic gravity anomaly with a range of -126 to 66 mgal. To date, seismic images of the deep structure of the mid-continent have not shown a similarly strong or otherwise correlated seismic-velocity anomaly beneath the failed rift. The SPREE aims to address this issue by densifying the seismic station coverage along and across the MGA, as well as extending the TA style station coverage into Canada, north of the MGA.

In anticipation of seismic data from the SPREE, we compiled teleseismic delay time data from the Abitibi Transect (Rondenay et al., 2000), TWiST (Kay et al., 1999), Polaris stations from southern Ontario (Aktas and Eaton, 2006). The delay times were found by using the Multi-Channel Cross Correlation method of VanDecar and Crosson (1990) to pick the S-wave arrivals and then the true delay times were calculated with respect to Xiaoting Lou's XC35 earth structure model.

The Abitibi delays show a range of roughly 1 second. This is very different than what is expected for the delay times beneath the MGA. Due to the shallower Moho beneath the failed rift (French et al.) the delay times of vertically arriving rays will arrive around two seconds earlier than the delay times from stations on either side of the rift where the crust is thicker. This difference could be due to little or no variations in the lithosphere of the Abitibi region while the lithosphere beneath the rift has drastic changes.

The tomography that Andrew Frederiksen has been doing with in the area of interest shows that the speed of the P-waves through the crust is positive in the area surrounding the MCR but increasingly slower as you move into the plains states. This is most likely due to the sedimentary basin located in the plains and the superior craton, which is underlain by igneous and metamorphic rock and only a small amount of sedimentary rock.

We will systematically compare the geographic distribution of teleseismic S wave delay times with the magnetic and gravity anomalies to assess the degree of correlation between the different geophysical properties. This will help in our understanding of the structure of the earth beneath and around this anomaly.

Using EarthScope and MAGNET GPS to determine the slip rate on the Honey Lake Fault, northern Walker Lane, California

Bormann, Jayne M.
jbormann@unr.edu

Hammond, William C.
whammond@unr.edu

Kreemer, Corné
kreemer@unr.edu

Nevada Geodetic Laboratory, Nevada Bureau of Mines and Geology, University of Nevada, Reno

The Walker Lane is a complex zone of active intracontinental transtensional faulting in the western United States. This ~100 km wide zone accommodates 10 mm/yr of right lateral deformation between the northwest translating Sierra Nevada/Great Valley (SNGV) microplate and the west-northwestward extending Basin and Range province. In the northern Walker Lane, to the north of Lake Tahoe, at least 5 mm/yr of right lateral shear occurs across a zone spanning the Honey Lake/Warm Springs and Mohawk Valley faults. These parallel, northwest striking, dextral faults work together as a cooperative pair to accommodate the deformation, however it is unclear which fault is dominant.

Geologic studies suggest that the Honey Lake fault slips at a rate of ≥ 1 mm/yr with a minimum of 0.3 mm/yr slip on the Mohawk Valley fault. In contrast, a regional geodetic study estimates a dextral slip rate of 1.2 ± 0.3 mm/yr on the Honey Lake fault and 2.9 ± 0.2 mm/yr for the Mohawk Valley fault. The distribution of slip between the two faults plays an important role in determining the regional distribution of seismic hazard for the nearby communities of Susanville and Truckee, CA, and Reno, NV.

To improve the estimate of slip rate on the Honey Lake fault, we have increased the density of GPS stations along a transect spanning the Mohawk Valley fault and Honey Lake faults. These stations are a part of the semi-continuous Mobile Array of GPS for Nevada Transtension network (MAGNET, http://geodesy.unr.edu) that forms a dense complement to the EarthScope Plate Boundary Observatory. We use preliminary results to solve for slip rates, fault dip and locking depth on both faults using a block model specifically designed for the Honey Lake/Mohawk Valley fault system. This analysis will allow us to address questions regarding the trade-off between slip rates on neighboring faults, uncertainties in fault geometries and linkages, and the potential role of normal faulting in regional deformation.

Episodic tremor and slip along the entire Cascadia subduction zone

Devin C. Boyarko[1], Michael R. Brudzinski[1], Stephen Holtkamp[1], Timothy I. Melbourne[2], Robert W. Porritt[3], Richard M. Allen[3], and Anne M. Tréhu[4]

[1]Department of Geology, Miami University
[2]Department of Geological Sciences, Central Washington University
[3]Department of Earth and Planetary Sciences, UC Berkeley
[4]College of Oceanic and Atmospheric Sciences, Oregon State University

In recent years, advances in seismic and geodetic monitoring systems have led to the discovery of a new family of slow earthquakes, including extended duration episodes of tectonic tremor and transient slip, originating downdip from the primary seismogenic portion of the plate interface in many subduction zones. In order to provide overall spatial and temporal constraints of tectonic tremor, specified time periods of elevated tremor energy during the period from 2005 to 2010 are investigated with the application of an automated location routine to seismic data spanning the full length of the subduction zone. In addition, geodetic estimates of slow slip episodes occurring along the entire the subduction zone are compared with our catalog of tremor solutions. Source parameters of individual episodes of tectonic tremor and slow slip are estimated and compared in an effort to facilitate a better understanding of these two processes. Investigation of the spatial and temporal progression of individual tremor episodes clarifies several unique modes of simple and complex propagation with components of motion parallel and orthogonal to the strike of the subducting plate. Segment boundaries that are defined based on the lateral extent, relative timing, and recurrence of tremor episodes are found to coincide with along strike structural variations in the continental and oceanic plates. Spatial distributions of tremor and slip are compared to the distribution of ordinary earthquakes, finding the tremor and slip source region coincides with a corridor of reduced seismic production inside the continental and oceanic plates along the subduction zone.

THE WESTERN IDAHO SHEAR ZONE, WEST MOUNTAINS, IDAHO: CHARACTERIZING DEFORMATION THROUGH A SEISMIC TRANSECT

Braudy, N.[1], Tikoff, B.[1], Gaschnig, R.[2], Vervoort, J.[2]

1. Department of Geoscience, University of Wisconsin-Madison, Madison, WI 53706; basil@geology.wisc.edu, nbraudy@gmail.com
2. School of Earth and Environmental Sciences, 1228 Webster Physical Sciences Bldg., Washington State University, Pullman, Washington   99164

The Earthscope Idaho-Oregon (IDOR) project is an integrated study of the tectonic boundary, from East to West, between the Precambrian North American and accreted island arc terranes of the Blue Mountains. The boundary is marked by the sharp discontinuities in wall rock lithology, geochemistry (Sr, O), and the presence of the western Idaho shear zone (WISZ).

Within the longitudes of 116° 15' and 116°15'30'', the IDOR seismic transect (occurring in the summer of 2012) cuts directly through the WISZ. Along this transect, three major plutonic complexes are found (from East to West): 1) Plutonic rocks containing both biotite and white mica (Idaho Batholith); 2) A tonalite sill with solid-state deformation on its western margin (Payette River tonalite); 3) Orthogneisses and paragneisses with strong solid-state deformation (correlative to Little Goose Creek complex); and 4) Variably deformed, epidote-bearing granitoids (correlative with Hazard Creek complex).

Gneissic zones mark the location of the WISZ. The zone is dominated by orthogneisses, with sillimanite-grade paragneisses localized along petrologically distinct boundaries. The gneisses have a strong, steeply east-dipping, solid-state foliation as defined by ribboned quartz grains and biotite stringers. There is also a pervasive vertical lineation defined by biotite stringers and aligned hornblende prisms. Shear sense is defined by sheared mafic enclaves, sheared augens of both Kspar and Plagioclase feldspar, isolated folds indicate dextral shear sense on sub-horizontal faces; this finding is consistent with previous reports from this zone.

New geochronological dates (U/Pb on zircon) from this area are consistent with results obtained from further north (McCall area) in the same shear zone. A pluton located E of the WISZ, intepretted to be the western edge of the Idaho batholith, is dated at 86 Ma (Little Valley pluton); this pluton do not contain a solid-state fabric. The tonalite sill (Payette River tonalite) is dated at 88.4 Ma, providing a minimum age of solid-state deformation associated with the WISZ at this locality. The zircons in the orthogneisses are complex. They indicate an age of ~106 Ma, but contain inherited cores that date around 200 Ma or slightly older.

It is unknown when the WISZ initiated and whether deformation occurred in a single episode of deformation. Additional geochronologic data may help resolve these issues. Results of the seismic transect will be used in conjunction with detailed field mapping on the WISZ in order to fully understand the deformational history in this area.

Seismic anisotropy in forearcs from antigorite crystal preferred orientations (CPOs)

Sarah J. Brownlee[1,*], Bradley R. Hacker[1,2], George E. Harlow[3], Gareth Seward[2]

1. Earth Research Institute, University of California, Santa Barbara
2. Department of Earth Science, University of California, Santa Barbara
3. Department of Earth and Planetary Sciences, American Museum of Natural History
* sbrownlee@eri.ucsb.edu

Seismic anisotropy is often used to infer flow directions in the mantle, but anisotropy in the upper plate nose of a subduction zone may be more directly related to alteration of mantle material (i.e. hydration of olivine). Understanding the mechanisms responsible for anisotropy in subduction zones provides a link between seismic observations and the processes occurring in subduction zones. It has been suggested that olivine B-type fabric alone cannot explain shear wave splitting observations in the shallow tip of the mantle-wedge [*Kneller et al.,* 2008]. We investigate the mechanisms of mantle-wedge tip anisotropy by measuring the crystal preferred orientation (CPO) of antigorite in serpentinites from central Guatemala using electron backscatter diffraction (EBSD), and using the published mineral elastic constants to calculate the aggregate seismic properties of the rock. This method has been demonstrated to return velocities within ±5% of laboratory measurements [*Barroul and Kern,* 1996; *Brownlee et al.,* in press]. Antigorite, like all sheet silicates, has highly anisotropic elastic properties [*Bezacier et al.,* 2010]. The CPO of antigorite is related to the geometry and strength of deformation [*Bezacier et al.,* 2010; *Hirauchi et al.,* 2010] and the CPO of the parent olivine [*Boudier et al.,* 2010]. Our measurements of CPO in 6 antigorite serpentinites doubles the number of available measurements on natural antigorite. The CPOs indicate slip within the basal plane and have a similar degree of variability in CPO strength as previous studies. The antigorite CPOs may retain information on the parent olivine CPO, and have the potential to distinguish between A- and B-, or C-type olivine CPOs. The calculated anisotropies of these rocks vary from ~14-28% in V_P, and ~13-32% in V_S, which is similar to previous studies. The symmetry of V_P anisotropy varies from orthorhombic to uniaxial with increasing anisotropy; the slowest velocities are found ~perpendicular to the foliation. Our results suggest that a combination of B-type olivine CPO and sheared antigorite on the subducting slab interface may account for shear wave splitting observations in the mantle-wedge tip.

References:
Barroul, G., and H. Kern: *PEPI, **95**,* 175-194, 1996.
Bezacier, L. et al.: *EPSL, **289**,* 198-208, 2010.
Boudier, F. et al.: *J. Petrology, **51**,* 495-512, 2010.
Brownlee, S.J. et al.: in press with *JGR-Solid Earth.*
Hirauchi, K. et al.: *EPSL, **299**,* 196-206, 2010.
Kneller, E.A. et al.: *EPSL, **268**,* 268-282, 2008.

Featuring EarthScope Science for K-12 Teachers and Students in the Pacific Northwest

Robert Butler, Department of Environmental Sciences, University of Portland, 5000 N. Willamette Blvd., Portland, OR 97203, butler@up.edu; Frank Granshaw, Portland Community College, Sylvania Campus, 12000 SW 49th Ave, Portland, OR 97219, fgransha@pcc.edu; Roger Groom, Mt. Tabor Middle School, 5800 SE Ash, Portland, OR 97215, rgroom@pps.k12.or.us; Chris Hedeen, Oregon City High School, 19761 S. Beavercreek Rd Oregon City, OR 97045, Chris.Hedeen@orecity.k12.or.us; Jenda Johnson, Volcano Video Productions, 1924 NE 47th St., Portland, OR 97215, jendaj@comcast.net; Bonnie Magura, Jackson Middle School, 10625 SW 35th, Portland, OR 97219, bmagura@pps.k12.or.us; Beth Pratt-Sitaula, Department of Geological Sciences, Central Washington University, 400 E University Way, Ellensburg, WA 98926-7418, psitaula@geology.cwu.edu; Denise Thompson, Orting High School, 320 Washington Ave. North, Orting, WA 98360, thompsond@orting.wednet.edu; Jill Whitman, Department of Geosciences, Pacific Lutheran University, Tacoma, WA, 98447, whitmaj@plu.edu.

Teachers on the Leading Edge (TOTLE) is an Earth science teacher professional development program featuring EarthScope science and Pacific Northwest geologic hazards. During summers of 2008 to 2010, TOTLE offered a six-day workshop for 35 Pacific Northwest K-12 teachers and 5 community college area team leaders each year. Workshop participants learned how geoscientists developed our current understanding of Pacific Northwest earthquakes, tsunamis, volcanoes and associated hazards and how EarthScope research is advancing frontiers of geoscience knowledge. This cutting-edge science content learning was blended with pedagogical sessions led by award-winning K-12 Master Teachers of Earth science. Workshop participants' confidence on content topics increased on a 4-point scale (1 = "not at all confident"; 4 = "very confident") from 2.7 to 3.2 to 3.7 on pre, immediately-post, and 8-month follow up surveys, respectively. TOTLE lesson plans feature analyses of EarthScope observations that apply directly to regional plate tectonics and geologic hazards and align well with national and state science education standards. Many lesson plans are regional adaptations of teaching resources developed by IRIS and UNAVCO. A key feature was developing lesson plans that progress from a basic one-class-period lesson (e.g. "Gum Drop GPS") to an intermediate-level enhancement (e.g. "Cascadia Locked and Loading") to a more advanced enhancement (e.g. "Episodic Tremor and Slip"). To facilitate transfer of TOTLE–EarthScope workshop learning to classroom teaching, participants received an extensive collection of maps, posters, and experimental apparatus along with a digital-resource DVD of lesson plans, animations, video lectures, and PowerPoint presentations. Greater than 75% of participating teachers implemented at least six of the curricular elements in the school year following their TOTLE–EarthScope workshop.

Title:
Mechanical Behavior of the Active San Andreas Fault: Insights from laboratory experiments on intact core

Authors:
Brett M. Carpenter, Chris Marone, and Demian M. Saffer
bmc245@psu.edu

Affiliation:
Department of Geosciences and Energy Institute Center for Geomechanics, Geofluids, and Geohazards, The Pennsylvania State University, University Park, Pennsylvania, USA

One primary motivation for recent major ICDP and IODP initiatives to drill into active plate boundary fault systems, including the San Andreas Fault Observatory at Depth (SAFOD) and the Nankai Trough Seismogenic Zone Experiment (NanTroSEIZE), has been to evaluate hypotheses for the apparent low strength of tectonic faults. Here, we report on laboratory experiments aimed at understanding controls on both (1) absolute fault strength, and (2) the nature of fault slip. We focus on results of experiments on core material recovered during SAFOD Phase III drilling. All samples in this study are adjacent to and within the Central Deforming Zone (CDZ) penetrated at 3302m MD in the SAFOD borehole. We sheared intact wafers of wall rock and fault gouge in a single-direct shear configuration, subject to true-triaxial loading, under constant effective normal stress, confining pressure, and pore pressure. We also sheared gouge derived from intact core in a double-direct shear configuration under similar conditions of effective stress, confining pressure, and pore pressure. Our experimental program included measurements of frictional strength, frictional velocity dependence, and time-dependent healing.

Our results show that: 1) material from the actively slipping San Andreas fault zone is frictionally weak (friction coefficient, $\mu=\sim0.1$) compared to the surrounding wall rock ($\mu > 0.40$); 2) the fault zone material exhibits velocity-strengthening frictional behavior, ($a\text{-}b > 0$), consistent with aseismic slip; 3) the actively creeping fault zone exhibits near-zero healing rates; and 4) damage zone and wall rock east of the active fault exhibit velocity-weakening behavior and high rates of frictional healing, both of which are consistent with the observed location of repeating small earthquakes. Additional analysis shows that intact wafers from the active fault are characterized by pressure-independent strength above ~50 MPa effective normal stress, suggesting that fault frictional strength may remain constant and low to depths of at least 5 km. XRD analysis documents large amounts (possibly greater than 60% by weight) of smectitic minerals (saponite) within the actively slipping fault strand, directly linking observations of mechanical behavior to mineralogy.

Potential contribution of seafloor geodesy offshore Cascadia to science goals of the PBO

Dave Chadwell, Scripps Institution of Oceanography

Space geodetic observations of crustal deformation using GPS and Interferometric Synthetic Aperture Radar (InSAR) have contributed greatly to understanding plate subduction. Measurements of interseismic strain have documented the active accumulation of strain. Denser arrays have begun to show the varying character of slip along the interface ranging from regions of full slip to regions of no slip. Continuous GPS measurements discovered and have documented a variety of slow slip phenomena. Measurements following earthquakes have constrained the area and amount of co-seismic slip, with longer time series capturing afterslip and viscoelastic response.

However, techniques based solely on electromagnetic energy (GPS, InSAR, etc.) stop at the water's edge while elastic strain build up and release, afterslip and viscoelastic response, and the thrust fault itself continues offfshore. GPS positioning of a surface vessel combined with underwater acoustic ranging to seafloor transponders can measure deformation of the offshore portion of a subduction zone. The GPS-Acoustic approach combines kinematic GPS on a floating platform (ship or buoy) and acoustic signals from the platform to an array of permanent seafloor transponders. The GPS-A method has permitted the accurate determination of plate velocities at a dozen or so locations on the seafloor. Offshore Peru, the displacement of two seafloor arrays on the submerged continental slope was measured, and found the slope moving towards the interior of South America. The observed rate is consistent with no significant slip on the subduction interface between the Nazca and South American plates. A series of GPS-A measurements offshore Japan, observed interseismic strain followed by co-seismic release after a subduction earthquake, then the re-establishment of interseismic strain accumulation. This site is within rupture area of the recent Tohoku Earthquake.

Offshore measurements are a natural complement to dense onshore geodetic measurements. Here we discuss the present state of technology, work in progress and a notional design for an array of seafloor sites along the submerged slope of the North American plate.

Postseismic Deformation of the Large 1959 Hebgen Lake, MT, and 1983 Borah Peak, ID, Earthquakes, With Implications for Lithospheric Rheology

Wu-Lung Chang[1] and Robert B. Smith[2]

[1]Department of Earth Sciences, National Central University, Jhongli, Taiwan (wuchang@ncu.edu.tw)

[2]Department of Geology and Geophysics, University of Utah, Salt Lake City, UT 84112

Time-dependent deformation of the Hebgen Lake, MT, normal fault zone was measured by campaign mode GPS and trilateration from 1973 to 2000 following the 18 August 1959 M_s=7.5 Hebgen Lake earthquake that occurred at the northwest edge of the Yellowstone volcanic field in an extensional tectono-volcanic regime. Since 2005, the EarthScope-PBO project has deployed an array of 10 continuously operated GPS stations across the Hebgen Lake fault and aftershock zone to assess intraplate post-seismic deformation and to model lithospheric rheology. Integrated analysis of these data shows time-dependent extension of baseline-length across the area with rates of 2 to 4 mm/yr. Rheological models derived by these data suggest that the lithosphere is stronger near the fault zone, and weaker in the vicinity of the Yellowstone caldera with much higher heat flow and a thinner brittle crust. Our models also imply a more viscous lower crust than the upper mantle, in agreement with a corollary that the continental mantle has relatively small long-term stress. In addition, we evaluated continuous GPS data from 10 stations that span the Lost River fault zone, ID, to measure the postseismic deformation associated with the1983 M_s=7.3 Borah Peak, ID earthquakes. The 08-09 data reveal extensional rates of 1-2 mm/yr across the Lost River fault zone. Our preliminary results of viscoelastic modeling suggest that the combined postseismic relaxation of both of these earthquakes produced horizontal ground motions up to ~1-2 mm/yr in the Yellowstone-Snake River Plain region, affecting the total deformation field of the eastern Basin-Range. This study provides new insights into the widespread effects on regional deformation from postseismic relaxation of large earthquakes that need to be considered in kinematic models and earthquake hazards of intraplate tectonic regions.

Mapping lithospheric structure using depth phase precursors recorded by EarthScope's USArray

Chen Chen (cc669@cornell.edu), Larry Brown, Suzanne Kay
Department of Earth and Atmospheric Sciences, Cornell University, Ithaca NY 14853
U.S.A.

Abstract:

Precursors to teleseismic depth phases such as pP or sS have been used to detect MOHO and possible intracrustal boundaries (Schenk et al., 1989; Zandt et al., 1994; McGlashan et al., 2008a), the LAB lithosphere-asthenosphere boundary (McGlashan et al., 2008b) and various within mantle boundaries at 80 km, 210 km, 330 km, 440 km and 660 km (Zhang and Thorne, 1993; Flanagan and Shearer, 1998; Shearer and Flanagan, 1998; McGlashan et al. 2008b). However, new large scale, high density seismic arrays such as EarthScope's provide much more powerful means of detailing such features with these phases. EarthScope's USArray has a station spacing about 70 km and covers a large area of the continental US. From the EarthScope open dataset we have extracted recordings of intermediate to deep (150 km to 700 km) earthquakes from subduction zones around the Pacific Rim. With proper phase alignment, filtering and coherency enhancement, we use the precursors to pP from slab earthquakes beneath South America to image the underside reflections from Moho (pmP), from the LAB (plP) and from possible 410 (p410P) discontinuities. The redundancy provided by the EarthScope's USArray allows us to enhance signal-to-noise ratios by stacking within common reflection point bins and application of multichannel coherency filters. In the Andean case, we gathered the underside reflection points in 4 km * 40 km bins for stacking, resulting in substantial improvement in the resulting image. Synthetic seismograms confirm that the observed arrivals are appropriate for reflections from the Moho and LAB. The observation of specular reflections from the underside of the LAB is particularly significant, as this boundary has been proven difficult to image by traditional seismic techniques. Comparable results have been obtained from deep earthquakes beneath western Pacific island arcs for the adjacent oceanic lithosphere and interpretation of these reflections needs to be further considered. We suggest that this technique applied to recordings from new seismic arrays like EarthScope's USArray can make significant new contributions to our understanding of lithospheric structure around subduction zone.

Crustal and upper mantle structure beneath the High Lava Plains from scattered-wavefield migration and receiver functions

Chin-Wu Chen and David E. James

Department of Terrestrial Magnetism
Carnegie Institution of Washington
5241 Broad Branch Rd. NW
Washington, DC 20015
{cwchen; james}@dtm.ciw.edu

The High Lava Plains (HLP) in eastern Oregon represents one of the most active intraplate magmatic provinces on Earth. This region's recent tectonic history is dominated by voluminous mid-Miocene outpourings of the Steens and Columbia River flood basalts, followed by a period of bimodal volcanic activities, generating two roughly orthogonal time-progressive rhyolitic hotspot tracks: the northeastern-trending Snake River Plain and the northwestern-trending High Lava Plains. The causes of this complex tectonomagmatic evolution are not well understood, and geophysical constraints have been lacking regarding the detailed crustal and upper mantle structure in this region. From 2006 to 2009, a passive seismic experiment with the deployment of 118 broadband seismic stations was carried out as part of the multidisciplinary High Lava Plains project, which aims to investigate the causes of continental intraplate tectonomagmatism. These stations covered central and eastern Oregon, northern Nevada, and southwestern Idaho, with average spacing of 15-20 km, yielding unprecedented data density in the HLP region. A number of tomographic and receiver function (RF) studies has revealed complex structures beneath HLP. These include irregular Moho topography across the HLP, and concentrated low velocity anomalies in the uppermost mantle beneath regions of Holocene volcanism in southeastern Oregon (including areas of the Owyhee Plateau), as well as beneath volcanic centers near Steens Mountain and Newberry volcano. We complement these previous studies by generating high-resolution seismic images from scattered wavefield to detect seismic discontinuities beneath the HLP. We process 80 high-quality teleseismic events with good azimuthal coverage using a 2-D teleseismic migration algorithm based on the Generalized Radon Transform. The resulting migration images indicate the presence of two main features: 1) a prominent and varying Moho topography: the Moho is at ~40 km depth east of the Cascadian arc, thinning to ~35 km depth beneath the HLP hotspot track, and dips southeasterly to ~45 km depth toward the Owyhee Plateau, and 2) a pronounced subhorizontal low-velocity layer underlying the thickened crust beneath the Owyhee Plateau. The varying Moho topography observed in our migration images corroborates results from previous RF analysis. However, the previous RF study did not resolve the low-velocity layer beneath the Owyhee Plateau. We perform additional RF analysis on individual stations in this region to verify the presence of the low-velocity layer, which may correspond to partial melt ponding at the base of the thickened crust in the eastern end of the HLP.

Initiation of the great Mw=9.0 Tohoku-Oki earthquake and location of aftershocks

Risheng Chu, Don Helmberger, and Zhongwen Zhan

Seismological Laboratory, California Institute of Technology, Pasadena CA 91125, USA

Large subduction zone earthquakes generally lack location precision in the off-shore direction mainly due to lack of regional stations. Other measurements are needed to refine the epicenters. Fortunately, stacking of the USArray data from a 2008 small earthquake yields a clear water phase (pwP) reflected from the air-water interface after the depth phase (pP) reflected from the water-crust interface. Here we use the differential timing between water phase and the depth phase to help locate smaller events in the area which have well-resolved global source inversions. After calibrating the global arrays at short periods for timing and amplitude of the master earthquake, we are able to examine the initiation process of the main event, which began with an Mw = 4.9 thrust event at 38.19N, 142.68E with a depth of 21 km. The same calibrations are applied to 80 aftershocks of the Mw=9.0 Tohoku-Oki earthquake. These focal mechanisms and locations will be presented in this poster.

Diverse slip propagation speeds and directions in simulations of slow slip events

Harmony V. Colella[1] (hcole001@ucr.edu), James H. Dieterich[1], and Keith Richards-Dinger[1]

[1]University of California – Riverside, Department of Earth Sciences, Riverside, CA 92521

We model slow slip events (SSEs) using the 3D simulation code, RSQSim, which employs rate- and state-dependent constitutive properties to set different modes of fault slip. For computational efficiency we impose the slip speed for SSEs, otherwise the simulations are fully deterministic in the nucleation, propagation speed, extent of slip, and final distribution of slip. Results from simulations are broadly consistent with a variety of SSE observations. Simulated SSEs initiate slowly over 1-5 days, followed by unilateral and/or bilateral growth of the slip region. Simultaneous slip often originates at multiple locations. Separate slip regions often merge to form a single SSE. Additionally the simulations show diverse rupture propagation speeds associated with renewed slip during a SSE. Propagation speeds for initiation of slip range from 7-21 km/day. Simulations also show renewed slip that propagates parallel to, but in the opposite direction (back propagation), and perpendicular (along-dip propagation) to the rupture front at higher speeds. If one assumes tremor is a proxy for slip, these may be analogous to rapid tremor reversal (RTRs) and along-dip streaks identified along the Cascadia and Nankai Subduction Zones. This rapid propagation for renewed slip may be related to incomplete fault healing that allows for re-initiation of slip at low stresses behind the slip pulse.

Title: Integrated 2-D Models of Crustal Structure in the High Lava Plains Region of Eastern Oregon

Cox, Catherine M

cmcox@ou.edu

Geology and Geophysics, University of Oklahoma, Norman, OK, USA

Keller, G. Randy

grkeller@ou.edu

Geology and Geophysics, University of Oklahoma, Norman, OK, USA

Harder, Steven H.

harder@geo.utep.edu

Geological Sciences, University of Texas, El Paso, El Paso, TX, USA

This study uses data from the High Lava Plains (HLP) controlled-source experiment collected in September of 2008. A total of 2612 Texan short-period seismic recorders and 120 RT-130 recorders were spaced across the HLP of eastern Oregon and adjacent parts of Nevada and Idaho to record 15 seismic sources thanks to the help of the 67 scientists, students, and 6 staff members from the PASSCAL/Earthscope Instrument Center who deployed. Seismic and gravity data were integrated to create 2-D crustal scale P-wave velocity and density models for the long NW-SE and N-S profiles that were a major effort in the HLP project. These models provide a better understanding of the crustal structure and upper mantle beneath the path of migratory, bi-modal volcanism that dotted the High Lava Plains during the past 16 Ma, in addition to the extension experienced in the region since 35 Ma. Our results show that the crustal structure across the HLP region is similar to that of the

northern Basin and Range. However, a thick cover (5–7 km) of sediments and volcanics covers most of the area and are thicker in the Harney Basin area. We interpret denser/faster material in the lower to middle crust under the southern Harney Basin area to be mafic intraplating. We have also identified a region of denser/faster material in the upper crust in the vicinity of Jordan Valley. The crust thickens (34km –37km), and the lower increases in density (2.8–2.85 gm/cc) from west to east across eastern Oregon in close proximity to the interpreted position of the 0.706 Sr isotope line. There is layer of relatively high velocity (7.2–7.4 km/s) and density of (2.95 gm/cc) layer in the lowermost crust of the southeastern HLP region that suggests underplating. The HLP region has undergone moderate extension, and the average crustal velocity is somewhat higher that in the adjacent Basin and Range suggesting some magmatic modification in the lower crust, but not as much as might be expected given the voluminous surface volcanism.

Slow-Slip Initiation and Stress Transfer Inferred from Cascadia Tremor Swarms

Kenneth C. Creager, Aaron G. Wech, and Amanda Klaus

University of Washington - Earth and Space Sciences

We have applied an automatic waveform envelope cross-correlation and clustering (WECC) algorithm to seven Cascadia-wide subarrays to search for non-volcanic tremor in 50%-overlapping, 5-minute windows, revealing about 100,000 tremor epicenters. The tremor epicenters cluster in time and space into 450 tremor swarms with durations ranging from 1 to 450 hours. The smaller tremor swarms generally locate along the downdip side of the larger Episodic Tremor and Slip (ETS) swarms and occur much more frequently. In northern Washington, which is currently best monitored, the ETS events, as well as the larger inter-ETS tremor swarms initiate downdip and propagate updip over a period of several days. During this time the amplitudes appear to increase linearly with time, perhaps due to a linear rate of increase of slipping area owing to a diffusional process causing radius to grow as square root of time. For the large ETS events, tremor swarm duration is proportional to geodetically determined seismic moment. We consider tremor swarms to be a proxy for slow slip for the smaller events as well, even though slip would be below current geodetic detection thresholds. We interpret the observed transition from longer-duration, less-frequent tremor swarms up dip to smaller more frequent tremor swarms down dip, in terms of fault strength decreasing with depth and with slip initiated by an updip stress transfer process originating from the stable sliding region at greater depth.

EarthScope resources and the multi-disciplinary search for seismogenic faults

Vincent S. Cronin, Geology Department, Baylor University, Waco, TX 76798-7354,

Vince_Cronin@baylor.edu

Several damaging earthquakes have occurred in recent decades along existing faults that had not previously been mapped, or along known faults that were not recognized as seismogenic. Three resource sets associated with EarthScope (and their respective data managment infrastructures) are particularly useful in recognizing seismogenic faults, making them excellent candidates for continued support and development beyond the current EarthScope Project: dense seismograph networks, PBO-style geodetic GPS networks, and airborne LiDAR surveys of structurally active areas. Geodetic GPS allows determination of the present-day crustal strain of an area, which is likely to be manifested by seismogenic faulting. With dense seismograph networks come better single-event focal locations, better data for joint-relocation studies, the possibility of developing 3-D crustal velocity models that will yield optimal single-event locations, and a more abundant supply of well-constrained focal mechanism solutions. Given more accurate focal locations and focal mechanism solutions, the approximate locations of seismogenic faults can be discerned by 3-D mapping of foci combined with analysis of seismo-lineaments on the ground surface (Cronin *et al.*, 2008, *Env. & Eng. Geosci.*, v. 14, p. 199-219). Seismo-lineaments can be used to define areas for airborne laser swath mapping, particularly in areas where fault mapping is incomplete or non-existent and where vegetation obscures the ground surface. Aerial LiDAR has proven effective in detecting geomorphic indicators of faulting. LiDAR-based geomorphic analysis combined with seismo-lineament analysis and traditional paleoseismology allows the surface location and offset history of seismogenic faults to be documented. That documentation provides critical information for seismic hazard source models used by earthquake engineers in probabilistic seismic hazard assessments, (hopefully) leading to a reduction in earthquake losses through well designed and administered building codes. Beyond the academic search for understanding about our planet, EarthScope resources will help us recognize seismic hazards and manage seismic risk.

INVESTIGATING 3D STRAIN PATTERNS DUE TO THERMAL INTRUSIONS: DEATH VALLEY FAULT ZONE, DEATH VALLEY, CA.

Cecilia Del Pardo[1], Benjamin P. Hooks[2], Bridget R. Smith-Konter[1], Laura F. Serpa[1] and Terry L. Pavlis[1]

[1]Department of Geological Sciences, University of Texas at El Paso, El Paso, TX 79968
[2]Department of Agriculture, Geosciences, & Natural Resources, University of Tennessee at Martin, Martin, TN 38238

Shallow (~ 10 km deep), high temperature (> 800 °C) intrusions have been suggested to play an important role in the development of surface deformation patterns associated with the Death Valley Fault Zone (DVFZ). The DVFZ, located in southeastern California, consists primarily of two dextral strike-slip faults whose motion produces a pull-apart basin that has been extending since its formation approximately 6 Ma. This study develops three-dimensional thermo-mechanical numerical models to analyze the strain evolution of the DVFZ driven by thermal perturbations resulting from a plausible intrusion beneath the Death Valley pull-apart basin. The model is created using the Fast Lagrangian Analysis of Continua in 3 Dimensions (FLAC3D) and consists of a 350 x 500 x 35 km rectangular grid representing the crust within the DVFZ area. A pressure-dependent, non-associative, Mohr-Coulomb plasticity and a temperature-dependent viscous model are used to define the mechanical behavior of the upper and lower crust, respectively. A basal drag velocity is applied in the fault-parallel direction, with a gradient along the same axis, which produces a surface velocity field approximating EarthScope PBO geodetic velocities spanning the region. An intrusion (represented by a 20 x 50 x 4 km rectangular-shaped box) is placed at a depth of 10 km. To evaluate the response of the model to several parameter variations (friction angle, conductivity, viscosity and intrusion temperature and location) a sensitivity test was first conducted. These results show that the strain rate appears to be largely insensitive to changes in friction angle, conductivity, and viscosity. The initial intrusion temperature also appears to have little impact on the strain distribution, however the spatial distribution and magnitude of the strain field is highly sensitive to intrusion location. Strain evolution was simulated for three different hypothetical locations (east, center and west of the current pull-apart basin) within the area of extension. We utilize visualization software (ParaView) to further explore the stress distribution with depth in a 3D volume. These results show that the central and southern regions of the fault zone are most sensitive to intrusion location and that the largest strain rate variations (~ 30 – 40 nStrain/yr) are produced if the intrusion is placed in the center or to the west of the pull-apart basin. Additional extensional stresses produced by the models in this analysis imply that other faults in the vicinity of the DVFZ (i.e. Garlock fault) might have significantly influenced the formation of the present day structures in the area.

GPS Time Series Analysis of Southern California Associated with the 2010 M7.2 El Mayor/Cucapah Earthquake

Robert Granat
Jet Propulsion Laboratory, California Institute of Technology

Andrea Donnellan
*Jet Propulsion Laboratory, California Institute of Technology and
University of Southern California*

The M 7.2 El-Mayor/Cucapah earthquake that occurred in Mexico on April 4, 2010 was well instrumented with continuous GPS stations in California. Large offsets were observed at the GPS stations as a result of deformation from the earthquake providing information about the co-seismic fault slip as well as fault slip from large aftershocks. Information can also be obtained from the position time series at each station. Hidden Markov models (HMMs) allow us to segment GPS time series into discrete modes in order to extract information. This can be done in the absence of labeled training data or other human supervision, and is entirely a data-driven approach. In general, fitting a hidden Markov model in the absence of a priori information using the standard expectation-maximization (EM) method is a difficult problem, due to the presence of numerous local maxima in the objective function. We address this problem through the use of the regularized deterministic annealing EM (RDAEM) algorithm, which produces stable, high-quality model fits. The QuakeSim project has implemented this algorithm in the RDAHMM software package. RDAHMM results are available through the QuakeSim web portal, which allows both micro-scale (individual station) and macro-scale (whole network) exploration of data sets and analysis results via Google Maps. Users can focus in on or scroll through particular spatial or temporal time windows, or observe dynamic behavior by created movies that display the system state. Analysis results can be exported to KML format for easy combination with other sources of data, such as fault databases and InSAR interferograms. Analysis of time series data around the 2010 El-Mayor/Cucapah earthquake shows that GPS stations change state near the rupture as expected. GPS stations also change state farther from the rupture, but near other faults, such as the San Andreas and San Jacinto faults. The GPS stations that change state associated with the earthquake tend to be in close proximity to faults that exhibited creep events associated with the earthquake in Baja.

Transportable Array Outreach Activities: Engaging Students and the Public

Perle Dorr, Robert Busby, Katrin Hafner, John Taber, and Robert Woodward

IRIS Consortium • 1200 New York Avenue, NW • Suite 800 • Washington, DC 20005
202-682-2220 • dorr@iris.edu

One of the goals of EarthScope is to actively engage students who will become the next generation of Earth scientists. The Transportable Array contributes to this goal by offering university students an opportunity to perform site reconnaissance for future seismic stations. In addition, other outreach activities are conducted to increase awareness and understanding of seismology concepts and scientific discoveries enabled by the EarthScope facilities, including several in collaboration with the EarthScope National Office and the Plate Boundary Observatory.

The Student Siting Program is a 10-week effort that begins with a multi-day workshop to introduce selected students and their faculty sponsors to seismic station requirements and a variety of mapping tools. The workshop includes presentations on topics such as siting criteria and communications options, and includes a day in the field to enable the students to evaluate actual sites and to gain experience using GPS units, modems, and other field equipment and techniques. Students work in pairs for the remaining 9 weeks under the supervision of a local advisor. Surveys at the end of the summer show that the students are enthusiastic about their active involvement in a major research project. From 2005 through 2010, more than 100 students from 31 universities have conducted site reconnaissance for about 1000 sites across the US. Beginning in May 2011, 18 students from nine institutions will identify a total of 205 sites in Lower Michigan, Indiana, Ohio, central and eastern Kentucky, central and eastern Tennessee, Georgia, Florida, and parts of Ontario and Quebec, Canada.

The Transportable Array also keeps current and former station hosts engaged in the program by producing and distributing *onSite* two times per year. This publication includes articles on exciting USArray science discoveries, the status of the Transportable Array and information about basic seismology concepts. Using data recorded by Transportable Array stations, hundreds of earthquake visualizations are routinely generated and posted on the web, illustrating the arrival of seismic waves across the array. Other outreach activities include the development of USArray and EarthScope pages for the Active Earth Display, teacher workshops, classroom seismographs and a DVD of earthquake-related educational materials.

Telling the EarthScope Story: Engaging Colleges, Universities and the Public in USArray

Perle Dorr, Robert Busby, Katrin Hafner, John Taber, and Robert Woodward

IRIS Consortium • 1200 New York Avenue, NW • Suite 800 • Washington, DC 20005
202-682-2220 • dorr@iris.edu

Since its inception as a pilot program in 2005, the highly successful Transportable Array Student Siting Program has involved students and faculty from colleges and universities in the identification of sites for future Transportable Array stations in their region. To date, more than 100 students from 31 institutions have conducted site reconnaissance for about 1000 sites in 26 states from the West Coast to the Great Lakes and the Gulf of Mexico. Participation in the program has provided students the chance to grow both personally and professionally. Other outcomes involve exciting informal education and media opportunities where information about EarthScope and its discoveries are shared with educators and the public. Examples include Ground Motion Visualizations and content sets for the Active Earth Display to articles in university, local and regional newspapers and stories appearing in national and international print and broadcast media.
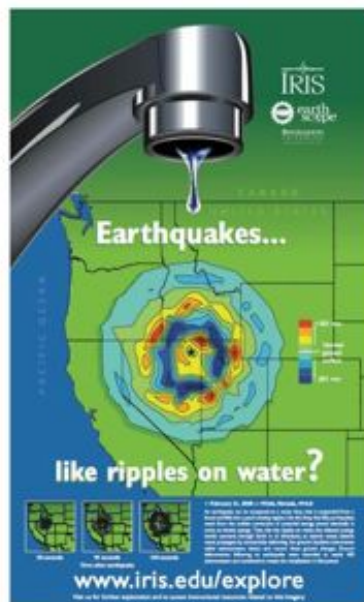
Seismic imaging beneath the Colorado Rockies from the CREST project

Ken Dueker[#], Rick Aster[*], Steve Hansen[#], Zhu Zhang[#], Josh Stachnik[#], Jon McCarthy[*], Brandon Schmandt[‡], Karl Karlstrom[Δ] and the CREST group: [#]Univ. of Wyoming, [*]New Mexico Tech, [‡]Univ. of Oregon, [Δ]Univ. New Mexico

The passive seismic component of the CREST project sampled the Colorado Rocky Mountain region to constrain how the existing crust and mantle structure is supporting the 1400 m of excess topography with respect to the adjacent Colorado Plateau and High Plains regions. Sixty IRIS PASSCAL seismic stations were operated for 15 months that, when combined with the EarthScope Transportable Array stations, resulted in a 94-station array with a mean station spacing of 25-40 km. This seismic component is complemented by geomorphic and thermochronologic studies that provide new constraint on the exhumation and uplift history of the Colorado Rockies. This poster presents results from P- and S-wave receiver function images and ambient/earthquake Rayleigh wave imaging by the University of Wyoming; the body wave P- and S-wave tomograms, gravity modeling and shear-wave splitting results are presented in a separate poster. The P-wave receiver function image is migrated using our Rayleigh wave shear velocity image and a mean Vp/Vs ratio of 1.76. This P-wave receiver function image resolves the Moho beneath the Colorado Rockies at a mean depth of 43 km. This mean depth is similar to the Moho depth beneath the surrounding Colorado Plateau and High Plains provinces. Thus, compensation of the high standing topography of the Colorado Rockies is not due to crustal Airy compensation. The Rayleigh wave image finds that the mean crustal velocity beneath the Colorado Rockies is reduced by 0.2 km/s with respect to the surroundings. This low velocity crust is consistent with the high heat flow and extensive granitic batholiths. Ignoring the flexural filter of a 25-35 km elastic thickness plate (Lowry, pers. com.), at best this low density crust could provide a 600 m isostatic effect. Hence, buoyancy from the mantle is required to support an additional 800 m of Colorado Rockies topography. Integrated interpretation of the buoyancy effects from the Rayleigh wave and body wave images is difficult because the images find a complex mantle lithosphere, upper mantle, and transition zone. The Rayleigh wave image finds a mean 4.2 km/s low velocity channel beneath the southern Colorado Rockies (south of Leadville) with a maximum negative velocity gradient at about 95 km depth, but beneath the northern Colorado Rockies a low velocity channel is not present. Further constraint on lithospheric thickness is provided by a S-wave receiver function image. The body wave tomograms find a complex pattern of low velocity anomalies generally beneath the high standing topography. In 2-3 areas, about 100 km diameter low velocity blobs extend down to 300-400 km depth. Interestingly, our P-wave receiver function image of the 410 km discontinuity finds a low velocity layer atop the 410 km discontinuity (410-lvl) within about 30% of the sampled area. This 410 low velocity layer is interpreted to manifest a partially molten layer (Bercovici and Karato, 2003) and we speculate that the 410-lvl has become unstable in the last 20 Ma to shed blobs of buoyancy upwards beneath the Colorado Rockies. An upwelling 410-lvl diapir would be promoted by both a high 410-lvl melt water content and upflow across the 410 km discontinuity. Local convective upflow could be associated with the edges of high velocity features (slabs) imaged in the lower transition zone about the Colorado Rockies (Schmandt and Humphreys, 2010): i.e., the convection modeling of Faccenna et al. (2010) find concentrated upflow at the edges of slabs. Given the temporal constraints on the uplift history of the Colorado Rockies by the CREST geologic research that find a 10-8 Ma uplift signal, mantle buoyancy must be emplaced beneath the Colorado Rockies by some process: be it via 410-lvl diapirs and/or thermal plumes.

GPS Monitoring of the San Bernardino Mountains and Inland Empire for Slip Rate Modeling of Southern California Plate Boundary Faults

By: B. J. Anderson 1, J. C. Duncan 2, J. N. Bywater 3, K. K. Chung 4, M. R. Swift 5, S. F. McGill 5, J. C. Spinler 6, A. Hulett 5, R. A. Bennett 6

1: Pasadena City College 2: Baylor University 3: California State University Sonoma 4: Wellesley College 5: California State University San Bernardino 6: University of Arizona

Although there has been no major earthquake on the southern San Andreas fault (SAF) in more than two centuries, the surrounding crust still moves. This crustal deformation causes strain accumulation on the SAF as well as the San Jacinto fault (SJF) and many others in the area. To get a better picture of how much strain is currently building on these faults, we used precise Global Positioning System (GPS) surveying to measure site velocities within the San Bernardino Mountains and surrounding areas, and we modeled these data along with site velocities from SCEC's Crustal Motion Model 4 (CMM4) to characterize crustal deformation within a transect across the plate boundary using two-dimensional elastic half-space models in MS Excel. We tested hundreds of thousands of slip rate combinations to find which combinations provide a good fit to the site velocities. From the combinations that produce the best-fitting lines, our results showed that the faults west of the SJF system could have total slip values of 4.5 to 13.5 mm/yr with the individual faults at: San Clemente: 0-1mm/yr, San Diego Trough: 0-1mm/yr, Palos Verdes: 0-5mm/yr, Newport-Inglewood: 0-3mm/yr, and Elsinore: 0-8mm/yr. The SJF-SAF system could have total slip of 15 to 26 mm/yr with the two faults at: SJF: 2-24mm/yr, SAF: 0-20mm/yr. The Eastern California Shear Zone had totals from 13 to 17 mm/yr with the individual faults at: Helendale: 0mm/yr, Lenwood: 1.5-2mm/yr, Emerson: 6.7-8.7mm/yr, West Calico: 0mm/yr, Pisgah: 2.2-2.9mm/yr, Ludlow: 1.5-2mm/yr, Red Pass Lake: 0.7-1mm/yr, and Baker: 0.4-0.5mm/yr.

Operations at the EarthScope USArray Array Network Facility (ANF)

Eakins, J.A (*jeakins@ucsd.edu*), Vernon, F.L., Astiz, L, Newman, R.L., Davis, G.A., Reyes, J., Martynov, V., Tytell, J., Cox, T.A., Karasu, G.
IGPP, Univ. of California San Diego, MC-0225, 9500 Gilman Dr., La Jolla, CA 92093-0225

The Array Network Facility (ANF) has been responsible for the metadata, collection of, and initial quality control and the transmission of the seismic data for the Earthscope USArray Transportable Array. Starting in February 2011, additional infrasound (NCPA) and pressure (Setra) sensors are being deployed at all newly installed TA stations. Procedures have been implemented for review of this data and these new data channels are available at the DMC. In addition, the ANF is reconfiguring procedures for initiating and confirming the results of individual station calibrations. In the past year we have implemented new methods to retrieve archived data from the balers to maximize data completeness within three months of real-time. The web-based ANF tools continue to evolve with an emphasis placed on station engineer needs and improving the speed and efficiency of the current tools and interfaces. Significant infrastructure updates have occurred increasing our storage capacity and reliability. A major undertaking was the complete physical move of all servers from the buildings at IGPP to more secure and climate controlled operations at the San Diego Super Computer Center. Analysts continue to review all seismic events recorded on 10 or more TA stations making associations against externally available bulletins and/or generating ANF authored locations.

Title: Integrated 2-D Models of Crustal Structure in the High Lava Plains Region of Eastern Oregon

Cox, Catherine M

cmcox@ou.edu

Geology and Geophysics, University of Oklahoma, Norman, OK, USA

Keller, G. Randy

grkeller@ou.edu

Geology and Geophysics, University of Oklahoma, Norman, OK, USA

 Harder, Steven H.

harder@geo.utep.edu

Geological Sciences, University of Texas, El Paso, El Paso, TX, USA

This study uses data from the High Lava Plains (HLP) controlled-source experiment collected in September of 2008. A total of 2612 Texan short-period seismic recorders and 120 RT-130 recorders were spaced across the HLP of eastern Oregon and adjacent parts of Nevada and Idaho to record 15 seismic sources thanks to the help of the 67 scientists, students, and 6 staff members from the PASSCAL/Earthscope Instrument Center who deployed. Seismic and gravity data were integrated to create 2-D crustal scale P-wave velocity and density models for the long NW-SE and N-S profiles that were a major effort in the HLP project. These models provide a better understanding of the crustal structure and upper mantle beneath the path of migratory, bi-modal volcanism that dotted the High Lava Plains during the past 16 Ma, in addition to the extension experienced in the region since 35 Ma. Our results show that the crustal structure across the HLP region is similar to that of the

northern Basin and Range. However, a thick cover (5–7 km) of sediments and volcanics covers most of the area and are thicker in the Harney Basin area. We interpret denser/faster material in the lower to middle crust under the southern Harney Basin area to be mafic intraplating. We have also identified a region of denser/faster material in the upper crust in the vicinity of Jordan Valley. The crust thickens (34km –37km), and the lower increases in density (2.8–2.85 gm/cc) from west to east across eastern Oregon in close proximity to the interpreted position of the 0.706 Sr isotope line. There is layer of relatively high velocity (7.2–7.4 km/s) and density of (2.95 gm/cc) layer in the lowermost crust of the southeastern HLP region that suggests underplating. The HLP region has undergone moderate extension, and the average crustal velocity is somewhat higher that in the adjacent Basin and Range suggesting some magmatic modification in the lower crust, but not as much as might be expected given the voluminous surface volcanism.

Teleseismic full Green's Function finite fault inversion and its application to the 2011 Tohoku Oki Earthquake

Shengji Wei[1], Risheng Chu[1] , Zhongwen Zhan[1] and Don Helmberger[1]

1. Seismolab Caltech
   shjwei@caltech.edu

Simplified teleseismic green's functions are used in traditional finite fault inversion methods, which assumed a simple geometric spreading to approximate seismic wave propagation in the mantle. However, for earthquakes with source time function longer than 100s, the following phases, rather than direct P and S arrivals such as PP and ScS, will arrive within the duration at many distance ranges. These phases, if not included in the green's functions, will be attributed to the source process during the inversion causing extended slip-distribution at least in testing theoretical data sets. To better handle the following phases, we use frequency-wave number (FK) synthetics, which have all possible theoretical arrivals, instead of the simplified green's functions. It turns out that the slip model becomes more compact and clean with full green's functions. The high quality USArray dataset is then used to verify our slip models at different frequency bands. Some clean paths are identified which are useful for refinement of the source process especially the high frequency features associated with changes in rupture velocity and large slip offsets. We also separate the FK green's functions into up-going and down-going portions, which allow us to better understand the different behavior between direct phases and depth phases and assess the impact of shallow crustal geology and differential amplitude and timing corrections.

Uppermost mantle velocity structure obtained from USArray regional phase data

J.S. Buehler and P.M. Shearer
Institute of Geophysics and Planetary Physics, U.C. San Diego, La Jolla

USArray has now provided several years of high-quality seismic data and improved ray coverage for much of the western United States. This allows for regional studies of the lithosphere and deeper structure of the North American continent with increased resolution. In this study, we use Pn and Sn phases in the USArray data set to solve for velocity structure in the uppermost mantle in the western United States. Travel-time tomography using the Pn picks provided by the Array Network Facility seismic analysts reveals prominent features of crustal thickness, velocity perturbations and anisotropy, as for example the low velocities in the Snake River Plain near the Yellowstone hotspot track and mostly fault-parallel fast axes in central California.

Extending the study, we apply waveform cross-correlation to obtain inter-station travel times between the closely and uniformly spaced USArray stations. This allows us to use traces without phase picks and reduces errors associated with the picking. Starting with Pn, we obtain differential times that can directly be used to fit locally for slowness and, depending on the approach, for the direction and curvature of the incoming wavefront. We test the method on a small number of earthquakes to obtain optimal cross-correlation and filtering parameters. Next we select a larger set of events considering epicenter location and magnitude and automate the process. The various measurements of incoming wavefronts at different sub-arrays provide constraints on azimuthal variation in velocity.

The traditional tomography approach and the local fitting method reveal similar large scale features. No regularization is applied with the local method, and the resulting velocity maps seem to show structure with better resolution. Applying similar methods to Sn is more challenging, but in principle should resolve the nature of upper mantle anisotropy better than Pn analysis alone. If we succeed in separately resolving Sn-SH and Sn-SV, we will obtain radial and azimuthal anisotropy parameters in the uppermost mantle, which can then be compared to crust and uppermost mantle models obtained using surface waves and SKS splitting.

The Mobile Margin of Far North America: GPS Constraints on Active Deformation in Alaska and the Role of the Yakutat Block

Julie Elliott, Jeffrey T. Freymueller, Christopher F. Larsen, and Roman J. Motyka
Geophysical Institute, University of Alaska Fairbanks
julie@gi.alaska.edu

GPS data from southern Alaska and the northern Canadian Cordillera have helped redefine the region's tectonic landscape. Instead of a comparatively simple interaction between the Pacific and North American plates, with relative motion accommodated on a single boundary fault, we find a margin made up of a number of small blocks and deformation zones with relative motion distributed across a variety of structures. Much of this complexity can be attributed to the Yakutat block, an allochthonous terrane that has been colliding with southern Alaska since the Miocene.

We present a GPS-derived tectonic model for the Yakutat block collision and its effects on southern Alaska and eastern Canada. The Yakutat block moves NNW at a rate of 50 mm/a, resulting in ~ 45 mm/a of NW-directed convergence with southern Alaska. Along its eastern edge, the Yakutat block is deforming, represented in our model by two small northwesterly moving blocks outboard of the Fairweather fault. Part of the strain from the collision is transferred east of the Fairweather – Queen Charlotte fault system, causing the region inboard of the Fairweather fault to undergo a distinct clockwise rotation into the northern Canadian Cordillera. Further south, the region directly east of the Queen Charlotte fault displays a much slower clockwise rotation, suggesting that it is at least partially pulled along by the northern block motion. About 5% of the relative motion is transferred even further east, causing small northeasterly motions well into the northern Cordillera.

Our GPS results indicate that the present-day deformation front between the Yakutat block and southern Alaska runs along the western side of the Malaspina Glacier. Multiple narrow crustal slivers bounded by N- to NW- dipping thrust faults that sole into a decollement are required to explain the observed deformation south of the Bagley Ice Valley. The majority of the relative convergence is accommodated over a fairly short distance across the St. Elias Mountains. The crustal slivers continue west until the vicinity of the Bering Glacier, where the GPS vectors show a northward rotation as the collision and accretion of the Yakutat block transitions to subduction along the Aleutian Megathrust.

The Plate Boundary Observatory Alaska Region – Operation and Maintenance, Lessons Learned During the First Two Years

Max Enders, Ellie Boyce, Karl Feaux, Mike Jackson - UNAVCO

UNAVCO is now in its third year of operation of the Plate Boundary Observatory network which includes 138 continuous GPS stations, 12 tiltmeters and 41 communications relays installed in Alaska. Two complete years of state of health data from our stations in the Alaska region has allowed us to better identify problem stations and common failure modes. This poster will present some the solutions we have implemented to deal with many of these issues in the previous two years, as well as highlight areas we are still improving upon.

In 2011 two areas we will focus on improving are data telemetry and power systems. This year, two new station components will be tested to address these issues and increase the reliability of our most problematic stations. The first, methanol fuel cells will supplement solar battery charging at remote stations that have high power demand and perform poorly due to insufficient solar input. Secondly, we plan to begin test deployments of Inmarsat BGAN satellite internet terminals. These will be deployed at remote stations where traditional data communications solutions are not practical, or reliable.

In addition to testing these new components and our routine maintenance activities, we plan to deploy 8 webcams at GPS stations. These will compliment the current data set available from these stations and provide near real time weather images to aid in remote helicopter operations. Data from the all PBO stations, including those located in Alaska is available from the UNAVCO archive.

The EarthScope Bighorn Project: The Power of Integrated Geoscience

Eric Erslev* and Karen Aydinian, University of Wyoming; Anne F. Sheehan, William L. Yeck, Zhaohui Yang, Colin O'Rourke, and Joshua C. Stachnik, University of Colorado; Kate C. Miller and Lindsay L. Worthington, Texas A&M University; Megan L. Anderson and Christine S. Siddoway, Colorado College; and Steve H. Harder, University of Texas at El Paso
*speaker

The collaborative Bighorn Project amply demonstrates the importance of integrating varied geoscience expertise and specialties in seeking to understand the lithospheric and plate tectonic mechanisms of basement-involved foreland arches by complementary structural and passive/active seismic experiments. Structural investigations have confirmed our selection of the Bighorn Arch of northern Wyoming as an optimum study location lacking syn/post-Laramide magmatic activity and post-Laramide faulting that might complicate our attempts to image the full crust.

Integration of basin and arch geometries from industry seismic and well data with geologic maps has defined the asymmetrical arch geometry, which verges towards the ENE. Kinematic data from fractures measured all the way around the arch have defined ENE-WSW thrust slip patterns and led to the creation of a new model for sequential foreland deformation,

These structural geometries and kinematics suggest lower-crustal detachment causing upper crustal thickening under the arch by a combination of rotational fault-bend folding and trishear. Two active source experiments involving up to 1850 "Texan" seismometers and a total of 20 blasts have generated crustal velocity models that will provide essential constraints for modeling the project's seismic results. Initial profiles are consistent with geometries of lower-crustal detachment, and furthermore suggest low velocity zones where the major master thrust and back thrusts cut the upper crust. These observations suggest that the lower North American lithosphere was not involved in the deformation, and this is also suggested by laterally-variable shear wave splitting results that can not be explained solely by Laramie-to-recent asthenospheric flow or lower lithospheric reworking with consistent strain across the region.

The active profiles provide detailed resolution of the mid and upper crust. The passive seismic results from three experiments, ranging from a year+ deployment of 38 broad band seismometers to a two week deployment of 800 "Texans", provide constraints throughout the crust and upper mantle.
While we are still in data compilation mode, instruments sited in crystalline rocks show a remarkably flat interface (Moho or top of 7XX) at ~40 km depth, which also supports upper crustal detachment. Intriguing results from the basins show that integration of our results will be essential to remove basin reverberations that could have been confused with teleseismic arrivals from the Moho.

As the project progresses, additional constraints from 3D structural and gravity modeling, more distant energy sources (e.g., mine blasts and earthquakes), and seismic noise and reverberation studies will be used to develop a highly constrained model for foreland arch development.

An Unexpected Discovery: PBO Tsunami Measurements

Kathleen Hodgkinson, Wade Johnson, Adrian Borsa, Dave Mencin, Brent Henderson and Mike Jackson
UNAVCO, 6350 Nautilus Drive, Boulder, Colorado 80301, USA

The Plate Boundary Observatory (PBO) includes over 110 continuously operating GPS, 75 borehole strainmeter/seismic sites, 6 laser strainmeters and 28 tiltmeters. The purpose of the observatory is to characterize the three-dimensional deformation field across the western United States plate boundary over the broadest spatial and temporal range possible. An unexpected finding, , is that PBO strainmeters located within a few hundred meters of the coastline have repeatedly recorded tsunamis as they arrive along the west coast of North America. In this presentation we document the signal recorded by PBO strainmeters, tiltmeters and GPS as the devastating tsunami generated by the March 2011, M9 Tohoku earthquake reached the coast of North America.

Several PBO strainmeters, some as far as 13 km inland, recorded the arrival of Tohoku tsunami. Long term trends, teleseisms and the background ocean-load plus earth tide signals are removed from the strainmeter data by band pass filtering the time series at 5 to 180 minutes. The tsunami strain signals stand well above the noise in the filtered time-series and the arrival times are consistent with those recorded by tide gauges along the west coast. Areal strain recorded by strainmeter B928 on Vancouver Island, British Columbia, yields a predicted wave height to within 4 cm of that recorded by a nearby tide gauge. While the unfiltered time series from PBO GPS site NEAH, near the Washington coast seems to follow the tidal loading signal, the spectral evidence for the tsunami signal is slim. A small signal is evident in the PSD when the data are sidereally filtered to reduce multipath noise but it does not have enough power to be visually identifiable in the time series. Our initial investigation shows that although PBO tiltmeters do have the potential to record a tsunami signal the instruments, all in Alaska, are installed too far inland to record the signal.

Although the Plate Boundary Observatory was designed to study the interaction of faults and patterns of strain accumulation and release along the western United States plate boundary, it is possible that the strainmeter component of the observatory could complement existing tsunami warning systems by providing a land-based continuous, high-rate, tsunami measurement system.

The Colorado Plateau: Integration of geophysical observations through dynamic modeling

Lucy Flesch, Corné Kreemer, and Hersh Gilbert

The Colorado Plateau has long been interpreted as a strong lithospheric block passively rotating within the highly deforming western United States. Resent results from seismic, geodetic and geologic observations and numerical modeling have shown that there is a fundamental difference between the eastern and western Colorado Plateau, thus necessitating a reevaluation of models. Specifically, variations between the eastern and western plateau include crustal and lithospheric thickness and deviation of SKS splitting observations away from absolute plate motion. There is migration of volcanism across the plateau from west to east. GPS observations on and surrounding the plateau indicate that the western side of the plateau is currently undergoing east-west extension. Previous models have shown that the strain rates associated with the GPS observations are not consistent with modeled stress directions; however, deviatoric stresses associated with gravitational potential energy variations are consistent with geologic stress measurements. Here, we explore the dynamics of the Colorado Plateau through observationally driven modeling investigating the role of gravitational potential energy variations, shearing of the Pacific plate and mantle flow caused by both eastward mantle flow and possible small-scale localized convection responsible for the present day break up of the Colorado Plateau.

Observations of arrival angles on the USArray

Anna Foster[1]*, Göran Ekstrom[1], Vala Hjörleifsdottír[2]

1. Lamont-Doherty Earth Observatory, Columbia University, Palisades, NY USA
2. Universidad Nacional Autónoma de México, Mexico City, Mexico

We have made estimates of the arrival angle of Love and Rayleigh waves at periods between 25-100 seconds at stations in the USArray Transportable Array. These estimates are made by fitting predictions of phase from an effective source location to the observed single-station phase measurements at all stations within some radius (100-200 km) of the station of interest. The back azimuth to the best-fit "effective source" corresponds to the best-fit arrival angle. The arrival angles are used to improve our two-station phase measurements, by correcting the geometry of the stations and source. However, on the scale of the TA, arrival angles can also be used to investigate the sources of refraction. As energy from an event propagates across the array, arrival angles tend to be largely unchanged along a given great-circle path. Variations up to 15° are observed perpendicular to the great-circle path direction. These banded patterns indicate that most refraction occurs as a result of large-scale structure outside of the study area. Within the array, the small changes in arrival angle observed in the propagation direction may be due to velocity contrasts within the array, or wave-front healing effects. We compare these observations to equivalent measurements made on synthetic seismograms calculated using SPECFEM3D_GLOBE. The synthetic data show the same banded patterns parallel to the propagation direction as the real data, but with major differences in the magnitude and occasionally even sign of the arrival angles. This comparison of real and synthetic observations can be used as a diagnostic tool to evaluate and improve global earth models.

*afoster@ldeo.columbia.edu

USING SHORT-TERM POSTSEISMIC DISPLACEMENTS TO INFER THE LONG-TERM TECTONIC ENVIRONMENT OF THE UPPER MANTLE AT AN ACTIVE PLATE BOUNDARY

Andrew M. Freed[1], Greg Hirth[2], and Mark D. Behn[3]

[1] Earth & Atmos. Sciences, Purdue University, West Lafayette, IN: freed@purdue.edu
[2] Geological Sciences, Brown University, Providence, RI
[3] Geology & Geophysics, Woods Hole Oceanographic Institution, Woods Hole, MA

Abstract

Postseismic surface displacements are associated with viscoelastic relaxation of the hot lower crust and/or upper mantle in response to sudden coseismic loading. The spatial and temporal characteristics of these displacements tell us something about the tectonic environment (temperature, pressure, background strain rate, water content, creep mechanism) within which postseismic flow occurs. In order to understand how to interpret postseismic observations in terms of the tectonic environment, however, the constitutive relationship utilized to relate strain rates to coseismic stress changes must also take into account a weak initial transient phase of flow. Here we develop a flow law that combines the influences of tectonic environment and a transient phase and apply it to understand the nature of the upper mantle beneath the Eastern California Shear Zone in southern California following the 1999 M7.1 Hector Mine earthquake. This is accomplished using a finite element model of the relaxation process constrained by surface displacement time-series recorded by 55 continuous GPS stations for 7 years following the earthquake. Results suggest that postseismic flow following this earthquake occurs below a depth of ~50 km and is controlled by dislocation creep of wet olivine. Significant diffusion creep is ruled out, as it would require a grain size (3.5 mm) much smaller than what is compatible (~1 cm) with inferred mantle conditions at these depths. Model results suggest an initial transient phase of flow that lasts ~2 years and is ~10 times weaker than subsequent steady-state flow, in general agreement with laboratory observations. The observed postseismic response is best explained as occurring within a relatively hot upper mantle (e.g., 1300° C at only 50 km depth) and a long-term background mantle strain rate of ~0.1 µstrain/yr, consistent with the observed surface strain rate. Long-term background shear stresses at the top of the mantle are ~4 MPa, then drop with depth to a minimum of 0.1-0.2 MPa at 70 km depth before increasing slowly with depth due to increasing pressure. This corresponds with a background viscosity of 10^{21} Pa s within a thin mantle lid that drops to ~5×10^{19} Pa s within the underlying asthenosphere. The earthquake is shown to have induced an immediate order of magnitude drop in viscosity within the upper mantle, which recovers to background levels within a few years. This study shows the utility of using short-term postseismic observations to infer long-term mantle conditions that are not readily observable by other means.

Distributed Continental Deformation Across Northwest North America

Jeff Freymueller (jeff.freymueller@gi.alaska.edu), and Julie Elliott
Geophysical Institute and Department of Geology and Geophysics
University of Alaska Fairbanks
Fairbanks, AK 99775

Pervasive fragmentation of continental lithosphere at plate boundaries is the rule, not the exception. The lithosphere of western and northwestern North America is fragmented into several large rigid or very slowly straining regions, most likely small plates within the plate boundary zone; a pattern familiar from the western part of the lower 48 US states. The same is true for northwestern North America (Alaska and the Northern Cordillera of Canada), which features a broad band of distributed deformation that extends around the northern Pacific Rim, and into Asia. We find evidence for distributed active deformation zone extending into the continent not only in the subduction part of the margin, but also along the strike-slip Queen Charlotte-Fairweather fault zone. Indeed, distributed continental deformation is continuous or nearly so from Baja California around the north Pacific to Tibet, and beyond.

The Salton Seismic Imaging Project: Investigating Earthquake Hazards in the Salton Trough, Southern California.

Sickler[1], R. R., G. S. Fuis[1], J. A. Hole[2], J. M. Stock[3], M. J. Rymer[1], R. D. Catchings[1], J. M. Murphy[1], E. J. Rose[1], C. J. Criley[1], C. J. Slayday-Criley[1], A. J. Ferguson[1], M. A. Gardner[1], S. Skinner[3], J. A. Cotton[1], J. R. Svitek[1], R. McClearn[1], M. R. Goldman[1], L. A. Butcher[1], D. S. Croker[1], E. G. Jensen[1], N. W. Driscoll[4], A. J. Harding[4], J. Babcock[4], G. M. Kent[4,5], A. Kell-Hills[5], and S. H. Harder[6]

[1] U.S. Geological Survey (USGS), Earthquake Science Center (ESC), Menlo Park, CA.
[2] Virginia Polytechnic Institute and State University, Dept. of Geosciences, Blacksburg, VA.
[3] California Institute of Technology, Seismological Laboratory 252-21, Pasadena, CA.
[4] Scripps Institution of Oceanography, La Jolla, CA.
[5] Nevada Seismological Laboratory, University of Nevada, Reno, NV.
[6] University of Texas, El Paso, TX.

The Salton Seismic Imaging Project (SSIP) is a collaborative effort to provide detailed subsurface 3-D images of the Coachella, Imperial, and Mexicali Valleys (the region here called the Salton Trough) of southern California and northern Mexico. Using both active and passive-source seismic data acquired both onshore and offshore in the Salton Trough, these images will provide insights into earthquake hazards, rift processes, and rift-transform interaction at the southern end of the San Andreas Fault system. The southernmost San Andreas Fault (SAF) is considered at high-risk of producing a large damaging earthquake, yet the structure of this and other regional faults and that of adjacent sedimentary basins are not currently well understood. To improve hazard models for southern California, SSIP will evaluate the geometry of the San Andreas and Imperial Faults, structure of sedimentary basins in the Salton Trough, and three-dimensional seismic velocity structure of the crust and uppermost mantle.

Data were acquired during the period of 2 March to 18 March 2011. One-hundred and twenty-six borehole explosions (10-1400 kg yield) were detonated along seven profiles in the Salton Trough region, extending from the Palm Springs, California, area to the southwestern tip of

Arizona, and airguns (1500 and 3500 cc) were fired along two profiles in the Salton Sea and at points in a 3-D array in the southern Salton Sea. Almost 2800 seismometers were deployed at over 4200 locations throughout the Salton Trough region, and 48 OBS's were deployed at 78 locations in the Salton Sea. Many of the onshore explosions were energetic enough to be recorded and located by the Southern California Seismograph Network (SCSN).

The focus of this abstract is geometry of the SAF and the depth and shape of the sedimentary basins in the Coachella Valley, where the only active-source data date from the early 1960's. Prior data (potential field, seismicity, InSAR) indicate that the SAF dips moderately to the northeast from its inception at the Salton Sea to Cajon Pass in the Transverse Ranges. Much of SSIP was designed to test models derived from this prior data. The geometry of the SAF has important implications for energy radiation in the next major rupture. We will present initial data from the Coachella Valley region.

Could Coseismic Compaction Inhibit Faults from Continued Failure?

Patrick M. Fulton[1]   pfulton@ig.utexas.edu
Andrew P. Rathbun[2]   andy.p.rathbun@gmail.com

[1] Institute for Geophysics, University of Texas at Austin, Texas, USA
[2] ISTerre (Institut des Sciences de la Terre), Université Joseph Fourier, Grenoble, France

Models of earthquake nucleation and slow unstable slip often invoke slip-induced dilation to reduce pore pressure P. This decrease in P is thought to discourage rupture by increasing the effective normal stress, thereby reducing the susceptibility for frictional failure (i.e. the difference between the shear stress on the fault and the failure criterion increases). This assumes effective stress is defined by $\sigma_n' = \sigma_n - P$. Here, we describe an additional process that can lead to an overall coseismic compaction and an increase in P and argue that a more comprehensive definition of effective stress is necessary to understand the how fault rocks respond to pore pressure changes.

We present results of experiments that exhibit stick-slip behavior representative of earthquake nucleation performed on analog fault gouge at a constant normal stress ranging from 7.5 to 50 MPa under dry conditions and a constant loading velocity of 200 µm/s. For each of the hundreds of slip events, the results consistently show coseismic compaction rather than dilation. Similar observations have been noted in previous studies that include strain release, although here we quantitatively explain how this results from a combination of slip-induced dilation along with an additional compaction process expected from the release of shear strain in order to maintain a force balance.

These results suggest that even without the effects of thermal pressurization unstable slip can lead to an increase in P rather than a decrease. However, using a more comprehensive poroelastic definition for effective stress we illustrate how for weak anisotropic fault rocks an increase in P can decrease the failure susceptibility, opposite of what it is commonly assumed. These results lead to a quite different conceptual model for how hydrologic and mechanical processes interact within fault zones during slip. Further characterization of these processes and how they relate to geologic and laboratory observations will be important for understanding and modeling earthquake mechanics.

Shear wave structure and radial anisotropy of the crust beneath the Rio Grande Rift

Yuanyuan V. Fu[1]*, and Aibing Li[1]

[1]Department of Geosciences, University of Houston, TX, USA

*Correspondent (pkucugfyy@gmail.com; 1-832-494-0986)

We have measured Rayleigh and Love wave phase velocities from 8 to 40 s using seismic ambient noise data recorded at 142 stations across the Rio Grande Rift in New Mexico and its vicinity from the transportable array component of the USArray in the EarthScope program. A 3-D shear wave velocity model of the crust with radial anisotropy is determined beneath the Rio Grande Rift, eastern Colorado Plateau, and western Great Plains from the inversion of the phase velocity maps. Significant low shear wave speed appears at the intersection of the Jemez lineament and the rift at shallow crust, beneath the Socorro area in the mid-crust, and beneath the Taos Plateau at the rift in northern New Mexico. All the low velocities are probably related to partial melt. The variable depth range of the low velocity anomalies at these places probably indicates different stages of melt propagation and accumulation along the rift. Radial anisotropy with $V_{SH} > V_{SV}$ is required in the mid and lower crust at most part of the area. The anisotropy is stronger beneath the rift and the Jemez lineament and weaker in the Great Plains. This can be explained as the mid and lower crust has been significantly weakened and stretched in the area that has experienced extension and rifting. Flat magma sills could also make contributions to the high radial anisotropy. However, anisotropy at the rift in northern New Mexico is close to zero or slightly negative ($V_{SV} > V_{SH}$), which might be caused by vertical movement of melt migration. The distinct crustal structure along the Rio Grande rift suggests that different rifting processes exist beneath the rift.

Initial full-wave tomography of the Cascadia subduction zone

Haiying Gao and Yang Shen

University of Rhode Island

A comprehensive and high-resolution velocity model is essential to understand the along-strike segmentation of the Cascadia subduction zone from northernmost California to the Vancouver Island, Canada, and the role of (de-)hydration of the slab/crust, which is thought to be critical for the occurrence of the episodic tremor and slip. In this study, we image the seismic structure of the crust and upper mantle with the application of a full-wave tomographic method (Shen and Zhang, 2010). About 600 stations are used in this study, including the EarthScope USArray Transportable array, the Canadian stations, the Pacific Northwest regional seismic network, the United States national seismic network, the Plate Boundary Observatory Borehole seismic network and the Wallowa flexible array in NE Oregon. The continuous seismic data obtained from the IRIS Data Management Center and the Canadian National Seismograph Network are re-sampled at 1 point/second. The empirical Green's functions (EGFs) are recovered from inter-station cross correlations at periods of 7-200 seconds. At the periods of our interest, the EGFs from cross correlations of vertical-vertical channels are primarily Rayleigh waves. We simulate full-wave propagation within a 3D reference velocity model. The travel time anomalies are measured from the observed and synthetic Green's functions at stations. The shear and compressional velocities are inverted jointly as Rayleigh waves are sensitive to both Vp and Vs. The solution from inversion is used to iteratively update the 3D reference model. Earthquake body and surface waves can be integrated with the empirical Green's functions. The integration of various waves in a physically consistent way holds promise for well-resolved absolute P and S velocities and Vp/Vs ratio, which will allow for more robust and reliable geodynamic interpretations.

Origin of the southern half of the Idaho batholith and its role as a window into the deep crust: Providing the temporal component of IDOR

Rich Gaschnig[1], Jeff Vervoort[1], Basil Tikoff[2], and Reed Lewis[3]
1. Department of Geology and Geophysics, University of Wisconsin-Madison, Madison, WI 53706; basil@geology.wisc.edu
2. School of Earth and Environmental Sciences, 1228 Webster Physical Sciences Bldg., Washington State University, Pullman, Washington 99164; gaschnig@wsu.edu, vervoort@wsu.edu
3. Idaho Geological Survey, University of Idaho, Moscow, ID 83844; reedl@uidaho.edu

The Idaho batholith represents a major tectono-magmatic component of the northern Cordillera. It occupies an estimated 23,000 km^2 and has been traditionally been divided into a larger Atlanta lobe to the south and smaller Bitterroot lobe to the north. The Earthscope Idaho-Oregon (IDOR) seismic experiment, scheduled to begin this year, will cross the center of the Atlanta lobe. In preparation for the geophysical work, we have conducted a geochronological and geochemical investigation of the batholith in order to provide a "fourth dimensional" view to the seismic interpretation of the batholith and the overall structure of the crust in this region. Geochronological studies of the Idaho batholith have lagged significantly behind other major batholiths of the Cordillera because a large amount of zircon inheritence has been an obstacle to dating these rocks using tradition ID-TIMS analysis.

The geochronology indicates that there are distinct pulses of magmatism that comprise the Idaho batholith. Each has unique geochemical signatures that provide important clues about the assembly and evolution of this major crustal feature. The Atlanta lobe, in particular, contains multiple generations of Cretaceous granitoids with major differences in composition. Two belts of metaluminous hornblende-bearing granodiorites and tonalites were emplaced on both the eastern and western (adjacent to the western Idaho shear zone) edges of the batholith. These granitoids were emplaced between 95 and 85, and are similar in composition to time-contemporaneous granitoids of the Sierra Nevada batholith to the south. These bodies also have mixed radiogenic isotopic signatures and relatively heavy oxygen isotope signatures, suggesting a petrogenesis involving the mixing of mantle melts with supracrustal rocks. The similar ages and compositions to the Cretaceous Sierra Nevada batholith suggest a similar origin in a continental arc environment.

The metaluminous plutons were intruded between 83 and 67 Ma by an enormous volume of peraluminous biotite granodiorite and two-mica granite that comprises the bulk of the Atlanta lobe. We call these rocks the Atlanta peraluminous suite. They have radiogenic isotopic signatures consistent with a Precambrian crustal source. Isotopic compositions vary with geographic location and geochemical evidence indicates an origin by the melting of different lithologies and ages of Precambrian crust rather than genesis by large-scale mixing of crust and mantle components.

The ages of inherited xenocrystic zircons provide important constraints on the nature of some of the crust that was melted or assimilated to form the Atlanta peraluminous magmas. Samples in the southern half of the Atlanta peraluminous suite contain xenocrystic zircons characterized by a bimodal age distribution, with peaks at

~680 Ma and 2550 Ma, which we interpret to represent the age of metaigneous basement. In contrast, xenocrystic zircons from the northern Atlanta peraluminous suite yield a continuum of Proterozoic ages, which is consistent with derivation from melted Neoproterozoic metasedimentary rock.

The cause in the shift from metaluminous to peraluminous magmatism and inferred shift from crust-mantle hybridism to primarily crustal melting after 85 Ma can be explained by two models, both of which call upon well-documented regional crustal thickening to thermally incubate the crust and screen out most mantle melts. One model attributes thickening to intra-arc to back-arc thrusting caused by a greater rate of convergence and/or greater coupling between the upper and lower plate in a subduction environment. The other model attributes thickening to the outboard collision of the Insular superterrane to the west, which was then translated northward to its present-day position.

High-resolution tremor imaging in Cascadia using multiple seismic arrays

Abhijit Ghosh, John E. Vidale, Kenneth C. Creager, and Heidi Houston
(aghosh.earth@gmail.com)
Department of Earth & Space Sciences
University of Washington, Seattle WA

Cascadia subduction zone under Washington experiences large slow quakes every 14.5 months or so. Each such event is characterized by geodetically observed slow slip and deep seismic tremor. This remarkably periodic coupled phenomenon is known as episodic tremor and slip (ETS). We installed 8 small aperture seismic arrays in northern Washington to capture the intimate details of tremor activity in Cascadia. The Array of Arrays focuses on the tremor-active megathrust in this region, including the area we previously imaged with a solo seismic array in 2008 [*Ghosh et al.*, 2009]. Each array consists of 10 to 20 three-component sensors recording in continuous mode. Since it became operational in June 2009, the Array of Arrays recorded several tremor episodes, including the recent episodic tremor and slip (ETS) event in August 2010. During the ETS, each array was augmented by 10 additional single-channel, vertical-component sensors.

We have developed a Multi-Beam Backprojection (MBBP) technique to image tremor in high resolution using data from multiple seismic arrays. We apply a beamforming technique at each array to stack the seismic energy at every 0.2 Hz from 2 to 20 Hz using 1-minute sliding time window. During tremor episodes, the arrays show stable slowness, and azimuth over the tremor frequency band (generally 3-8 Hz). We get the best slownesses from all the available arrays, and backproject to find the tremor source location in 3-D space. While P-wave energy stacks coherently up to 10 Hz and higher, S-wave extends only up to 6 Hz or so.

The MBBP algorithm is applied to 15.5 months of continuous seismic data from multiple seismic arrays to detect and locate tremor. We observe tremor streaks, bands, and patches confirming the observations made in our previous studies [*Ghosh et al.*, 2010a, 2010b; *Ghosh et al.*, 2009]. Moreover, MBBP algorithm has reasonable depth resolution. We found that majority of the tremor in the vicinity of the arrays is located near the plate interface, aligns parallel to the dip of the interface, and form a layer above the ordinary earthquakes (Figure 1). This algorithm is able image the details of rupture propagation of slow earthquakes not only during the ETS 2010, but also smaller events during inter-ETS time period. Generally, slow quakes show complex rupture pattern. Particularly interesting is the change of propagation velocity from 8 km/day to 18 km/day during the August 2010 ETS in this area. Tremor locations appear to illuminate a discontinuity in the oceanic crust separating highly tremor-active north from the feebly active south, possibly indicating variation in frictional properties across the discontinuity. These intriguing observations are providing new insights into the physics of slow earthquakes and tremor.

References:

Ghosh, A., J. E. Vidale, J. R. Sweet, K. C. Creager, A. G. Wech, H. Houston, and E. E. Brodsky (2010a), Rapid, continuous streaking of tremor in Cascadia, *Geochem. Geophys. Geosyst., 11*, Q12010, doi:10.1029/2010GC003305.

Ghosh, A., J. E. Vidale, J. R. Sweet, K. C. Creager, A. G. Wech, and H. Houston (2010b), Tremor bands sweep Cascadia, *Geophys. Res. Lett., 37*, L08301, doi:10.1029/2009GL042301.

Ghosh, A., J. E. Vidale, J. R. Sweet, K. C. Creager, and A. G. Wech (2009), Tremor patches in Cascadia revealed by seismic array analysis, *Geophys. Res. Lett., 36*, L17316, doi:10.1029/2009GL039080.
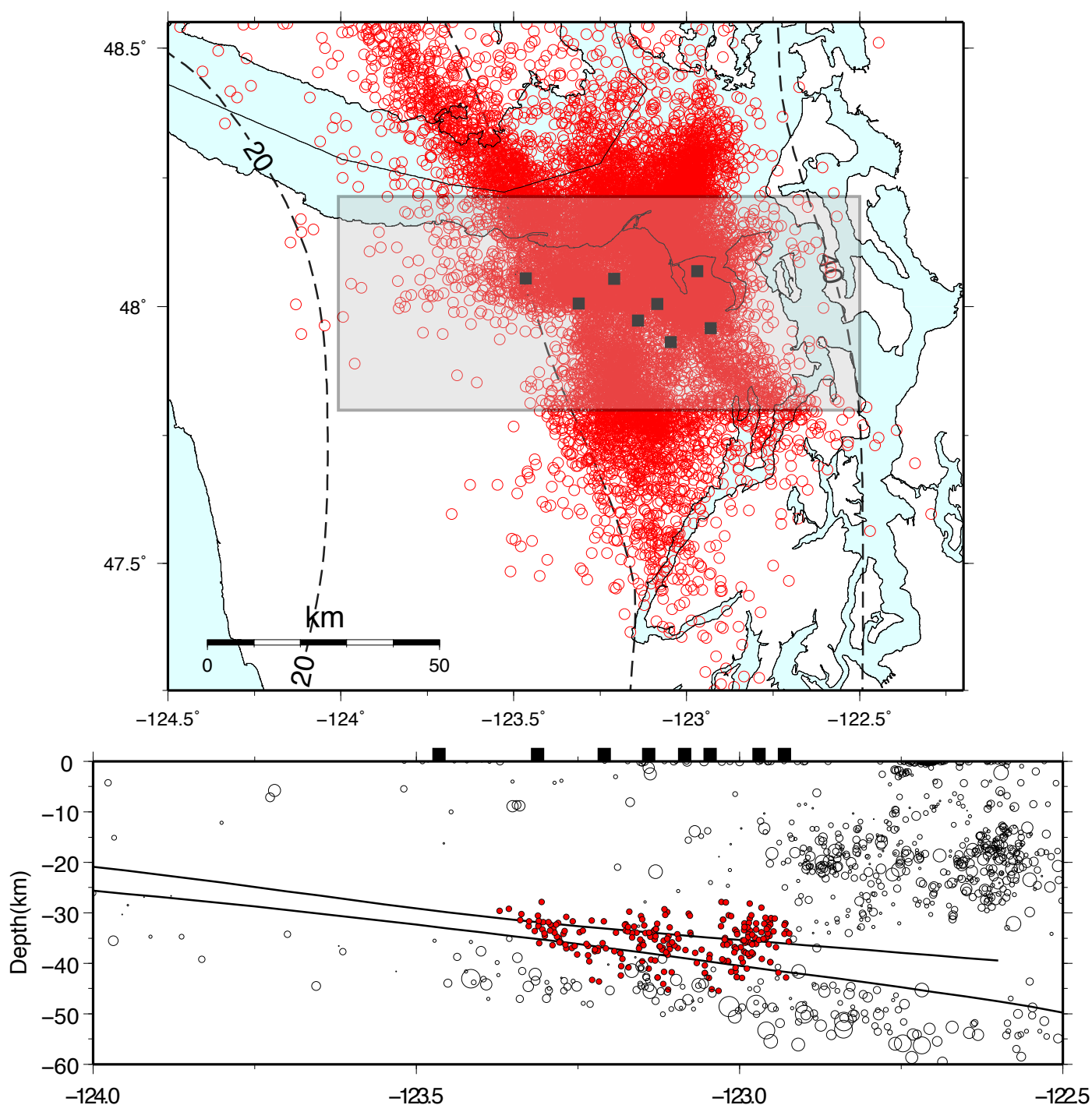
Figure 1: Top panel shows tremor location (red circles) using MBBP method for the entire 15.5 months. Black boxes marks the arrays. Gray rectangle covers the area tremor and earthquake locations are taken from to make the cross-section below. Gray dash lines are the contours showing the plate interface (*Audet et al.*, 2009). Bottom panel shows the cross-section along a E-W line going right through the middle of the gray rectangle in the top panel. Red circles are tremor location. Black circles are ordinary earthquakes scaled by their magnitude. Two lines represent two models of the plate interface; shallow one is by *Audet et al.*, 2009; deep one is by *McCrory et al.*, 2006. For tremor location in depth, only well-constrained locations every 30-minutes are plotted in the cross-section.

Understanding the deformation of the North American continent

Attreyee Ghosh,* University of Southern California

Thorsten Becker, University of Southern California

Gene Humphreys, University of Oregon

* Now at Stony Brook University

The goal of this study is to understand the possible deep mantle causes of deformation of the North American continent by trying to match the regional geoid, dynamic topography, plate motion and deviatoric stress field based on flow modeling. We evaluate the importance of shear tractions beneath the North American continent in a global high resolution, finite element convection code, CitcomS. This takes into account both radial and lateral viscosity variations arising from weak plate boundaries, strong keels as well as temperature dependent viscosity. We test different tomography as well as slab models. In addition, we also include the effects of shallow lithospheric buoyancies that give rise to gravitational potential energy (GPE) differences in the convection models by applying them as stress boundary condition. Moreover, we investigate the effect of anisotropic viscosity along the San Andreas on local velocity and stress field.

Step Discontinuity Detection in GPS time series

Jay Goldfarb, William C. Hammond, Geoffrey Blewitt, Hans-Peter Plag
(jgoldfarb@unr.edu)
Nevada Geodetic Laboratory, Nevada Bureau of Mines and Geology
University of Nevada, Reno

We routinely use GPS station coordinate time series to measure tectonic strain accumulation and other geophysical processes in the Sierra Nevada and Great Basin (SNGB) of the western United States. While tectonic strain accumulation is ostensibly slow and steady, the GPS time series are punctuated by step discontinuities as well as other periodic and aperiodic transient signals of both known and unknown origin. To estimate the parameters of geophysical motion most accurately, all known non-geophysical effects must be identified and removed from the time series. The occasional abrupt discontinuities that appear in the time series are attributable to a number of equipment or system-related causes. We have developed an algorithm to automatically detect step discontinuities and to separate discontinuities due to equipment and software changes from those having geophysical causes. In order to identify those steps which are due to equipment changes, the algorithm retrieves metadata in International GNSS Service (IGS) log files available on the internet and correlates this information with automated step detection results. Examples of events listed in the log files are antenna and receiver changes. We have applied this algorithm to generate statistics on step distribution in several hundred time series across the SNGB. We examined several representative time series and found that there is great variability in the character of these individual series. After correcting for the effect of equipment-related changes, many unmodeled non-linear transients remain. Examples of these include rate changes (ramps) which cause the automated algorithm to detect spurious steps. We suggest modifications to the method which might alleviate these problems.

Capturing a seismic wave field: Animation of kinematic GPS data recorded during the 2011 Tohoku-oki Earthquake, Japan.

Ronni Grapenthin,[1*] Jeffrey T. Freymueller[1]

[1]Geophysical Institute, University of Alaska Fairbanks,
903 Koyukuk Drive, P.O. Box 757320 Fairbanks, Alaska 99775-7320

[*]Correspondence to: ronni@gi.alaska.edu.

Earthquakes displace the ground during rupture and create seismic waves, which involve dynamic displacements that travel around the globe. Only recently did we measure dynamic displacements directly with high-rate Global Positioning System (GPS) data rather than using inferred displacements from seismic records. However, due to sparse station coverage, such data are traditionally presented as timeseries of a few GPS stations neglecting spatial correlation in the signal presentation. Here, we visualize directly measured dynamic and permanent displacements caused by the March 11, 2011, M_w 9.0 Tohoku-oki earthquake as a vector field based on data recorded by the dense Japanese GPS Earth Observation System (GEONET). The data was processed by the ARIA team (JPL/Caltech) using RINEX files provided to Caltech by the Geospatial Information Authority (GSI) of Japan. Our animations show the growth of the earthquake rupture over time

and illustrate differences of earthquake magnitude using two smaller aftershocks. We identify dynamic ground motion due to S-waves (body waves), Love waves and Rayleigh waves (surface waves). The displacements in map view are easily understandable by specialists and non-specialists alike. Real time availability of such displacements could be of great use in earthquake early warning, tsunami warning, and earthquake response.

Surface deformation in Central Nevada Seismic Belt observed by Satellite Radar Interferometry

Presentation - Poster

Fernando Greene[1] (fgreene@rsmas.miami.edu) and Falk Amelung[1] (famelung@rsmas.miami.edu).

[1]Rosenstiel School of Marine and Atmospheric Sciences.

We present the contemporary velocity field in the western Basin and Range province observed by satellite radar interferometry. A recent study in the Central Nevada Seismic Belt (CNSB) reported a broad area of uplift (~ 2-3 mm/yr) explained by postseismic mantle relaxation after a sequence of four earthquakes (M ~ 7) that occurred in the first half of the 20th century. To investigate the contemporary crustal deformation at the CNSB we use SAR imagery that covers a swath nearly 700 km long (seven conventional SAR frames) acquired by the European Remote Sensing Satellites ERS-1 and ERS-2 between 1992 and 2009, and Envisat between 2004 and 2010. In order to observe variations in the rates of velocity in CNSB, we produce line of sight (LOS) velocity fields for different time periods (1992 – 2000, 1999 – 2009 and 1992 - 2009) by averaging independent interferograms with small perpendicular baselines (< 150 m). Time-Series results from ERS 1/2 suggest that the uplift velocity decreased for the last decade, which is consistent with models of postseismic relaxation. Additionally we identify high rates of deformation at Long Valley Caldera, land subsidence due to water pumping on mines and agricultural exploitation areas, and ground deformation associated with moderate earthquakes.

PROCESSING INNOVATIONS NECESSARY TO MAXIMIZE RESOLUTION OF MODELS OF THE NORTHERN GULF COAST PLAIN USING BROADBAND DATA FROM THE "GUMBO" SEISMIC STUDY

GURROLA, Harold[1], PRATT, Kevin[1], PULLIAM, Jay[2], and John Dunbar[2] (1) Geosciences, Texas Tech University, Box 41053, Lubbock, TX 79409, harold.gurrola@ttu.edu, (2) Department of Geology, Baylor University, One Bear Place #97354, Waco, TX 76798

In summer of 2010, 21 broadband seismographs were installed at 16-18 km spacing along a transect running from Johnson City, TX (on the Edwards Plateau) to Matagorda Island to study the current structure of this rifted passive margin. Scientists at the UT Institute for Geophysics conducted a seismic refraction study along an offshore extension of the onshore transect called the "Gulf of Mexico Basin Opening" (GUMBO) seismic experiment.

GUMBO's onshore broadband component has data problems not typically encountered in recent PASSCAL or EarthScope flexible array experiments. This project is funded by a grant from the Norman Hackerman Advanced Research Program (NHARP), a biannual competition among Texas Universities to support research, and makes use of Texas Tech, Baylor and UT Austin equipment. As a result, the deployment includes a less uniform array of seismic equipment (10 Trillium compact seismometers and 10 Guralps; including 40Ts, 3Ts and 3ESPs) than most modern projects supported by the IRIS PASSCAL center.

Our vault construction was to PASSCAL standards, but Gulf Coast provides a more challenging environment for deployment than most encountered in the western US. The shallow water table and loose sediment can become almost fluid when storms deluge the area with rain. In dry periods, mud cracks near the vaults which cause the vaults to tilt. As a result, even high quality, shallow seismic vaults can "float" or shift sufficiently to cause one or two components of the seismic stations to drift against their stops in days or weeks. The stations with what is typically considered to be lower quality seismometers (e.g., Guralp 40T) were able to provide more consistent three component data than the higher quality seismometers (e.g., 3ESP), which require the mass to be centered regularly. As a result, the only data consistently available from all our stations (so far) are vertical components.

To address the data's shortcomings we will average the vertical components from our stations and nearby EarthScope TA stations (up 300 km away) to isolate the cleanest representation of the incoming P-wave (with local Ppp reverberations averaged out). The clean P-wave will then be deconvolved from the vertical components at each station to produce a vertical component receiver function that will enable us to model and stack local P-wave reverberations for lithospheric structure. To produce traditional receiver functions from time periods in which we lost one component of the seismic recordings, we will treat neighboring stations as arrays and recover an "array averaged three-component seismogram" for each location. These "beamed" seismograms will allow imaging of the lithospheric mantle and transition zone beneath the broadband array using traditional receiver function stacking or migration.

Seismicity and Active Crustal Deformation in the Wabash Valley Seismic Zone: A Postseismic Effect of the 1811-1812 New Madrid Earthquakes?

Michael Hamburger[1], Gerald Galgana[1,2], and Kaj Johnson[1]
[1]Department of Geological Sciences, Indiana University, Bloomington, IN 47405
[2]Lunar and Planetary Institute, USRA, Houston, TX 77058

The Wabash Valley Seismic Zone (WVSZ) and the New Madrid Seismic Zone (NMSZ) are intraplate seismic zones characterized by high-angle faults that define Precambrian grabens underlying relatively undeformed Phanerozoic rocks. The two regions are separated by an enigmatic tectonic zone characterized by basement uplift, Precambrian strike-slip and normal fault zones, and Mesozoic and Cenozoic magmatism. We examine active deformation in the two zones using campaign and continuous GPS networks, notably a 56-station campaign-based regional GPS network in Illinois, Indiana, and Kentucky, and a dense 35-station campaign network in the Fluorspar district of southern Illinois, a transitional zone between the Wabash and New Madrid seismic zones. The observed velocity field shows systematic motion of network sites with respect to the Stable North American Reference Frame at 1-2 mm/yr in a N-NE direction. The average strains for the entire network show marginally significant strain rates, with 1.4 ± 0.7 ns/yr NW-SE compression, and 1.6 ± 0.6 ns/yr NE-SW extension. While the systematic north-trending velocities and systematic internal strain may suggest several plausible tectonic interpretations of the surface deformation (e.g., slow strain accumulation associated with glacial unloading, or motions arising from slow rotations of relatively rigid but "jostling" tectonic blocks), we theorize that the present-day seismicity and deformation rates at the WVSZ may be an effect of the 1811-1812 New Madrid Earthquakes. We examine numerical models that test the effect of the 1811-1812 New Madrid earthquakes on the near- and far-field strain and seismicity rates in the region through instantaneous elastic deformation in the lithosphere and associated postseismic viscoelastic flow in the asthenosphere. Our results indicate that significant changes in strain and seismicity rates in the WVSZ can persist for several hundred years following the New Madrid earthquakes. The seismicity rate can increase by as much as 7x the background rate in the near-field, but by a much smaller amount in the far-field, with modeled seismicity rates highly dependent on the choice of lower-crust viscosity. Our results demonstrate that elevated seismicity and strain in the WVSZ could result from aseismic slip triggered by viscous relaxation in the lower crust long after the New Madrid earthquakes. The resultant strain is low enough that it might remain undetectable for earthquakes as large as Mw 7.5.

EarthScope Plate Boundary Observatory Reveals Uplift of the Sierra Nevada

W.C. Hammond[1], G. Blewitt[1], Z. Li[2], H.-P. Plag[1], C. Kreemer[1]

[1] Nevada Geodetic Laboratory, University of Nevada, Reno, Reno NV, 89557, USA, *whammond@unr.edu*
[2] School of Geographical and Earth Sciences, University of Glasgow, Glasgow G12 8QQ, United Kingdom

The history, driving forces, and rate of uplift of the Sierra Nevada have been the subject of some controversy. For example, estimates of the age of the modern topography based on geologic, paleoseismic, and isotope paleoaltimetry vary by over one order of magnitude, from less than 3 to greater than 40 million years. Present peak elevations exceed 4 km, and thus the most rapid of the possible uplift rates are >1 mm/yr, which is large enough to be detected by precise GPS measurements. Stations from the EarthScope Plate Boundary Observatory (PBO) now have time series long enough to provide estimates of vertical rates with uncertainties less than 0.5 mm/yr, and can be used to distinguish between a rapidly uplifting vs. inert range.

Additionally, 19 years of ERS and ENVISAT radar data that span the Sierra Nevada-Great Basin transition are available from the GeoEarthScope and WinSAR archives. We have performed interferometric and time series analysis of these data and combined them with three component GPS rates to separate vertical and horizontal components of motion.

Our results show that GPS stations on the west slope of the Sierra Nevada move upward at rates between 0.6 and 1.7 mm/yr with respect to eastern Nevada, and with respect to the Earth center of mass as estimated by the location of the origin of ITRF2005. The InSAR+GPS geodetic image of the southern Sierra Nevada uplift shows a gradient of between 1-2 mm/yr of vertical motion that coincides with the eastern edge of the Sierra Nevada/Great Valley microplate, corroborating the interpretation of the GPS results as a measurement of tectonic uplift of the Sierra Nevada.

These uplift rates are similar along most of the length of the Sierra Nevada, between latitude 35° and 39° north, and are similar to slip rates on normal faults along the eastern Sierra Nevada range front. Thus our results agree with models that call for a relatively young modern Sierra Nevada elevation, whose age is ~3 Ma or less.

For more information and figures see: http://geodesy.unr.edu/billhammond/vertical_gps.html

The Salton Seismic Imaging Project (SSIP): Active rifting in the Salton Trough, California

Liang Han[1], Kathy K. Davenport[1], J. A. Hole[1], J. M. Stock[2], G. S. Fuis[3], N. W. Driscoll[4], G. M. Kent[5], E. Carrick[1], S. Skinner[2], J. Persico[2], F. Sousa[2], B. Tikoff[6], M. J. Rymer[3], J. M. Murphy[3], R. R. Sickler[3], L. A. Butcher[3], E. A. Rose[3], J. Babcock[4], A. J. Harding[4], A. Kell-Hills[5], A. Gonzalez-Fernandez[7], O. Lazaro-Mancilla[8]

1. Virginia Tech, Blacksburg, VA, USA.
2. Caltech, Pasadena, CA, USA.
3. U. S. Geological Survey, Menlo Park, CA, USA.
4. Scripps Inst. Oceanography, La Jolla, CA, USA.
5. University of Nevada, Reno, NV, USA.
6. University of Wisconsin, Madison, WI, USA.
7. CICESE, Ensenada, Baja California, Mexico.
8. Universidad Autonoma de Baja California, Mexico.

The Salton Seismic Imaging Project (SSIP) acquired seismic data in and across the Salton Trough in southern California and northwestern Mexico in March 2011. SSIP is investigating both rifting processes at the northern end of the Gulf of California extensional province and earthquake hazards at the southern end of the San Andreas Fault system. SSIP acquired seven lines of land refraction and low-fold reflection data in the Coachella, Imperial, and Mexicali Valleys, airguns and OBS data in the Salton Sea, and a line of broadband stations across the trough. The controlled-source projects utilized over 90 field personnel, a majority of whom were student volunteers. Seismometers were deployed at 4235 locations at 50-500 m spacing onshore, and at 78 locations on the floor of the Salton Sea. These stations recorded 126 onshore explosive shots of up to 1400 kg and several lines of airgun shots.

This poster focuses on data acquired to investigate active rifting processes in the central Salton Trough. Previous studies suggest that North American lithosphere has been rifted completely apart. Based primarily on a 1979 seismic refraction project, the 20-22 km thick crust is apparently composed entirely of new crust added by magmatism from below and sedimentation from above. Active rifting in this part of the Salton Trough is manifested by normal faults observed in modern surface sediments, seismicity in the Brawley seismic zone between transform faults, and volcanism at the Salton Buttes. SSIP acquired seismic refraction and reflection lines across and along these features in the Imperial Valley, in the Salton Sea, and between onshore and offshore. Data were acquired inline for dense 2-D coverage and in grids for 3-D coverage. We will present initial data that will constrain the role and mode of magmatism, the effects of rapid Colorado River sedimentation upon extension and magmatism, and the partitioning of oblique extension in this transform-dominated rift system.

Diurnal and sub-diurnal variations in slow slip in Cascadia: comparison of PBO borehole strain observations with tidal loading and tremor

Jessica C. Hawthorne and Allan M. Rubin, Princeton University

A number of studies have observed variations in non-volcanic tremor on timescales between a few minutes and a few days. Observations from borehole strainmeters allow us to detect variation in slow slip on some of these timescales. We examine data from PBO borehole strainmeters in Cascadia in order to look for tidal modulation of slow slip and for a correlation between slip and tremor. To do so, we combine data recorded at six strainmeters during four major slip events between 2007 and 2010. We find that, on average, the strain due to slow slip is tidally modulated, with 20 to 30% more slip during the favorable portion of the tidal period. Comparison with tidal loading calculations suggests that the maximum slip rate occurs between the maximum shear stressing rate and the maximum shear stress, but given changes in tidal loading along strike, it may be at either. This observed tidal modulation of slip can be compared relatively directly with tidal modulation in simulated slow slip events that are controlled by one of the mechanisms proposed to explain slow slip events.

The method of fitting the strain data is described in *Hawthorne and Rubin* (2010). We slightly modify our earlier method so that we can compare the strain data with a predicted time series, rather than simply looking for signals at the tidal periods. We obtain similar estimates of tidal modulation of slip by comparing the predicted tidal stresses with the observed strain. We also use this modification to compare the strain data with tremor. We find that the strain rate during slow slip is correlated with tremor detected by *Wech and Creager* (2008) and with the amplitude of seismic signals recorded at colocated stations. This is true even when we consider only variations in strain and tremor with periods shorter than two hours.

References

Hawthorne, J. C., and A. M. Rubin (2010), Tidal modulation of slow slip in Cascadia, *J. Geophys. Res.*, *115*, B09,406, doi:201010.1029/2010JB007502.

Wech, A. G., and K. C. Creager (2008), Automated detection and location of Cascadia tremor, *Geophys. Res. Lett.*, *35*, L20,302, doi:10.1029/2008GL035458.

GLOBAL SEARCH FOR REMOTE TRIGGERING SEISMICITY CAUSED BY THE 2011, M9.0 TOHOKU, JAPAN EARTHQUAKE

A. A Velasco, H. Gonzalez-Huizar, M. Cameron and L. M. Sandoval

Geological Sciences, University of Texas at El Paso

(hectorg@miners.utep.edu)

Observations show that large earthquakes can trigger seismicity at large distances from the mainshock. The passing of seismic waves changes the stress conditions on previously over stressed regions causing the triggering of small earthquakes and tremors, this phenomenon is know as remote or dynamic triggering seismicity. We performed a global search of earthquakes and tremors potentially triggered by the surfaces waves from the 2011, M9.0 Tohoku, Japan earthquake. We used EarthScope's seismic stations and other seismic networks and catalogs to search for instance of instantaneous triggering of earthquakes and tremors during the passing of the seismic waves, as well as for statistically significant changes in seismic rate at several regions after the passing of the waves. Instantaneous triggering of tremor and earthquakes was observed in places as Taiwan, Armenia, Russia, Ecuador and the Caribbean, and changes in the local seismic rate where observed in places as USA, Mexico and the Solomon Sea. In order to have a better understanding of this phenomenon, we analyzed the seismic waves and modeled the stress changes caused by them and their relationship with the local stress where triggering occurred.

Studying the atmosphere and atmospheric phenomena using the USArray Transportable Array

Michael A.H. Hedlin[1], Catherine de Groot-Hedlin[1], Kris Walker[1] and Bob Woodward[2]

[1] Laboratory for Atmospheric Acoustics, Institute of Geophysics and Planetary Physics, Scripps Institution of Oceanography, University of California, San Diego

[2] Incorporated Research Institutions for Seismology

Abstract

Although the USArray TA was intended for studies of the solid Earth it is proving invaluable for studies of the structure of the atmosphere and atmospheric phenomena. It is well known that atmospheric acoustic signals couple to seismic at the Earth's free-surface and often register clearly on seismic channels. With this fact in mind we migrate the dense, Cartesian, USArray TA data at sound speeds (280 to 350 m/s) to detect and locate large atmospheric infrasonic sources. The infrasonic catalog developed using TA seismic data contains several hundred events per year. We take further advantage of the dense TA network to observe and study branches of acoustic signals. The seismic TA data allows us to observe for the first time the emergence of tropospherically and stratospherically ducted infrasound branches and their eventual decay – features that are well below the resolving power of the current network of infrasound stations but are very useful for understanding how sound is ducted in the atmosphere. Stations in the TA are now being upgraded with a suite of sensors that sample air pressure from D.C. to the Nyquist frequency. In this talk we will present new results from our study of seismically recorded infrasound from ground-truthed explosions in northern Utah and very long-period air pressure variations as recorded by newly installed pressure sensors.

Contact information for Michael Hedlin: 1 858 534-8773 (voice), 1 858 534-6354 (fax), hedlin@ucsd.edu

Comminution and Mineralization of Subsidiary Faults in the Damage Zone of the San Andreas Fault at SAFOD

Bretani Heron, Judith S. Chester, Renald Guillemette, and Frederick M. Chester
Center for Tectonophysics, Department of Geology & Geophysics, Texas A&M University, USA

Spot core from the San Andreas Fault Observatory at Depth (SAFOD) borehole provides the opportunity to characterize and quantify damage and mineral alteration of siliciclastics within an active, large-displacement plate-boundary fault zone. Deformed arkosic, coarse-grained, pebbly sandstone, and fine-grained sandstone and siltstone retrieved from 2.55 km depth represent the western damaged zone of the San Andreas Fault, approximately 130 m west of the Southwest Deforming Zone (SDZ). The sandstone is cut by numerous subsidiary faults that display extensive evidence of repeating episodes of compaction, shear, dilation, and cementation. The subsidiary faults are grouped into three size classes: 1) small incipient faults, 1 to 2 mm wide, that record early fault development, 2) intermediate-size faults, 2 to 3 mm wide, that show cataclastic grain size reduction and flow, extensive cementation, and alteration of host particles, and 3) large subsidiary faults that have cataclastic zones up to 10 mm wide. The cataclasites contain fractured host-rock particles of quartz, oligoclase, and potassium feldspar, in addition to albite and laumontite produced by syn-deformation alteration reactions. In general, grain shapes and size distributions indicate that potassium feldspar and quartz primarily are deformed through fracture, whereas the oligoclase phase has been fractured and altered to produce albite and laumontite. Five structural domains are distinguished in the subsidiary fault zones: fractured sandstones, brecciated sandstones, microbreccias, microbreccias within distinct shear zones, and principal slip surfaces. We have quantified the particle size distributions of the host rock mineral phases and the volume fraction of the alteration products for these representative structural domains. Overall, the particle sizes are consistent with a power law distribution down to a grain size of at least several microns in diameter. We find that the exponent (fractal dimension) increases with shear strain and volume fraction of laumontite, recording a general transition from constrained comminution to abrasion processes with increasing shear strain. The macroscopic and microscopic structure of the subsidiary faults is consistent with an evolution from the early formation of compacting shear bands while the sandstone was porous, followed by alteration and cementation, and repeated reactivation of the bands by shear and dilation, alteration, and cementation. Later stages of deformation involved localization of slip within the larger bands that contain a very high volume fraction of laumontite.
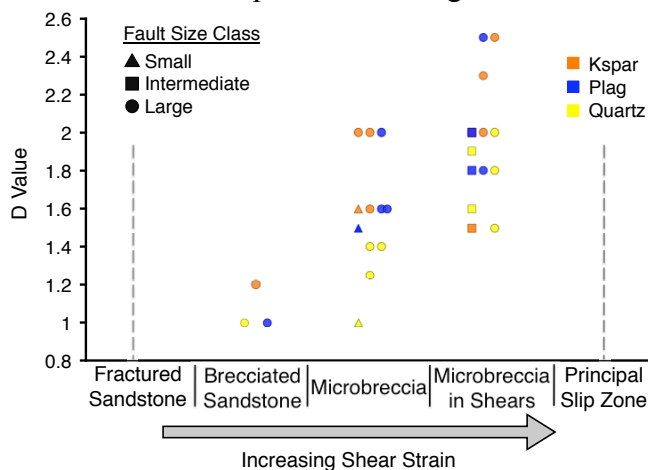

Figure 1: Fractal dimension, D, of particle size distribution as a function of increasing shear strain for different host minerals
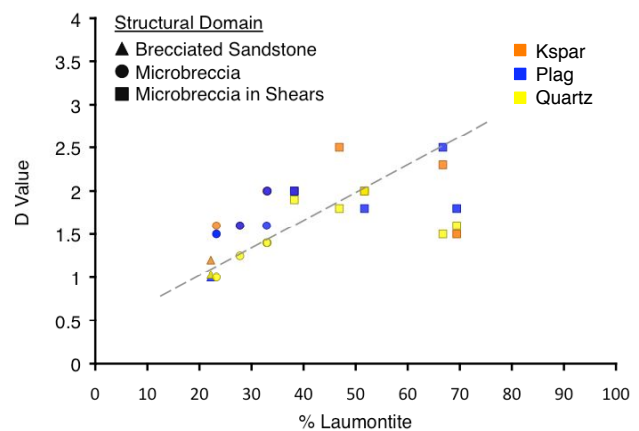

Figure 2: Fractal dimension, D, for different volume fractions of laumontite

PBO Borehole Strainmeter Data Products and Data Quality Metrics

Kathleen Hodgkinson, Adrian Borsa, Dave Mencin, Warren Gallaher, Mike Gottlieb, Brent Henderson, Wade Johnson, Jeremy Smith, Liz VanBoskirk and Mike Jackson.

UNAVCO, 6350 Nautilus Drive, Boulder, Colorado 80301, USA

The Plate Boundary Observatory (PBO), built and maintained by UNAVCO, includes 75 4-component Gladwin Tensor Strainmeters installed in arrays distributed between southern California and Vancouver Island, Canada. Strain, seismic, barometric pressure, rainfall and temperature data are collected at all PBO strain boreholes while pore pressure, accelerometer and tilt data are collected at a subset of sites. Ensuring complete, rapidly available and high quality data sets are collected for the scientific community is an essential function of the Observatory. Each PBO strain site records at least 70 data channels and presenting the entire suite of data products available to the community in an easily understandable manner is a challenge in itself.

This presentation will focus on the data products from the PBO borehole strain network and the metrics that have been developed to monitor strain data quality. Strain data products include raw time-series, processed time-series, nominal and *in-situ* calibrations calculated using the method of Roeloffs (2010), tidal models, barometric pressure response and data quality metrics. Metrics allow potential problems to be identified in network operations plus give the scientific community a sense of which instruments perform well over the broad operating range of borehole strainmeters. We assess each strainmeters recording of seismic signals, the signal to noise ratio in the tidal band, the presence of steps in the data and the state of borehole compression. These metrics are made available to the community in the strainmeter processing section of the UNAVCO strainmeter web pages and as a network table that is updated every three months. More information on PBO strainmeters and all other instruments within the observatory can be found at http://pboweb.unavco.org.

Using GPS Derived Shear Strain Rates to Constrain Fault Slip Rate, Locking Depth, and Residual Off-Fault Strain Rates

William Holt and Yu Chen, Stony Brook University, Stony Brook, NY 11794-2100

Strain rate fields within strike-slip regimes often possess complexity associated with along strike slip rate variations. These along strike slip rate variations produce dilatational components of strain rate within and near the fault zones and within the adjacent block areas. These dilatation rates do not directly reflect the slip rate magnitude on the strike slip fault, but rather the relative change in along strike slip rate. Displacement rates measured using GPS observations reflect the full deformation gradient field, which may involve significant dilatational components. Thus, using displacement rates to infer slip rate and locking depth of major strike-slip faults may introduce errors when along strike slip rate variations are present. On the contrary, the shape and magnitude of the shear strain rates (pure strike-slip component) reflect true strike-slip parameters of interest (locking depth and slip rate). In this study we investigate the use of shear strain rates alone (obtained from the full displacement rate field of the SCEC 4.0 velocity field in southern California) to infer fault slip rate and locking depth parameters along the San Andreas and San Jacinto fault zones.

The first step in the study involves benchmarking tests to determine if accurate shear strain rates can be obtained from a synthetic fault slip rate field. The synthetics were derived using Okada's [1992] elastic dislocation routine and synthetic displacement rates were generated. These displacement rates were interpolated using bi-cubic Bessel interpolation to infer shear strain rates (associated with pure strike-slip deformation) and dilatation rates. In order to test realistic conditions, along strike slip rates were put into the elastic dislocation model and model displacements were output at the true GPS station spacing in southern California (the same as the SCEC 4.0 velocity field). The modeled strain rate field shows negligible strain rate artifacts in most regions and both shear strain rates and dilatation rates obtained from the bi-cubic interpolation were well resolved. The inferred shear strain rate field was then inverted, using a simple screw dislocation forward model for the best-fit fault location, fault locking depth, and fault slip rate. Model parameter estimates were well resolved both near and away from fault slip rate transitions (± 1 km for fault locking depth; ± 1-2 mm/yr for fault slip rate).

The inferred shear strain rate field from the true GPS field in southern California (SCEC 4.0 velocity field) shows remarkably well resolved and prominent shear strain rate bands that follow both the San Andreas and San Jacinto fault systems. The shear strain rates reflect dramatic along strike slip rate variations, and locking depths that vary between 5-6 km south of the Salton Trough to 8-12 km elsewhere. Results to date suggest that dilatation rate estimates are largely not artifacts of strain interpolation but instead reflect true along-strike fault slip rate variation. Moreover, because displacement rates may be 'contaminated' by dilatational

components of the field, the modeling of well-resolved shear strain rates may be a more optimal way of inferring accurate fault locking depth and slip rate estimates within strike-slip fault regimes.

Earthquake Swarms Occur at the Edges of Great Earthquake Rupture

S.G. Holtkamp[1] (stephen.holtkamp@gmail.com) and M.R. Brudzinski[1], [1]Miami University Geology Dept.

A key question in seismology and earth science is why certain subduction zones appear to have a characteristic size for the largest earthquake possible at that margin. A manual search for earthquake swarms by Holtkamp and Brudzinski (2011) documented 180 megathrust earthquake swarms at Circum-Pacific subduction zones and found that regions of the megathrust with large along strike gaps in swarm activity experience larger magnitude earthquakes. Consistent with this, Holtkamp et al. (2011) show that the 2010 Chile earthquake rupture was bracketed to the north and south by previous megathrust earthquake swarms. Subsequently, we have found evidence for similar relationships in Sumatra, Peru, Alaska, Kamchatka, and Japan. Holtkamp and Brudzinski (2011) found 10 earthquake swarms in the Sendai region on or near the subduction margin that ruptured during the 2011 Tōhoku earthquake. The swarms occurred exclusively in two regions which appear to closely bound the northern and southern extent of the Tōhoku rupture, with the Tōhoku earthquake and the M_w 7.9 aftershock occupying the ~400 km gap between swarms. In this study, we examine the relationships between earthquake swarm occurrence from 1973 to 2010, interseismic coupling, and co-seismic moment release for recent great earthquakes. The two swarm regions in Sendai Japan occur at zones of reduced plate coupling, determined by Loveless and Meade (2010), while the gap between the swarm regions, which ruptured during the Tōhoku earthquake, was determined to be a region of high interseismic coupling. We suggest that earthquake swarms can be used as a proxy for either subduction zone coupling or stress heterogeneity, both of which have been hypothesized to influence the size to which an earthquake can grow. If aseismic slip is a driving mechanism for megathrust earthquake swarms and is releasing a large percentage of the overall convergence, the lack of long term (earthquake cycle scale) stress accumulation in these regions may explain why rupture termination seems to occur in earthquake swarm regions.

The Importance of USArray Data for Understanding the Nature of the Mantle Transition Zone

Christine Houser
Department of Earth and Planetary Sciences, University of California Santa Cruz, Santa Cruz, CA, 95064
cthouser@ucsc.edu

The density and current extent of USArray as it advances eastward across the country are improving our resolution of the 410 and 600 km discontinuities which define the mantle transition zone. Here I present a couple of examples where USArray either provides an unprecedented volume of data or illuminates previously sparsely sampled regions. There are no seismic stations in the northwest Pacific, so SS precursors are one of the few observations from the transition zone in this region. Fortunately, there is an unprecedented concentration of SS reflections off of the 410 and 600 km discontinuities under the NW Pacific from earthquakes in the western Pacific recorded on the USArray Transportable Array. Since there are now more than 1000 traces contributing to these NW Pacific waveform stacks, the S410S and S660S reflections are exceptionally clean. Thus, we can use details of these observed stacks to test predictions from different temperature and composition profiles to determine which thermo-chemical models best fit the data. Closer to home, the Transportable Array is making it possible to obtain the triplication structure of the 410 and 660 km discontinuities. A source-receiver distance around 20° is necessary to study triplications, but very few earthquakes occur at this distance from the western US where most seismic stations have been concentrated in the past. As the TA moves eastward, the stations are now within 20° of events in Central America and the Caribbean. The triplications are critical for understanding the nature of the 410 and 660 km discontinuities since they constrain not only the depth and magnitude of the discontinuity but also the impedance contrast (i.e. density) which is sensitive to composition. Here I demonstrate, using the current extent of the TA, that we can now begin to understand the nature of the mantle transition zone along the southern US border.

The role of fluids in promoting seismicity in active spreading centers of the Salton Trough, California

Musa Hussein, Laura Serpa and Aaron A. Velasco

Department of Geological Sciences, University of Texas at El Paso, El Paso, TX 79968-0555

We interpret seismic activity in the active spreading centers of the Salton Trough at the Brawly, Cerro Prieto, Imperial and San Jacinto faults to indicate 1) a magmatic body in the lower crust that lies beneath these active faults and 2) fluids in the upper crust that have been released from that magmatic body. The absence of a magmatic body and fluids at the location of fossil spreading centers along the Sand Hill and Algodones faults is consistent with the weak or absent seismic activity in those areas. We show several lines of evidence to indicate that melt and fluids are related to the seismic activity. In particular, receiver functions analysis, and tomographic data reveal high *Vp/Vs* ratios. Low velocity zones coincide with the location of the active spreading centers. High *Vp/Vs* ratios and low velocity zones in the lower crust and upper mantle are attributed to melt inclusion, while low *Vp/Vs* ratios in the upper crust are caused by the inclusion of H_2O. Frequency-magnitude distributions, "*b-values*", are high in southern California; high "*b-values*" have also been associated with fluids. A crustal scale model created from the receiver functions, gravity, and magnetic data support the existence of a magmatic body at a depth of about 20 km to the southwest of Salton Sea. That body extends for 90 km in SW-NE direction.

Data products in development at the IRIS DMC

Alexander Hutko, Manoch Bahavar, Chad Trabant & Rich Karstens

alex@iris.washington.edu
IRIS DMC, 1408 NE 45th St, Seattle, WA 98105

As part of a data product development effort, the IRIS DMC is offering higher order data products generated internally or by the community in addition to the raw times series data traditionally managed at the DMC. These products are intended to serve many purposes: stepping-stones for future research projects, data visualizations, data characterization, research result comparisons as well as outreach material. We currently have automated receiver functions (EARS) and two event based products in production: USArray Ground Motion Visualizations (GMVs) and Event Plots. The GMVs and Event Plots are available, along with other products, through our Searchable Product Depository (SPUD).

We are developing or exploring many new products that will be of great interest to the EarthScope community. The Earth Model Collaboration (EMC) will serve as a standardized repository for contributed regional and global tomography models. The EMC allows users to download models as well as generate standard and custom map views, vertical cross sections and depth profiles for any one or multiple models. We are also developing more event-based products. For earthquakes larger than M7.0, we intend to generate back-projection rupture movies using USArray and GSN array geometries. For earthquakes larger than M6.0, we will be generating either body or surface wave source-time functions or both, depending on the magnitude. Finally we plan on generating aftershock sequence animations that include maps, histograms and statistics. These may either be available as user generated custom requests or standardized for all large earthquakes. Example figures and animations for these new event-based products will include results from the recent M9.0 Tohoku event.

More details on these and other existing products are available at:
http://www.iris.edu/dms/products/

Flat slab subduction, continental faults, and surface uplift: 3D numerical models of south-central Alaska

Margarete A. Jadamec*+, Magali I. Billen*, and Sarah M. Roeske*

Plate boundaries are inherently three-dimensional (3D) tectonic features with variations in geometry and physical properties along their length. For example, subduction zones have significant changes in slab dip along strike, including flat slab segments, as in the eastern Alaska subduction zone, the Peru-Chile Trench, and the southwestern Japan Trench. In addition, the lithospheric structure often includes spatial heterogeneity, including major faults inboard of the plate boundary such as the Denali fault, the Altyn Tagh fault, and the North Anatolian fault. Here we present results from regional 3D numerical models of the eastern Alaska subduction-transform plate boundary system that explore the role of the flat slab geometry and the Denali fault on the surface velocity and dynamic topography in south-central Alaska. The shape of the Aleutian-Wrangell slab is defined by Wadati-Benioff zone seismicity and seismic tomography. The thermal structure for both the subducting and overriding plate is based on geologic and geophysical observables, thereby capturing the regional variability in the plate boundary system. We employ a composite viscosity, which includes both the diffusion and dislocation creep mechanisms. The models suggest the flat slab geometry beneath south-central Alaska controls several first order deformation features in the overriding plate, including subsidence in the Cook Inlet Basin. To reproduce the localized uplift observed in the central Alaska Range, the models require a non-Newtonian rheology and a localized lithospheric weak zone representative of the Denali fault, as well as the shallow slab geometry. Models with only a Newtonian viscosity do not reproduce the observed uplift, even when the Denali fault is included. 3D numerical models of this kind can provide a tectonic framework for observational based studies in Alaska as a part of the upcoming EarthScope deployment.

* Geology Department, University of California, Davis, CA 95616 USA
+ School of Mathematical Sciences, School of Geosciences, Monash University, Clayton, VIC 3168 Australia

Contact email: Margarete.Jadamec@ucdavis.edu

Use of Synthetic Receiver Functions to Interpret their Behavior When Encountering Several Boundaries

Helen A. Janiszewski (Rutgers University, New Brunswick, NJ, USA)
helenj78@eden.rutgers.edu
Vadim Levin (Rutgers University, New Brunswick, NJ, USA)
vlevin@rci.rutgers.edu

Analysis of synthetic receiver functions generated for structures containing several layers yields new insights on the determination of the depth and average Vp/Vs in similar complex geologic environments. Teleseismic receiver functions used to determine the depth of the Moho and other crustal features by stacking Ps, Ppms, and Psms multiples typically operate under the assumption that the impedance contrast at a single boundary is much greater than at others beneath the station. However, preliminary results suggest that a stacking method can also reasonably estimate the properties of two interfaces when using stacks of synthetic receiver functions generated with three layers (two above the halfspace). The stacking produces two maximum agreements between the three multiples at depths and Vp/Vs ratios both consistent with the values used to generate the synthetics. This approach is applicable, for example, in areas that contain both the Moho boundary and a mid-crustal discontinuity, such as seen along the Aleutian island arc. Several seismic stations along the arc produce this pattern of two maximum agreements between the multiples.

Furthermore, this modeling technique offers an improved perspective on systematic errors that arise due to using a two-layer technique (one layer over the halfspace) in an area containing multiple layers. Using an incorrect estimate of the average Vp will produce errors of different magnitude for the depth and the Vp/Vs estimates of the two boundaries. Understanding how these errors may be skewed can improve predictions of crustal structure. With the progression of the USArray and creation and expansion of additional seismic networks, new and complex geological environments are currently being explored at a rapid pace. As such, a comprehensive understanding of the seismic techniques used to interpret these structures is essential. Use of these synthetic receiver functions gives invaluable information on how receiver functions can reliably be used to determine properties of the crust where multiple boundaries are present.

Slow Slip Events in Costa Rica Detected by Continuous GPS Observations, 2003-2010

Yan Jiang, Marine Geology and Geophysics, Rosenstiel School of Marine and Atmospheric Science, University of Miami, 4600 Rickenbacker Causeway, Miami, FL, 212300, USA. (yjiang@rsmas.miami.edu)

Shimon Wdowinski, Marine Geology and Geophysics, Rosenstiel School of Marine and Atmospheric Science, University of Miami, 4600 Rickenbacker Causeway, Miami, FL, 212300, USA.

Timothy H. Dixon, University of South Florida, Department of Geology, 4202 E Fowler Ave, Tampa, FL, 33620, USA

Marino Protti, Universidad Nacional Costa Rica – OVSICORI, Heredia, Costa Rica

Victor Gonzalez, Universidad Nacional Costa Rica – OVSICORI, Heredia, Costa Rica

Abstract. A network of continuously operating GPS stations have operated in the Nicoya Peninsula of northern Costa Rica since 2002. A slow slip event was identified here in 2007, releasing accumulated seismic strain equivalent to a M 6.7 – 7.0 earthquake. We reprocessed all available data from this network for the period 2002-2010 to investigate the occurrence of other slow slip events. A new technique that enables us to find slow slip events in the presence of noise is described and applied to the GPS data. We find four significant slow slip events during the 2002-2010 period, defining an average recurrence interval of approximately two years. The data also suggest that, for the 2007 event, slow slip starts near the coast, then migrates inland (down-dip) over a period of ~30 days. The 2009 event has a significantly longer event duration (~ half year) compared to other events.

Did a slow earthquake follow the Jan 12-13, 2011 earthquake series on the San Andreas fault at San Juan Bautista?

Ingrid A. Johanson, Roland Bürgmann, Robert Nadeau, Taka'aki Taira, Pascal Audet,
Berkeley Seismological Laboratory, University of California, Berkeley

The San Juan Bautista section of the San Andreas fault is the transition zone between the creeping section in the south and the locked fault section in the north that last ruptured in the 1906 San Francisco earthquake. It is an area of heterogeneous creep, with locked patches, possibly capable of producing ~M6 earthquakes, embedded in the otherwise creeping fault (*Johanson and Bürgmann*, 2005). It has a history of producing slow earthquakes of about the same size as its largest recorded seismic events. The largest of these is a slow earthquake that followed a $M_W5.1$ seismic event in 1998 and itself has a moment of $M_W5.0$ (*Gwyther et al.*, 2000; *Uhrhammer et al.*, 1999). This slow earthquake was detected by strain- and creep-meters, but was also detectable in data from a nearby BARD continuous GPS station (SAOB). At the time, this was the only continuous GPS station in the region, but since completion of PBO installation, there are several more GPS stations and strainmeters that would be capable of detecting a 1998-like slow earthquake (Figure 1).

A recent series of earthquakes (Jan. 12-13, 2011) on the San Juan Bautista segment were followed several days later by a moderate creep event. We have brought together data from continuous GPS stations from the BARD and PBO networks, creepmeters, strainmeters and seismic data, including repeating earthquakes, to investigate whether the increased surface creep was indicative of a more widespread slip transient and to determine its extent and temporal evolution. The expression of both the earthquake and possible slow earthquake in the GPS data is subtle, but by leveraging multiple data sources we expect to have much better constraints than we could from any one source alone.
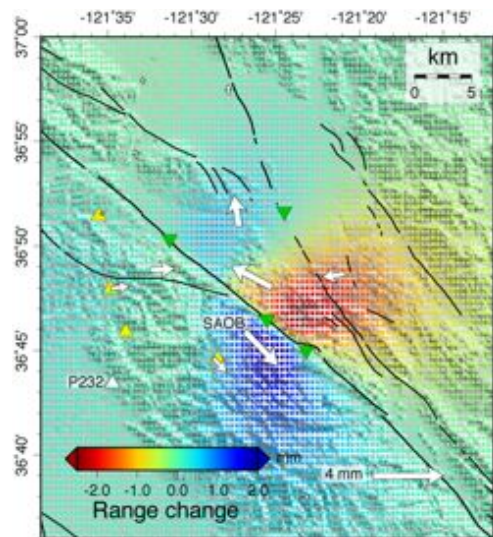

Figure 1: Forward model of 1998 slow earthquake given the current BARD and PBO GPS networks and for InSAR range change. Forward-modeled GPS motions are white arrows and are relative to station P232 (white triangle). Colored points show the projected range change magnitude and extent from the 1998 event. Yellow triangles are PBO borehole strainmeter locations and green triangles are USGS creepmeters.

References

Gwyther, R. L., C. H. Thurber, M. T. Gladwin, and M. Mee (2000), Seismic and aseismic observations of the 12th August 1998 San Juan Bautista, California M5.3 earthquake, paper presented at 3rd San Andreas Fault Conference, Stanford Univ., Stanford, Calif.

Johanson, I. and Bürgmann, R. (2005). Creep and quakes on the northern transition zone of the San Andreas fault from GPS and InSAR data. *Geophys. Res. Lett*, 32.

Uhrhammer, R., L. S. Gee, M. Murray, D. Dreger, and B. Romanowicz (1999), The Mw 5.1 San Juan Bautista, California earthquake of 12 August 1998, Seismol. Res. Lett., 70, 10-18.

The lithosphere structure across the Yellowstone hotspot and the Wyoming craton from S receiver functions

While the Yellowstone Hotspot and the Rocky Mountain region in the western United States have been subjects of many geophysical studies in the past, the neighboring Wyoming craton, covering an area of ~100,000 km^2 in the Wyoming, Montana and Idaho regions, has been largely understudied in deep structure surveys. The USArray component of the EarthScope program has collected a large amount of seismological data in this area, which allows for producing detail images of crust and mantle structure. The goal of this study is to investigate how the lithosphere beneath the Wyoming craton has been modified by the Yellowstone hotspot activity. We applied S receiver function technique at 18 stations of the transportable array in one NE and one EW profiles in Wyoming. S receiver functions can be used to determine seismic discontinuities and is especially useful in determining the lithosphere-asthenosphere boundary (LAB). It is obtained by deconvolving Sv component from P component that are found by coordinate rotation of the original three component seismograms. Individual receiver functions using both S and SKS phases have been analyzed from over 200 events with epicentral distances ranging from 55 to 117 degrees. The receiver functions will be stacked by station along both profiles. Preliminary results indicate a consistent S to P converted phase at ~8-10 s before the S arrival, which is probably associated with the LAB. The variation of the LAB and its tectonic implication will be explored after stacking receiver functions at more stations.

Seismic Analysis of the Tonga Subduction Zone and Implications on the Thermo-Petrologic Evolution of Deep Subduction

Patrick Karel[1], Michael Brudzinski[1], Wang-Ping Chen[2], Harry Green II[3], Robert Pillet[4]

[1]Geology Department, Miami University; [2]Department of Geology, University of Illinois at Urbana-Champaign; [3]Institute of Geophysics and Planetary Physics, University of California at Riverside; [4]IRD, Geosciences Azur, New Caledonia

Utilizing high-resolution waveform analysis of triplicate P and S waves recorded by a broadband seismic array, we show that the subhorizontal, leading-edge ("toe") of the Wadati-Benioff zone (WBZ) in the Tonga subduction zone exhibits characteristics of a petrologic and petrofabric anomaly. Based on seismicity alone, the "toe" clearly connects with the rest of the WBZ and extends westward by about 300 km. The source region of earthquakes exhibits ~1% polarization anisotropy, a phenomenon rarely observed in the mantle transition zone, indicating the existence of a localized petrofabric. High P and S wave speeds (~3%) are expected to accompany the low temperature in the source region of seismicity, yet velocities are low within the anisotropic zone of earthquakes itself, requiring a petrologic anomaly that counteracts the effect of low temperature. In addition, sporadic fault plane solutions from earthquakes defining the toe show no clear pattern, so a localized stress must be responsible for the deep seismicity.

Each component in this unusual collection of observations has also been documented for a zone of so-called outboard earthquakes – a remarkable swath of subhorizontal seismicity that extends over 1,000 km further to the west of the toe. Given the fact that the toe is still connected with the WBZ or the trajectory of active-subducting slab, there seems little doubt that shared properties between the toe and the outboard earthquakes reflect consecutive stages in deep subduction, with the toe being the immediate predecessor of a large-scale remnant of detached lithosphere.

As documented in previous work, the only candidate for a petrologic and petrofabric anomaly that satisfies all available observations is metastable olivine – a buoyant material when present in the transition zone, promoting slab deflection near the 660-km discontinuity and acting as a barrier to deep-slab penetration. Over time, a positively-buoyant, anisotropic thermo-petrologic anomaly would evolve into a negatively-buoyant, pure thermal anomaly. As the petrologic anomaly dissipates with rising temperature over time, so does its anisotropy and seismicity – a prediction borne out by observations of high wave speed, isotropic slab remnants in the aureole surrounding the outboard earthquakes in Tonga, and in many aseismic slab anomalies elsewhere in the mantle transition zone of the western Pacific.

Crust and upper mantle electrical conductivity beneath the Yellowstone Hotspot Track

Anna Kelbert[1], Gary D. Egbert[1] and Catherine deGroot-Hedlin[2]

(1) College of Oceanic and Atmospheric Sciences, Oregon State University, Corvallis, OR, USA

(2) Scripps Institution of Oceanography, University of California, San Diego, La Jolla, CA, USA

We have performed a set of three dimensional inversions of magnetotelluric data in the Snake River Plain and Yellowstone areas. We used a total of 91 sites from Earthscope MT Transportable Array, covering much of Idaho and Wyoming, southern Montana, eastern Oregon and northern Nevada, in addition to 34 sites from an earlier long-period MT survey, collected in two denser profiles along and across the eastern Snake River Plain (SRP). Data for 14 periods from 7.3 secs to 5.2 hours were inverted for 3D inverse conductivity models on a grid with horizontal resolution of 10 km. We obtained a class of models that fit the data adequately and were therefore able to identify the features that were recovered robustly. After removal of outliers in the data, our preferred model (Figure 1) fits both the impedances (with 5% error floors) and the vertical magnetic transfer functions to an RMS of 1.8.

The images reveal the presence of a large, interconnected conductive body beneath the Eastern and central SRP. Consistent with the surface-wave [Pollitz & Snoke 2010; Obrebski et al. 2011] and ambient noise [*Gao et al.*, 2011] tomography, we resolve highly anomalous upper mantle beneath the Yellowstone hotspot track at lithospheric depths. However, in contrast to the seismic wave velocities which stay negative to 200-250 km depth, the electrical conductivity anomaly peaks in the uppermost mantle around 40-80 km depth. There, conductivities of the order of 0.1 S/m or higher are present. These conductivities are too high to be explained by maximum 1% partial melt content usually estimated in this area [e.g., Leeman et al. 2009], unless we also allow for the presence of volatiles such as water, or alternative explanations such as carbonatite melts. Our resolution of the deeper asthenosphere is limited below the SRP, but the conductivities stay elevated throughout the upper mantle, with at least 0.02 S/m beneath the Wyoming craton in the Yellowstone vicinity. The seismically imaged thermal anomaly [Obrebski et al., 2011; Smith et al., 2009; Yuan & Dueker, 2005] interpreted as the Yellowstone plume is likely to be poorly resolved by the MT data, which are much more strongly impacted by partial melt and fluids present at shallower depths.

The lithospheric anomaly extends to at least 200 km southwest of Yellowstone, roughly parallel to the direction of North America absolute motion. The anomaly connects to the near-surface in several

locations along and to the North of the SRP, as well as directly beneath the Yellowstone caldera. There, highly conductive (~ 1 S/m) shallow anomalies are to be found. This leads us to believe that the complex lithospheric feature beneath the SRP represents a partially molten magma reservoir, possibly rich in volatile constituents, that feeds the Yellowstone hotspot. Additionally, in several locations beneath the Eastern SRP very high conductivities (a few S/m) are imaged at or near the base of the lower crust. These can probably be explained by a combination of partial melt, and highly saline fluids exsolved during magmatic underplating.
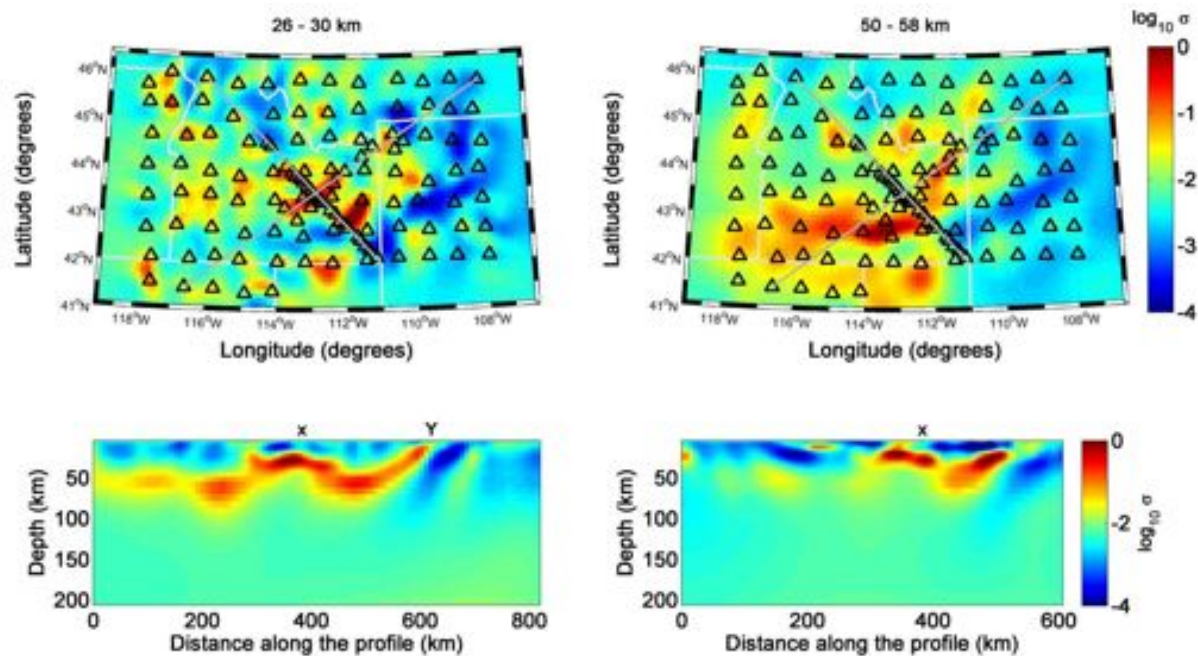

Figure 1: Inferred electrical conductivity distributions for representative depths in the lower crust and uppermost mantle. Two profiles of higher station density (grey lines) along (bottom left) and across (bottom right) the eastern SRP are also shown. Crosses indicate their point of intersection; Yellowstone caldera's Sour Creek Dome is indicated by the letter Y.

Our model suggests that the state of the uppermost mantle beneath the eastern SRP needs to be re-evaluated in terms of melt content and possibly the presence of free volatiles. The modest temperature anomaly estimated for the Yellowstone plume [Leeman et al. 2009; Adams & Humphreys 2010] even in conjunction with up to 1% partial melt does not provide an adequate explanation for the high conductivities imaged at lithospheric depths beneath the Yellowstone hotspot track.

References:

Adams, D. C., and E. D. Humphreys (2010), New constraints on the properties of the Yellowstone mantle plume from P and S wave attenuation tomography, *Journal of Geophysical Research*, *115*(B12), B12311--. [online] Available from: http://dx.doi.org/10.1029/2009JB006864

Gao, H., E. D. Humphreys, H. Yao, and R. D. van der Hilst (2011), Crust and lithosphere structure of the northwestern U.S. with ambient noise tomography: Terrane accretion and Cascade arc development, *Earth and Planetary Science Letters*, *304*(1-2), 202-211, doi:10.1016/j.epsl.2011.01.033. [online] Available from: http://linkinghub.elsevier.com/retrieve/pii/S0012821X11000598 (Accessed 22 March 2011)

Leeman, W. P., D. L. Schutt, and S. S. Hughes (2009), Thermal structure beneath the Snake River Plain: Implications for the Yellowstone hotspot, *Journal of Volcanology and Geothermal Research*, *188*(1-3), 57-67, doi:DOI: 10.1016/j.jvolgeores.2009.01.034. [online] Available from: http://www.sciencedirect.com/science/article/B6VCS-4VP667P-1/2/83f669bdbd6998a076c04e868606531f

Obrebski, M., R. M. Allen, F. Pollitz, and S.-H. Hung (2011), Lithosphere-asthenosphere interaction beneath the western United States from the joint inversion of body-wave traveltimes and surface-wave phase velocities, *Geophysical Journal International*, no-no, doi:10.1111/j.1365-246X.2011.04990.x. [online] Available from: http://doi.wiley.com/10.1111/j.1365-246X.2011.04990.x (Accessed 28 March 2011)

Pollitz, F. F., and J. A. Snoke (2010), Rayleigh-wave phase-velocity maps and three-dimensional shear velocity structure of the western US from local non-plane surface wave tomography, *Geophysical Journal International*, *180*(3), 1153-1169, doi:10.1111/j.1365-246X.2009.04441.x. [online] Available from: http://doi.wiley.com/10.1111/j.1365-246X.2009.04441.x (Accessed 25 January 2011)

Smith, R. B., M. Jordan, B. Steinberger, C. M. Puskas, J. M. Farrell, G. P. Waite, S. Husen, W.-L. Chang, and R. O Connell (2009), Geodynamics of the Yellowstone hotspot and mantle plume: Seismic and GPS imaging, kinematics, and mantle flow, *Journal of Volcanology and Geothermal Research*, *188*(1-3), 26-56, doi:DOI: 10.1016/j.jvolgeores.2009.08.020. [online] Available from: http://www.sciencedirect.com/science/article/B6VCS-4X5JSS3-1/2/29d05cc90f7cef363c4df04b687b56a6

Yuan, H., and K. Dueker (2005), Teleseismic P-wave tomogram of the Yellowstone plume, *Geophysical Research Letters*, *32*, 7304-+, doi:10.1029/2004GL022056.

The Meers Fault: A prominent Holocene scarp in southern Oklahoma with a history of repeated movement

G. Randy Keller and Hamed Al-refaee
College of Earth and Energy, University of Oklahoma

The Meers Fault is the only documented Holocene fault scarp east of Colorado. It is the southernmost element of the complex and massive (>10 km of throw) frontal fault zone that forms the boundary between the Anadarko basin, which is the deepest intra-continental basin in the United States, and the uplifted igneous rocks of the Wichita Mountains. The most recent movement occurred 1100-1300 years ago with an earlier movement 2,000-2,900 years ago. There is as much as 5 m vertical and probably appreciably more left-lateral strike slip displacement on the fault. Motion on the Meers Fault represents continued activity on one of the largest structural features in North America. The Wichita uplift and the Anadarko basin, which are separated by the Meers Fault and related sub parallel fault strands, indicate significant intra-plate deformation along the trend of the Southern Oklahoma aulacogen, which is a classic example of a failed and massively inverted rift. In addition to the tectonic significance of these structures in Oklahoma, two well dated, late Holocene events occurred on the Meers Fault and another in the middle-Pleistocene. As such, this fault represents one of the highest potential seismic hazards in the central/eastern United States. However, its relative seismic quiescence is in contrast with the fact that Oklahoma has a well-documented history of seismicity elsewhere with more than 600 events being located in 2010, including a 4.7 $M_b$lg event in October that was felt from Kansas City to Dallas.

A phenomenological description of stress-driven melt segregation for application to experimental data and geodynamic models: Steady-state viscosity with partitioned deformation

Daniel S.H. King - Penn State University (dking@psu.edu)
Benjamin K. Holtzman - Lamont-Doherty Earth Observatory
David L. Kohlstedt - University of Minnesota

Experimental studies have demonstrated significant interactions between deformation and melt distribution in partially molten rocks. Driven by pressure gradients that develop when a partially-molten rock is sheared, melt segregates into melt rich bands at a low angle to the macroscopic shear plane and synthetic to the shear direction. The melt-rich bands act as zones of localized deformation, significantly reducing the overall strength of the rock. A major focus of experimental studies has been to constrain the length scales of this process, which depend upon the permeability of the rock as well as the viscosities of the solid and liquid. In this contribution, we explore the effects of melt segregation on the rheological properties of partially molten rocks. In the Earth, the effects of a small amount of melt could vary significantly depending upon the degree of segregation. Quantifying the effects of segregated melt on the rheological properties of Earth materials could be critical to understanding the nature of the lithosphere-asthenosphere boundary and the dynamics of other regions where deformation and magmatism interact. The difficulty in understanding the roles of stress-driven melt segregation in the Earth is that it occurs at the meso-scale. Laboratory-based flow laws describe processes at the grain scale, smaller than the length scales of melt segregation, while geodynamic models describe processes at much longer length scales. Here, we discuss the segregation factor, S, that describes melt distribution in an average sense. We also present a framework for the homogenization of viscosity for layered media, which yields effective constitutive equations as a function of S. We apply this approach to gain insights from experimental data and discuss settings in the Earth where the possible effects of melt segregation could be explored.

Back-Projection Results for the March 11, 2011 Tohoku, Japan Earthquake

Eric Kiser and Miaki Ishii

Department of Earth and Planetary Sciences

Harvard University

20 Oxford St.

Cambridge, MA 02138

kiser@fas.harvard.edu

The March 11, 2011 Mw 9.0 Tohoku, Japan earthquake is investigated using a back-projection method applied to data from the USArray Transportable Array. In addition to investigating the mainshock, we perform a continuous back-projection analysis of data from March 9, 2011 to March 12, 2011. This approach allows us to more accurately determine the rupture distributions of foreshocks and aftershocks with respect to the mainshock distribution.

Our results show that the mainshock lasted about 220 seconds and had rupture dimensions of 250 km by 175 km. Most of the energy release during the mainshock occurred in the first 110 seconds near the downdip edge of the seismogenic zone. These rupture dimensions are small for a Mw 9.0 earthquake, which suggests relatively high stress drop. Comparing these results with historic seismicity shows that the 2011 event ruptured four segments of the plate interface that have individually produced tsunamigenic earthquakes in the past 150 years.

In addition to the mainshock, continuous back-projection results show that large segments of the plate interface ruptured during the March 9th Mw 7.3 foreshock and the two hours of aftershocks directly following the March 11th mainshock. Including these episodes of rupture leads to a total rupture area that is almost three times that of the mainshock alone. Given the closeness in time of the different ruptures, we hypothesize that this almost total failure of the plate interface nearly occurred during a single event with a moment magnitude of 9.4.

Frictional behavior of the CDZ gouge at seismic slip rates

Hiroko Kitajima[1], Melodie E. French[2], Judith S. Chester[2], Frederick M. Chester[2], and Takehiro Hirose

[1] *Department of Geosciences and Energy Institute, The Pennsylvania State University, USA*
[2] *Center for Tectonophysics and Department of Geology & Geophysics, Texas A&M University, USA*
[3] *Kochi Core Center Japan Agency for Marine-Earth Science and Technology, Japan*

The lack of a heat flow anomaly and the large angle between the San Andreas Fault and the maximum principal compressive stress orientation has led scientists to conclude that the fault system is weak. However, the strength of the fault and the weakening mechanisms are still debated. Recent friction experiments on fault gouge recovered from the Central Deforming Zone (CDZ) at SAFOD show small friction coefficients (0.14-0.2) and velocity-strengthening behavior at low slip rates (0.01-300 micron/s) [Carpenter et al., 2010, 2011; Lockner et al., 2011; Coble, 2010]. Although these findings are consistent with observations of active creep and a weak San Andreas Fault, the frictional behavior of the fault gouge at seismic slip rates and the possibility of seismic slip along the actively creeping segment have not been studied experimentally.

In order to characterize the frictional behavior of CDZ fault rocks at seismic slip rates, we conducted friction tests on SAFOD core samples at slip velocities of 0.1-1.3 m/s and normal stresses of 0.3-1.5 MPa. Flaked fault gouge from the CDZ and disaggregated samples of four distinct fault rocks from the 3067 m MD subsidiary fault were deformed in a high-speed rotary-shear apparatus at Japan Agency for Marine-Earth Science and Technology (JAMSTEC) Kochi Core Center (KCC). Samples were sheared between host blocks of gabbro under both room-humidity (dry) conditions and water-dampened conditions. The 3067 m fault samples sheared at 1.3 m/s have peak friction coefficients of 0.5-0.6, which decrease to steady state values of 0.05-0.12 after approximately 10 m of slip. The frictional behavior is similar to that of Punchbowl fault ultracataclasite reported by Kitajima et al. [2010]. On the contrary, the CDZ samples shows peak friction coefficients of approximately 0.3 and steady-state friction coefficients of 0.29 (0.1 m/s), 0.2 (0.35 m/s), and less than 0.02 (0.7 and 1.3 m/s). The friction coefficients of the CDZ at both low and high slip-rates are small relative to the other fault-rocks sampled at SAFOD. The low coefficients of friction for the actively creeping CDZ are consistent with the lack of a heat flow anomaly near the San Andreas Fault. The low peak friction coefficient at the onset of rapid slip implies a small mechanical barrier to dynamic rupture propagation along the creeping segment. Although the CDZ currently is creeping, the high-speed friction results suggest that seismic slip in this material also is possible.

Title: Space-Time Variations in Cascadia Tremor Amplitude

Authors: Amanda Klaus[1*], Ken Creager[1], Justin Sweet[1], Aaron Wech[2]
Affiliations: [1]University of Washington
                  [2]University of Victoria, Wellington
*Contact: aklaus@u.washington.edu

We present a new analysis of seismic energy based on tremor amplitudes in Washington state. The seismic energy release of non-volcanic tremor has not been fully quantified due to the complex nature of tremor. However, understanding the pattern of energy release is an important piece of the tremor puzzle. For larger ETS (episodic tremor and slip) events, the duration of tremor is observed to be a good proxy for slow slip seismic moment as estimated geodetically (Aguiar et al. 2009, Wech et al. 2010). Tremor duration, however, does not tell the whole story. For example, even during times of near-continuous tremor, amplitudes have been observed to be strongly modulated by tidal forcing (Rubinstein et al. 2008). We extend these past observations to a new data set in order to better understand this tidal forcing. Similarly, energy-based analyses shed light on what happens at the onset of tremor. Tremor amplitudes typically ramp up during the early days of a large tremor episode, perhaps as the faulted area grows. Quantifying released seismic energy is also a component of determining how slow slip events fit into earthquake scaling laws; the question of whether accumulated energy is a better measure of slip than event duration is an open question. In the future, we will further address this question by comparing spatial variations in energy release across different ETS events. Spatial patterns in patches of concentrated seismic energy release may have implications for the distribution of slip and the mechanism of tremor.

High-Resolution Strain Rate Models for the American Southwest and Alaska

Corné Kreemer[1] and Elliot C. Klein[1]

As part of the Global Earthquake Model (GEM) project (www.globalquakemodel.org), there is a need for geodetically constrained, high-resolution, strain rate models of plate boundary zones. These models can be used to assess the completeness of the moment rate budget implied by Quaternary faulting data bases and earthquake productivity rates, which are the typical foundations of any seismic hazard model. The ultimate goal is to create strain rate models that best satisfy the geodetic, geologic, and seismic observations simultaneously. Such models could reveal any significant discrepancy between Quaternary faulting slip rates and geodetic observations, and could constrain the maximum expected magnitude in light of a Gutenberg-Richter or Characteristic Earthquake distribution of seismicity.

We present strain rate models for southwestern North America and Alaska based on geodetic, geologic, and seismic observations. When solving for a continuous velocity gradient tensor field that best matches the horizontal GPS velocities, we use the seismic and geologic data as apriori constraints on the strain rate model covariance matrix. These constraints are essential to damp the solution, guarantee equal data fit in low and high straining regions, and avoid aliasing the strain rate model as a result of the uneven spacing of GPS stations. For the a priori strain rate variances, we use Quaternary fault slip rates from the USGS where available, and for all "non-faulting" cells of our model grid we combine unit summed moment tensors with strain rates associated with the moment release rate given an area's a- and b-value and assumed maximum moment. We will show results for this preferred model, but will also present the strain rate models that are based on either the geologic or seismic data alone. We will briefly discuss the significant differences between these models in terms of using these data sets in seismic hazard modeling.

[1]Nevada Bureau of Mines and Geology / MS 178
University of Nevada, Reno
Reno, Nevada 89557-0178, USA

Rupture Imaging of Recent Giant Earthquakes Using P-waves Recorded Across USArray: How Array Geometry and Frequency Band Affect Resolution

Keith D. Koper, University of Utah, Salt Lake City, UT (koper@seis.utah.edu)
Alex R. Hutko, Inc. Research Institutions for Seismology, Seattle, WA, (ahutko@gmail.com)
Thorne Lay, University of California Santa Cruz, Santa Cruz, CA, (tlay@ucsc.edu)
Charles J. Ammon, The Pennsylvania State University, University Park, PA (cja12@psu.edu)
Hiroo Kanamori, California Institute of Technology, Pasadena, CA (hiroo@gps.caltech.edu)

The rupture process of two recent giant earthquakes (M8.8 Chile in Feb. 2010 and M9.0 Japan in March 2011) is examined using back-projection of P waves recorded across USArray. In particular, we focus on the effects that array geometry and frequency band have on the details of the rupture images. A key issue is whether the short-period image of the source as determined from backprojection of P waves is significantly different than the long-period image of the source determined from inversions of continuous GPS, teleseismic body and surface waves, and tsunami observations. Preliminary work on both earthquakes has found evidence for a segmentation of the megathrust boundary in which short-period energy is preferentially radiated down-dip of the longer-period energy that contributes to the bulk of the moment release and tsunamigenesis. The backprojection is carried out in a series of overlapping frequency bands that vary from 0.2-2.0 Hz in which bandpass filters are applied after the alignment of the initial segments of the unfiltered P waves. For each frequency band, station weights are chosen that yield an array response function closest to a delta function in a least-squares sense. The resulting images are compared to those determined using uniform weights across all of USArray, and a spatially desampled version of USArray. Our results support the idea of segmentation for the Japan earthquake, but are more ambiguous for the Chile earthquake.
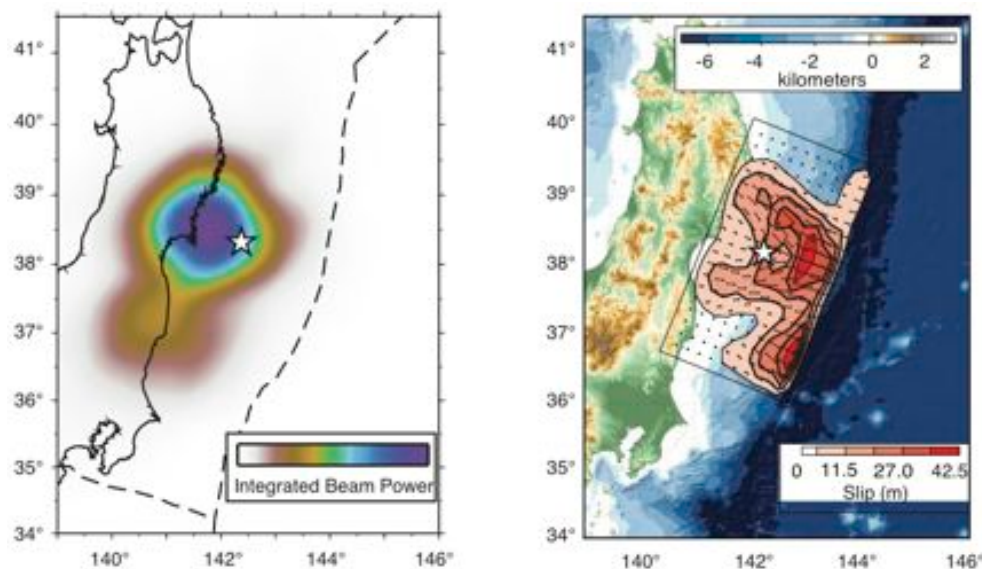
*Rupture Models of the 2011 Tokohu-oki M_w 9.0 earthquake. **(left)** Time integrated beam power from backprojection of short period P-waves recorded by USArray. **(right)** Seismically determined finite-fault rupture model developed from broadband teleseismic P-waves. In each panel the white star indicates the USGS epicenter. The dashed lines in the left panel show regional plate boundaries.*

New GPS Network to Measure the Motion and Deformation of the Colorado Plateau

C. Kreemer (University of Nevada, Reno), J. Broermann and R. Bennett (University of Arizona)

The Colorado Plateau, southwestern U.S., has played an important role in the geologic evolution of the Pacific-North America plate boundary zone. Unlike most other parts of the western U.S., the Colorado Plateau has remained largely intact during most of its geologic history, while significant extension has occurred in the Basin and Range to the plateau's west and south. The area has few active earthquake faults. However, earthquakes do happen within the Colorado Plateau, and some very large ones have occurred in southern Arizona and northern Mexico.

We installed 34 new continuous GPS stations in Arizona, southern Utah, and southeastern Nevada in 2010/11 (see figure). Many stations are in National Parks and Monuments and state parks. These stations complement and densify the long-running continuous GPS stations of NSF EarthScope's Plate Boundary Observatory. The additional stations are needed to create well-constrained kinematic models to describe the region's present-day tectonics. With a well-constrained model of the deformation can we investigate the origin of the motion and deformation of the Colorado Plateau. Some of the models that are considered include a rigid motion of the plateau causing opening of the Rio Grande Rift, crustal extension encroaching into the plateau due to evolving mantle processes, extension in the plateau due to stresses associated with crustal thickness variations, and the effect of Pacific plate motion on the deformation of the southern Basin and Range.

We will present an overview of the network, science goals, and the most up-to-date results using other GPS stations.
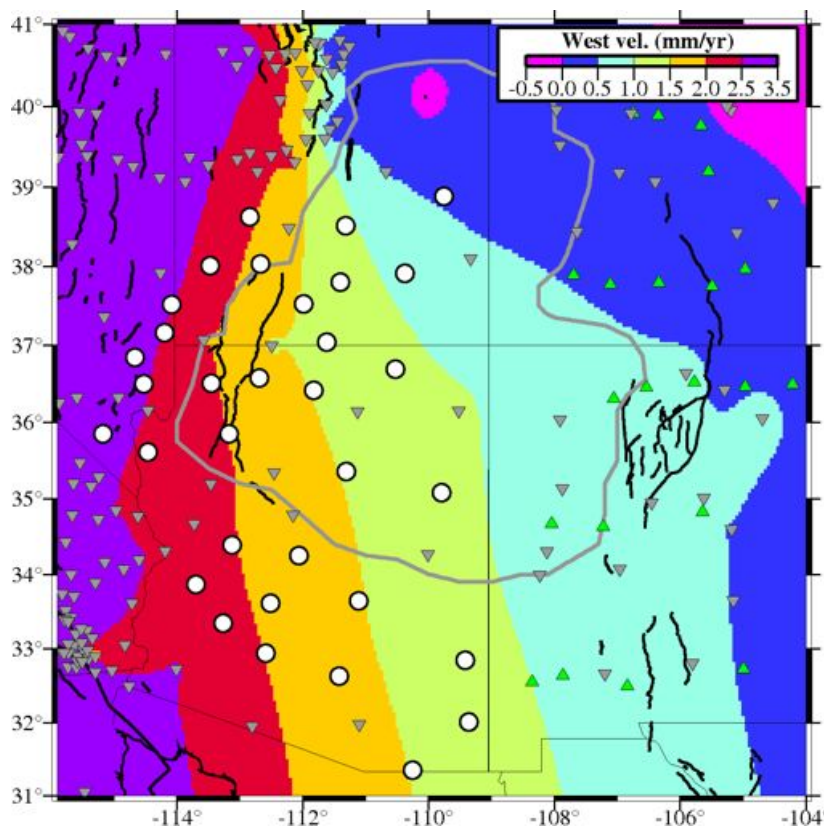
Left: colors indicate a model of the westward motion of SW U.S. relative to North America based on few long-running GPS stations. Colorado Plateau outline in grey. White circles are stations installed by this project (station in Capitol Reef, NP, shown above), grey triangles are (mostly) EarthScope stations and green triangles are stations from EarthScope's Rio Grande Rift project.

Scientific Problems and Lithospheric Targets for the Northern Mississippi Embayment

Charles A. Langston[1]
Heather R. DeShon[1]
Stephen P. Horton[1]
Christine A. Powell[1]
Robert B. Herrmann[2]
Charles J. Ammon[3]
William A. Thomas[4]

[1] Center for Earthquake Research and Information
[2] St. Louis University
[3] Pennsylvania State University
[4] University of Kentucky

Passage of the EarthScope TA stations across the Mississippi Embayment (ME) provides an opportunity to investigate lithospheric structure associated with active deformation and an ancient, major, intracratonic rift. The ME is a first-order geological structure of the North American continent but the reason for basin subsidence is enigmatic; subsidence began in Late Cretaceous and is not linked to a major tectonic episode. The lithosphere below the ME has a long and complex geological history of rifting, uplift, and subsidence over at least two Wilson cycles. In addition, the active New Madrid seismic zone (NMSZ) is located in the upper crust below the northern ME. We suspect that lithospheric heterogeneity ultimately controls the dynamic processes associated with ME subsidence and the NMSZ. We further suspect that the mantle lithosphere will show anomalous heterogeneity related to surface features and buried Phanerozoic rift geology. Investigating ancient failed rift lithospheric structure helps constrain the mantle dynamics associated with the rifting process. Major issues we wish to address are 1) the primary differences in lithospheric structure between the ME and the surrounding region, 2) the nature of early Cambrian rifting and relationship to pre-existing structure, 3) the dynamic processes responsible for ME subsidence, and 4) the relationship of the NMSZ to lithospheric structure. Joint interpretation of compressional and shear velocity tomography, potential fields, transfer/receiver functions, and depth-dependant anisotropy images generated using traditional and new techniques, should help unlock the enigma of the NMSZ and reveal how ancient tectonic events continue to influence the present via inherited lithospheric structure.

PBO H2O: Plate Boundary Observatory Studies of the Water Cycle

Authors: Kristine M. Larson, Eric E. Small, John J. Braun, Felipe Nievinski, Clara Chew, Ethan Gutmann, and Valery Zavorotny

The Plate Boundary Observatory was built to measure mm changes in position of GPS stations over time periods of days to years. The resulting station velocities derived from these data provide important constraints on how the North American continent is deforming. PBO stations can also be used to measure ground displacements at much higher frequencies (5-Hz) for studies of fault slip during large earthquakes (Hammond et al., 2011) and for warnings of volcanic eruptions (Cervelli et al., 2006). There is also a long history of using atmospheric delays on the GPS signals to estimate precipitable water vapor (for weather and climate studies) and total electron content (space weather studies). Now that the PBO network has been completed, new and innovative uses of these GPS data have been demonstrated which are providing a strong link between this new, state of the art geodetic facility and non-geodetic fields of research, specifically water cycle research. It is now clear that PBO data are sensitive to signals that reflect from the nearby environment. These GPS reflections can thus be used for water cycle studies by measuring how much water is in the soil, how much snow is on its surface, and the water content of vegetation surrounding the GPS station (Larson et al., 2008; Larson et al, 2009; Small et al., 2010). Observing and monitoring spatial and temporal changes in the water cycle is critical for both understanding and predicting the Earth's climate. Since GPS reflections encompass an area of ~1000 m^2, they provide a spatial footprint that complements satellite systems which sense much larger areas and in situ systems that sense regions < 1 m^2. After summarizing the techniques used for GPS reflection research, we will update the EarthScope community on our new results for snow and vegetation sensing.
See also http://xenon.colorado.edu/reflections/GPS_reflections/PBO_H2O.html

Continuing Colorado Plateau Uplift by Delamination-Style Convective Lithospheric Downwelling

A. Levander[1], B. Schmandt[2], M. S. Miller[3], K. Liu[1], K. E. Karlstrom[4], R. S. Crow[4], C.-T. A. Lee[1] & E. D. Humphreys[2]

[1]Earth Science Department, Rice University, Houston, Texas 77005-1892, USA. (alan@rice.edu, lkjcammit@gmail.com, ctlee@rice.edu)

[2]Department of Geological Sciences, University of Oregon, Eugene, Oregon 97403, USA. (bschmand@uoregon.edu, genehumphreys@gmail.com)

[3]Department of Earth Sciences, University of Southern California, Los Angeles, California 90089-0740, USA. (msmiller@usc.edu)

[4]Department of Earth and Planetary Sciences, University of New Mexico, Albuquerque, New Mexico 87131, USA. (kek1@unm.edu, crow.ryan@gmail.com)

We've combined finite-frequency teleseismic P and S body wave and Rayleigh wave tomography with PdS and SdP receiver functions to image the west-central Colorado plateau. The images, made largely with USArray data, resolve a high-velocity drip extending from the base of the crust to more than 200 km depth The upper surface of the delaminating body, very clearly defined by the PdS receiver functions, dips from the lower crust to depths of 70-90 km. The base of the crust above the drip has a shape almost identical to the top of the drip, with an elevated Moho and a low seismic contrast.   The structure appears to us to be an ongoing delamination-style downwelling of the lowermost crust and the pre-existing, Proterozoic age Colorado plateau continental lithospheric mantle. The structure of the lithosphere-asthenosphere boundary (LAB), imaged with the receiver functions and the Rayleigh wave tomography support this view.

We associate this delamination feature with Pliocene and ongoing uplift of the Colorado Plateau, and envision uplift driven by a succession of these events propagating inward from the Plateau margins, associated with the magmatic invasion of the Colorado Plateau from its margins.   Petrologic and geochemical observations suggest that Laramide-age lithospheric hydration weakened this lithosphere and that mid-Cenozoic to Recent magmas infiltrated the Colorado plateau mantle, creating the negative buoyancy required to destabilize the lithosphere. Using Grand Canyon incision rates and Pliocene basaltic volcanism patterns, we suggest that substantial plateau uplift resulted from the underlying delaminations over the last ~6 Ma. We also note that hydration of a craton with subsequent magmatic invasion of melts that freeze to increase the bulk density of the lithosphere can be a general means to destabilize a craton.

High-Resolution Characterization of Fault Damage and Healing at SAFOD Viewed by Fault-Zone Trapped Waves

Yong-Gang Li[1], Peter E. Malin[2], Elizabeth S. Cochran[3]and Po Chen[4]

[1]Department of Earth Sciences, University of Southern California, Los Angeles California 90089, USA

[2]Institute of Earth Science and Engineering, University of Auckland, Auckland 1142, New Zealand

[3]Department of Earth Sciences, University of California-Riverside, Riverside California 92521, USA

[4]Department of Geology and Geophysics, University of Wyoming, Wyoming 82071, USA

Abstract

Highly damaged rocks within the San Andreas fault (SAF) at Parkfield form a low-velocity waveguide to trap seismic waves. The amplitudes and dispersion feature of trapped waves are sensitive to the geometry and physical properties of the fault zone due to the constructive interference conditions of these waves. We use fault-zone trapped waves (FZTWs) generated by earthquakes and explosions and recorded at surface and borehole seismographs at the San Andreas Fault Observatory at Depth (SAFOD) site (Fig. 1) to document fault zone structure and rock damage at seismogenic depths with high-resolution. Observations and 3-D finite-difference simulations of these FZTWs at dominant frequencies of 2-10 Hz (Fig. 2 to Fig. 7) show the downward tapering SAF characterized by a 30–40-m wide fault core with the maximum velocity reduction up to ~50% embedded in a 150–200-m wide zone with velocities reduced by 25-40% in average from wall-rock velocities. The width and velocity reduction of the damage zone at 3 km depth delineated by FZTWs are verified by the direct measurements in SAFOD drilling and logging studies at this depth [*Hickman et al.*, 2007] (Fig. 4). The results indicate the localization of severely damaged rocks along the SAF caused by historical earthquakes, including the 2004 *M*6 event on it. The magnitude of damage varies with depth and along the fault strike due to rupture distributions and stress variations over multiple length and time scales. The damage is not symmetric across the main slip plane but extends farther on the southwest side of the main fault trace. Based on the depths of earthquakes generating prominent FZTWs, we estimate that the low-velocity damage zone along the SAF at Parkfield extends at least to depths of ~7-8 km.

Fig. 1 Location of the study area (box in inset map). Circles denote ~350 aftershocks of the 2004 *M*6 Parkfield earthquake, signals from which were recorded at the SAFOD borehole seismographs. The aftershocks marked by black outlines occurred within the fault zone and are divided into 5 groups based on epicentral distance from the SAFOD site. Grey dots are 120 microearthquakes and stars are 5 explosions SP1-SP5, signal from which were recorded at the surface seismic array deployed near the SAFOD site in 2003. Event A, the SAFOD drilling target, occurred at ~3 km depth while Events B, C and D are deep events occurring within and away from the fault zone were recorded at the SAFOD surface array in 2003. Two explosions PMM and PARK detonated within the fault zone, signals from which were recorded at the cross-fault array deployed ~1.5 km northwest of the town of Parkfield in the experiment in 2002 [*Li et al.*, 2004].
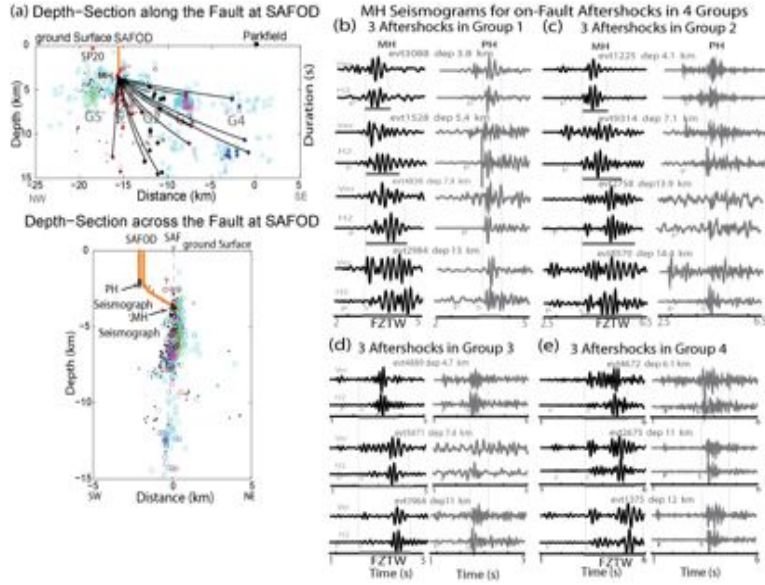
Fig. 2 (a) Depth-sections along and across the SAF, showing the locations of ~350 aftershocks (circles) of the 2004 *M*6 Parkfield earthquake recorded at the SAFOD main-hole (MH) seismograph located at ~3 km depth on the SAF and pilot hole (PH) seismographs. The aftershocks are grouped into G1 to G5. Black lines denote ray paths between SAFOD MH seismograph and aftershocks in 4 groups shown in (b) to (e). Vertical and horizontal seismograms recorded at the MH and PH for aftershocks occurring within the fault zone at different depths in 4 groups with different epicentral distance ranges. **(b)** Aftershocks in G1 located at 1-2 km SE of the array, **(c)** G2 located at 4-6 km SE of the array, **(d)** G3 at 8-10 km SE of the array, **(e)** G4 at 14-16 km SE of the array. Earthquakes are ordered by source depth and aligned on the *S*-arrival. Event index and focal depths are listed above the seismograms. Seismograms have been <6 Hz filtered and are normalized by amplitude. Prominent FZTWs with large amplitudes and long wavetrains are observed after *S*-arrivals in MH seismograms while the high-frequency body waves with brief wavetrains are dominant in PH seismograms.
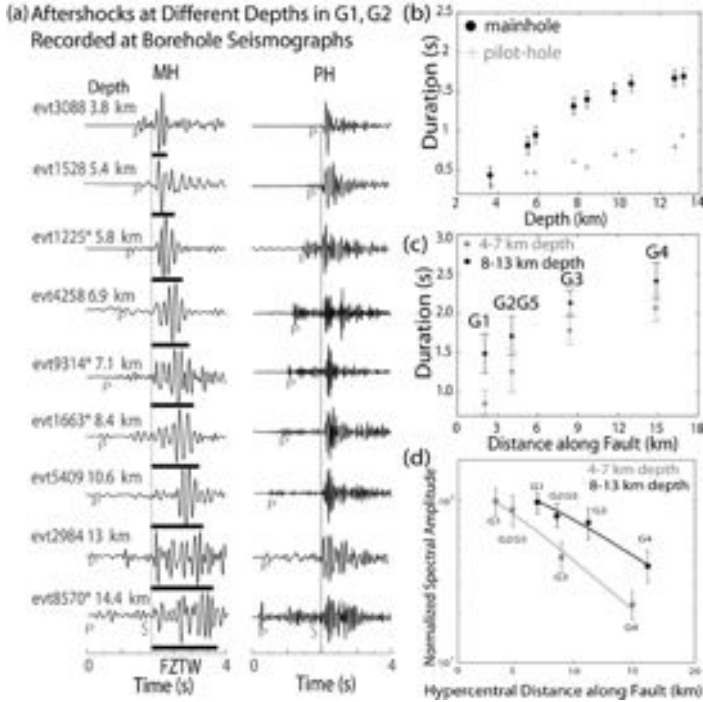

Fig. 3 (a) Vertical-component seismograms recorded at the SAFOD MH and PH seismographs for 9 on-fault aftershocks at different depths in groups G1 and G2. Traces are aligned at *S*-arrivals. Seismograms have been <6 Hz filtered. **(b)** Measured FZTW durations from the MH (black dots) and PH (grey crosses) seismograms plotted versus focal depths for 9 on-fault aftershocks in groups G1 and G2. Each data point is the average FZTW duration measurements on the 3 component earthquake data. Error bars indicate standard deviations of the measured durations. **(c)** Measured FZTW durations from MH seismograph for ~80 aftershocks in groups G1–G5 versus epicentral distance from the SAFOD site. Each data point is the averaged for all on-fault aftershocks in each group. Violet and red dots denote the measurements for aftershocks occurring at depths of 4-7 km and 8-13 km, respectively. Error bars indicate standard deviations of the measured durations in each group. **(d)** Normalized spectral amplitudes of FZTWs versus hypocentral distances for aftershocks in 5 groups G1 – G5. Each point denotes the mean of coda-normalized spectral amplitude peaks at 4-8 Hz at the SAFOD MH seismograph. We fit the measurements using the formula $\ln(A_1/A_i) = \pi f (r_i - r_1)/QV_s$. Spectral amplitudes of trapped waves are multiplied by a factor of $(r_i/r_1)^{1/2}$, $i = 1$, n, to correct for geometrical spreading. The light line fits the data for shallow events at depths of 4-7 km using Q of 30 while the black line fits the data for deep events at depths of 8-13 km using Q of 60.
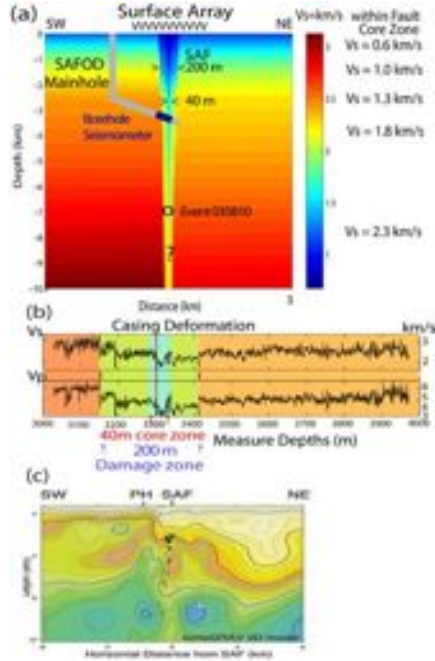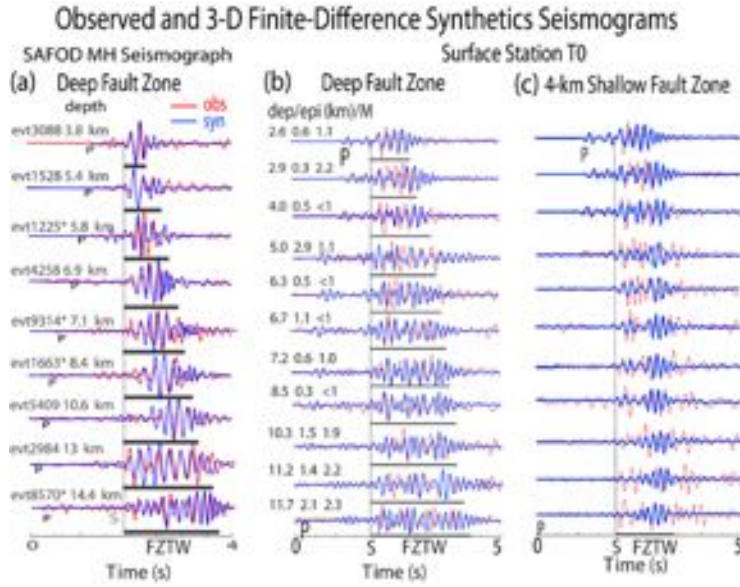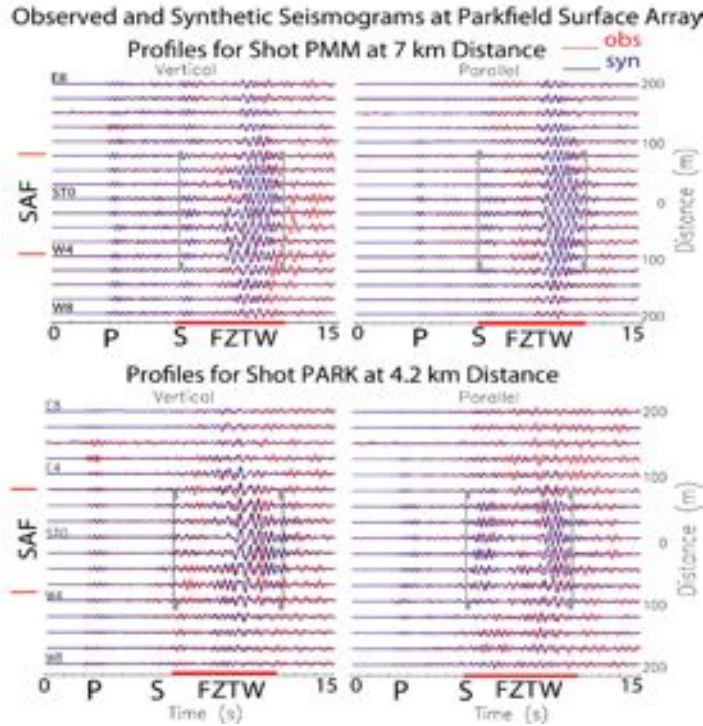
Fig. 4 (a) Cross-section of the *S*-wave velocity model across the SAF used to compute synthetic fault-zone trapped waves (FZTWs). The velocities within the 100-200-m wide waveguide on the SAF and surrounding rocks were found by 3-D finite-difference fits to the FZTWs generated by explosions and aftershocks. Model parameters are listed in Table 1. **(b)** SAFOD drilling log data showing a 40-m fault core surrounded by a 200 m low velocity zones [*Hickman et al.*, 2007]. The red line indicates the location where fault creep is deforming the borehole casing. **(c)** The cross-section through the SAFOD site from the tomography DD 3D velocity model [*Thurber et al.*, 2004]. Earthquakes within 1 km of the section are shown (filled circles), and the positions of the Pilot Hole (PH) and SAF trace (SAF) are indicated. Depths are relative to sea level. The 0.2 contour of the diagonal element of the model resolution matrix is shown in the result (dashed line).
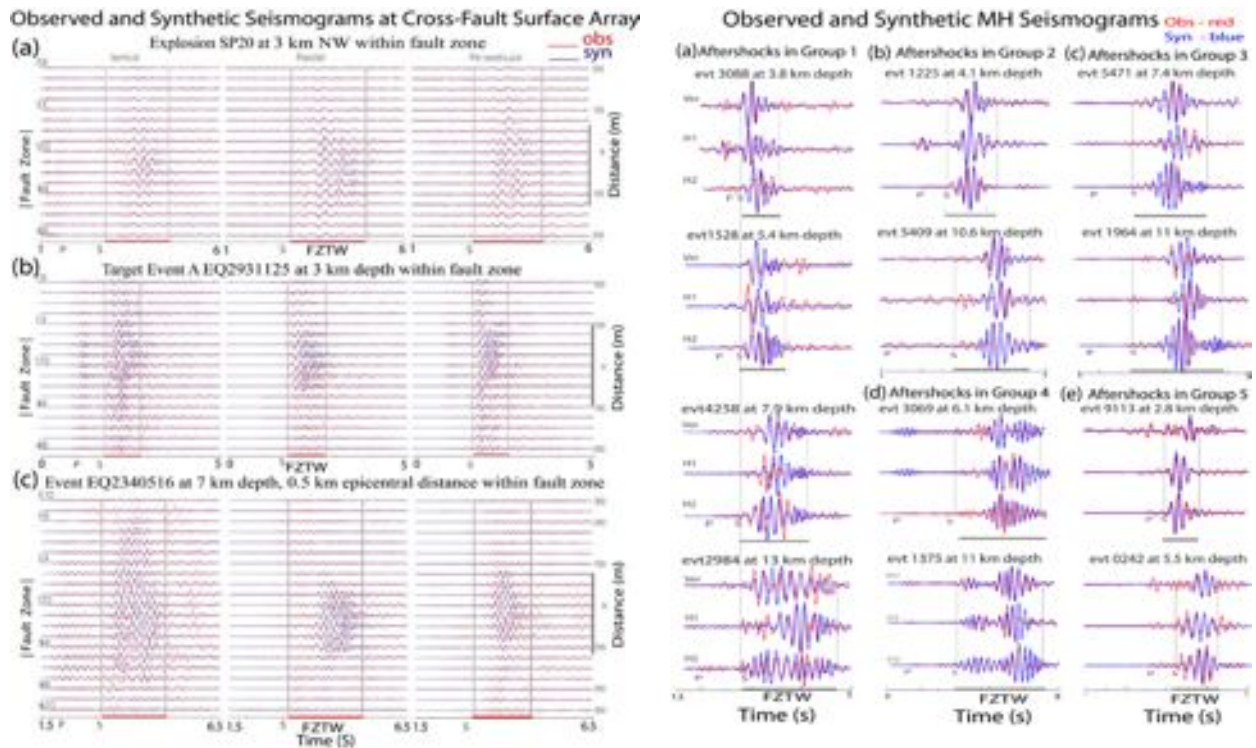
Fig. 5 Left: Comparison of observed (red lines) and synthetic (blue lines) seismograms at the SAFOD surface array for **(a)** shot SP20, **(b)** the SAFOD drilling target event A at ~3 km depth and **(c)** a micro-earthquake occurring at 7 km depth and 0.5 km epicentral distance from the surface array. An explosive source is used for the shot and a double-couple source is used for the earthquakes. Seismograms have been low-pass filtered at 6 Hz and are plotted using a fixed amplitude scale. **Right:** Comparison of observed and synthetic seismograms from the SAFOD MH for Groups 1-5. The observed seismograms are shown in red and synthetic seismograms are shown in blue. Synthetic seismograms are computed using 3-D finite difference techniques, as described in the text, and the velocity model shown in **Fig.4**. Observations and synthetics are shown for a range of source depths from 2.8 – 13 km. The model adequately reproduces the observed FZTW amplitudes and durations. Data have been low-pass filtered at 6 Hz.

Observed and 3-D Finite-Difference Synthetics Seismograms

(a) Deep Fault Zone — SAFOD MH Seismograph

(b) Deep Fault Zone — Surface Station T0

(c) 4-km Shallow Fault Zone — Surface Station T0

Fig. 6 (a) Observed (red line) and synthetic (blue line) vertical-component seismograms at the SAFOD MH seismograph at ~3 km depth for 9 on-fault aftershocks in groups G1 and G2 (with stars) at depths between 3.8 km and 14.4 km. The *S*-arrivals for these events are aligned at the same time. Bars denote the post-*S* wave durations. **(b)** Observed and synthetic vertical-component seismograms at station ST0 of the cross-fault surface array for 11 on-fault microearthquakes at depths between 2.6 km and 11.7 km. **(c)** Synthetic seismograms at ST0 for 11 on-fault events using a 4-km shallow fault zone for comparison with observations. The synthetic waveforms with short wavetrains for events at depths below 4 km cannot match the long wavetrain of observed FZTWS.

Observed and Synthetic Seismograms at Parkfield Surface Array

Profiles for Shot PMM at 7 km Distance

Profiles for Shot PARK at 4.2 km Distance

Fig. 7 Observed and 3-D finite-difference simulations of seismograms for shots PMM and PARK detonated within the fault zone at distance 7 km NW and 4.2 km SE from Parkfield surface array across the SAF ~1.5 km NW of the town of Parkfield in 2002. Station ST0 of the array were located on the SAF main trace. Seismograms have been <3 Hz filtered. Prominent fault-zone trapped waves (FZTWs) with large amplitudes and long wavetrains (marked by brackets) following are observed at stations located close within ~200-m-wide fault zone, and show the lower velocities and higher damage magnitude of fault rocks on the SAF segment between the array and Shot PARK where the highest surface slip was found in the 2004 *M*6 Parkfield earthquake [*Langbein et al.*, 2005; *Ammon et al.*, 2005]. Seismic velocities of the waveguide southeast of the Parkfield array used in simulations of FZTWs for shot PARK are lower by ~20% in average than waveguide velocities northwest of the array in Fig. 4a.

Waveform cross-correlation measurements from repeated explosions and microearthquakes recorded at the same array deployed near Parkfield before and after the 2004 *M*6 Parkfield earthquake show the velocity decrease of ~2.5% within the fault zone likely due to the coseismic rock damage in the *M*6 mainshock and then increase of ~1.2% in the first 3-4 months owning to post-seismic fault healing with rock rigidity recovery (Fig. 8 and Fig. 9). Results from this investigation illuminate the spatial extent of fault-zone damage and the loss and recouping of strength across the earthquake cycle, suggesting that inelastic processes such as fracture fluid migration and pore pressure solution may lead to mechanical failure and nucleation of earthquakes at the plate boundary.
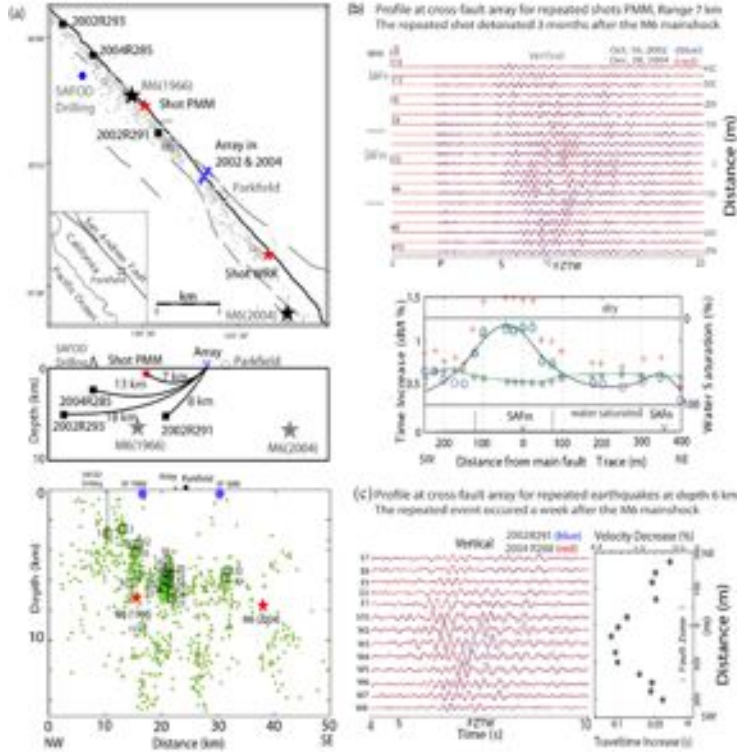
Fig. 8 (a) Map shows locations of the seismic array deployed across the SAF main and north fault strands near Parkfield in 2002 and 2004, and repeated shots. Dots denote aftershocks recorded at the array in 2004. Open squares are clusters of repeated aftershocks used to examine fault healing. Solid squares - earthquakes recorded on Julian date R291 and R293 in 2002 and their repeated events in 2004. Stations ST0 and E15 were located on fault main and north strands. **(b)** Vertical-component seismograms recorded at cross-fault array for repeated shot PMM before and after the 2004 *M*6 Parkfield earthquake, showing seismic waves traveled slower after the 2004 *M*6 mainshock. Traveltime increases for *P* (red), *S* (blue), and trapped waves (green) measured by moving-window waveform cross-correlations, showing seismic velocity decreased after the *M*6 mainshock. The blue curve fits to traveltime increases of *S* waves in 2004. A pair of vertical grey bars denotes a ~200-m-wide zone with greater travel time increases. **(c)** Seismograms at the cross-fault array for two repeated micro-earthquakes before and after the 2004 *M*6 Parkfield earthquake. The *P*-wave arrivals are aligned. The increases were measured by waveform cross-correlations between the 2002 and 2004 events.
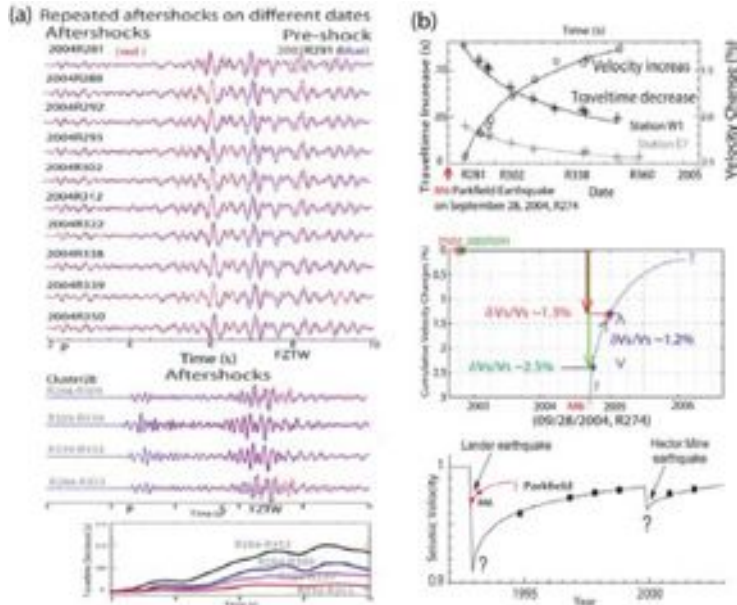
Fig. 9 (a) Vertical-component seismograms recorded at a within the fault zone for the microearthquake occurring on R291 in 2002 (blue line) and the 2004 aftershocks (red lines) occurring at the same place, showing that waves traveled slower in 2004 with the largest time delay in the earliest stage after the 2004 M6 Parkfield *M*6 mainshock. Waveform cross-correlations show the larger for earlier repeated aftershocks **(b) Top:** The maximum traveltime and *S* velocity variations measured by waveform cross-correlation of between the event in 2002 and 10 repeated events in 2004. The curve is the logarithmic fit to measurements with a constant of velocity change 0.012 /day. **Mid:** *S*-wave velocity changes within the rupture zone caused by the 2004 *M*6 Parkfield earthquake. *S* velocity decreased by ~1.3% between the two repeated shots in 2002 and 2004. Measurement for repeated microearthquakes in 2002 and aftershock in 2004 show ~2.5% decrease in *S* velocity. Then, *S* velocities increased by 1.2% in the following 3 months. **Bottom:** Damage and healing at rupture zones of the 1992 *M*7.4 Landers and 1999 *M*7.1 Hector Mine earthquakes ,show healing as a logarithm of time, and the larger damage magnitude for larger earthquake size.

Discovery Using Ducttape Excessively (DUDE), with EarthScope Data

Pei-Ying Patty Lin* and Edward J. Garnero

School of Earth and Space Exploration, Arizona State University, Tempe, Arizona, USA
*patty.lin@asu.edu

The USArray's Transportable Array (TA) is a large seismic network of about 400 stations. Combined with global data, 1000's of seismic recordings can be collected nearly immediately following current earthquakes. Here, we present an approach to view global and/or TA data quickly and easily, for a comprehensive preview of an earthquake for research, education, and general interest purposes. We developed a software package named "Discovery Using Ducttape Excessively" (DUDE). The philosophy behind this effort is to seamlessly generate plots for viewing earthquake data for the entire earthquake (all distances, all components of motion, and a large time window) for potential discovery of unexpected phenomena, combining a number of freely available special purpose software packages (i.e., the "duct-tape"), such as the TauP Toolkit (http://www.seis.sc.edu/taup), Standing Order for Data, SOD (http://www.seis.sc.edu/sod), the Seismic Analysis Code, SAC (http://www.iris.edu/software/sac), the Generic Mapping Tool, GMT (http://www.soest.hawaii.edu/gmt), and shell-scripting. DUDE plots include maps of the earthquake and stations along with great circle paths, seismic record sections of raw and filtered seismograms, radiation patterns for P, SH, and SV components, along with piercing points of a number of common seismic phases, as well as an empirical source time function for the direct P and S waves. Thus, DUDE provides a quick graphical view of an earthquake through directly viewing data in a number of ways. Our research commonly focuses on some piece of data (e.g., solely a time window around some seismic phase of interest), and hence the motivation for constructing DUDE is to gain a more complete view of earthquakes. We have found that DUDE-generated plots are also useful for other things, such as teaching (all levels), identifying unanticipated research projects, and applying towards other research by simply modifying the DUDE scripts. Viewing plots from different earthquakes readily emphasizes the building blocks of what we call "good data" for different seismic phases: earthquake radiation pattern, strength, and source-time function. The relatively dense TA station spacing ($\sim$ 70 km) permits high-resolution Earth structure studies from a single event; hence DUDE plots provide quick assessment of desired, as well as unanticipated, data analysis opportunities.

We will present examples from a number of recent earthquakes, which highlight a number of important seismic phases for imaging mantle and/or core structure. These will include S and ScS from an unusual deep focus Spain earthquake (04/11/2010), multiple ScS from an Argentina earthquake (01/01/2011), and PKP from an Indonesia earthquake (04/03/2011). DUDE's flexibility allows the user to regenerate plots zooming in on phases, time windows, and distances of interest, and hence, is a method and philosophy that helps to support discovery of the unexpected.

Title: Surface wave tomography with USArray: incorporating amplitude measurements to estimate elastic and anelastic structures

Authors: Fan-Chi Lin, Michael H. Ritzwoller, & Weisen Shen

Affiliation: Center for Imaging the Earth's Interior, Department of Physics, University of

Colorado at Boulder, Boulder, CO 80309-0390 USA

Email: linf@colorado.edu

Abstract

The deployment of the EarthScope/USArray Transportable Array has permitted the detailed study of crustal and upper mantle structures in the western US based on surface wave measurements. While elastic structures can be constrained based on phase travel time measurements alone, accurate amplitude measurements are not only essential to estimate the attenuation but also crucial to account for finite frequency effects and resolve unbiased elastic structures. In this presentation, we present two different applications that incorporate amplitude measurements. In the first application, we demonstrate how amplitude measurements can be used along with empirical phase front tracking to estimate local directionally dependent phase velocities by applying the Helmholtz equation. This method, referred to as Helmholtz tomography, accounts for the finite frequency effects, reduces both random and systematic errors, and improves the resolved of isotropic and azimuthally anisotropic structures at long period (>50 sec) compared to its ray theoretic based predecessor, eikonal tomography. In the second application, we examine the possibility of using amplitude measurements from ambient noise cross-correlations to constrain attenuation structures. We show at two periods (10 and 18 sec) and locations (northeastern Nevada and eastern Wyoming), after correcting for the duration of noise time series and the azimuthal variations of the amplitude measurements, that the spatially averaged attenuative decay based on ambient noise amplitude measurements are consistent with those from a nearby earthquake and mining blast. The fact that attenuation can be estimated from ambient noise cross-correlations is somewhat surprising considering that the ambient noise amplitudes are strongly altered by data processing methods such as temporal normalization and spectral whitening before cross correlating. Further studies such as comparing positive and negative lags amplitude measurements remain to be performed, however, to understand the potential bias due to uneven source distributions prior to estimating local variations in attenuation.

A new asthenospheric upwelling model in the California slab window near the Mendocino Triple Junction region

Kaijian Liu[1, 2*], Yongbo Zhai[1], Alan Levander[1], Rob Porritt[3], Richard Allen[3]
1. Department of Earth Science, Rice University, Houston, TX, United States
2. Applied Physics Program, Rice University, Houston, TX, United States
3. Earth & Planetary Science, UC Berkeley, Berkeley, CA, United States
* Email: lkjcammit@gmail.com

The Mendocino Triple Junction (MTJ) region in the northern California marks the progressive replacement of Gorda convergent motion by the strike-slip transform regime in the San Andreas Fault system. It provides a natural laboratory to examine the lithospheric and asthenospheric evolution associated with the northwestward migration of the MTJ and the deformation resulting from three plates interacting (Gorda, Pacific, North American). Northward migration of the MTJ results in removal of the Gorda slab from beneath North America, leaving in its wake the so-called 'slab window'. Knowledge of the geometry and pathways of asthenospheric sources filling the slab window have been unclear. Previous active source profiles and body-wave traveltime tomography are limited to either crustal or a deeper upper mantle scale, respectively.

In this study, we have developed a new 3-D shear velocity model from joint inversion of the surface wave, ambient noise and receiver functions to examine the structure of the slab window model and lithospheric evolution. We first used finite-frequency Rayleigh wave tomography to analyze the surface waves recorded by the Flexible Array Mendocino Experiment (FAME), EarthScope/USArray TA stations, and UC Berkeley Digital Seismic Network stations in the period band 22-100 s. After incorporating our surface wave dispersion data (22-100 s) with the short-period ambient noise data (8-30 s) provided by Porritt et al. (unpublished), we jointly inverted for shear velocity structure with the combined Rayleigh wave phase velocities and PdS receiver functions (Zhai and Levander, unpublished). The resulting Vs model reveals strong lateral heterogeneity and provides estimates of Moho and LAB depths in the MTJ region.

In the crust, we have clearly imaged low upper crust Vs (<3.0 km/s) in parts of the Coast Range Franciscan Complex bounded by relatively high-Vs Klamath block to the northeast. The relatively high-velocity ophiolite in the Great Valley abuts the lower-Vs Sierran basement. In the upper mantle, we have clearly imaged the subducted Gorda plate and the associated mantle wedge to the east under the Cascades. Extremely low uppermost-mantle shear velocities provide new seismic evidence for the hydration and serpentinization in the forearc mantle with fluid released from the subducted oceanic lithosphere. From both the Vs model and LAB maps, we have identified three young and shallow LABs (<60 km), one beneath the California slab window in the transform region, one under the Gorda plate under the shallow parts of the subduction zone near the trench, and the final under the arc volcanoes at the southern terminus of the Cascadia margin. The shallow LABs can be

related to partial melt occurring under different conditions: the slab window is related to decompression melting; the Gorda LAB could be associated with the sheared melt or simply due to proximity of the ridge; the mantle wedge might be caused by the fluid-mediated melting. In the slab window, the emplaced asthenosphere was suggested to originate from the depleted mantle beneath the oceanic slab, while geochemical data by Whitlock et al. (2001) preferred a mantle wedge type instead. To reconcile the contradiction among the existing models for the origin of the slab window asthenosphere, we further proposed a 'staggered upwelling' model that can explain both the mantle wedge-derived geochemical signature and the time lag between the recent Clear Lake volcanics and pullout of the Gorda slab.

Subduction dynamics of western US since Oligocene

Lijun Liu & Dave Stegman

IGPP, Scripps Institute of Oceanography, University of California, San Diego, CA, 92093

We model the Farallon-Juan de Fuca plate subduction during the past 40 Ma using high-resolution numerical models. By assimilating plate motion history, paleo-age of sea floor, and paleo-geography of plate boundaries, we attempt to reproduce the recently observed complex mantle structure beneath western U.S. as reported by seismic tomographic models using EarthScope data (e.g., Burdick et al., 2008; Roth et al., 2008; Tian et al., 2009; Schmandt & Humphreys, 2010; Sigloch, 2011).

We find that a laterally varying viscosity is crucial in order to generate reasonable mantle structures that resemble tomographic models. The best-fit models favor a viscosity contract of 4 orders of magnitude across the plate boundary and three orders of magnitude within the upper mantle. The inferred depth-dependence of ambient mantle viscosity from these forward models is similar to our conclusion reached by adjoint (inverse) modeling of the Farallon subduction since Late Cretaceous (Liu et al., 2008; Spasojevic et al., 2009).

Using forward models, we show that the highly segmented western U.S. upper mantle structure is a result of the Farallon-Juan de Fuca subduction, subject to the opening of a slab window and Basin & Range (B&R) extension since 30 Ma. The imaged fast seismic anomalies located between 300-700 km depth bear little resemblance with the shallower portion (above 200 km), as suggested by most recent tomography inversions. We find that these 'circular'-shaped fast anomalies presently beneath the four corners region are subducted slabs younger than 15 Ma, while the linear slab imaged beneath the Cascades is younger than 5 Ma. In fact, the distinct morphology between these two parts of the subduction system indicates the strong influence of toroidal flow induced by the sinking slab, originating from the migrating JF-PA-NA triple-junction and the development of the B&R extension. Our subduction model for western U.S. also appears to be consistent with the evolution of several structural geologic features and the peculiar seismic anisotropy measurements at the present day.

Upper Mantle Structure Beneath the Gamburtsev Subglacial Mountains & East Antarctica from Body-Wave Tomography

Andrew Lloyd & Andy Nyblade, Penn State
Doug Wiens, Washington University in St. Louis
Samantha Hansen, University of Alabama

The geophysical mechanism responsible for the uplift of the Gamburtsev Subglacial Mountains (*GSM*) is poorly understood. Many uplift models for the region have been invoked, such as the existence of a hotspot or a series of Proterozoic/early Paleozoic orogenic events. Past seismic studies have been limited to continental scale surface wave tomography with spatial resolution no better than 600 km, leaving the *GSM* relatively unexplored. Using seismic data from the GAMSEIS array we investigate the geologic structure of this unique subglacial mountain range. The GAMSEIS array consisted of 26 temporary broadband stations: 12 stations were arranged in a linear array as a continuation of the TAMSEIS array, 6 stations were arranged in a second linear array intersecting the first array, and 8 stations were install between the two linear arrays to improve 3-D resolution. Here we investigate the upper mantle structure via regional body-wave tomography using P & S travel times from teleseismic events. Geometric crust and ice effects, determined by receiver functions or GPR, are removed when calculating the relative travel time residuals. P and S velocity models indicate that a near laterally homogenous upper mantle underlies the *GSM* indicative of an old stable craton. In addition a second set of P & S velocity models place the GSM and East Antarctica in the same context by incorporating seismic data from GAMSEIS, TAMSEIS, and POLENET seismic arrays as well as from several permanent stations, allowing us to more thoroughly evaluate the upper mantle structure of East Antarctica.

North American Mantle Velocity Structures from Joint Inversion of Body and Surface Waves

Xiaoting Lou (xlou@earth.northwestern.edu) and Suzan van der Lee (suzan@earth.northwestern.edu)
Department of Earth and Planetary Sciences
Northwestern University
Evanston, IL 60208

We have developed a Python/Matplotlib tool to measure teleseismic body wave arrival times. A graphic user interface is built to visualize seismograms and facilitate quality control. Seismic data from IRIS PASSCAL arrays and EarthScope's Transportable Array were processed with this tool to get teleseismic P and S relative delay times sampling both western and eastern North America. Within some scatter, the S delays are consistently about 3 times stronger than the P delays. Delay times corrected for crustal structures from earthquakes with Mw greater than 6.0 show that the mantle beneath the US east of the Rocky Mountains is at least as heterogeneous as the mantle beneath the US west of the Rockies. Inversion of the relative S delay times produced mantle velocity structure patterns familiar from previous studies. For example, a dipping, high velocity Juan de Fuca Slab, strong low velocities under Yellowstone and all along Snake River Plain, a relatively high velocity Colorado Plateau surrounded by low velocity arms, high velocity structures in the transition zone which could represent older fragments of Farallon Plate, and a strong velocity contrast across the Proterozoic-Paleozoic basement boundary on the eastern margin. Although focused on different wavelengths, the teleseismic body wave model seems generally consistent with surface wave models such as NA04. However, important differences exist and we will report on our ongoing attempts to reconcile these differences through a joint inversion of body and surface wave data for crust and mantle heterogeneity.

Crustal quartz plays a surprising role in controlling Cordilleran deformation

Anthony R. Lowry[1] and Marta Pérez-Gussinyé[2]

[1]Department of Geology, Utah State University, Logan, UT 84322-4505, USA. Contact: Tony.Lowry@usu.edu.

[2]Department of Earth Sciences, Royal Holloway, University of London, Egham, Surrey TW20 0EX, UK.

As highlighted in the EarthScope 2010-2020 science plan, large-scale deformation of continents remains poorly understood more than forty years after the plate tectonic revolution. Rock flow strength and mass density variations both contribute to stress, so both are certain to be important, but these depend (somewhat nebulously) on rock type, temperature, and whether or not unbound water is present. Hence, it is unclear precisely how Earth material properties translate to continental deformation zones ranging from tens to thousands of km in width, why deforming zones sometimes intersperse with non-deforming blocks, and why large earthquakes occasionally rupture in otherwise stable continental interiors. An important clue comes from observations that mountain belts and rift zones cyclically form at the same locations despite separation across vast gulfs of time (the Wilson tectonic cycle), accompanied by inversion of extensional basins and reactivation of faults and other structures formed in previous deformation events. We will present surprising evidence that the abundance of crustal quartz, the weakest mineral in continental rocks, may strongly condition both continental temperature and continental deformation. We used a combined analysis of EarthScope seismic receiver functions, gravity, and surface heat flow measurements to estimate thickness and seismic velocity ratio, V_P/V_S, of the continental crust in the western United States. V_P/V_S is insensitive to temperature but very sensitive to quartz. Our results demonstrate a surprising correlation of low crustal V_P/V_S with both higher lithospheric temperature and Cordilleran deformation. The most plausible explanation for the relationship to temperature is a robust dynamical feedback in which ductile strain first localizes in relatively weak, quartz-rich crust, and then initiates processes that promote advective warming, hydration, and further weakening. The feedback mechanism hypothesized here not only would explain stationarity and spatial distributions of deformation, but also would lend insight into the timing and distribution of thermal uplift and observations of deep-derived fluids in springs.

A lower bound on crustal driving stress in megathrust regions from topography and gravity

Karen Luttrell[1] and David Sandwell[2]

[1] U.S. Geological Survey, Menlo Park, CA – kluttrell@usgs.gov

[2] Scripps Institution of Oceanography, La Jolla, CA – dsandwell@ucsd.edu

We use a static force balance model to constrain the crustal shear stress required to support observed subduction zone forearc topography while maintaining a thrust regime stress field. The model uses a semi-analytic solution for the stress field exerted by surface and Moho topography loading the crust, and it places a lower bound on the driving stress exerted by tectonic forces. The shape of the Moho load is constrained by gravity data. When compared with coseismic stress drops from earthquakes with large rupture area, the estimates of crustal stress have implications for fault strength. We show model results from southern Chile and the 2010 Maule earthquake, which indicate that the depth-averaged crustal shear stress must be at least 7 MPa while the depth-averaged coseismic shear stress drop was at most 4 MPa. This suggests either the Maule event ruptured a weak portion of the megathrust fault plane or it achieved only partial stress release. Additionally, we show model results from the northern Chile subduction zone, the Japan Trench, the Nankai Trough, and the Cascadia subduction zone. Comparison of the wedge topography-induced stress at each of these regions reveals that crustal driving stress can vary widely at different subduction regions, possibly indicating differences in the seismic behavior of these plate boundaries.

Earthscope in the Central US: Unraveling the lithospheric evolution of the southern margin of Laurentia and its long-term effect on intraplate seismicity

M. Beatrice Magnani*, Heather DeShon*, Samantha Hansen**, Kate Miller***, Suzan van der Lee****, Katie Keranen*****

*Center for Earthquake Research and Information, University of Memphis, Memphis, TN
** Department of Geological Sciences, University of Alabama, Tuscaloosa, AL
***Department of Geology and Geophysics, Texas A&M, College Station, TX
****Department of Earth and Planetary Sciences, Northwestern University, Evanston, IL
*****School of Geology and Geophysics, University of Oklahoma, Norman, OK

The heart of the stable North American continent hosts the New Madrid Seismic Zone (NMSZ), a system of faults that ruptured repeatedly in the last 3000 years generating large magnitude earthquakes (M>7). The processes responsible for triggering these earthquakes still elude us, but numerical models invoke the presence of a lithospheric anomaly, either at the lower crustal or upper mantle depth beneath the NMSZ, to store stress and concentrate strain in the active zone, suggesting a correlation between the lithospheric structure and the location of the seismogenic zone. Indeed refraction profiles in the Mississippi Valley model a high velocity layer at the base of the crust, generally interpreted as a "rift pillow", associated with the Reelfoot rift extensional tectonics, and spatially coincident with the NMSZ.

Evidence is mounting, however, that the NMSZ might not be the only system of faults active during the Holocene, and that deformation is accommodated along structures additional to the NMSZ and spanning an area that extends at least to the southern edge of the Laurentia Proteorozoic continent, marked to the south by the Alabama-Oklahoma transform fault. These new findings suggest that a more widespread lithospheric structure might create the zone of weakness controlling the extent of the seismogenic zone, and that this structure might be associated with the 1.4 Ga granite-rhyolite province and the extent of the Proterozoic lithosphere to the south.

Here we summarize the research opportunities these new findings unfold in the Mississippi Valley, the Southern Laurentia margin, and the Gulf of Mexico coastal plains, as the Earthscope arrays move to the Central U.S.

Crustal xenoliths from central Montana: heterogeneity and incremental assembly of high seismic velocity (7.x) lower crust in cratonic North America

K.H. Mahan[1], K. Barnhart[1], T. Blackburn[2], S.A. Bowring[2], F. Dudas[2], Schulte-Pelkum, V. [1]

[1] Department of Geological Sciences, University of Colorado at Boulder, 2200 Colorado Ave., Campus Box 399, Boulder, CO 80309

[2] Department of Earth, Atmospheric, and Planetary Sciences, Massachusetts Institute of Technology, 77 Massachusetts Ave., MIT Bldg 54, Cambridge, MA 02130

The presence (or absence) of continental lower crustal layers with unusually high seismic P velocities of over 7 km/s provides fundamental information about lithospheric growth and destruction processes. Where such layers are present, their thickness, composition and degree of heterogeneity can also have a profound influence on the rheological properties and behavior of the lower crust during younger tectonic events. In Montana and Wyoming, seismic experiments reveal an anomalously thick 7.x layer that comprises up to half the ~55 km thickness of the crust in the region. Our studies of xenoliths exhumed in Eocene volcanics in central Montana emphasize the heterogeneity in composition, age, physical properties, and modes of formation of the lower crust. The sample suites include mafic garnet granulite, mafic eclogite, and felsic granulite. Multiple samples preserve evidence for prograde burial and some are polymetamorphic. Peak pressures of some samples exceed 1.7 GPa whereas pressures interpreted to represent residence depths are consistent with derivation from 25-50 km. Calculated seismic velocities are also heterogeneous with data from samples within the seismically defined 7.x layer ranging from 6.9 to >8.0 km/s. A variety of U-(Th)-Pb data from zircon, monazite, titanite, and rutile record multiple igneous, metamorphic and/or fluid flow events from Archean to Mesoproterozoic time with discrete pulses at 2.1 Ga, 1.8 Ga, 1.7 Ga, and 1.3 Ga. Collectively, the data suggest a protracted history of incremental assembly of the 7.x layer in Montana, allowing significant improvements to models for the formation, evolution and present day structure of the North American lithosphere.

Structure and Dynamics of the Central North American Craton: An EarthScope Swath from the Ozark Plateau, Across the Illinois Basin, to the Grenville Front

Marshak, S. *Department of Geology, University of Illinois, Urbana, IL*
Pavlis, G.L. *Geological Sciences, Indiana University, Bloomington, IN*
Hamburger, M. *Geological Sciences, Indiana University, Bloomington, IN*
Gilbert, H.J. *Earth & Atmospheric Sciences, Purdue University, West Lafayette, IN*
Larson, T. *Illinois State Geological Survey, University of Illinois, Urbana, IL*

EarathScope's Transportable Array is beginning its sweep across the Midcontinent of North America. The central portion of this swath, between latitudes 36°N and 38°N, covers a "type example" of cratonic-platform lithosphere, where a veneer of Paleozoic sedimentary strata overlies Precambrian crystalline basement. A collaborative project has just begun to utilize additional instruments of the Flexible Array to increase subsurface resolution in the type example, a region that includes the eastern Ozark Plateau, the southern Illinois Basin, and the western edge of the Appalachian Basin. Notably, in spite of low topographic relief, the region has large subsurface structural relief. Specifically, the elevation difference between the Cambrian-Precambrian unconformity at the crest of the Ozark Plateau and the same horizon at the base of the Illinois Basin (< 100 km to the east) is over 7.5 km. The region is also of interest because it includes the northern end of the Mississippi embayment (an anomalous depression), four major Proterozoic lithosphere accretionary boundaries (including the Yavapai, Mazatzal, and Grenville belts), one of the world's largest anorogenic igneous provinces (the Eastern Granite-Rhyolite Province), pronounced gravity and magnetic anomalies, and numerous fault-and-fold zones. Many of the fault-and-fold zones remain seismically active, both within and outside the notorious New Madrid seismic zone. The project is focused on operation of a three-dimensional, broadband, passive-seismic array. Over the three-year period that coincides with the operation of the Transportable Array, we will deploy 120 temporary seismograph stations. Site occupation will roll in four distinct stages using a maximum of 60 simultaneously operating stations. The acquired seismic data will be analyzed using a variety of state-of-the-art tools, such as: travel-time tomography using teleseismic P- and S-waves; wave-field imaging; and a detailed spatial analysis of recorded seismicity. Resulting observations have the potential to define the nature of lower crustal or upper-mantle features related to the process of crustal assembly and cratonization, as well as to provide insight in to origin and persistence of continental-interior epeirogenic structures (basins and domes). The project also will incorporate an integrated education and outreach component.

Receiver Function Transect Across Tibet, Tarim, and Tien Shan

Ben Marshall (benjmars@gmail.com), Vadim Levin, Guochin Huang, Earth and Planetary Sciences, Rutgers University NJ, USA Steven Roecker, Earth and Environmental Sciences, Rensselaer Polytechnic Institute, NY, USA Huaitao Wang, Xinjiang Earthquake Administration, Xinjiang, China

We investigate the region of the ongoing collision between the Indian and Eurasian tectonic plates that results in widespread deformation of the continental lithosphere. Over the past decade numerous regional studies were conducted between the Himalaya and the Tien Shan mountains, each illuminating a small part of the area. We combine the data from a number of portable and permanent networks to construct an ~1800 km long profile of the lithospheric properties across three very different tectonic domains: the Tibetan plateau, the Tarim basin, and the Tien Shan mountains. We use data from 60 stations operated in the region by US, Chinese and French researchers. We use records of distant earthquakes to construct receiver function gathers for each station. The uniformity of processing ensures that our results are comparable along the transect. We examine receiver function gathers at each site, and rank their quality on the basis of number of records, noise levels, and directional stability of the wavefield. We select 32 sites with high-quality data. For these we construct average receiver function traces using data in 60-85 degree range, and use them as a guide to the lithospheric layering beneath the region. On most receiver functions we constructed the most prominent feature is a positive phase likely associated with the crust-mantle transition. The timing of this phase varies significantly over the length of the profile. Beneath the Tibetan plateau delay times ~7-8 s are seen close to the Himalayas, and nearly 10 s delays are found further north. Delays of 6 to 8 s are seen beneath sites in the Tarim basin and the Tien Shan mountains, and nearly 10 s delays are seen at the border between them. In addition to the pulse associated with the crust-mantle transition we see other locally-consistent features, for example a negative phase with delay values between 3 and 5 s beneath much of the Tibetan plateau.

UPDATE OF THE PACIFIC NORTHWEST GPS-DERIVED VELOCITY FIELD

Robert McCaffrey (r.mccaffrey@pdx.edu) Department of Geology, Portland State
 University, Portland OR 92707
Robert W. King (rwk@chandler.mit.edu) Dept. of Earth, Atmospheric & Planetary
 Sciences, Massachusetts Institute of Technology, Cambridge, MA 02139
Suzette J. Payne (Suzette.Payne@inl.gov), Idaho National Laboratory, P.O. Box 1625,
 Idaho Falls, Idaho 83415

We present an update of the Pacific Northwest GPS-derived surface velocity field presented earlier by McCaffrey et al. (Geophys. Jour. Int., 2007) and Payne et al. (Geology, 2008). The velocity field combines new SOPAC daily solutions for 1994-2010 for the BARGN, EBRY, PANGA, PBO, and WCDA networks (http://sopac.ucsd.edu/processing/gamit) with our solutions using data from field surveys conducted by us and several other institutions from 1991-2010. The new field reveals that the large-scale clockwise rotation seen in western Washington and Oregon also extends southward into southern Idaho and the Snake River Plain as well as into the northern Basin and Range of Nevada. The axes of rotation generally fall near the Oregon-Washington-Idaho border. Significant permanent strain rates are localized at the Wasatch fault, the Walker Lane, and parts of the Basin and Range. Otherwise large areas of the Pacific NW rotate relative to North America as nearly rigid blocks. The Cascadia subduction zone imparts an elastic strain rate of up to 10^{-7} /yr on the western edge of North America. We present a revised locking model for Cascadia based on these velocities and coastal uplift rates from leveling by Burgette et al. (J. Geophys. Res., 2009). Detailed interpretations of the Snake River Plain region based on this velocity field are presented by Payne et al. (this meeting).
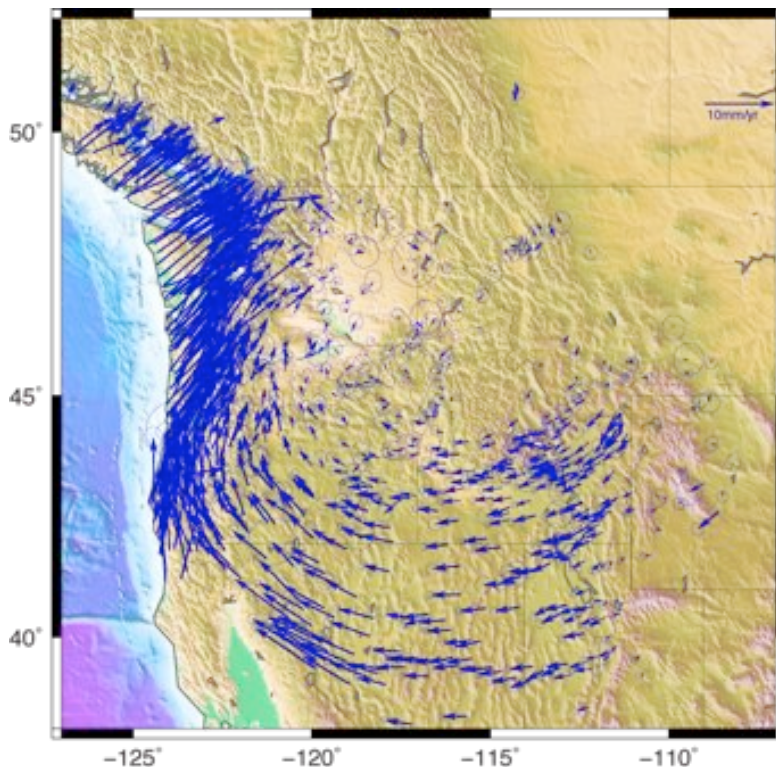
A joint geophsysical investigation of the Cascadia subduction system using data from dense arrays of passive seismic and magnetotelluric stations

R Shane McGary[*][1,2], Stephane Rondenay[1], Rob Evans[2],

Philip Wannamaker[3], Geoff Abers[4], and Chin-Wu Chen[5]

1. Massachusetts Institute of Technology
2. Woods Hole Oceanographic Institution
3. University of Utah
4. Lamont-Doherty Earth Observatory
5. Carnegie Institute of Washington

* r_shane@mit.edu

Abstract:

Joint analyses that combine multiple geophysical methods can yield improved characterization of the subsurface over that acheived by single methods. Here, we investigate the Cascadia subduction zone using dense seismic and magnetotelluric (MT) data sets collected along three profiles, each roughly perpendicular to the strike of the dipping slab at that location. (figure 1)

We present images generated by 2-D Generalized Radon Transform (GRT) inversion of scattered teleseismic data, along with results from 2-D Non-Linear Conjugate Gradient (NLCG) inversion of roughly collocated MT data. The seismic and MT images in A-A' and the seismic image in C-C' have been previously published, but the MT image in C-C' and both images in B-B' represent new work in various stages of completion.

The migrated seismic image for B-B' (figure 2a) clearly shows the subducted oceanic crust as a dipping low velocity layer that persists to ~40-50 km depth. It also depicts the region within which eclogitization is taking place, along with a disrupted continental Moho that may be weakened by serpentinization and weakened fluid phases within the underlying mantle wedge. The collocated MT image (figure 2b) shows highly resistive features corresponding to sections of the subducted slab. There are also conductive features associated with the release of fluids during eclogitization as well as fluids/partial melt within the mantle wedge that appear to be linked with the volcanic arc.

The real strength of this approach comes into play when we not only use both the seismic and MT methods to constrain one another, but also look at how the interpretation varies along strike. All three profiles show conductive regions associated with both eclogitization and fluid/melt phases in the mantle coincident with disruption in the Moho. There are also some potentially important differences between the profiles, such as a strong resistive feature present between these two conductors in A-A' and B-B', but not in C-C'. This resistor could be indicative of a decoupling of the tip of the mantle wedge, a cooling, serpentine saturated region that affects fluid pore pressures upstream and fluid release downstream. It may be a glimpse into the reason why C-C' is the only line of the three along which earthquakes are very rare. This sort of combination of techniques and use of multiple along strike images promises much insight into the nature of subduction settings, and speaks to the value of large-scale data collection projects such as Earthscope.
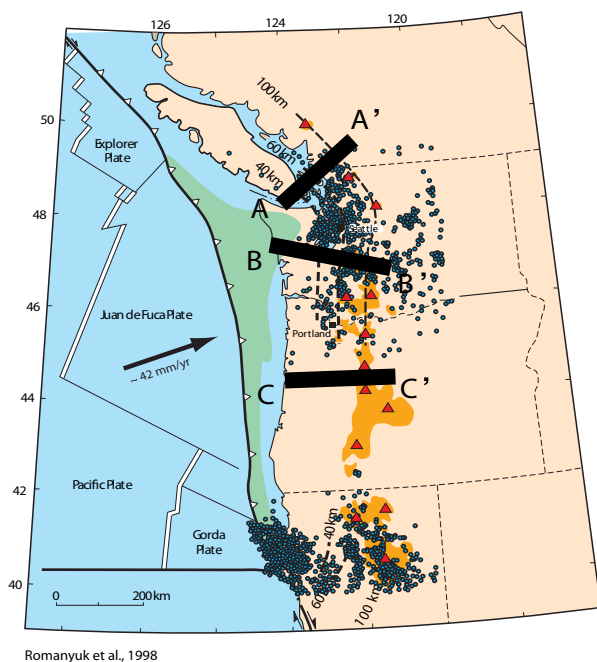

Figure 1: Map of the Cascadia region showing the three primary transects, plate boundaries, the volcanic arc, and earthquake activity
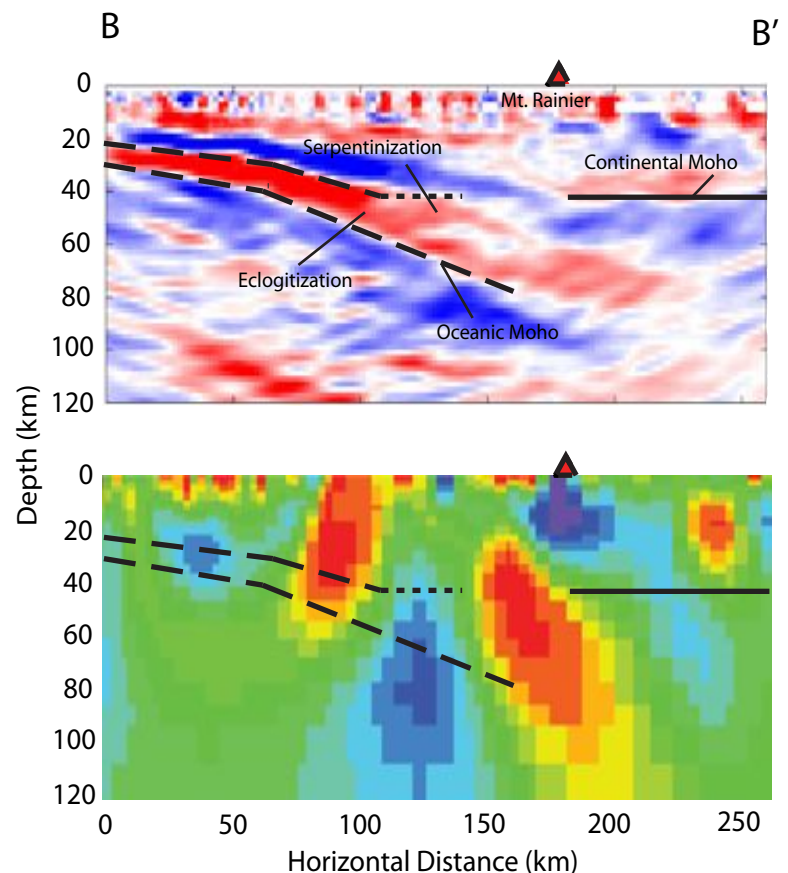

Figure 2: GRT migration (top) and NLCG MT inversion (bottom) for the B-B' transect across central Washington

References:
Nicholson et al., New constraints on subduction zone structure in Northern Cascadia, Geophys J. Int, 2005.
Rondenay et al., Multiparameter two-dimensional inversion of scattered teleseismic body waves, JGR, 2001.
Soyer and Unsworth. Deep electrical structure of the northern Cascadia subduction zone, Geology, 2006.

# Collaborative Education and Research in Crustal Deformation Studies

Sally McGill, *Department of Geological Sciences, California State University, San Bernardino*
Robert deGroot, *Southern California Earthquake Center*
Rick Bennett, *Department of Geosciences, University of Arizona, Tucson*
Joshua Spinler, *Department of Geosciences, University of Arizona, Tucson*

Crustal deformation research offers many opportunities for undergraduate students, high school teachers and high school students to participate in the scientific research process. Collaborations that span multiple levels including research scientists, graduate students, faculty and undergraduate students at comprehensive universities, and high school teachers and their students can be productive and beneficial to all parties. Undergraduates and high school teachers and their students benefit by gaining valuable research experience, and they have the satisfaction of contributing significant new data to publishable scientific research. These participants grow in the confidence that they can become part of the research process and are more likely to pursue further study in the geosciences. Research scientists and graduate students benefit by gaining access to new data that is labor-intensive to collect, and they support undergraduate and high-school-teacher research by processing the GPS data into a form that can be used those parties. Research institutes also benefit from new applicants to graduate school who have prior research experience. Faculty who act as mentors to the high school teachers and undergraduate students further develop their own professional skills in addition to nurturing the development of their mentees. Participants at all levels benefit from a deeper understanding of the Earth and its processes, as does society in general.
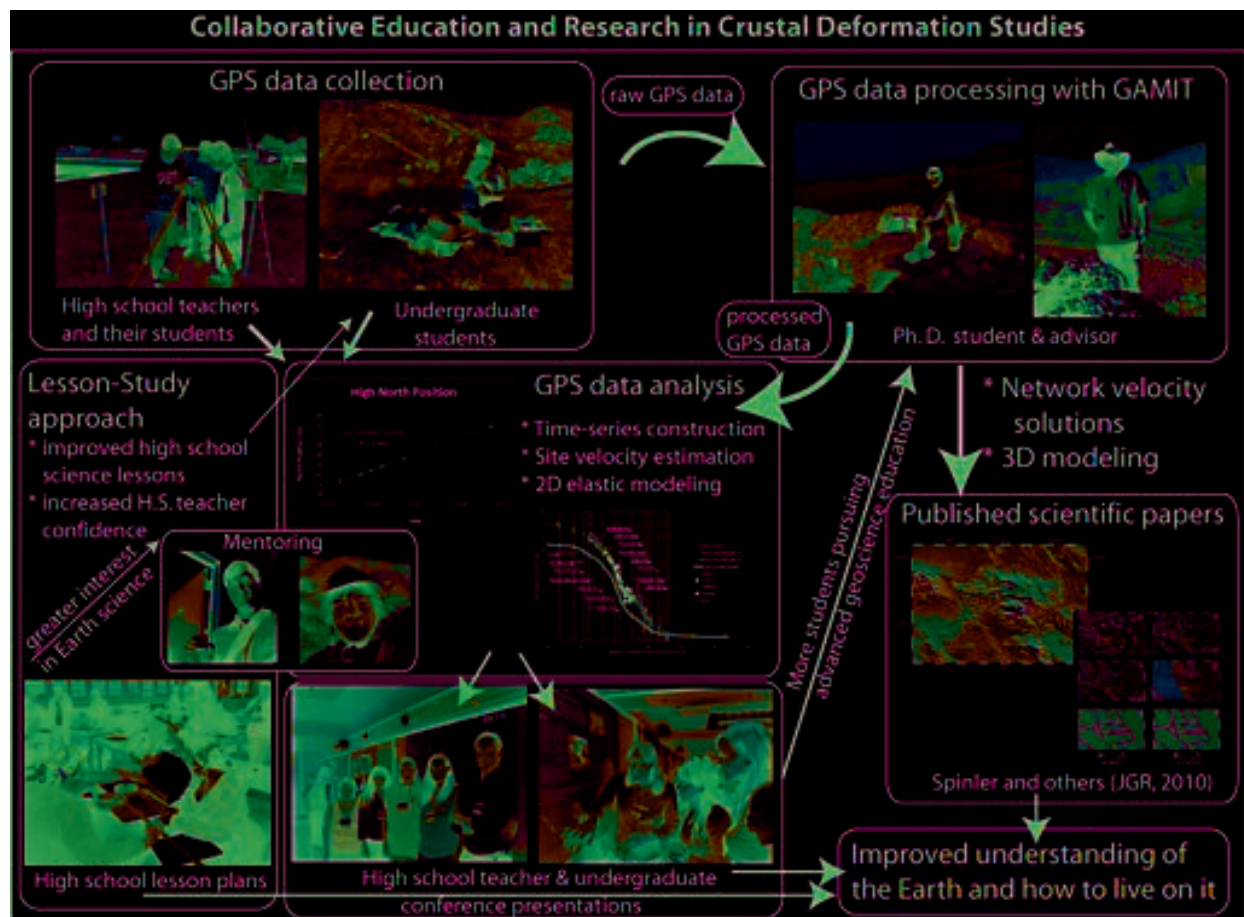
Earthscope funding is supporting campaign-style GPS data collection in the San Bernardino Mountains and vicinity, California from 2009-2011, building upon data collected previously (2002-2008) with other funding from the National Science Foundation and Southern California Earthquake Center. Each year, 7-10 high school teachers, 10-20 high school students and 8 undergraduate students participate in a 2-week long GPS workshop that includes training, data collection and data analysis and interpretation. Participants collect 5 days of campaign GPS data from 25 or more benchmarks in the San Bernardino Mountains and vicinity, where GPS data had previously been sparse. These data are important for understanding the partitioning of slip onto various faults that make up the transform plate boundary in southern California and for understanding differences between geologically and geodetically estimated fault slip rates. Previously published estimates of elastic strain accumulation across the San Bernardino strand of the San Andreas fault from geodetic data are at least two times smaller than slip rates estimated geologically over tens of thousands of years. The GPS data we are collecting will help to better constrain the models in this region.

Each year 5 of the 8 undergraduates who participated in the 2-week workshop used the GPS data they collected for undergraduate research projects that culminated either in conference presentations and/or oral presentations to faculty and students at their home institutions. These students constructed time series, estimated velocities for each site and conducted two-dimensional elastic modeling, systematically testing combinations of slip rates on 11-15 sub-parallel faults that make up the plate boundary. Of the five undergraduates who pursued undergraduate research projects during the first year of the project, one is continuing GPS-related research in a Ph.D. program and three others are currently applying to begin graduate studies in the 2011-12 academic year.

The high school teachers also continued their professional development beyond the two-week summer workshop. They presented their GPS time series and best-fitting models for fault slip rates at the annual meeting of the Southern California Earthquake Center, and each teacher displayed a copy of the research poster in their classrooms. The teachers also worked collaboratively in groups of 2-4 to develop a (or refine an existing) science lesson, related to earthquakes or to the scientific method and to test and improve the lesson using the Lesson Study approach (Stigler and Heibert, 2009). Lesson Study is a professional development process where teachers systematically examine their practice with the goal of becoming more effective. This examination centers on teachers working collaboratively on a small number of Research Lessons. "Lesson Study" is different from "lesson planning" because it focuses on what teachers want students to learn rather than on what teachers plan to teach.   In Lesson Study, a group of teachers develops a lesson together and ultimately one of them teaches the lesson while the others observe the student learning. The entire group comes together to debrief after the lesson and often revises and re-teaches the lesson to incorporate what has been learned (Lewis, 2002).   In their evaluations of the program, the participating teachers agreed that planning a lesson with other teachers produces a richer, better-designed lesson because everyone brings something to the process. They also felt that Lesson Study could develop leadership in teaching because of the increase in confidence, which encourages teachers to share what they have learned.   In the final year of the project, we plan to recruit multiple teachers from each of a few schools, to make it easier to sustain over the long term the teacher communities that we help to develop.

Many other opportunities for collaboration between education and research probably exist within the interdisciplinary EarthScope community. The key is finding the synergisms, where each party has something to gain from the collaboration and something to contribute to it.

References

Lewis, Catherine C. *Lesson Study: A Handbook of Teacher Led Instructional Change.* (2002). Philadelphia, PA: Research for Better Schools.

Stigler, J. & Hiebert, J. (2009). *The Teaching Gap: Best Ideas from the World's Teachers for Improving Education in the Classroom.* New York, NY: The Free Press.

Geophysical characterization of transtensional fault systems in the Eastern California Shear Zone-Walker Lane Belt

Matthew McGuire[1](matt.mcguire@ou.edu), Katie Keranen[1], Daniel F. Stockli[2], Joshua Feldman[2], and G. Randy Keller[1]

[1]University of Oklahoma, Norman, Oklahoma, USA

[2]Unversity of Kansas, Lawrence, Kansas, USA

The Eastern California Shear Zone (ECSZ) and Walker Lane belt (WL) currently accommodate ~25% of plate motion between the North American and Pacific plates. Linking the ECSZ and WL are the east-northeast striking faults of the Mina deflection, which transfer strain from the Owens Valley and Death Valley-Fish Lake Valley (DVFLV) fault systems to the transcurrent faults of the central Walker Lane. During the mid to late Miocene the majority of the strain was transferred through the Silver Peak-Lone Mountain extensional complex via a northwest dipping detachment. The primary location of strain transfer has since migrated to its present day location in the Mina Deflection, however the SPLM complex may still transfer some percentage of the strain from the ECSZ to the WL on a younger set of high-angle faults. Determining the amount of strain transfer through the SPLM complex can thus help in understanding strain accommodation throughout the entire step-over system, and intra-continental strain transfer more generally. To map recent strain accommodation in the SPLM region we collected seismic reflection and refraction profiles and a dense gravity grid, merged with existing gravity data, to map the young fault system, relative offsets along each fault set, and the geometry of the Miocene detachment. Preliminary results from the seismic profiles image the high-angle basin-bounding normal faults as well as the detachment in both the footwall and hanging wall and indicate strong lateral and vertical velocity boundaries. Detailed models of the velocity structure and improved MCS imaging are in progress. Gravity data spatially extend the mapped fault systems throughout the region and provide constraint on spatial variations in long-term strain accommodation. Our data and analyses will provide insight into long-term strain rates and strain distribution in the SPLM region, and more broadly, strain accommodation within the North American plate.

Coupling, Detaching and Sinking: How stages of Farallon subduction influenced topography of the 410-km discontinuity beneath North America

Melissa McMullen, Hersh Gilbert
Department of Earth and Atmospheric Sciences, Purdue University
mmcmulle@purdue.edu; hjgilber@purdue.edu

Prior to USArray, it was not possible to examine topography along the 410- and 660-km discontinuities at the spatial scale necessary to track the path of the Farallon plate into the transition zone. Equipped with this new capacity, we use P-to S-wave receiver functions to infer mantle processes through a comparison of thermally induced topography along the discontinuities to tectonic regimes on the surface. We explore the degree to which specific stages of Farallon subduction appear to have influenced small-scale mantle dynamics that led to the formation of distinct tectonic regimes. Similar to tectonics on the surface, the presence, absence, and the removal of the slab are still represented by three individual topographic regions along the 410-km discontinuity. This suggests that these three stages of subduction initiated processes large enough to extend to the transition zone. However the depth extent is limited as there is no such pattern on the 660-km discontinuity.

Related to the removal of the flattened portion of the Farallon and the influx of warm asthenosphere, we find that in the area to the west of the Rocky Mountains (region A in image below), the 410-km discontinuity is predominantly depressed by ~10 km. The continuity of the deepened topographic trend is disrupted by smaller localized processes that have occurred in the last 50Ma, resulting in an increase in topographic range of ±30 km. A central domain (B) extends from the easternmost portion of the Rocky Mountain province through most of the Great Plains, and is defined by an absence of topography with less than 10 km variation. This domain may represent a thermal transition from the warmed upper mantle of the west to the cooler stable craton in the east. The final domain (C), which extends eastward from the Dakotas, is consistently ~15km shallow. We interpret this discontinuity topography to result from the current location of the Farallon slab, which coincides with the location where prior tomographic studies and plate reconstructions place the slab. The presence of these three topographic domains demonstrates the association of stages of Farallon subduction and topography on the 410-km discontinuity. This also suggests that processes above the transition zone of North America are the dominant source of topography along the 410-km discontinuity.
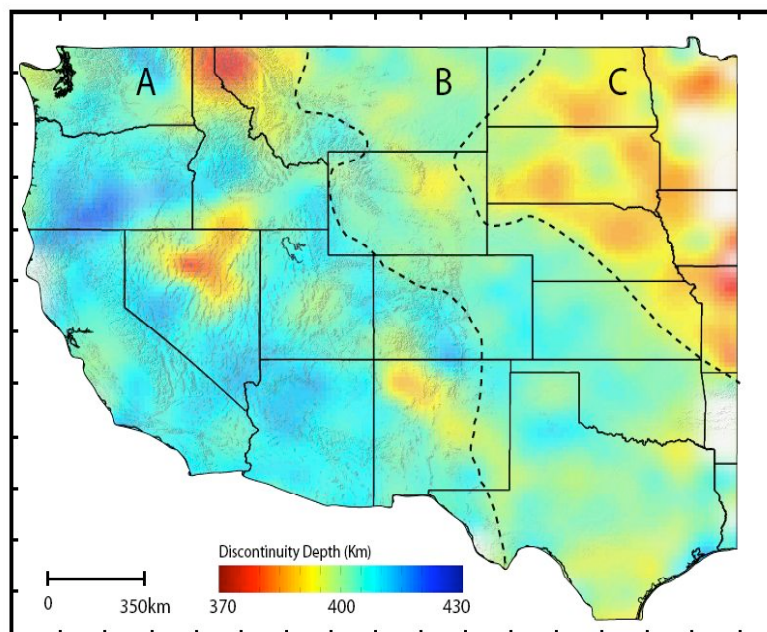
Figure: Three domains of the 410 discontinuity. Depth of the 410 is indicated by the color scale, which is overlain on surface topography. Lateral heterogeneities in seismic wavespeeds were accounted for using the tomographic model of Schmandt and Humphreys 2010.

EarthScope Content Module for Active Earth Display

Patrick McQuillan[1], Russ Welti[1], Jenda Johnson[2], Celia Rose Shiffman[3]
Shelley Olds[3] and John Taber[1]

[1] IRIS Consortium • 1200 New York Avenue, NW • Suite 800 • Washington, DC 20005
202-682-2220 • mcquillan@iris.edu
[2] Volcano Video Productions and IRIS Consortium • 1924 NE 47th Avenue • Portland, OR 97213
503-281-1814 • jendaj@comcast.net
[3] UNAVCO • 6350 Nautilus Drive • Boulder, CO 80301
303-381-7562 • celias@unavco.org

The Active Earth Display is an interactive computer-based display for formal and informal learning educational organizations (small museums, visitor centers, schools and libraries). It runs in a web browser using kiosk mode. The display consists of a customizable set of 76 web pages that describe a range of topics including tectonic regions (e.g. Cascadia, Basin and Range), real-time seismicity and seismic recordings and the EarthScope project. Low-cost and simple-to-implement, the Active Earth Display provides a way to engage educational audiences with earth science information without spending resources on a large exhibit.

Currently in production, the EarthScope Content Module consists of chapters that focus on What is EarthScope?, EarthScope Observatories, and EarthScope Science Results. Content topics are easily explored using a web page button type navigation interface via a touch screen or mouse. A formative evaluation of general public users informed the interface design.

Chapters in the EarthScope Content Module start with a general overview and proceed to detailed specifics. Each chapter utilizes at least one set of live research data (often more than one). This exposes the general public to active ongoing research that is engaging, relevant to the individual user, and explained in easy to understand terms. All live content is updated each time a user accesses the individual page displaying the live data.

All scientific terms are defined using pop-up boxes. Leading questions are presented allowing the user to examine the content before accessing the answer via pop-up box. Diagrams and charts of research data have explanatory keys that allow users to self explore all content.

Additional content pages can be created and inserted in the Active Earth Display by utilizing the Style Sheet templates or by simple html coding.

Regional conductivity structures of the northwestern segment of the North American Plate derived from 3-D inversion of USArray magnetotelluric data

Naser Meqbel, Gary D. Egbert and Anna Kelbert
College of Oceanic and Atmospheric Sciences, Oregon State University, Oregon, USA
Contact: naser@coas.oregonstate.edu

Long period (10-20,000 s) magnetotelluric (MT) data are being acquired in a series of temporary arrays deployed across the continental United States through EMScope, a component of EarthScope, a multidisciplinary decade-long project to study the structure and evolution of the North American Continent. MT deployments in 2006-2010 have so far acquired data at 272 sites on an approximately regular grid, with the same nominal spacing as the USArray broadband seismic transportable array (~70 km), covering the Northwestern US, from the Oregon-Washington coast across the Rocky Mountains, into Montana and Wyoming. Preliminary 3-D inversion results (Patro and Egbert; 2008) were based on data from the 110 westernmost "Cascadia" sites collected in the first two years. These revealed extensive areas of high conductivity in the lower crust beneath the Northwest Basin and Range (NBR), inferred to result from fluids (including possibly partial melt at depth) associated with magmatic underplating, and beneath the Cascade Mountains, probably due to fluids released by the subducting Juan de Fuca slab. Here we extend this study, refining and further testing the preliminary results from Cascadia, and extending the inversion domain to the East and to the South, to include all of the EarthScope data.

Although site spacing is very broad, distinct regional structures are clearly evident even in simple maps of apparent resistivity, phase and induction vectors. For instance, the phase of the Zyx impedance at periods longer than 2000 s shows a sharp transition to higher phases at the Cascade arc. Apparent resistivity and phase maps for both Zxy and Zyx components at ~ 100-2000 s are indicative of extensive areas of low resistivity in the crust and upper mantle in the southern part of the study area, extending from near the coast in the west, across the NBR and the Snake River Plain, then extending northeastward to Yellowstone in Idaho and Wyoming. The volcanic arc of the Cascadia subduction zone appears in the apparent resistivity maps as a low resistive structure elongated in the N-S direction, with reversal of induction vectors in the period range 300-3000 s.

For the 3-D inversion we are using the parallelized version of our recently developed Modular Code (ModEM), which supports Non-Linear Conjugate Gradient and several Gauss-Newton type schemes. Our initial inversions use data from 272 MT sites, fitting impedances and vertical field transfer functions (both together and separately). We obtained 3-D electrical conductivity models of the area, distinguishing the stable features that are seemingly required by the data. These include:

- A conductive structure elongated in the N-S direction underneath the volcanic arc of the Cascadia subduction zone starting at a depth of about 20-30 km.
- A pronounced conductive feature at or just below the base of the crust. This coincides with the NBR conductor of Patro and Egbert (2008), but our results show that this extends (and becomes even more pronounced) further to the east, where it connects with a conductive zone in the Yellowstone "hot spot" area.
- Resistive crustal structure in the coast range, and beneath the Columbia Plateau, consistent with the interpretation of Humprheys (2008) that these two sections of crust represent the accreted Siletzia terrane (broken subsequently by arc volcanism).
- A clear contrast between continental and oceanic mantle, with higher conductivities to depths of at least 150 km above the subducting Juan de Fuca Plate; the highest conductivities appear to be in the back arc in northern Washington.
- Higher deep mantle conductivity to the east, in particular beneath Yellowstone.

Multiple 3-D inversion and forward modeling tests will be required to verify the resolution and stability of these and other more subtle conductive and resistive structures in our 3-D models. Our efforts in this direction will be presented at the meeting.

Modern active and passive rifting analogs for the Mid-Continent Rift

Miguel Merino, miguel@earth.northwestern.edu

Seth Stein, seth@earth.northwestern.edu

Department of Earth and Planetary Sciences
Northwestern University, Evanston, IL 60208, USA

The Mid-Continent Rift (MCR) origin has been attributed to either tectonic forces, or rifting initiated by a plume. Petrologic and geochemical models favor the MCR having formed by active rifting over a mantle plume. In such scenarios, the two arms are analogous to today's East African rift - Red Sea - Gulf of Aden system that is splitting Africa into three plates. A new tomographic image of the Red Sea region shows how an upper mantle linear low velocity channel extending from a plume can form. Alternatively, many tectonic models view the rift as having formed by passive rifting a consequence of the Grenville orogeny, a series of 1.3-0.9 Ga tectonic events. In such interpretations, northwest-directed convergence at the southern margin of Laurentia (North America) caused extension and magmatism to the northwest, including formation of the MCR. This scenario could be similar to the way the Baikal rift results from the Himalayan collision. Comparing the MCR to present rifts will give insight into what features to look for.

Imaging the evolution of lithospheric structure in the Western U.S. from receiver functions

Meghan S. Miller, University of Southern California, Los Angeles, CA 90089, msmiller@usc.edu

Alan Levander, Rice University, Houston, TX 77005, alan@rice.edu

We have produced common conversion point (CCP) stacked Ps and Sp receiver function image volumes of the lithosphere and uppermost mantle beneath the western United States using teleseismic data recorded by the USArray Transportable Array. Since Ps and Sp receiver functions are made with different frequency bands and distance range events, they produce images of different resolutions, and therefore can provide independent estimates of depths for the crust-mantle and lithosphere-asthenosphere interfaces. We have imaged a large volume of the western United States, which includes a series of distinct of tectonic environments, allowing us to investigate existing views of the evolution of these structural boundary layers. From these structural image volumes we identify the Mohorovičić discontinuity (Moho) as a nearly continuous topographic surface, varying in depth between 22-52 km with a few tectonically understandable discontinuities associated with regions of convective downwelling or unusual material properties. Two of these features are known anomalies associated with the Wallowa mountains and the southern Sierra Nevada. Another, newly imaged, drip-like feature beneath the central Colorado Plateau is clearly imaged in our receiver functions. In contrast to the Moho, the lithosphere-asthenosphere boundary (LAB) has a much greater depth variation (~40-150 km), is weaker in amplitude than the Moho signal and and unlike the Moho cannot be described as a single continuous surface. Beneath some regions the LAB has a very complex expression as a series of partially overlapping surfaces, which we attribute to multiple physical sources for a seismic impedance contrast of the correct polarity (fast to slow velocity change). Despite the complex structure of the asthenosphere and mantle lithosphere throughout most of the region, it is clear that the lithosphere is almost uniformly twice as thick east of the Cordilleran hinge line in comparison to the west. This boundary marked the edge of the passive margin bordering the Precambrian terranes along much of southwestern North America. Other tectonic boundaries are also clearly defined by the Moho and LAB depths, and much of the seismicity and recent volcanism in the western U.S. not associated with the Pacific-North America-Juan de Fuca plate boundaries are found concentrated along these steep gradients in either crustal or lithospheric thickness. This suggests that lateral gradients in integrated lithospheric strength act as loci of deformation and furthermore we infer that the depths of the Moho and the LAB can be reset by small scale convection and erosion at these gradients or boundaries within the lithosphere.

Evidence of transient increases of fluid pressure in SAFOD phase III cores

Silvia Mittempergher[1,2], Giulio Di Toro[1,3], Jean Pierre Gratier[2], Jafar Hadizadeh[4], Steven A. F. Smith[3], Richard Spiess[1]

1 Università di Padova, Dipartimento di Geoscienze, Padova, Italy; 2 Université Joseph Fourier – Grenoble I, ISTerre, Observatoire, Grenoble, France;3 Istituto Nazionale di Geofisica e Vulcanologia, Roma, Italy; 4 Department of Geography and Geosciences, University of Louisville, KY, United States

Abstract

The San Andreas Fault Observatory at Depth (SAFOD) in Parkfield, central California, has been drilled through a fault segment that is actively deforming through creep and microearthquakes. Creeping is accommodated in two fault strands, the Southwest and Central Deforming Zones, embedded within a damaged zone of deformed shale and siltstone. During drilling, no pressurized fluids have been encountered, even though the fault zone acts as a permeability barrier to fluid circulation between the North American and Pacific plates. Microstructural analysis of sheared shales associated with calcite and anhydrite-bearing veins found in SAFOD cores collected at 1.5m from the Southwest Deforming Zone suggests that transient increases of pore fluid pressure have occurred during the fault activity, causing mode I fracturing of the rocks. Such build-ups in fluid pressure may be related to permeability reduction during fault creep and pressure-solution processes, resulting in localized failure of small fault zone patches and providing a potential mechanism for the initiation of some of the microearthquakes registered in the SAFOD site.

Serpentinite within the Creeping Bartlett Springs Fault, Northern California: An Analogue for the San Andreas Fault near SAFOD?

D. E. Moore, R. J. McLaughlin, J. J. Lienkaemper, and M. J. Rymer, U. S. Geological Survey, Menlo Park, CA 94025 USA

The Bartlett Springs Fault (BSF) is an active, right-lateral strike-slip fault, about 170 km in length, that is part of the San Andreas Fault system north of San Francisco, California. Its slip rate is currently estimated to be ~6 mm/yr, and along a segment that crosses Lake Pillsbury half the slip (3.1 ± 0.3 mm/yr) is taken up by creep. An exposure of the BSF ~1.6 km northwest of Lake Pillsbury (Figure 1) consists of sheared serpentinite that has risen buoyantly during right-lateral shear within Late Pleistocene to Holocene (?) fluvial deposits. Some serpentinite has extruded onto the ground surface. The serpentinite-rich mass contains a large concentration of porphyroclasts distributed in a sheared and foliated, fine-grained matrix that varies from light greenish- to dark bluish-gray in color. The lighter-colored zones are dominated by antigorite serpentinite that shows some retrograde recrystallization to chrysotile and lizardite. The darker zones are rich in porphyroclasts containing one or more of the minerals talc, chlorite, and tremolite-actinolite in a sheared matrix of the same minerals. The mineral assemblage of the darker areas is characteristic of metasomatic reaction zones formed between ultramafic and crustal rocks at greenschist- to subgreenschist-facies conditions. Incipient low-temperature alteration accompanying shear has formed Mg-rich smectitic clays, with local development of foliated, clay-rich gouge containing clasts of the other rock types. Textures and mineral assemblages of the gouge in this exposure of the BSF are very similar to those observed in samples of Phase 3 SAFOD core from the southwest and central deforming zones (SDZ and CDZ, respectively). The main difference is that the low-temperature, clay-forming reactions have progressed to a substantially greater extent in the SAFOD gouge zones. This outcrop of the BSF therefore warrants more detailed study as a possible analogue of the early stages in the development of the SDZ and CDZ.
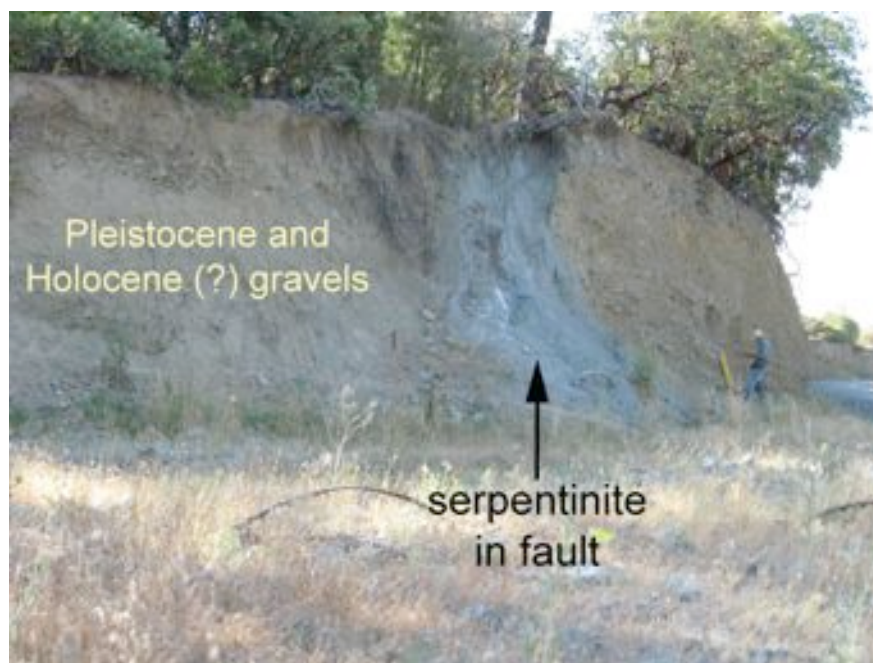

Figure 1. The serpentinite-filled Bartlett Springs Fault, exposed along a scarp roughly 1.6 km northwest of Lake Pillsbury in northern California. Photo by J. J. Lienkaemper.

Textural and Mineralogical Comparison of Fault Gouge from the Two Actively Creeping Strands at SAFOD

Diane E. Moore and Michael J. Rymer, U.S. Geological Survey, Menlo Park, CA 94025

Fault creep at SAFOD is highly localized to two narrow zones of foliated gouge, the 2.6-m-wide Central Deforming Zone (CDZ) and the 1.6-m-wide Southwest Deforming Zone (SDZ). The CDZ takes up the majority of the creep, as evidenced by the more-pronounced well-casing deformation associated with it. Preliminary petrographic examination of recently obtained Phase 3 core samples indicates that both gouge zones record shear-enhanced metasomatic reactions between serpentinite tectonically entrained in the fault and adjacent sedimentary rocks. The gouges consist of porphyroclasts of serpentinite and sedimentary rock dispersed in a foliated matrix of the Mg-rich clay minerals saponite ± corrensite. Porphyroclasts of all types are variably altered to the same Mg-rich clays as the gouge matrix, and fractures lined with Mg-clays extend for a short distance (<1 m) into the sedimentary damage-zone rocks adjoining the gouge zones. Differences in texture and mineral composition between the CDZ and SDZ may be attributable to their different shearing rates. The SDZ core contains larger serpentinite porphyroclasts than the CDZ (Phase 3 Core Atlas, www.earthscope.org), and powder X-ray diffraction analysis of the gouge suggests a larger sedimentary component (e.g., quartz and feldspar contents) in the SDZ than in the CDZ. Veinlets of calcite up to 5 mm in length are preserved in the SDZ gouge matrix; these are more than an order of magnitude longer than the ≤200 µm long veinlets of anhydrite (?) found in the CDZ. The gouge-matrix clays in the CDZ are largely saponitic, with ~5-8 wt% Al_2O_3. In contrast, the SDZ is dominated by more corrensitic clays (~9-12 wt% Al_2O_3). Where age relations can be determined, saponitic clays are younger than corrensitic ones in the SDZ; for example, saponite concentrations are greatest adjacent to the late calcite veinlets. Smaller sizes and lower abundances of of both serpentinite and sedimentary porphyroclasts in the CDZ are consistent with a greater degree of shear-enhanced reaction to form the Mg-rich clays. The differences in clay-mineral compositions may reflect a change in physico-chemical conditions such as temperature or fluid chemistry, with clays in the more actively deforming CDZ adjusting more completely to the new conditions than those in the SDZ. Clay-mineral chemistry may prove useful for tracking variations in slip rate across the widths of the gouge zones.

Preliminary Measurements of Permeability, Electrical Resistivity and Frictional Strength of SAFOD Fault Gouge and Damage Zone Rocks

C. Morrow*, D. Lockner, D. Moore and S. Hickman

U.S. Geological Survey, Menlo Park, CA 94025 USA

*cmorrow@usgs.gov

The San Andreas Fault Observatory at Depth (SAFOD) scientific drillhole near Parkfield, California crosses two actively deforming shear zones at a vertical depth of 2.7 km. Core samples retrieved from these active strands consist of a foliated gouge containing the magnesium-rich clay minerals saponite ± corrensite, with porphyroclasts of serpentine and sedimentary rock. The adjacent damage zones are comprised of fine-grained sandstones, siltstones, and mudstones. We have conducted laboratory tests to measure the permeability, electrical resistivity and frictional strength of these various samples at effective confining pressures, P_{eff}, up to the maximum estimated *in situ* P_{eff} of 120 MPa under saturated conditions, using a brine formulated to duplicate the *in situ* formation fluid chemistry. Permeability values of intact damage zone samples were around 10^{-18} to 10^{-19} m^2 at 10 MPa P_{eff} and decreased with applied pressure to 10^{-20} to 10^{-22} m^2 at 120 MPa. Permeability of the foliated gouge was distinctly lower than the damage-zone rocks (10^{-20} to 10^{-23} m^2 over the same pressure range) due to the fine-grained, clay-rich nature. Corresponding electrical resistivity values increased with increasing P_{eff}, but were also lower for the foliated gouge (3 to 30 ohm-m) compared to the damage zone rocks (40 to 1000 ohm-m). In addition, foliated gouges showed a marked increase in the pressure sensitivity of resistivity at P_{eff} above 70 MPa. Permeability of crushed-and-sieved foliated gouge was measured during shearing between Berea sandstone forcing blocks at 120 MPa effective normal stress. These permeability values were insensitive to shear displacement, at around 3 x 10^{-22} m^2, indicating that most of the permeability loss occurred during initial compaction due to the application of normal stress. Such extremely low permeability would constitute a cross-fault barrier to fluid flow at depth, in agreement with mud gas analyses carried out across the San Andreas Fault in SAFOD (Wiersberg and Erzinger, 2008).

The coefficient of friction in the two shear zones (μ = 0.15-0.2) was much lower than that of the damage zone rocks ($\mu \sim$0.4-0.6) due to the presence of the weak phyllosilicate mineral saponite.   Thus, the apparent weakness of the San Andreas Fault, based on stress orientation and heat flow data, can be explained entirely by the rheologic properties of the fault gouge at the SAFOD location without appealing to high fluid pressure, shear heating or other stress reducing mechanisms (Lockner et al., 2011, *Nature*).

An interseismic Global Positioning System velocity field for the central California coast region and preliminary deformation models

Jessica R. Murray-Moraleda[1], Wayne Thatcher[1], Jerry Svarc[1], Tiemi Onishi[1]

[1]U.S. Geological Survey, Menlo Park, CA 94025

Abstract

The central California coast, from north of Point Piedras Blancas (36°N) southward to Point Arguello (34.6°N) and west of the Rinconada and East Huasna faults, is a structurally complex region cut by several subparallel, late Quaternary faults. Studies of the way in which strain is partitioned across the Central California Coast Region (CCCR) have concluded that observed deformation patterns arise from transpression due to the clockwise rotation of the Transverse Ranges (McLaren and Savage, BSSA 2001) or, alternatively, the westward transfer of right lateral strike slip motion in a left-stepping fashion across the region (Hardebeck, BSSA 2010). Despite relatively low rates of deformation inferred from geologic studies of the CCCR, the occurrence of the 2003 M_w 6.5 San Simeon earthquake southeast of Point Piedras Blancas highlights the need to better understand the ongoing patterns of deformation here as a means for assessing the seismic hazard.

Geodetic data can be used to elucidate how strain is currently partitioned between shear parallel to the San Andreas Fault (SAF) and contraction within the CCCR, and on what structures active deformation is occurring. We have compiled a new, spatially dense secular velocity field for the CCCR derived from Global Positioning System (GPS) measurements. We leveraged the EarthScope Plate Boundary Observatory (PBO) permanent GPS network and existing survey-mode GPS (SGPS) data available in archives. To this we added newly-collected SGPS observations and data from nine semi-permanent GPS (SPGPS) sites established by USGS to improve spatial coverage and obtain well-constrained velocities in a short amount of time. Using time series analysis techniques that incorporate the white and colored noise typically present in GPS time series (Langbein, JGR 2004), we estimated secular rates. We accounted for the effects of the 2003 M_w 6.5 San Simeon and 2004 M_w 6 Parkfield earthquakes by excluding data likely to be affected from the analysis and reassessing the uncertainties on estimated rates. Notably, the postseismic signal following the San Simeon event is considerably longer-lived than reported in earlier papers making it difficult to estimate secular rates for sites in the affected region.

We have used the resulting secular velocities, in combination with velocities from the Southern California Earthquake Center Crustal Motion Map v.4 and the Plate Boundary Observatory velocity field, to constrain block models of deformation for central and southern California. We follow the approach of McCaffrey (2005) using his *defnode* software to solve for the rotation of fault-bounded blocks, fault slip rates, and internal strain within blocks. Preliminary results show that while significant internal strain occurs in the Salinian block (which extends west from the SAF to the coast in central California) this is largely due to displacement patterns observed near the junction of the SAF and the Garlock fault. The data do not require substantial slip on the Rinconada fault or, alternatively, a fault bounding the eastern edge of the CCCR; estimated slip rates are ~2 mm/yr and <1 mm/yr respectively. The data also do not

suggest that significant internal strain is occurring within the CCCR. Ongoing work is focused on exploring different block geometries in an effort to better constrain slip rates on the Hosgri and San Andreas faults. These results will contribute to development of a coherent regional tectonic model and help characterize the potential seismic sources in the region.

References

Hardebeck, J. (2010), Seismotectonics and Fault Structure of the California Central Coast, *Bull. Seis. Soc. Am.*, **100**(3), 1031–1050, doi: 10.1785/0120090307.

Langbein, J. (2004), Noise in two-color electronic distance meter measurements revisited, *J. Geophys. Res.*, **109** (B04406), doi:10.1029/2003JB002819.

McLaren, M. and W. Savage (2001), Seismicity of South-Central Coastal California: October 1987 through January 1997, *Bull. Seis. Soc. Am.*, **91**(6), 1629–1658.

Crustal strain across a deeply exhumed continental fault

NADIN, Elisabeth S., Department of Geology and Geophysics, University of Alaska Fairbanks, Fairbanks, AK 99775, enadin@alaska.edu
HIRTH, Greg, Geological Sciences, Brown University, Box 1846, 324 Brook St, Providence, RI 02912

Strike-slip faults commonly arise in transpressional environments—the Denali fault is a salient modern-day example—and are associated with large earthquakes. Geodetic data can be used to assess the relative components of shortening and strike-slip shear of modern transpressional faults. However, understanding the crustal strain accommodated by such faults, which arise from long-term plate tectonic forces, requires study of fault zones exhumed from mid- to lower-crustal levels. The 130-km-long Proto-Kern Canyon fault (PKCF) in the southern Sierra Nevada, CA, is one such fault that accommodated ~15 km of dextral displacement in response to obliquely directed forces imparted during Farallon plate subduction. The PKCF traverses exposure levels of ~25 km, allowing investigation of structures and microstructures that provide constraints on the distribution of stress and strain from ductile through brittle conditions, including the transition zone. A regional geobarometric database of >200 locations through the batholith constrains the paleodepths of PKCF exposures. The fault is ~2 km wide in most places—typical of mid-crustal shear zones—and across its width, different rock types including marble, phyllite, quartzite, granodiorite, and amphibolite are variably deformed. Thus, the PKCF provides a natural laboratory to investigate crustal strain as a function of temperature, depth, and composition.

Samples from the study analyzed thus far crystallized at depths of 11–13 km and temperatures of 700–725 ˚C. The Titanium-in-quartz thermometer (TitaniQ of Wark and Watson, 2006) yields recrystallized quartz temperatures of ~480 ˚C for four igneous and quartzite mylonite samples. The oldest deformed plutonic rocks within the shear zone are 104 Ma, and the youngest igneous member was deformed as it was emplaced ca. 85 Ma. From the younger intrusion, two-feldspar thermometry on plagioclase with stretched orthoclase overgrowths yields T = 480 ± 22˚ C, and TitaniQ on recrystallized quartz yields T = 461 ˚C ± 22˚ C. Such uniform recrystallization temperatures in intrusions spaced by up to 20 Ma indicated that temperature equilibrated fairly quickly across the shear zone while it was active.

Deformation temperatures help refine our ability to determine strain rate along the PKCF. Quartz piezometry-derived stresses for several samples are 50–95 MPa; incorporating the TitaniQ-derived deformation temperature of 480 ˚C places natural strain rates at 10^{-15}–10^{-13} s^{-1}. Compositional studies were paired with EBSD-derived crystallographic preferred orientation (CPO) data for rocks of all compositions from the shear zone. Quartz CPO is absent in micaceous quartzite that forms the western boundary of the shear zone, indicating mica dictates the strength (or weakness) of mid-crustal shear zones. In contrast, the shear zone's eastern boundary displays progressively diminishing quartz CPO of igneous mylonites, suggesting that when

temperature is high, it plays the greater role in imparting weakness through multi-mineralic rocks. This exhumed fault zone points to enhanced crustal weakness along a long-lived structure.

Illinois EarthScope: a new view of integrated Earth sciences

Robert S. Nelson and David H. Malone
Department of Geography-Geology
Illinois State University
Normal, Illinois 61790-4400

Illinois EarthScope is a 72-hour workshop for middle and high school science teachers. The workshop consists of four components. The first component is a week-long introduction to EarthScope and teacher resources available through EarthScope, IRIS and UNAVCO. The early evolution of the Earth is presented and teachers examine meteorites and produce an expanded slice of the Earth. Continents are then developed and the plate tectonics model is examined. Earthquakes are presented along with three-component seismograms and Plate Boundary Observatory data. Teachers visit the Mackinaw, Illinois Backbone Seismic Station and Plate Boundary Observatory HDIL. The first component includes a discussion of the deployment of the transportable array and campaign arrays.   The nature plate boundary and intra-plate earthquakes are examined. The first component concludes with an examination of large scale climate change, glaciation and fluvial modification of continental interior. Component two is a four day field trip to examine the midcontinent geology starting with the granite-rhyolite terrain in the St. François Mountains of Missouri and concluding with neotectonics and mineralization along the Commerce City Geophysical Lineament. Component three is a weekend session on the geochemistry and geophysics of volcanism. Yellowstone, the Cascades and the Chilean Andes volcanoes and volcanic hazards and risks are discussed.   Component four is a weekend session on earthquake hazards and earthquake risk. Cascadia subduction, the San Andreas Fault, and the New Madrid and Wabash Valley seismic zones are examined.

Accessing EarthScope and Complementary Data Sets at the Northern California Earthquake Data Center

Douglas Neuhauser, Mario Aranha, Stephane Zuzlewski, Barbara Romanowicz (UC Berkeley Seismological Laboratory)

The NCEDC is an official archive of EarthScope PBO and SAFOD time series data, which are complemented by the seismic, strain, geodetic, and other geophysical data sets for northern California at the NCEDC from UC Berkeley, USGS and other contributors. The NCEDC archives a broad range of time series data; broadband, strong motion, and short period seismic data, borehole seismic and strain data, low frequency geophysical data (strain, creep meter, and well water level), and continuous and campaign GPS data. All NCEDC data are available to all users over the internet through a variety of data request and retrieval methods.

Earthquake catalog, phase, and amplitude data from the Northern California Seismic System (NCSS) and the entire ANSS catalog are accessible through web search and retrieval interfaces.   Time series data from can be queried and retrieved through web forms, email request methods such as NetDC, BREQ_FAST, and EVT_FAST, and programmatic interfaces such as FISSURES DHI, STP, and the NCEDC Simple Wave Server (SWS). GPS data in RINEX and raw format at both normal rate (30 and 15 second) and high rate (1 second) are available through HTTP, FTP, and are accessible through other data distributors via GPS Seamless Archive (GSAC) clients at UNAVCO and SOPAC.

The NCEDC Simple Wave Server (SWS) and companion program Simple Wave Client (SWC) provide a simple programmatic interface for retrieve continuous segments or event time series data in MiniSEED format. Data can be requested by SEED Station, Network, Channel, Location, time interval, and/or eventid. SWC runs on Linux, Solaris/Unix, and MacOS systems. The NCEDC provides 2 Simple Wave Servers – one for the NCEDC data archive, and one for real-time data from the NCEDC DART (Data Available in Real Time). Dataless SEED volumes providing complete metadata for all channels are available by FTP or HTTP from the NCEDC. The current data request servers provide a basis for future data access methods such as web services.

The Northern California Earthquake Data Center (NCEDC) is joint project of the UC Berkeley Seismological Laboratory and the USGS, with additional funding provide by NSF EarthScope and the Department of Energy.

GPS interferometric reflectometry (GPS-IR): Forward and inverse modeling results

Felipe G. Nievinski,[1] Kristine M. Larson,[1] Valery U. Zavorotny [2]
[1] *Department of Aerospace Engineering Sciences, University of Colorado, Boulder*
[2] *Earth Systems Research Laboratory, National Oceanic and Atmospheric Administration, Boulder, CO*

GPS interferometric reflectometry (GPS-IR) is a method that exploits multipath for ground-based remote sensing in the surroundings of a GPS antenna. It has been demonstrated to be capable of retrieving a number of environmental parameters of importance to the study of the water and carbon cycles, such as soil moisture changes, snow accumulation and melting, and vegetation growth. Initial results for GPS-IR adopted a mostly empirical data processing approach: changes in observation frequencies and amplitudes have been correlated with changes in environmental parameters. More recently, we have developed a physically-based forward model and a statistically-rigorous inverse model for optimal exploitation of GPS-IR observations; the former is based on geometrical optics and the latter is based on non-linear least squares. The intent is to make GPS-IR environmental retrievals less sensitive to equipment changes (antenna), to alleviate site feasibility requirements (regarding topography, both large-scale deterministic undulations and small-scale stochastical surface roughness), and to be able to separate different environmental effects (e.g., accumulation vs. densification of snow, soil moisture vs. soil type, vegetation growth vs. ground roughness). We will show results for GPS sites of the EarthScope Plate Boundary Observatory, comparing GPS-IR environmental retrievals to *in situ* observations of snow depth where available.

Anomalous upper mantle structure of Central Kamchatka indicated by results of beam-averaged receiver function migration.

Alex Nikulin[1], Vadim Levin[1], Michael West[2].

[1]*Rutgers University, Department of Earth and Planetary Sciences, 610 Taylor Rd., Piscataway, NJ 08854*

[2]*University of Alaska, Fairbanks, Geophysical Institute, 903 Koyukuk Dr., Fairbanks, AK 99775*

Volcanoes of the Klyuchevskoy Group (KG) form the most active arc volcanic system in the world. They are also quite unusual in a number of attributes of their tectonic setting and eruptive output.

The upper mantle structure beneath the KG is far from the textbook model of a convergent plate margin. While at present the subduction zone terminates shortly to the north of the KG, the existence of 5-10 Ma old volcanic centers in northern Kamchatka requires this to be a tectonically recent development. A zone of low seismic velocities and high attenuation is reported ~100 km beneath the KG by a number of studies using local earthquakes. Investigations of mantle deformation by means of seismic anisotropy suggest a complex 3D flow pattern.

We develop and implement a new beam-averaged method of migrating multi-taper correlated (MTC) teleseismic receiver functions to image the seismic structure of the upper mantle beneath the KG. We migrate and stack receiver functions from a set of observatories on the Bezymianny volcano to show that the upper mantle contains a surprising feature - a sharply delineated planar inclined low-velocity body at ~70 to 100 km depth. A convecting mantle wedge over the subducting plate is not expected to have strong gradients in seismic velocity. In our images this body is clearly distinct from the much deeper subducting plate. Intriguingly, it occupies the "textbook" depth for the formation of island arc volcano magmas.

We demonstrate that beam-averaged MTC receiver function migration enables generation of high-resolution images of the upper mantle velocity structure relying on seismic data recorded over a relatively short station deployment period (~3 years). We propose the future use of beam-averaged MTC migration method for previously deployed EarthScope TA sites in Cascadia and sites yet to be deployed in Alaska.

Large contrasts in crustal structure and composition between the Ordos plateau and the NE Tibetan plateau from receiver function analysis

Fenglin Niu[1], Suzhen Pan[1]
*Department of Earth Science, Rice University Houston, Texas, USA*

Abstract

The Ordos plateau located in the western side of the North China craton is a distinct aseismic block. The plateau is bounded on the south and east, respectively, by the Paleozoic-Mesozoic Qinling orogenic belt and the Taihangshan mountain range. A series of graben systems were developed late in Cenozoic around the southern and eastern margins of the plateau. The Ordos is also bordered on the southwest by the northeastern (NE) margin of the Tibetan Plateau formed by the Cenozoic India-Eurasia collision. Tapponnier et al. (2001) suggested that the rise of the Tibetan plateau occurred progressively from south to north, and that crustal thickening was accommodated by shortening along the compressional direction. On the other hand, Clark and Royden (2000) proposed that the topographic relief along the eastern and NE margins of the plateau is maintained by dynamic pressure from a lower crust flow. Injection of lower crustal material from the central plateau to the edges inflated the crust along the borders of the plateau. In other words, crustal thickening occurred mainly in the lower crustal level. In general mafic rocks have higher Vp/Vs ratios than felsic rocks (Zandt and Ammon, 1995; Christensen, 1996). Thus seismic measurements of Vp/Vs ratio across the area could be used to diagnose whether the crustal shortening model or the lower crustal flow model is a more appropriate explanation for the crustal thickening observed along the NE corner of the Tibetan plateau.

We analyzed thousands of receiver-function data recorded by 182 national and regional stations of the broadband seismic network operated by the China Earthquake Administration to study the crustal structure beneath the Ordos plateau and the northeastern margin of the Tibetan plateau. Crustal thickness and average crustal Vp/Vs ratio were measured at each station. The Ordos plateau is underlain by a moderate thick crust with an average Moho depth ~40 km. The Trans-North China Orogen east to the Ordos is featured by a thin crust varying from 25-35 km. The Weihe Graben at the southern border of the Ordos plateau is lying above a ~30-km thin crust, while its southern neighbor, the Qinling organic belt has a thick root extending to as much as 45 km deep. Crust beneath the northeastern margin of the Tibetan plateau varies from 55 to 65 km (Figure 1).

We found a remarkable contrast between the Tibetan and Ordos plateaus in the measured Poisson's ratio: the Ordos plateau is featured by a high Poisson's ratio (*Vp/Vs* = 1.761, σ =0.261) while the Tibetan margin has a very low Poisson's ratio

(*Vp/Vs* = 1.714, σ =0.240). Laboratory studies indicated that the Poisson's ratio is a good indicator of crustal composition (e.g., Christensen, 1996). Pressure and temperature appear to have little effect on it. The relative abundance of quartz (*Vp/Vs* = 1.49, σ =0.090) and plagioclase (*Vp/Vs* = 1.87, σ =0.300) has a dominant effect on the Poisson's ratio of common igneous rocks and their metamorphosed equivalents. An increase in plagioclase content or a decrease in quartz content can increase the Poisson's ratio of a rock. For example, the Poisson's ratio increases from 0.240 for granitic rock, to 0.269 for diorite, and to 0.300 for gabbro (Tarkov and Vavakin, 1982). The mafic/ultramafic igneous rocks generally have high Poisson's ratios because they usually contain gabbro and peridotite or dunite, which originate from magmatic differentiation. The measured lower ratio thus indicate that the crustal column beneath the NE margin of the Tibetan Plateau is rather felsic and is inconsistent with the lower-crust injection model. This lower crustal flow model also has difficulty in explaining the thin crust beneath the Weihe Graben. The observed contrast in the Poisson's ratio, on the other hand, agrees with the observed surface deformation that indicates the Ordos plateau is mechanically stronger than the Tibetan plateau.
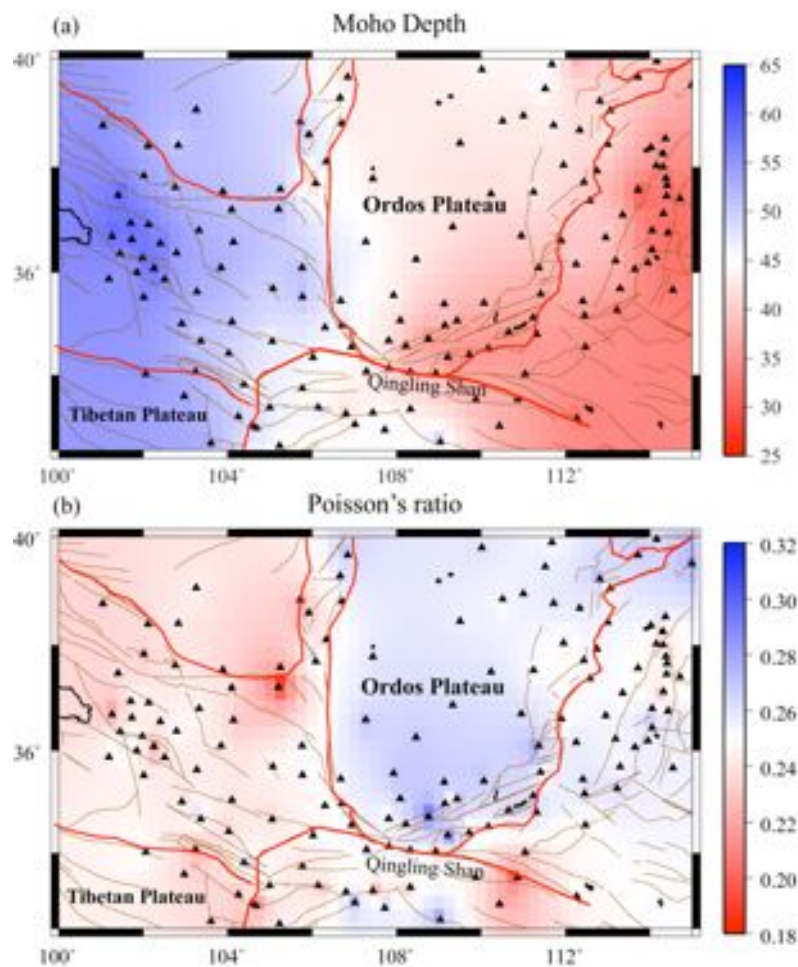
Figure 1. *(a) Moho relief map inverted from observations at stations shown as black triangles..*

Note the gradual increase of Moho depth from east to west. Also note the thin crust beneath the Weihe graben at the southern edge of the Ordos plateau. (b) Map of lateral variations for the Poisson's ratio. The color contour is calculated from observations at stations shown by black triangles.

Reference:

Christensen, N.I., 1996. Poisson's ratio and crustal seismology. J. Geophys. Res. 101, 3139–3156.

Clark, M. K., Royden, L. H., 2000. Topographic ooze: Building the eastern margin of Tibet by lower crustal flow, Geology 28, 703-706.

Tapponnier P., Xu, Z. Q., Roger, F., Meyer, B., Arnaud, N., Wittlinger, G., Yang, J. S., 2001. Oblique Stepwise Rise and Growth of the Tibet Plateau, Science 294, 1671-1677.

Tarkov, A. P., Vavakin V. V., 1982. Poisson's ratio behavior in crystalline rocks: Application to the study of the Earth's interior, Phy. Earth Planet. Inter. 29, 24-29, doi:10.1016/0031-9201(82)90134-0.

Zandt, G., Ammon, C. J. 1995. Continental crust composition constrained by measurement of crustal Poisson's ratio, Nature 374, 152– 154.

Toward an Understanding of the Geometry of the Farallon Plate in North America: Synthesis of Three-dimensional Imaging Results from the Transportable Array

Gary L. Pavlis, Xin Liu (Department of Geological Sciences, Indiana University, Bloomington, Indiana); Scott Burdick, Robert D. van der Hilst (Department of Earth, Atmospheric, and Planetary Sciences, Massachusetts Institute of Technology, Cambridge, Massachusetts); and Frank L. Vernon (Institute of Geophysics and Planetary Physics (IGPP), University of California, San Diego, La Jolla, California)

We compare all accessible, three-dimensional, P and S velocity models and wavefield imaging results produced from TA data with the objective of defining the geometry of the Farallon slab. We use three-dimensional visualization techniques to compare these results in a common coordinate system linked to surface geographic line data and topography. We evaluate two fundamentally different classes of models for the geometry of the Farallon slab: (1) a single, continuous body linking current and past subduction zones to high velocity anomalies in the eastern US imaged by global tomography; and (2) a series of recently proposed interpretations that fragment the slab into pieces of different scales. The basic tool we use to evaluate these divergent models is to define one or more surfaces that define the geometry suggested by the authors. We then evaluate whether the geometry these surfaces define is kinematically reasonable and if a particular model is consistent with independently determined results. We find the results to date have major inconsistencies in relation to the Farallon slab geometry problem. Work is ongoing to evaluate additional newly published results and to develop quantitative metrics for cross-validation of different results.

Kinematics of the Snake River Plain and Adjacent Basin and Range Regions from GPS

Payne, Suzette J. (Suzette.Payne@inl.gov), Idaho National Laboratory, P.O. Box 1625, Idaho Falls, Idaho 83415-2025; **McCaffrey, Robert** (r.mccaffrey@pdx.edu) Portland State University, Department of Geology, PO Box 751, Portland, OR 97207. **King, Robert W.** (rwk@chandler.mit.edu) Dept. of Earth, Atmospheric & Planetary Sciences, Massachusetts Institute of Technology, Cambridge, MA 02139; **Kattenhorn, Simon A.** (simkat@uidaho.edu) University of Idaho, Dept. of Geological Sciences PO Box 443022, Moscow, ID 83844-3022;

Horizontal Global Positioning System (GPS) velocities together with geologic, volcanic, and seismic data indicate very little deformation at present within the Snake River Plain, Idaho. The Snake River Plain, a prominent physiographic feature in the western U.S., exhibits low topography, seismic quiescence, and Holocene to Quaternary basalt volcanism in the wake of the Yellowstone hotspot contrary to the surrounding higher mountainous terrain, seismically active, and rapidly-stretching Basin and Range province. We present an updated velocity field within the Stable North American Reference Frame (SNARF) using GPS data collected from 1994 to 2009 over the Northern Basin and Range Province. Our results show contraction for the Snake River Plain extending over a 125 x 650 km region, including the Owyhee-Oregon Plateau. The slow internal deformation in the Snake River Plain is in contrast to the rapidly-extending adjacent Basin and Range provinces to the north in the Centennial Tectonic belt and south in the Intermountain Seismic belt. Tests with dike-opening models indicate rapid extension by dike intrusion in volcanic rift zones does not occur in the Snake River Plain at present as previously hypothesized. If we assume the low rate of deformation is reflected in the length of time between eruptions on the order of 10^4 to $>10^6$ yrs, the interlude of a low-strain field in the Snake River Plain and Owyhee-Oregon Plateau would extend at least through the Quaternary. Also, regional GPS velocity gradients are best fit by nearby poles for rotation over much of the Northern Basin and Range Province including the Snake River Plain, Owyhee-Oregon Plateau, Oregon, Centennial Tectonic belt, and Idaho batholith. The proximity of the poles for the regions indicates that clockwise rotation is driven by extension to the south in the Great Basin and not localized extension in the Basin and Range or Yellowstone hotspot volcanism.

Real-Time PBO for Tsunami Early Warning along the Pacific Coast of North America

Hans-Peter Plag[1], Geoff Blewitt[1], William C. Hammond[1], Corne Kreemer[1], Yoaz Bar-Sever[2], Yuhe T. Song[2]

1) Nevada Bureau of Mines and Geology and Seismological Laboratory, University of Nevada, Reno, Mail Stop 178, Reno, NV 89557, USA
2) Jet Propulsion Laboratory, 4800 Oak Grove Drive, Pasadena, CA 91109-8099, USA

The Pacific Coast of North America is exposed to potentially devastating tsunamis. Tsunamis originating from major earthquakes at the Cascadia subduction zone would result in very short warning times. Reliable tsunami early warning requires a rapid assessment of the tsunamigenic potential of an earthquake as well as a prediction of the likely propagation pattern of the tsunami. Low-latency availability of the coseismic Earth's surface displacements can support the assessment of the tsunamigenic potential of an earthquake and improve predictions of the propagation pattern of the tsunami. Observational constraints for the estimation of of the surface displacement field come from sufficiently dense GPS networks. The GPS network of the Plate Boundary Observatory (PBO) would allow for the low-latency estimation of the coseismic displacement field if a sufficient number of stations could be integrated in a real-time processing. We have developed a fingerprint methodology for the rapid determination of the surface displacement field from GPS-determined displacements. The fingerprint methodology depends on a priori knowledge of the faults potentially involved in a rupture. The known faults are parametrized with standard elements and for each element so-called fingerprint functions are computed for unit strike and dip slips. After an event, the model space of all reasonable fault-element combinations is searched for the element-slip combination best fitting the observed displacements using GPS time series as observational constraints. Application to the recent large earthquakes demonstrates that this combination provides the best estimate of the displacement field and earthquake magnitude consistent with observations. The uncertainties in displacement field and magnitude estimates are a function of the GPS station network geometry. We will present the fingerprint method, consider requirements for the real-time GPS network, and discuss the applicability to tsunami early warning for the Pacific Coast of North America.

Extending a Continent: Magmatism and Dynamics of the Lithosphere across the Basin and Range, US

Terry Plank, Esteban Gazel, Claire Bendersky: LDEO, Palisades, NY
Don Forsyth, Christina Rau: Brown University, Providence, RI
Erik Hauri, DTM, Carnegie Institution of Washington
Cin-Ty Lee, Rice University

On-going extension across the Basin and Range has generated topography, faults and volcanoes, and yet the relationship between these features is yet not clear. Moreover, recent work points to a driving role for small-scale convective phenomena in the mantle, such as lithospheric drips, edge-driven convection, or flow around subducting slabs. Here we use the Earthscope platform to constrain the dynamics of melting and evolution of the continental lithosphere, by integrating the shear wave velocity structure derived from inversion of Rayleigh waves, with petrological information in volcanic rocks that record the conditions of their formation in the mantle.

We contrast here the western boundary of the Basin and Range, in Owens Valley California (the Big Pine Volcanic Field), with the eastern boundary within the Transition Zone to the Colorado Plateau (Snow Canyon Volcanic Field). Big Pine basaltic melt inclusions, trapped in primitive olivines, record in their low FeO and moderate H_2O contents low mantle equilibration temperatures, that mark a shift over the last 500 ka from melting of 1300°C potential temperature asthenosphere at 50-75 km depth, to melting or melt percolation and equilibration at 1200-1250°C within a thin lithospheric layer at 40-50 km, just below the Moho. Correlations between trace element ratios, and melting temperatures and pressures support this shift to shallower, lithospheric melting with time. The shallow melt equilibration beneath Big Pine is consistent with the lack of a high velocity seismic lid here, and supports the notion that mantle lithosphere has been severely thinned or lost, possibly due to its foundering in the last several Ma. In contrast, Snow Canyon basaltic melt inclusions record in their high FeO and low H_2O contents high mantle equilibration temperatures (1375-1425°C, at 65-75 km), very near the seismically inferred lithosphere-asthenosphere boundary, and at the top of a very low velocity zone (V_s < 4.1 km/s) that extends to > 100 km. Such high melt temperatures and low seismic velocities might require active upwelling of hot mantle, in support of recent proposals for the thermal erosion of Colorado Plateau lithosphere along its margins. The large variation in the temperature of the shallow mantle, and the evolution of mantle lithosphere across the Basin and Range point to the potential importance of lithospheric downwellings and asthenospheric upwellings as drivers of magmatism and consequences of continental extension.

Investigation of Cascadia Segmentation with Ambient Noise Tomography

Robert W. Porritt, Richard M. Allen,

Dept. Earth and Planetary Science, UC Berkeley

Devin C. Boyarko, and Michael R. Brudzinski.

Dept. Geology, Miami University

Corresponding author: Robert W. Porritt, Email rwporritt@berkeley.edu, Tel 906-281-3675, Fax 510-643-5811, Dept Earth and Planetary Sciences, UC Berkeley, 307 McCone Hall, Berkeley CA 94720, USA.

Abstract

Along strike variation in the characteristics of subduction zone processes has been observed throughout the Cascadia Subduction Zone through analysis of arc magmas and the distribution of seismicity. We investigate links between these observations and subduction zone structure by imaging three-dimensional lithospheric scale shear velocity structure using ambient noise tomography (ANT). The crustal portion of the model is well resolved through typical ANT processing techniques. We expand the methodology to use longer period phase velocities in order to recover structure to ~120km depth. The resulting model, PNW10-S, represents structural information in terms of relative shear velocity in the crust and uppermost mantle. Crustal structure mirrors surface geology to ~10 km depth and then transitions to a structure that is dominated by the subducting slab. The subducting slab and overriding crust appear segmented into three parts with boundaries near 43°N and 46°N. This three-way structural segmentation is aligned with the variation in recurrence of episodic tremor and slip along the subduction zone (Brudzinski and Allen, 2007). Upper to middle crustal boundaries between the Klamath Mountains and Siletzia Terrane and between the Crescent Formation and Olympic Peninsula are also coincident with locations of increased occurrence of tremors raising the question of whether there is a link between the intensity of tremor activity and shallow (<10km) crustal structure. The slab-segment boundary at 43°N is a stronger feature than the northern segment boundary at 46°N and appears to be the continuation of the Blanco Fracture Zone separating the Gorda segment of the plate from the rest of the Juan de Fuca plate. The southern half of the arc system, south of 45°N, shows lower velocities from the surface to ~80 km depth relative to the northern portion of the arc. We propose this is due to clockwise plate rotation, which causes extension in the south, and results in increased melting. Along the arc, four broad low-velocity features are also imaged just below the Moho and centered at 42°N, 44°N, 47°N, and 49°N. We interpret these as ponding of melt just below the crust where differentiation can occur before further ascent through the crust.

Seismic Tomographic Imaging of an Upper Mantle Anomaly beneath the Rio Grande Rift

Carrie V Rockett[1], Jay Pulliam[2], and Stephen P Grand[3]

[1]*Department of Geology, Baylor University, Waco, TX, carrie_rockett@baylor.edu*
[2]*Department of Geology, Baylor University, Waco, TX, jay_pulliam@baylor.edu*
[3]*Jackson School of Geosciences, University of Texas at Austin, Austin, TX, steveg@geo.utexas.edu*

In 2004 tomographic results from the La Ristra array revealed a fast seismic velocity anomaly beneath the eastern flank of the Rio Grande rift. The location and geometry of the anomaly led to the hypothesis that it was the result of edge-driven convection. The linear array imaged the anomaly in only two dimensions, however, warranting further three-dimensional modeling. To investigate the hypothesis, a two-dimensional array was deployed through the *S*eismic *I*nvestigation of *E*dge-*D*riven *C*onvection *A*ssociated with the *R*io Grande Rift (SIEDCAR) project.

We present P and S traveltime tomographic images of the crust and upper mantle beneath the southeastern edge of the Rio Grande rift. Broadband seismometers belonging to six different networks including the Transportable Array (TA) and SIEDCAR (XR) networks covered southwestern New Mexico and West Texas with a station spacing of ~35 km in the center of the array and ~70 km along the outer bounds. We used a total of 282 events of magnitude 5.0 or greater occurring at distances of 30° to 90° recorded from August 2008 to July 2010. P and S velocity models were created with FMTOMO, a robust non-linear, grid-based inversion program.

Our models confirm the fast seismic anomaly exists and show that it extends from near Portales, New Mexico southward to West Texas and northeastern Chihuahua, Mexico. We also show that this anomaly is disconnected from the Great Plains craton and is dipping southeast. The geometry and location of the anomaly suggest that edge-driven convection is a likely mechanism for the fast seismic structure. To further investigate the origin, ρ/V_S values should be examined to investigate the thermal and compositional effects within the anomaly. Additionally, joint P and S inversions provide further information which can assist in the understanding of the anomaly and its origin.

Improved Removal of Long-term and Seasonal Trends from PBO Borehole Strainmeter Data

Evelyn Roeloffs, U.S. Geological Survey, Vancouver, WA 98683
evelynr@usgs.gov

Abstract

The Plate Boundary Observatory borehole strainmeter (BSM) network in northern Cascadia is well-distributed to constrain the time-dependent slip distribution of slow slip events (SSE's) on the subduction interface. Since 2007, four SSE's have been recorded by up to six BSM's. Each BSM produces two shear-strain time series containing transients of ten's of nanostrain over three to 20 days, generally consistent with thrust displacement propagating along strike of the subducting slab at 30-40 km depth, simultaneously with large-scale tremor.

It has proven difficult, however, to process the BSM data so that the results may be used to constrain detailed models. The main challenges are calibration of the BSM data, removal of long-term borehole relaxation trends, and correction for seasonal signals.

Shear-strain transients from Cascadia SSE's cannot be discerned without removing borehole relaxation trends of 10's of microstrain per year. For many BSM's, seasonal signals are at least as large as the strain transients from SSE's. Roeloffs (JGR, 2010) showed that tidal calibration of some BSM's requires improved tidal models; here the borehole relaxation trends and seasonal signals are addressed.

Although BSM's exhibit random-walk noise at periods of several days or more, the borehole relaxation trend is recorded at high signal-to-noise ratio and can be modeled by fitting a linear trend plus a small nonlinear component, such as a fractional power of time. Seasonal variations are often common-mode signals similar on all four gauges, and can therefore be reduced even when modeling them is not possible.

Improved removal of long-term and seasonal trends preserves shear-strain offsets left by SSE's, which helps answer two questions. First, do SSE's represent pure thrust displacement, or instead oblique slip parallel to plate

motion? Second, do SSE's stop near certain strainmeters, or are network gaps simply missing continued propagation? Simple dislocation models show that both questions require observing whether SSE's leave permanent strain offsets. For pure thrust slip, engineering shear strain in fault-perpendicular and -parallel coordinates undergoes an excursion as the slip front passes the BSM, but leaves no net offset, while oblique slip leaves offsets of both shear strains. Engineering shear strain offsets are also caused by edge effects if the slip front stops near the BSM.   Combining these data processing techniques with improved calibrations renders BSM data much better able to constrain quantitative models.

Lithospheric modification beneath the Mid-Continent Rift System: Geochemistry as a temporal probe.

Tyrone O. Rooney[1]

Dept. of Geological Sciences, Michigan State University, East Lansing, MI 48824, USA

Anthony Pace

Ontario Geological Survey, Ministry of Northern Development, Mines and Forestry, Sault Ste. Marie, Ontario, Canada.

Thomas Hudgins

Dept. of Geological Sciences, University of Michigan, Ann Arbor, MI 48109, USA

Timothy Matthews

Dept. of Geology & Geophysics, University of Wyoming, Laramie, WY 82071, USA

The multi-year snap-shot of the lithosphere that comprises the North America continent provides an unprecedented glimpse of the current-day lithospheric structure, however, this modern lithospheric configuration may be the result of overlapping processes that acted upon the lithosphere during its lifetime. To fully appreciate the origin of structures now imaged, the results of modern geophysical techniques can be interpreted within the temporal record of lithospheric processes preserved in the rock record. The Mid-Continent rift is a dominant geologic feature of the mid-western United States and contains a magmatic record of a plume-influenced and magma-rich rifting environment. Chemical and mechanical modification of the lithosphere is a widely acknowledged feature of continental rifting, therefore unraveling the modern structure in the region is largely dependent on establishing the lithospheric modification processes active during the development of the Mid-Continent Rift. We have undertaken a pilot study of Mid-Continent Rift-related magmatism in the most southern portion of Ontario, Canada, where a particularly complete temporal record is preserved. We have utilized the ongoing interdisciplinary studies in East Africa to place our observations within the broader context of the processes currently active there. The geochemical heterogeneity in basaltic magmas erupted in the Mid-Continent Rift largely preserves variability in contributions from the sub-lithospheric reservoirs contributing to magmatism (e.g. plume, upper mantle), however the effects of lithospheric modification by assimilation and intrusion are also evident. Rhyolites in the region preserve evidence of crustal processes such as magma hybridization/fractionation, and importantly show clear evidence for gabbroic cumulates in the local lithosphere. We also present preliminary geochemical data on newly discovered kimberlites, lamprophyres and other silica under-saturated magmas which will be used to directly probe the composition of the sub-continental lithospheric mantle. These magmas, which largely originate from areas away from the flood basalts and rift may provide key evidence of the composition of the regional lithospheric mantle and form a baseline from which the lithospheric modification associated with the Mid- Continent rift may be evaluated. The ongoing study of the magmatic products associated with the Mid-Continent Rift system will assist in unraveling the sequence of events that has led to the current lithospheric configuration and highlights the potential for future interdisciplinary studies in this region.

[1]email: rooneyt@msu.edu, phone: +1-517-432-5522

Using Continuous GPS Data to Learn About Earthquakes

Ricardo Ruiz, Chaffey High School, Ontario, CA
Bernadette Vargas, Etiwanda High School, Rancho Cucamonga, CA
Sally McGill, California State University, San Bernardino, CA
Robert de Groot, Southern California Earthquake Center, University of Southern California

Are you interested in enhancing student learning while incorporating real GPS data related to recent earthquakes into classroom activities? We share a GPS lesson plan that is easily incorporated into the teaching of plate tectonics. Designed and tested by secondary science educators, this activity is an interactive approach to enhancing student knowledge about fault motion. Students are introduced to GPS and its real world applications and to mapping the movement of tectonic plates. Students learn how to interpret real data from continuously operating GPS stations in the Plate Boundary Observatory network with respect to tectonic motions both during an earthquake and during the interseismic interval. In this lesson students graph continuous GPS data from a station near the April 4th, 2010, M7.2 Sierra El Mayor-Cucapah earthquake in northern Baja California, México. This earthquake offers an opportunity for a teachable moment since it is still fresh in students' memories. The lesson can easily be adapted to use other continuous GPS data sets from future earthquakes to keep the lesson relevant (and timely) as the April 4th earthquake becomes a distant memory. Developed collaboratively using the Lesson Study Model this lesson was tested twice in high school classrooms and subsequently modified through feedback provided by the activity developers and two outside observers.

This lesson is relevant to several of the California state science content standards (grades 9 – 12). It reinforces student understanding of how and why earthquakes occur (Earth science standard 3d). Students learn how plate motion creates elastic bending near the fault that is eventually released as slip on the fault during an earthquake. This lesson promotes an awareness of natural hazards in different parts of California (Earth Science standard 9b) by emphasizing the causes behind an event that was personally experienced by many students in Southern California. The lesson also addresses several Investigation and Experimentation content standards such as displaying data and analyzing relationships (I&E standard 1a), formulating explanations using logic and evidence (I&E standard 1d), and analyzing sequences of natural phenomenon over time (I&E standard 1i).

REMOTE SENSING OF SEISMOTECTONIC PROCESSES IN GLACIATED SOUTHERN ALASKA WITH MULTI-BEAM LIDAR AND L-BAND INTERFEROMETRIC SYNTHETIC APERTURE RADAR DATA

J. Sauber[1], M. Hofton[2], R. Bruhn[3], E. Burgess[3], R. Forster[3] and M. Cotton[3]

In 2007 the U.S.A. National Research Council Earth Science Decadal Survey, Earth Science Applications from Space, recommended a L-band InSAR and multibeam Lidar mission to study deformation, ecosystem structure, and dynamics of ice. The recommended Lidar and InSAR capabilities were optimized for studying geohazards and global environmental change. The complex plate boundary in southern coastal Alaska provides an excellent setting for testing multi-beam Lidar and L-band SAR geodetic imaging capabilities to recover fundamental parameters of glacio-seismotectonic processes. Although the rate of ongoing deformation associated with subduction and accretion of the Yakutat terrain has been constrained by campaign style geodetic, and more recent PBO, measurements, the nature and magnitude of long-term deformation accommodated on faults and folds is still poorly constrained. Also, thick coastal forest and brush mask important aspects of the geomorphology of marine terraces, faults, and folds on standard digital elevation models (DEM) derived from optical methods and C/X-band SAR images.

Geodetic imaging results from Lidar and L-band SAR are providing new structural and geomorphic information in this remote glaciated region of steep terrain and high relief. Based on simulations of the multi-beam Lidar performance over marine terraces west of Icy Bay, uplift associated with the 1899 Yakataga seismic event, and glaciers, a medium footprint (25m) satellite Lidar with contiguous elevations along profiles spaced less than 1 km apart will provide an accurate georeferenced surface for local and regional scale geohazard and climate change studies needed for interdisciplinary, EarthScope-related studies in Alaska. An additional challenge to understanding the tectonics and seismic risk of this area is that the mountain glaciers flow over major faults and folds. Using L-band SAR data from ALOS/PALSAR (Mode: Fine beam, HH, 46 days apart) we have been able to estimate ice velocities (0.2-4.0 m/day) from offset tracking in the Upper and Lower Seward Basin, Bagley Ice Valley and the upper Malaspina Glacier. We are using the morphology and dynamics of glaciers derived from these L-band SAR ice velocities to infer the large-scale sub-ice structures that form the structural framework of the Seward-Bagley Basins and to test regional tectonic models.

[1]Planetary Geodynamics Laboratory, NASA's GSFC, Greenbelt, MD
[2]University of Maryland, College Park, MD
[3] University of Utah, Salt Lake City, UT

Teleseismic Tomography Beneath the Colorado Rocky Mountains and Mantle Support for High Topography

Schmandt, B. (University of Oregon); MacCarthy, J. Aster, R., (New Mexico Tech); Dueker, K. (University of Wyoming); Karlstrom, K. (University of New Mexico); and the CREST group.

We present new P and S mantle tomography results for the broadly uplifted Colorado Rocky Mountains region, which sits at the eastern extent of the tectonically active and provincially heterogeneous western U.S. This region is bounded to the east by the abrupt north-trending Rocky Mountain Front (RMF), across which lies the tilted but tectonically intact Great Plains. The Colorado Rockies Experiment and Seismic Transects (CREST) team deployed 60 broadband seismometers in the Colorado Rockies as part of a multi-disciplinary effort to understand the sources of buoyancy that presently support the 2-3.5 km elevation of the Colorado Rockies, constrain the timing of regional uplift, and gain insight into the crust and mantle processes that gave rise to multiple episodes of intra-continental tectonic and magmatic activity since the late Cretaceous. We invert P and S teleseismic travel-time residuals from the CREST array, USArray and more than 1800 additional stations for 3-D perturbations in mantle velocity structure to a depth of 1200 km. The inversion uses recent advances in western U.S. crust models including new regional constraints from CREST data to better isolate the mantle component of travel-time residuals. We use frequency-dependent 3-D sensitivity kernels to map travel-time residuals, measured in multiple frequency bands, into velocity structure. In addition to separate Vp and Vs models, we jointly invert the two datasets for Vp/Vs perturbations by imposing a smoothness constraint on the $\delta\ln Vs/\delta\ln Vp$ field. We find a broad low-velocity, high Vp/Vs anomaly underlies most of the Colorado Rockies from 60-200 km, and includes a more pronounced low-velocity anomaly trending northeast from the San Juan Mountains to North Park. Locations of <10 Ma basaltic volcanism in western Colorado are underlain by low-velocity upper mantle near a sharp transition to a high-velocity uppermost mantle beneath the northern Colorado Plateau and Wyoming. Interestingly, we do not find a sharp mantle boundary that is laterally coincident with the RMF. Weaker

low-velocity anomalies with sub-vertical "pipe-like" geometries extend from near the base of the lithosphere to 300-400 km depth beneath the Colorado Rockies and adjacent regions. We speculate these low-velocity anomalies may represent complex upward return flow induced by descent of high-velocity fragments of subducted ocean lithosphere imaged within and beneath the mantle transition zone. In this context, the low-velocity mantle in the upper 200 km may owe its origin to deeper mantle processes via this process. Regardless of specific origin, the magnitude of the low-velocity anomalies near the base of the lithosphere requires 300-500 C higher temperature than surrounding mantle and likely provides a significant source of buoyancy for the Colorado Rockies. This interpretation is strengthened by the positive regional geoid anomaly, by complementary CREST results for crustal thickness that preclude topographic support via Airy isostasy, and by geomorphic and thermo-chronologic evidence for epeiorogenic uplift during the last 10 Myr.

Evolution of the Pacific Northwest convergent margin, initiation of the Yellowstone hotspot track, and inherited influences on present-day deformation and volcanism

Schmandt, B. [1], Humphreys, E. [1], Gao, H. [1,2], Kelbert, A. [3], Meqbel, N. [3], and Egbert, G. [3]
[1]University of Oregon, [2]now at University of Rhode Island, [3]Oregon State University

Pacific Northwest U.S.A. (PNW) crust and upper mantle structure and geologic activity provide insight into major events in regional lithospheric evolution including early Cenozoic reconfiguration of the PNW/Farallon convergent margin and Miocene initiation of the Yellowstone hotspot track. We integrate recent geophysical observations with geologic constraints on tectonic and magmatic activity to provide a synthesis of PNW evolution since the Cretaceous. A westward jump of the PNW/Farallon convergent margin in the early Cenozoic is evidenced by termination of arc magmatism in Idaho and initiation of the Cascade arc following accretion of Farallon ocean lithosphere (Siletzia) in the Columbia Embayment. The oceanic affinity of Siletzia accounts for the low strain rates, low elevation, and distinctive seismic and electromagnetic properties of the Columbia Basin lithosphere today. In addition, mantle structure imaged by body-wave tomography suggests Siletzia accretion triggered rollback and north-south segmentation of the flat subducting Laramide-age slab. Present-day magmatic activity in the northern Cascade arc is typified by localized low-volume eruptions and seismically expressed as relatively high upper crustal velocities beneath arc volcanoes. The character of northern Cascades volcanism is attributed to crustal compression caused by post-accretion clockwise rotation of the relatively non-deforming Siletzia block as well as the presence of a sub-vertical Farallon slab segment that is stalled in the upper mantle beneath eastern Washington and western Idaho and impedes flow of asthenosphere into the northern portion of the Cascadia mantle wedge. Conversely, volcanism in the southern Cascades is more voluminous, occurs at numerous widespread vents, and is underlain by low-velocities and high-conductivity at all crustal depths. These characteristics are consistent with crustal extension on the trailing edge of Siletzia rotation and unimpeded flow of asthenosphere into the southern Cascadia mantle wedge. Nearly simultaneous large volume volcanic eruptions at ~17-15 Ma indicate the regional arrival of upwelling Yellowstone plume material which spread laterally at the base of the lithosphere along the western edge of Precambrian North America. The Columbia River Basalts (CRBs) primarily erupted from vents in northeast Oregon and were by far the largest of these volcanic events. Rapid uplift of the Wallowa Mountains pluton, which is spatially correlated with CRB crustal magma chambers, suggests that delamination aided by impact of hot low-viscosity plume material focused CRB eruption in the northeast Oregon by allowing plume ascent to relatively low pressures and providing fertile material. A large volume of high-velocity mantle beneath this region today is thought to be a combination of delaminated Siletzia lithosphere and a plug of depleted mantle created by CRB melt extraction.

Using EarthScope to Detect Upper Mantle Transition Zone Heterogeneity

Nicholas Schmerr[1,2]
Chin-Wu Chen[2]
Daoyuan Sun[2]

[1]NASA Goddard Space Flight Center
Code 698
Greenbelt, MD 20771

[2]Carnegie Institution of Washington
Department of Terrestrial Magnetism
5241 Broad Branch Rd. NW
Washington, DC 20015

nicholas.c.schmerr@nasa.gov
cwchen@dtm.ciw.edu
dsun@dtm.ciw.edu

A wide variety of reflected, converted, and refracted seismic waves are used to image the structure of the upper mantle transition zone. This region is delineated by discontinuities arising from solid-to-solid phase transitions in olivine at approximately 410, 520, and 660 km depth. Seismic imaging has provided a wealth of information about discontinuity topography, impedance contrast, and phase transition sharpness, giving important insights into the heterogeneity of mantle temperature and composition.

Here we use source and receiver topside reflections of SH energy to map the depth and sharpness of mantle discontinuities. Topside reflections, termed *sdsS* or *Ssds*, where *d* indicates discontinuity depth (Fig. 1A), arrive several hundred seconds after the direct *S* or *Sdiff* seismic phases and are observed in the epicentral distance range of 70-110º (*sdsS*) and 110-165º (*sdsSdiff*). The topside reflections have amplitudes that are 1-10% of the main arriving *S* or *Sdiff* phase, and energetic enough to be observed on individual traces of seismograms, though stacking is generally required for a robust analysis of this phase (Fig. 1B). A challenge arises from the ambiguity in which side of the path the topside reflection takes place, either on the source or receiver side. We eliminate this ambiguity using an array approach in our analysis that isolates structure to either side of the path.

The topside reflections are sensitive to discontinuity structure within 200-500 km of the source or receiver, and possess a quarter period Fresnel zone on the order of several hundred kilometers. This sensitivity is ideal for investigating transition zone structure near subduction zones, ridges, and continental cratons and margins. We apply our array technique to a dataset of Transportable Array stations, consisting of broadband, transversely polarized waveforms that sample the epicentral distance range of 70-165 degrees. The deep seismic structure of the Western United States is mapped using differential times of the *s660sS* and *s410sS* phases to map transition zone thickness (Fig. 1C). The differential times eliminate any travel time heterogeneity originating from paths through the crust and lowermost mantle. We find good agreement with past receiver function studies of the transition zone, and provide a detailed map of thermal and chemical heterogeneity beneath the western United States.
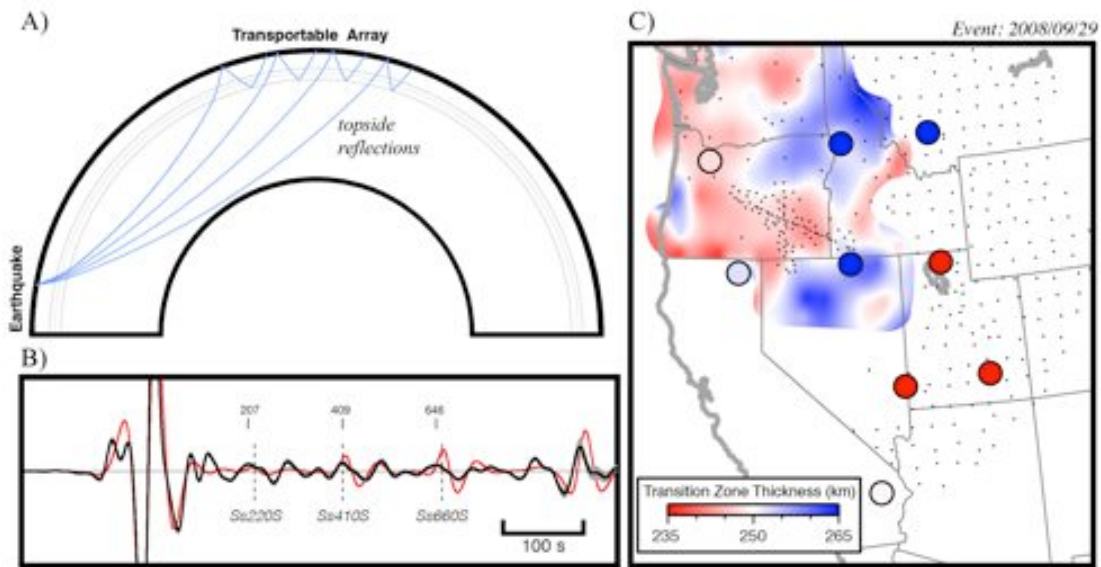
Figure 1. Details of the topside reflection approach to mapping transition zone structure. A) Raypaths of *Ssds* to the transportable array stations. B) A stack of seismograms (black) and stack of synthetic seismograms (red), indicating the presence of topside reflections from upper mantle structure. A bootstrap-resampling algorithm is used to compute the 95% confidence interval (gray shading). C) Mantle transition zone thickness results for a single event compared to the receiver function result of Eagar et al., 2010. Stations used to produce the stacks are shown as black triangles and transition zone thicknesses from stacks for topside reflections are colored circles.

Electrical conductivity structure in the NW Continental US from the US Array MT Program

The IRIS EM Working Group – (Paul Bedrosian[1], Gary Egbert[2], Matthew Fouch[3], Dean Livelybrooks[4], Maureen Long[5], Kevin Mickus[6], Stephane Rondenay[7], Adam Schultz[2], Martyn Unsworth[8], Phil Wannamaker[9], Chester Weiss[10])

[1]US Geological Survey, [2]Oregon State University, [3]Arizona State University, [4]University of Oregon, [5]Yale University, [6]Missouri State University, [7]Massachusetts Institute of Technology, [8]University of Alberta, [9]University of Utah, [10]Virginia Tech University

A picture of electrical conductivity structure in the mid-lower crust and upper mantle in the northwestern quadrant of North America has emerged that is spatially coherent with regional geologic structure, and with large scale features evident in seismic tomograms and in receiver function analyses. The data set used to build this emerging set of large-scale 3D conductivity inverse models has been acquired by the EarthScope US Array magnetotelluric program (i.e. "EMScope"), which includes seven quasi-permanent backbone stations (MT BB) installed at sites in Oregon, California, Montana, New Mexico, Minnesota, Missouri and Virginia, and a transportable array of stations (MT TA) installed typically for several weeks at sites located on an approximately 70 km spaced national grid of large regional footprints. The MT field program and data quality control activity is carried out on behalf of IRIS by Oregon State University and its subcontractors, with advice from the IRIS Electromagnetic Working Group (EMWoG). All EMScope time series data and primary derived data products (e.g. magnetotelluric impedances and induction vectors) are distributed without restriction through IRIS DMC.

From 2006-2010 EMScope acquired 271 MT TA stations, forming a contiguous grid covering all of Washington, Oregon, N. California to within 50 km N of Sacramento, and extending eastward through Idaho, Nevada and much of Montana and Wyoming. In 2011 the remainder of this first MT footprint will extend eastward through Utah and into the NW quadrant of Colorado and SW Wyoming before the next footprint is acquired in the upper Midwest targeting a region encompassing the Mid-Continent Rift.

We report on principal results-to-date of inversions of EMScope MT data carried out independently by a number of different groups, using data available from IRIS DMC. Key features in regional scale conductivity structure include electrically resistive crustal blocks along the western margins of continental Cascadia that correspond to inferred mechanically rigid blocks associated with the N and S Siletzia and Klamath provinces of Oregon; the S Cascades conductive anomaly that has been inferred to result from crustal magma accumulations and hydrothermal activity; the transition from the flood basalt province to the Basin and Range; substantial conductivity contrasts between the Juan de Fuca/Gorda mantle wedge and the ocean-ward mantle; extremely high conductance beneath the Yellowstone Caldera that extends toward and along the Snake River Plain to the west where it deepens; and areas of enhanced conductance that appear to be associated with large scale features of the Cascadia volcanic arc. A number of these features correspond to seismically delineated crust and upper mantle anomalies, including indications of crustal melt accumulations from receiver function analysis, and plume-like mantle melt sources from seismic tomography.

Additional fieldwork is underway (e.g. CAFÉ-MT) or proposed (Cascadia onshore-offshore MT) to provide high spatial resolution additions to the regional scale view provided by EMScope data. A large set of commercial contractor wideband MT data has also been made available to this effort, providing very high resolution 3D sampling of the upper through mid-crust. Various groups are currently working to advance the joint interpretation, and ultimately the joint inversion of magnetotelluric, seismic and other complementary data sets in order to constrain the underlying physical and compositional conditions in the crust and mantle.

Compositional variations in the mantle, and their velocity and density effects

A combination of laboratory, xenolith, and thermodynamic modeling studies on compositional variations among peridotites, and the density and velocity effects of these compositional trends, will be presented.   We find that both isobaric and decompression melting can cause subtle increases in S-wave velocity; notably decompression melting produces non-linear velocity effects that depend on the melting path.   A more significant cause of velocity change may be silica enrichment, which can produce up to a 2% P-wave velocity decrease compared to a typical mantle lherzolite velocity. Distinguishing compositional variations in the mantle with tomography will be a challenge.   Silica enrichment produces a distinct Vp/Vs drop, and melt depletion is best distinguished by the ratio Vs/density.   By examining the major element effects of melt depletion with multiple techniques, it is clear now that high cratonic velocities are not caused by changes in peridotite mineral content.   In addition, mantle melting does not produce isopycnic—neutrally buoyant—cratonic mantle.   Models of subsolidus compositional changes in peridotites show that melting cannot make cold cratonic mantle as dense as hot fertile asthenosphere.

Derek L. Schutt*
*corresponding author: Derek.schutt@colostate.edu
Department of Geosciences
Colorado State University

Juan Carlos Afonso
Department of Earth and Planetary Sciences
Macquarrie University

Charles E. Lesher
Department of Geology
University of California, Davis

Characterizing the evolution of permeability across the brittle-ductile transition in porous sedimentary rocks

M. Scuderi[1], H. Kitajima[1], B. Carpenter[1], C. Marone[1], D. Saffer[1]

[1] Department of Geosciences and Energy Institute Center for Geomechanics, Geofluids, and Geohazards,

The Pennsylvania State University, University Park, Pennsylvania, USA

It is commonly accepted that changes in porosity and fluid pressure within porous sedimentary rocks are capable of changing their mechanical response to an applied stress, from aseismic slip (stable) to seismic slip (stick-slip). In order to understand this transition, we investigated the mechanical behavior of porous sedimentary rocks within the Marcellus shale formation characterized by porosity ranging from 40 to 44%. Seven deformation experiments were conducted on cylindrical specimens 25 mm in diameter and 50 mm in length, using: 1) hydrostat loading path ($\sigma1=\sigma2=\sigma3$), during which P_c was increased 2.5 MPa every 10 minutes; 2) triaxial loading path ($\sigma1>\sigma2=\sigma3$), maintaining constant effective pressure (P_e) and an axial displacement rate of 0.1 μm/s ($2x10^{-6}$ s^{-1}). Pore pressure was maintained constant at 2MPa during each experiment, and changes in volume were monitored (drained conditions) to keep track of the change in porosity during both hydrostat and triaxial loading. Permeability was also measured at several stages of each experiment. We performed an experiment only in hydrostat condition to determine P* of 70 MPa, with P_e ranging from 1 to 90 MPa. For the triaxial loading experiments, data shows brittle behavior P_e=1MPa with an increase in permeability from $7.73x10^{-15}$ m^2 to $1.82x10^{-14}$ m^2 associated with mode I fractures. For P_e=2.5 and 5 MPa, we observed a transition from brittle to ductile behavior. At higher effective pressures, from 10 to 50MPa, we observed ductile (compactive) behavior. Sample behavior is characterized by: 1) an initial poro-elastic deformation, 2) yield stress (C*), and 3) grain crushing and pore collapse defining inelastic yield by shear enhanced compaction. P-q plots show shear localization at low values of P_e, and then a yield cap, marking the onset of shear enhanced compaction. The relationship between permeability and porosity is characterized by a log-linear evolution, unaffected by the loading path. In summary, we document an evolution from brittle to ductile behavior with increasing effective pressure during triaxial loading experiments. Moreover, we observe a log-linear decrease in permeability with porosity regardless of the loading path.

Back-projection study with a dipping fault plane

Guangfu Shao[1*]

Miguel Andres-Martinez[1]

Tomoko E. Yano[1]

Chen Ji[1]

1. Earth Science Department, University of California, Santa Barbara, CA

* shao@umail.ucsb.edu

Back-projection method has been widely applied to study the spatial and temporal evolutions of high frequency radiations associated with the earthquake rupture process using the data from dense local arrays or global networks. In the conventional approaches, high frequency seismic waves are first projected back to the source region and then stacked at hypothetical sources on a horizontal plane at the surface or at a certain depth. During this process, the far field P wave earth response is simplified as a delta function. The free surface reverberations have been ignored. Furthermore, the fault planes of giant subduction earthquakes might have significant change in fault dip angles, consequently affecting their far field radiation pattern. In this study, we will discuss the effects of these simplifications and study the 2011 Tohoku, Japan earthquake using more realistic earth response.

Variations in Tremor Activity and Implications for Lower Crustal Deformation Along the Central San Andreas Fault, California

D.R. Shelly[1]
[1]U.S. Geological Survey, Menlo Park, CA, USA; dshelly@usgs.gov

Tremor activity patterns can serve to illuminate spatially variable properties and deformation styles of the deep fault. Toward this goal, we use cross-correlation to separate tremor into more tractable individual events, called low-frequency earthquakes (LFEs). We then divide the LFEs into 88 families (groups of similar events) distributed along 150 km of the central San Andreas Fault, beneath creeping, transitional, and locked sections of the upper crustal fault [Shelly and Hardebeck, 2010].

For maximum accuracy, we locate these tremor families using a 3D velocity model and seismogram stacks of up to 400 events. These stacks reveal clear P and S body waves, even on analog surface stations, which tightly constrain event hypocenters. Depths are mostly between 18 and 28 km, in the lower crust, and below the maximum depth of regular earthquakes. Tremor epicenters are concentrated within 3 km of the surface trace, implying a nearly vertical fault. Combined with observations of tremor migration, this suggests that the San Andreas Fault remains a localized, through-going structure at least to the base of the crust in this area.

Using these 88 event families as waveform templates, we systematically scan 9+ years of continuous seismic data. We detect more than 600,000 events (LFEs) since mid-2001; typically multiple bursts per day. We find systematic variations in properties among families, including amplitudes, recurrence intervals, responses to the nearby M 6.0 Parkfield and M 6.5 San Simeon earthquakes, and sensitivity to small stresses imparted by the tides and by waves of regional and teleseismic earthquakes.

Joint inversion of Surface Wave Dispersion and Receiver Functions based on Earthscope/Transportable Array data

Weisen Shen[1], Vera Shulte-Pelkum[2], Fan-Chi Lin[1] and Michael H Ritzwoller[1]

1. Center for Imaging the Earth's Interior, Department of Physics, University of Colorado at Boulder
2. Department of Geological Sciences, University of Colorado at Boulder

The joint inversion of surface wave dispersion and receiver functions has proven feasible on a station by station basis (e.g., Julia et al. 2000). Joint application to a large number of stations across a broad region has been elusive, however, because of the different resolutions of the two methods. Improvements in resolution in surface wave studies derived from ambient noise and array-based methods applied to earthquake data now allow surface wave dispersion and receiver functions to be inverted simultaneously across much of the Earthscope/USArray Transportable Array (TA). We have developed a Monte-Carlo approach (Shapiro and Ritzwoller 2002) for joint inversion of surface wave dispersion and receiver functions. As a proof of concept we apply this procedure to a region spanned by ~180 TA stations in Nevada, Utah, and Colorado, including parts of the Colorado Plateau, the Basin and Range, the Colorado Rockies, and the Great Plains (Figure 1). This new approach includes: 1. construction of back-azimuth-independent receiver functions; 2. determination of uncertainties in surface wave dispersion and receiver functions; 3. determination of the appropriate parameterization needed to fit both data sets; and 4. a Monte Carlo search of model space to determine a 3-D model of the crust and uppermost mantle with associated uncertainty information.

We enlarge the Earthscope Automated Receiver Survey (EARS) (Crotwell and Owens 2005) receiver function database by adding more events within a quality control framework. On average, the number of individual receiver functions for a single station is doubled. Then a back-azimuth-independent receiver function and its associated uncertainties are constructed using a harmonic stripping algorithm. We demonstrate that in most cases the constructed receiver function provides a good approximation to the receiver function for the azimuthally averaged velocity structure near the station.

We apply a Metropolis Monte Carlo algorithm (Mosegaard and Tarantola 1995) to invert for the average velocity structure beneath each station. Rayleigh wave dispersion curves are generated from the recent Eikonal tomography maps (Lin, Ritzwoller and Snieder 2009) from 8 sec to 80 sec period. The initial model parameterization includes 4 cubic B-splines in the crystalline crust, Moho depth, and 4 B-splines in the mantle to a depth of 120 km. In sedimentary basins it is necessary to modify the parameterization to include a gradient sediment layer above crystalline crust.

This approach is applied to the TA stations in the study region. We show that the receiver functions and surface wave dispersion data can be reconciled (Figure 2) beneath more than 80% of the stations using the relatively simple parameterization. Compared with using surface wave data alone, uncertainty in crustal thickness is much lower and there are smaller depth-velocity trade-offs (Figure 3). This procedure may be applied automatically for most of the TA stations and future work aims to apply it systematically across the US.
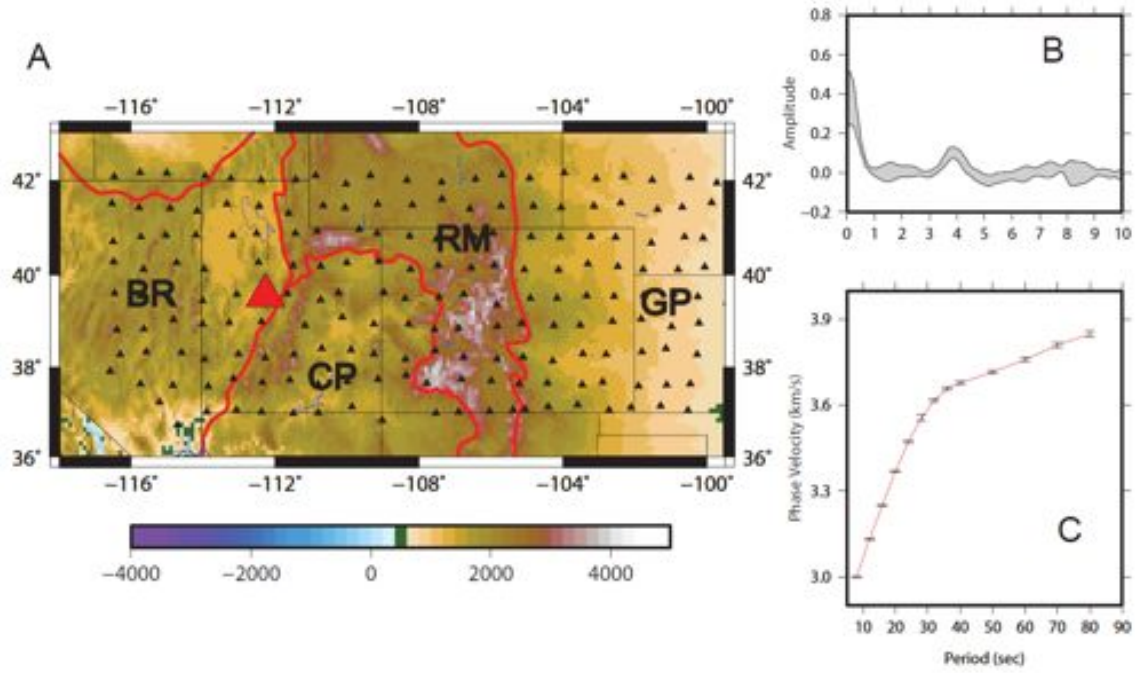
Figure 1. A. Stations used in this research are plotted as black triangles. Location of station P15A (red triangle) and the geological setting of this region is also shown (BR: the Basin and Range; CP: the Colorado Plateau, RM: the Rocky Mountains; GP: the Great Plains). B: The back-azimuth independent receiver function for station P15A; uncertainties are plotted as a gray corridor. C: Rayleigh wave dispersion from 8 sec to 80 sec. Uncertainties are plotted with error bars.
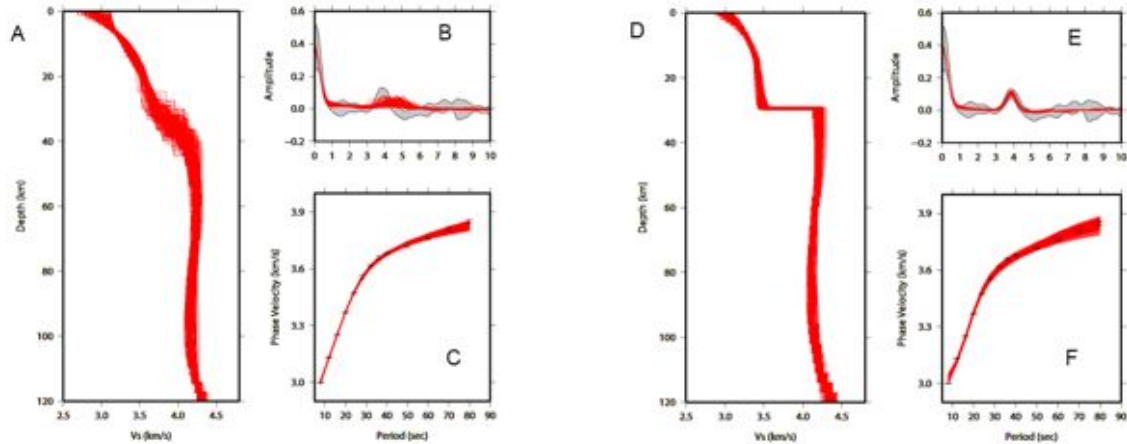

Figure 2. (A)-(C): Monte Carlo inversion of surface wave dispersion alone at the location of station P15A. 200 models accepted are plotted in (C); the fit to the receiver function and dispersion curve is shown in (B) and (C). (D)-(F): Monte Carlo inversion of surface wave dispersion and receiver function. 200 accepted models are plotted in (D); the fit to the data is shown in (E) and (F).
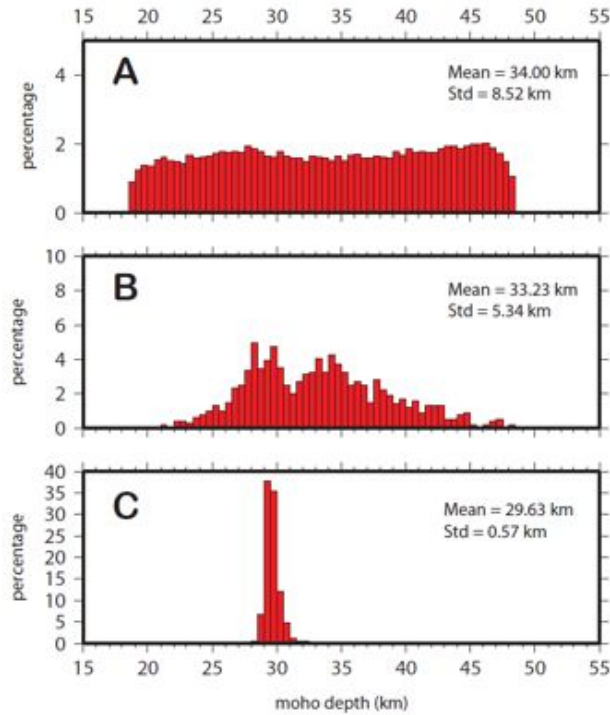
Figure 3: A. The prior distribution of Moho depth beneath station P15A. B. The posterior distribution of Moho depth from Monte Carlo search using surface wave dispersion alone. C. The posterior distribution of Moho depth using surface wave dispersion and the receiver function.

References

Crotwell, H. P. & T. J. Owens (2005) Automated receiver function processing. *Seismological Research Letters,* 76**,** 702-709.
Julia, J., C. J. Ammon, R. B. Herrmann & A. M. Correig (2000) Joint inversion of receiver function and surface wave dispersion observations. *Geophysical Journal International,* 143**,** 99-112.
Lin, F. C., M. H. Ritzwoller & R. Snieder (2009) Eikonal tomography: surface wave tomography by phase front tracking across a regional broad-band seismic array. *Geophysical Journal International,* 177**,** 1091-1110.
Mosegaard, K. & A. Tarantola (1995) MONTE-CARLO SAMPLING OF SOLUTIONS TO INVERSE PROBLEMS. *Journal of Geophysical Research-Solid Earth,* 100**,** 12431-12447.
Shapiro, N. M. & M. H. Ritzwoller (2002) Monte-Carlo inversion for a global shear-velocity model of the crust and upper mantle. *Geophysical Journal International,* 151**,** 88-105.

Opportunities for Earthscope science in the eastern US: rifting, magmatism and sutures

Donna J. Shillington[1], Daniel Lizarralde[2], James B. Gaherty[1], Harm J.A. Van Avendonk[3], M. Beatrice Magnani[4], Vadim Levin[5]

[1]Lamont-Doherty Earth Observatory of Columbia University; [2]Woods Hole Oceanographic Institution; [3]Institute for Geophysics, University of Texas; [4]Center for Earthquake Research and Information, University of Memphis; [5]Rutgers University

The eastern US offers rich opportunities to examine the evolution of heterogeneous continental lithosphere in response to extensional deformation and magmatism by examining the manifestation of accreted terranes, magmatism, extension and continental rupture at all levels of the lithosphere. Such observations can also provide important new insights into the relationships between continental stretching, magmatism, preexisting structures, and sediment transport. The lithosphere of the eastern US is the product of a series of continental amalgamation and rifting events since Paleozoic times. Successive orogenies have added exotic terranes to the eastern margin of North America, notably the addition of the large Carolina and Avalon terranes during the Alleghanian orogeny. The most recent extensional episode lead to the formation of a series of rift basins along eastern North America and its conjugate margins starting at ~230 Ma, and ultimately to the rupture of the Pangean supercontinent and opening of the Atlantic Ocean at least 30 Ma later. The east coast of the US also records one of the largest magmatic events in Earth's history: the Central Atlantic Magmatic Province (CAMP), whose emplacement spans three continents and appears to be contemporaneous with continental rupture. However, many questions remain about the lithospheric expression of sutures and rift structures, the distribution, composition and origin of CAMP magmatism, and interrelationships of sutures, rifting and magmatism. In this presentation, we will present previous work on the east coast of the US and elsewhere on these topics and highlight several long-standing questions raised by these previous studies that can be uniquely addressed by Earthscope investigations on the east coast of the US.

Previous studies of rifts and rifted margins document remarkable variability in the style of continental rifting, the volume and distribution of magmatism and the apparent influence on rifting of pre-existing lithospheric structural and compositional heterogeneity. This variability is observed globally between different rifts as well as within individual extensional systems, where changes are apparent between conjugate margins, along-strike and with depth. Much of what is known about spatial patterns of deformation, extension and pre-existing structure in extensional systems is based on surface geology, sparse 2D information on crustal structure, and limited observations of mantle structure. Thus, many questions remain about fundamental rifting processes and the resulting lithospheric architecture, including the 1) distribution of deformation, magmatism and associated depletion throughout the crust and mantle lithosphere beneath failed rift basins and successfully rifted margins; 2) patterns of magmatism and deformation within and between rift segments, and the evolution of segmentation from failed rift basins to the successfully rifted margin to the mid-ocean ridge; and 3) the manifestation of sutures and other structural and compositional heterogeneity from previous tectonic events through the lithosphere and their influence on rifting. Substantial progress on many of these questions can be made through Earthscope investigations of the east coast of the US.

Brittle fracture studies in post-Permian strata of the western flank and crystalline core of the Bighorn Arch, Wyoming: An undergraduate research component of the NSF EarthScope Bighorn Project

Molly Chamberlin[1], Elizabeth Dalley[2], Tyler Doane[3], Bryan McAtee[4], David Oakley[5], Charles Trexler[6], Brennan Young[7], Megan Anderson[3], Eric Erslev[8], and Christine Siddoway[3]†

1. Dept of Geology and Geophysics, Texas A&M University, College Station, Texas 77843
2. Geology Department, Oberlin College, 52 West Lorain Street, Oberlin, OH 44074
3. Geology Department, Colorado College, 14 E. Cache La Poudre St., Colorado Springs, CO 80903. †
    Corresponding author: csiddoway@coloradocollege.edu .
4. Dept. of Geology and Environmental Geosciences, Lafayette College, Easton, PA 18042
5. Department of Geosciences, Williams College, Williamstown, MA 01267
6. Department of Geology, Whitman College, Walla Walla, WA 99362
7. Department of Geology, Utah State University, Logan, UT 8432
8. Department of Geology and Geophysics, Dept. 3006, 1000 University Ave., University of Wyoming, Laramie, WY 82071

Pervasive brittle fractures within Phanerozoic strata and Precambrian basement of the Laramide Rocky Mountains (Figure 1) provide a rich repository of kinematic information for characterization of Laramide deformation and paleostress state. A regional inventory of the structures (Erslev and Koenig, 2009) determined average Laramide slip and compression to be oriented ENE-WSW, but persistent questions remain about the timing of formation and the deformation mechanisms for the prevalent fracture arrays. Exposures of the siliciclastic and carbonate succession on the central western flank of the Bighorn Mountains offer sites with contrasting bedding geometries where these questions can be explored. The contrasting geometries are a long continuous homocline, termed the "Shell shelf," between Shell and Greybull, WY, and the renowned Sheep Mountain anticline northwest of Greybull (Fig. 2). Formed in strata with extremely gentle westerly dips, the fractures within the "Shell shelf" represent a brittle response to very minor bedding rotation and layer-parallel shortening. Within the asymmetric doubly plunging anticline at Sheep Mountain where sedimentary formations attained moderate dips, fractures formed in response to greater bedding rotation and higher strain. Within the Archean granite and gneiss that forms the "basement arch" of the Bighorn Mountains, range-scale topographic lineaments (Figure 2) correspond to large faults containing meters-thick mylonitic zones; breccia and damaged rock; and/or extensive polished slickensides within narrow valleys. Distinct from the range-bounding faults that are *parallel* to the mountain arch, the basement structures transect the range (Figure 2).

RATIONALE: Of particular interest for analysis of Laramide fracture arrays are the Permian and younger formations that were deposited after the Ancestral Rocky Mountains orogeny and therefore contain a record of Laramide and younger events. Undergraduate researchers from the Keck Geology Consortium undertook a study of systematic fracture arrays in Permian and younger strata, with a primary aim to determine the prevalent fracture orientations (Figure 3) and mode of slip (Petit, 1987; Angelier, 1984) for the western flank of the Bighorns. Standard methods of brittle fracture analysis were used (e.g. Marrett and Allmendinger, 1990). In addition, a comparison of fractures in Cretaceous pre-tectonic units versus Tertiary syn- to post-tectonic deposits (Fort Union Formation). The results contribute to the creation of balanced serial cross sections and development of a 4D (3D space plus time) restorable Earth model of the Bighorns arch being constructed by the EarthScope Bighorn Project. A final aim was to compare the microstructural deformation mechanisms within Mesozoic carbonate units in the contrasting structural settings, as a means to gauge the response of a competent unit to the regional stress and clarify the mechanism of formation of a NW-SE fractures.

Within the crystalline core of the Bighorn Arch, structural inheritance is a virtual certainty due to the profound age of the rocks that have been affected by all of the tectonism imposed upon the Wyoming Province since 2.65 Ga. This is corroborated by observations of brecciated mylonite zones, crosscutting striae upon single slickenside surfaces, contradictory kinematic sense within single fault zones; and strongly differing striation orientations upon planes of a single geometrical array. The motivations for structural analysis within the complexly fractured basement are 1) to gather evidence for or against

Figure 1. Photographs of striated fracture surfaces in a) Archean granite and b) siliciclastic sedimentary rock. Such surfaces yield geometrical information (strike, dip, trend, plunge) that, together with a determination of motion-sense, can be used to determine strain and stress axes and slip trend.
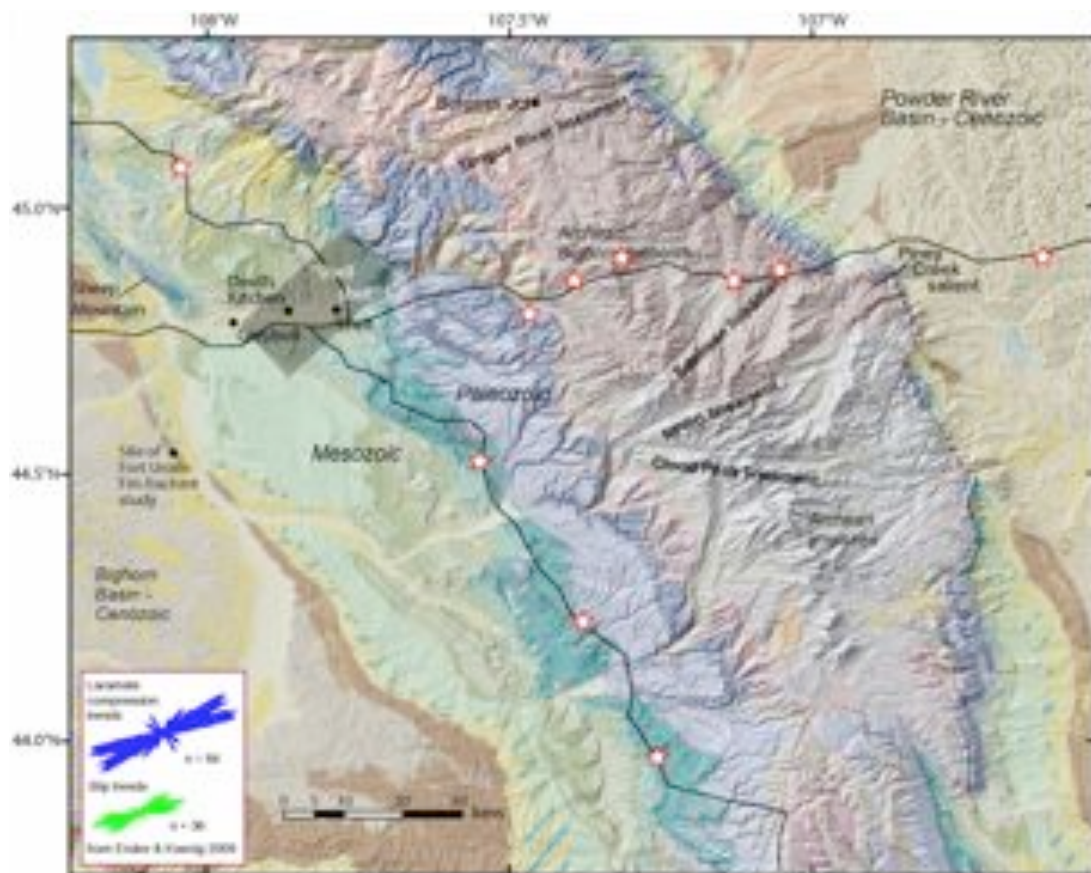

Figure 2. Location map for the Bighorn Mountains, northern Wyoming. Field research sites and selected structures are noted. The location for lines for the BASE active source experiment is shown. Inset provides the regional determination of compression trends and slip trends from Erslev & Koenig (2009). Digital elevation and geological data from Wyoming Geographic Information Science Center (WyGISC; www.uwyo.edu/wygisc).

2

Laramide reactivation of preexisting structures; 2) to characterize crustal scale faults that may project to depth and form seismic reflectors imaged by the Bighorns Arch Seismic Experiment (BASE) active profiles; and 3) to determine the mechanism(s) for deformation of competent Archean crystalline rocks into an arch. The outcomes also may bear on the question of sources of crustal anisotropy that is identified by the shear wave splitting analysis (Anderson et al., 2011) that makes part of the broadband seismology component of BASE. A hindrance to the investigation is that there are few/no prospects for determining the age of motion upon those faults that do not cut sedimentary cover.

RESULTS: Minor fault populations within the post-Permian cover strata of the "Shell shelf" consist of dip-slip conjugate reverse faults striking ~ 335 and 160, and conjugate strike-slip faults striking ~055° (right-lateral) and ~085° (left-lateral). The sites yield a ENE-WSW average maximum horizontal compression direction (σ_1) in good agreement with previous work (e.g. Erslev and Koenig, 2009). Joint arrays form a NW-SE set in an orientation consistent with formation as a longitudinal array parallel to the trend of the arch;
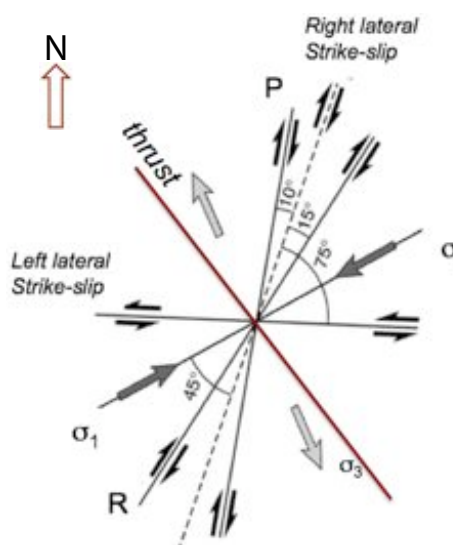

Figure 3. Diagram showing the average Laramide maximum principal stress direction oriented ENE-WSW, together with the predicted strike orientations for brittle fractures and faults that would form in response to the stress state. Preexisting fractures and faults in these orientations could be reactivated.

however, they exist in the near-flat-lying strata of the Shell Shelf as well as in the tight Sheep Mountain anticline, so they cannot be attributed to tensional opening over the crest of the arch or anticline. Another joint set oriented 110° has a transverse geometry with respect to the trend of the Bighorns arch. Joints in that orientation form an array in the Tensleep Formation at Sheep Mountain that has been attributed to pre-Laramide fracturing by Bellahsen et al. (2006). However the presence of 110°-striking fractures in sandstone of the Tertiary Fort Union Formation, with other fracture sets abutting against them, show that the 110° joint array is not pre-Laramide. There is some evidence for late development of normal faults oriented 320/47NE that may be a product of gravitational collapse.

Structural analysis of basement structures in the central Bighorns range makes use of a large fault and fracture data set collected within and adjacent to topographic lineaments (Figure 2) that correspond to steeply dipping fault zones that transect the range. There is wide variability in the geometry of fractures and faults and their striae, but two orientations occur in the greatest abundance. These are ~E-W striking and N-S to NE-SW-striking steep planes (Figure 4), documented from landform analysis using ArcGIS and from field data collection. The prevalent plunge of lineations on the fractures is shallow, indicating predominant strike-oblique motion, and two large-scale faults oriented NNE and ENE do displace Phanerozoic strata. Those faults (Figure 2) are the Tongue River lineament that exhibits north-side-down displacement and cuts the Dry Fork Ridge anticline of Laramide age, and the Johnny Creek fault with west-side-down displacement. The structures have orientations suitable for right lateral and left lateral components of slip (Figure 3) during Laramide compression oriented ENE-WSW (Erslev & Koenig, 2009). Together these observations are taken as evidence of Laramide-age displacement on the faults, and probably on minor faults and fractures that have similar geometries.

At the same time, there is abundant evidence for reactivation of basement faults and fractures: multiple orientations of striae were measured upon planes within a geometrical array, including dip-slip striae upon faults oriented ~E-W and ~N-S (that have prevalent strike-slip or very shallowly plunging striae), fabrics indicative of crystal-plastic deformation are overprinted by brittle cataclasis, and epidote±chlorite±quartz mineralization is variably associated with the shears. To assess the inference of reactivation, the Angelier (1984) paleostress inversion was performed on a set of fractures for which

Figure 4. An exposure of a highly polished, striated fault surface within the Edelman Pass fault zone. Oriented NE-SW, the orientation of the steeply dipping fault was favorable for right-lateral oblique motion that may have aided the relative motions that led to arch formation. In absence of post-Precambrian offset markers and dateable material, there is no means to date this fault, however.

complete fault plane, lineation, and kinematic sense determination are available (n>100). The approach determines what stresses would produce the observed slip on an existing fault plane, rather than the stress state that would *produce* the initial fracture; for this reason it is suitable for situations of structural inheritance. The result from the full data set gave principal stress orientations of $\sigma_1 = 02, 273$, $\sigma_2 = 17, 182$ and $\sigma_3 = $ subvertical, indicative of ~ E-W-oriented compression but with large dispersion. Tighter solutions come from subsets of faults defined by mineralization type; for example, chlorite-mineralized faults yield a maximum principle paleostress σ_1 oriented 69, 282, with the moderately steep plunge indicating an extensional state of strain during motion on chloritic faults. The mineralizing conditions (chlorite-quartz association indicative of crustal depths greater than those for the "upper basement" in the Bighorns arch) and the normal sense kinematics, if correct, are incompatible with the regional Laramide stress state and are likely to be the product of a pre-Laramide event.

 Conclusions and applications of the Bighorn Project fracture studies are as follows. Data from fractures within cover strata indicates ENE-WSW Laramide compression. Steep conjugate strike-slip fault arrays are more prevalent than dip-slip reverse faults in basement than the cover. The information on geometry, location, and timing of development of successive fracture arrays is being integrated into a restorable 4D model of basement arch development. There is wide variability in the geometry of basement structures and there is clear evidence for structural inheritance in the crystalline terrain, but the dominance of steep faults with strike-slip motion suggests Laramide ENE-WSW compression and axis-parallel extension. Field data acquisition in the Archean basement is ongoing, with the aim to characterize crustal-scale faults that may appear as seismic reflectors or as boundaries of anisotropic regions.

References cited
Anderson, M. L. and 10 others, 2011 Earthscope abstract, this volume.
Angelier, J., 1984, Journal of Geophysical Research 89: 5835-5848.
Bellahsen N., Fiore, P., and Pollard, D. D., 2006, Journal of Structural Geology 28: 850-867.
Erslev, E. A. and Koenig, N. V., 2009, Geological Society of America Memoir 204: 125-150.
Marrett, R. and Allmendinger, R. W., 1990, Journal of Structural Geology 12: 973-986.
Petit, J.-P., 1987, Journal of Structural Geology 9: 597-608.

Quantifying tectonic tremor in southern Mexico and its lack of correlation with slow slip

AUTHORS
Stefany M. Sit and Michael R. Brudzinski
Miami University, Department of Geology
Oxford, OH

ABSTRACT
Tectonic tremor, formerly known as non-volcanic tremor, along with slow slip episodes represent key new discoveries assisting in our abilities to learn more about how faults account for slip at major tectonic boundaries. Observations of tremor and slip were first made in Cascadia, but have now been observed in a variety of other subduction zones. Recent studies in Oaxaca, Mexico reveal both slow slip and tectonic tremor, but analysis of the most prominent tremor finds it recurs as often as every 2-3 months in a given region while slow slip occurs much less frequently on the order of 12-24 months. This result was surprising considering that tremor and slip are so well correlated in Cascadia that a linear relationship exists between the number of tremor hours recorded and the moment of concurrent slow slip. In contrast, the first study of tremor in Oaxaca found prominent tremor episodes were only slightly more common during the 2 month slow slip event than the 6 months before or after. However, tremor is more difficult to detect in Oaxaca than Cascadia considering the frequent microseismicity, seasonal storms, and limited seismic network. In this study, we investigate whether there were smaller periods of tremor that went undetected during the slow slip in the initial study, which was based on scanning average absolute amplitudes in the tremor passband. As an alternative, we will utilize a recently developed technique for detecting tremor that takes advantage of the narrow frequency content by calculating the ratio of amplitudes in the tremor passband relative to amplitudes in higher and lower passbands where microseismicity and surface waves are more common, respectively. In Cascadia, this frequency ratio method has been successful in the detection of low amplitude, short duration inter-ETS tremor and may assist in the detection of less prominent tremor in Oaxaca. Moreover, it will provide a more thorough estimate of tremor prevalence over time to test whether tremor is at all correlated with GPS-detected slow slip and if it provides any proxy to the degree of strain release on the deeper portion of the plate interface. Such a technique will also provide insight into the degree to which tremor is tidally modulated in Oaxaca, as recent modeling has indicated such a triggering relationship could be used to examine the state of stress and frictional properties on the fault interface.

3D VOLUME VISUALIZATIONS OF STRESS ACCUMULATION RATES OF THE SAN ANDREAS FAULT SYSTEM

Bridget Smith-Konter and Cecilia Del Pardo

Department of Geological Sciences, University of Texas at El Paso, El Paso, TX 79968
brkonter@utep.edu

While the present archive of EarthScope seismic and geodetic instruments is poised to capture critical details of major pending earthquakes along the San Andreas Fault System (SAFS), a 3D synoptic picture of stress evolution spanning the full earthquake cycle requires sophisticated computational models and powerful visualization tools. To investigate stress rate variations along the SAFS over multiple earthquake cycles, we developed a 3D kinematic model that simulates interseismic strain accumulation, coseismic displacement, post-seismic viscous relaxation of the mantle. Traditionally, modeled stress rates have been presented in map view or in cross-section, represented by 2D grids of scalar values. Stress rates have been analyzed for sensitivity to both horizontal (i.e., slip rates, interacting fault segment positions) and vertical (i.e., fault locking depth) parameters. These results suggest that such parameters are critical in controlling the present-day stress accumulation rate on active faults. Nevertheless, as stress rates cannot be directly observed, nor is their 3D behavior completely understood, visualization tools are becoming increasingly important for the display, analysis, and synthesis of model-derived crustal motions.

To investigate stress rates of the SAFS with a true 3D perspective, we use ParaView 3.10 (www.paraview.org), an open-source multi-platform visualization package. ParaView supports a wide variety of data formats (polygon data, images, structured and unstructured grids, etc.) and offers a feature-rich interface with several visualization algorithms for volume rendering, isosurfacing, plane cutting, filtering, etc. Model grid files are prepared for import into ParaView in a few simple steps. We first generate a suite of 2D model grids (GMT netcdf format), each reflecting stress rates calculated over a horizontal observation plane (~ 1000 x 1500 km) of constant depth. The stack of grids is then converted to a single rectilinear VTK object, which is then imported into ParaView. ParaView creates a 3D meshed volume spanning a ~1000 x 1500 x 50 km region of the SAFS that is easily manipulated and visualized. Here we present both volume and sliced views of stress rates at different viewpoints along the plate boundary. These visualizations lay the groundwork for future 3D time-series animations, an important forward in simulating stress evolution over multiple earthquake cycles spanning paleoseismic timescales.

INVESTIGATING STRESS DROP VARIATIONS OF MAJOR SAN ANDREAS FAULT EARTHQUAKES OVER THE LAST 1000 YEARS

Teira Solis and Bridget Smith-Konter
Department of Geological Sciences, University of Texas at El Paso, El Paso, TX 79968
tsolis2@miners.utep.edu

The periodic earthquake cycle model provides a simplified representation of stress accumulation on a fault throughout the interseismic period and a predictable coseismic stress drop that results from each earthquake. There is a large body of evidence, however, indicating that repeating earthquakes on a single fault segment are not periodic in time, nor do they generate equivalent amounts of coseismic slip or stress drop. Static stress drop is typically estimated using the ratio of the coseismic fault slip to an appropriate scale length (fault length, fault depth, or the square root of the fault area) over which the slip occurred [*Kanamori*, 1994]. 3-D earthquake cycle models also show that stress accumulation and static stress drop are a complex function of space and time. Stress concentrations can vary spatially, particularly near locations of complex fault geometry and interacting fault segments. Stress accumulation rates can also be considered quasi-static during an interseismic period, where the loading rate may change as a function of time.

In this study we investigate how earthquake cycle stress varies as a function of time and space using static stress drop estimates based on paleoseismic slip measurements and a 3-D crustal deformation model. Here we focus on the Wrightwood paleoseismic site, located along the Mojave segment of the San Andreas fault. We use published slip estimates from 8 paleo-events [*Weldon et al.,* 2004] and fault locking depths derived from regional GPS data [*Smith-Konter et al.,* 2011] to calculate the sequence of stress drops at Wrightwood over the last 1000 years. Using a 3-D Maxwell viscoelastic crustal deformation model, we also simulate 8 earthquake cycles of interseismic stress accumulation, coseismic stress drop, and postseismic stress relaxation at Wrightwood from the same paleoseismic dataset, assuming a constant slip rate of 33 mm/yr and a stress drop to zero for each event. Resulting paleoseismic-derived stress drops range from 1.5-14.6 MPa (std 4.5 MPa) while model-derived stress drops are much lower, ranging from 0.5-2.2 MPa (std 0.6 MPa). In the model, the stress field is distributed along the fault depth and is influenced by postseismic relaxation and neighboring fault interactions, which may contribute to the stress drop differences. Furthermore, unusually large paleoseismic slip estimates (for example, 7 m in 1563 following a 49 year earthquake cycle) yield large paleoseismic stress drop anomalies. To better approximate the paleoseismic stress drops and investigate the implications of such variations at Wrightwood, we develop a suite of models with slip rates that are adjusted over each earthquake cycle to match the recorded paleoseismic offsets. Future work will be aimed at applying this method to several other fault segments of the SAF with a rich paleoseismic history.

Testing models of complex anisotropy using teleseismic SKS data from broadband station RSSD in NW South Dakota

In this study, we examine complex anisotropy observed at station RSSD in NW South Dakota. A preliminary analysis of the RSSD data set using the Silver and Chan method yielded high quality results that clearly show back-azimuthal variation of apparent fast axis orientation and split time, indicating that complex anisotropy is present beneath the station. To model this anisotropy, we test and statistically rank possible models of multiple layer structure by comparing observed SKS from RSSD to predicted SKS. The cross convolution method of Menke and Levin is used to measure the goodness of fit, and a direct Monte-Carlo search method (the Neighborhood Algorithm) is used to guide the search through parameter space and produce maximum likelihood models. We then use the *F*-test to rank the significance of the relative error reductions between the different model parameterizations. This combination of methods provides for statistical examinations of the fit of various complex models, and proves more effective than fitting back-azimuthal variations of splitting times.

Melinda A. Solomon*
*corresponding author: melindasolomon@gmail.com
Department of Geosciences
Colorado State University

Derek L. Schutt
Department of Geosciences
Colorado State University

Orogeny, deformation, rifting, and sediment burial on the Texas Gulf Coast: An EarthScope target

Speckien, Mark[1], Jay Pulliam[1], John Dunbar[1], Harold Gurrola[2] , and Harm Van Avendonk[3] (1)
[1]Department of Geology, Baylor University, One Bear Place #97354, Waco, TX 76798;
[2]Geosciences, Texas Tech University, Box 41053, Lubbock, TX 79409;
[3]Institute for Geophysics, University of Texas at Austin, 10100 Burnet Rd, Bldg 196, Austin, TX 78758

The Texas Gulf Coast margin, located at the southeastern edge of Laurentia, has recorded a broad range of geological events, including rifting, subsidence, broad sedimentation, and uplift. However, despite its complex history and great interest to the oil and gas industry, it has not been subjected to intensive studies at deep crustal and mantle depths. The interaction between asthenospheric and lithospheric processes and their roles in the margin's evolution are therefore unclear. This is also the case for most passive margins, which are broadly distributed throughout the world.

Potential field data reveal a large magnetic maximum coupled with a Bouguer gravity high running parallel to the coast of Texas. Due to the depth of sediment on the Texas Gulf Coast, magnetic studies in the region have not shown as clear a view of the anomalies associated with the margin as may be present. Based largely on potential field modeling, Mickus et al. (2009) suggested that the Gulf Coast is a volcanic rifted margin with a triple junction to the south and extends to a non-volcanic margin to the east. Previous studies reached inconsistent conclusions regarding active vs. passive rifting models. For example, Skogseid (2001) showed no volcanic activity while Menzies (2002) showed volcanic dominance.

Recent work done with magnetic intensity data has shown that the Gulf Coast magnetic anomaly is not one anomaly but two distinct anomalies, with one portion trending northward through central Texas, conforming to the Balcones Fault Zone and the eastern trace of the Ouachita Deformation Front, and the other following the coastline into Louisiana. How the existence of two magnetic anomalies conforms to the hypothesis, currently popular, that the Gulf of Mexico was created as a result of the Yucatan peninsula rifting away from the Texas coast, is unclear. Given the margin's deep sedimentary cover, geophysical methods are needed to probe the lithosphere; the Texas Gulf Coast region—the shortest distance between true oceanic crust in the Gulf of Mexico and the relatively undeformed Laurentia on the Edwards Plateau—is therefore an excellent target for EarthScope tools and studies.

Some preliminary work is underway. In summer of 2010, 21 broadband seismographs were installed at 16-18 km spacing along a transect running from Junction, TX (on the Edwards Plateau) to Matagorda Island. The deep sediment package creates a challenge for broadband receiver functions but modeling suggests that beamforming techniques will create useful images of the upper mantle, at least. Results from the seismic survey, combined with a vector magnetic survey scheduled for summer of 2011, will hopefully yield information needed to interpret the interplay between, for example, the asthenosphere-lithosphere boundary, the mantle flow, and crustal thinning associated with ocean-continental transition zones.

Coseismic Displacements and Deep Aseismic Slip Associated with the April 4, 2010, Mw7.2 El Mayor-Cucapah Earthquake, northern Baja California, Mexico

Joshua Spinler and Richard Bennett
Department of Geosciences, University of Arizona

Contact: jspinler@email.arizona.edu

We present crustal motion measurements from an analysis of continuous (CGPS) data for southern California and northern Baja California, Mexico. The 2010 Mw7.2 El Mayor-Cucapah (EMC) earthquake is the largest event to occur along the southern San Andreas fault system in nearly two decades. We analyzed data from 102 locations within 250 km of the EMC earthquake, determining coordinate time series relative to a stable North America reference frame. We observe coseismic displacements greater than 200 mm for the three sites closest to the earthquake rupture. Inversion of the displacement observations using a purely vertical strike-slip model fault plane oriented along the mapped trace of the faults that ruptured, enable us to estimate the slip distribution associated with this earthquake. The maximum slip estimate is 1.52 m, which is consistent with reported field observations. Total seismic moment (Mo) calculated for our slip distribution results is 5.90×10^{26} dyne-cm, or the equivalent of a Mw7.1 earthquake.

We also observe a second offset in the coordinate time series that correlates temporally with the largest aftershock (Mw5.7) on June 15th, 2010, located ~75 km northwest of the initial EMC event. Maximum observed displacements for the second event are 15-16 mm. By inverting the displacement observations, we are able to estimate the slip distribution along a model fault plane for this event. The maximum slip estimate is 104.8 mm. The distribution for this model shows two areas of high slip, with the maximum estimates beneath the surface trace of the EMC rupture, and slightly lower slip estimates in the vicinity of the Mw5.7 aftershock. The total seismic moment (Mo) calculated for this slip distribution is 1.23×10^{26} dyne-cm, or the equivalent of a Mw6.7 earthquake. This estimate for seismic moment magnitude is an order of magnitude larger than the Mw5.7 aftershock, indicating the vast majority of the energy release was not associated with the aftershock. In addition, the area of maximum slip for the Jun 15th event is located at mid- to lower-crustal depths (~10-30 km) beneath the EMC rupture zone, with no significant seismicity observed. The large displacements observed by the GPS network in absence of a known seismic signal of comparable magnitude suggests that appreciable aseismic slip occurred in association with the M5.7 aftershock.

Session 5 solicited abstract

New Madrid and Beyond: what Earthscope can teach us about ancient structures, modern deformation, and the relation between them.

Seth Stein, Northwestern University

Eric Calais, Purdue University

Mian Liu, University of Missouri

A major question in central and eastern U.S. tectonics is how ancient structures formed, evolved, and influence modern deformation. The area contains paleorifts, basins, sutures, and other faults, all of which would seem likely to be somewhat weaker than their surroundings, and hence candidates for present seismicity. However, some - notably the Reelfoot Rift, Wabash Valley fault system, and St Lawrence valley - appear more seismically active at present. Similarly, some parts of the rifted continental margin - those off Canada, near Boston, and Charleston - appear more active. It is important to assess whether in the long term these locations will remain more active, or whether seismicity will migrate. Presumably a major factor is whether the active areas are weaker than other similar structures, either because of the way they formed or later modification, or whether their preferential activity primarily reflects the present stress field. Earthscope will address this question in several ways. High resolution seismic images of the crust and mantle will show similarities and differences between structures, for example allowing comparison of the Reelfoot and midcontinent rift structures. These will give insight into the difference in formation and evolution between a major rift that failed prior to continental breakup - but is seismically inactive today - and a smaller one that failed as part of a successful breakup but is more active today. The results will hopefully also give insight into what effects these differences have on the area's evolution. In addition, Earthscope GPS stations will help identify effects of Glacial Isostatic Adjustment and other tectonic deformation and assess their possible role in present day seismicity.

The Salton Seismic Imaging Project (SSIP): Rift Processes in the Salton Trough

J. M. Stock[1], J. A. Hole[2], G. S. Fuis[3], A. González-Fernández[4], O. Lázaro-Mancilla[5], N. Driscoll[6], G. Kent[7], S. L. Klemperer[8], S. Skinner[1], J. Persico[1], F. Sousa[1], L. Han[2], K. Davenport[2], E. Carrick[2], B. Tikoff[9], M. J. Rymer[3], J. M. Murphy[3], R. Sickler[3], L. Butcher[3], E. A. Rose[3], S. Barak[8], J. Babcock[6], A. J. Harding[6], A. Kell-Hills[7]

1. Seismological Laboratory, Caltech, Pasadena, CA, USA; jstock@gps.caltech.edu.
2. Geosciences, Virginia Tech, Blacksburg, VA, USA
3. Earthquake Science Center, U. S. Geological Survey, Menlo Park, CA, USA.
4. Geología, CICESE, Ensenada, Baja California, México.
5. Universidad Autónoma de Baja California, Mexicali, Baja California, México.
6. Scripps Inst. Oceanography, La Jolla, CA, USA.
7. University of Nevada, Reno, NV, USA.
8. Geophysics, Stanford University, Stanford, CA, USA.
9. University of Wisconsin, Madison, WI, USA.

The Salton Seismic Imaging Project (SSIP) acquired seismic data in and across the Pacific-North America plate boundary zone, at the Salton Trough in southern California and northwestern Mexico, in March 2011. SSIP is investigating both rifting processes at the northern end of the Gulf of California extensional province and earthquake hazards at the southern end of the San Andreas Fault system. SSIP acquired seven lines of land refraction and low-fold reflection data in the Coachella, Imperial, and Mexicali Valleys, airguns and OBS data in the Salton Sea, and a line of broadband stations across the trough. The controlled-source projects utilized over 90 field personnel, a majority of whom were student volunteers. Seismometers were deployed at 4235 locations at 50-500 m spacing onshore, and at 78 locations on the floor of the Salton Sea. These stations recorded 126 onshore explosive shots of up to 1400 kg and several lines of airgun shots. A separate installation of broadband sensors at 42 sites for up to 18 months was designed to record the controlled sources as well as ambient noise and regional and global seismicity.

This poster focuses on data acquired primarily to investigate the processes of continental breakup. Previous studies suggest that, in the central Salton Trough, North American lithosphere has been rifted completely apart. To investigate crustal and upper-most mantle structure and tectonics, we acquired two 220-230 km seismic refraction / wide-angle reflection lines across and along the Salton Trough. Line 1 comprises 35 shots on land along the trough axis, parallel to the direction of Pacific-North America plate motion; this will illuminate both active rifting and adjacent extended lithosphere in the rift valley. The southeastern end of this line, in Baja California, crosses the Cerro Prieto fault. Line 2 crossed perpendicular to the trough at the location of the northern Imperial Fault in order to image structural variations across the rift, the rift flanks, and the structure of the major bounding blocks: the Peninsular Ranges and southern Chocolate Mountains. We will show initial data from the onland shots, used to constrain the style of continental breakup and the partitioning of oblique extension.

High Density Pancakes Sitting on the Mantle-Core Boundary

Daoyuan Sun[1*], Don Helmberger[2], and Jennifer Jackson[2]
[1]DTM, Carnegie Institution of Washington, Washington, DC 20015;
[2]Seismological Laboratory 252-21, Caltech, Pasadena, CA 91125
[*]Email: dsun@dtm.ciw.edu

Deep events beneath the Philippines have produced dense sampling of the SKS-SPdKS and SKPdS bifurcations recorded on USArray at ranges 108 to 125 degrees. The short P-wave diffraction segment (Pd) provides unique information about the thermal-chemical boundary layer. This phase has been used extensively to study abrupt changes in P and S velocites resulting in the detection of ULVZ's near the edges of Large Low Shear Velocity Provinces (LLSVPs). Here we investigate these phases away from such LLSVPs in more normal regions. With the dense array we can measure the differential time (Δ_{LR}) between SPdKS/SKPdS and SKS following by a multi-pathing analysis [*Sun et al.*, 2009]. Strong variations in Δ_{LR} patterns are observed and using the multi-events to determine that SKPdS has the strongest anomalies which span a 20 deg patch covering the CMB region from western Canada-US boundary to southwestern US. There are many trade-offs between the model parameters involving Vp, Vs, and height. To generate an image of lateral variation at CMB, we matched records with 2D flat layer Generalized Ray Theory (GRT) synthetics by assuming $\delta Vs = -8\%$, $\delta Vp = -5\%$ and different thickness of the low velocity layer from a library. A topographic map is produced by merging several events. Then 2D synthetics are generated from the model along cross sections for validation. The map shows elongated dome structures sitting on the CMB. The most prominent one has 80-km height, ~8 deg length, and ~4 deg width. These structures are difficult to detect by most methods because they occur in the shadow zone caused by the high-velocity post-perovskite layer. Although we need to validate the existence of such structures in other regions, we suggest that these results can be explained by a dynamically-stabilized structures containing small amounts of iron-rich (Mg,Fe)O that may have fractionally crystallized from a primordial magma ocean or formed by reactions with liquid outer core [*Bower et al.*, 2011].

Low-Frequency Earthquakes in Cascadia: Results from Array of Arrays

Low-frequency earthquakes (LFEs) are a recently identified class of earthquakes that have been observed to occur coincidentally with tectonic tremor in time and space. These LFEs also have a frequency spectra that is nearly identical to that of tectonic tremor—implying a common source for these two phenomena. As demonstrated by Shelly et al. (2006, 2007, Nature), tremor in Japan can be thought of as a superposition of many individual LFEs. Accordingly, LFEs have been used to constrain the location and focal mechanism of tremor. LFEs have been identified within tectonic tremor at several subduction zones around the world (Brown et al., 2009, GRL), including Cascadia, as well as strike-slip faults like the San Andreas Fault. In 2008 we identified two LFE clusters in Cascadia using a single dense seismic array. These clusters each contained approximately 100 repeating LFEs over the course of about an hour. The clusters locate on the plate interface and individual LFE locations within the clusters varied by no more than ~200m. Here we show the detection of LFEs in northern Cascadia using newly collected data from the Array of Arrays (AOA) experiment. The AOA consists of 8 dense seismic arrays—containing 10 3-component and 10 single-component instruments each—deployed along the northern Olympic Peninsula, Washington State. These arrays are situated above the portion of the Cascadia subduction zone that sees regular episodic tremor and slip (ETS) events—approximately between the surface projections of the 30-45km depth contours of the subduction interface. The AOA recorded the August 2010 ETS event that began in southern Puget Sound and migrated along strike directly underneath our arrays. Using several of the arrays, we find nearly a dozen new LFE clusters that—when well-located—are found to lie on the plate interface. Most of these LFEs repeat hundreds of times per day and come in bursts of activity that correspond to increased levels of tremor in the same location. Interestingly, most LFE clusters appear to last for only about a day and do not appear to repeat, even over timescales of several months. LFEs from August 2010 occurred during the ETS event, while LFEs from March 2008 and March 2010 occurred during minor tremor swarms located farther east (downdip).

Evidence for Prehistoric Earthquakes along the San Jacinto Fault in
Trench 7 at the Mystic Lake Paleoseismic Site, Southern California

Mark Swift, Sally McGill, Nate Onderdonk,Tom Rockwell, Gayatri Marliyani

Mystic Lake occupies a closed depression in San Jacinto Valley within a releasing step-over between the Casa Loma and Clark faults in the San Jacinto fault zone. In July 2010 we excavated three new trenches (T5, T6 and T7) across the Claremont fault within the deposits of ephemeral Mystic Lake near the northwestern end of this step-over. This poster presents results from Trench 7, located 5-10 meters northwest of the original trench (T1), which was excavated in October 2009.   Six prehistoric faulting events were identified in Trench 1 over the past 1600 years, and two of these (events 3 and 4) were visible in Trench 7, along with a new event that is younger than any identified in Trench 1.

As in trench 1, there are a few faults that extend to the ground surface, vertically offsetting by a cm or two historical layers that contained a tin can in Trench 1. The lack of historical earthquakes along this portion of the fault, suggests that these small offsets are probably due to water withdrawal or fault creep rather being related to earthquakes.

Numerous cracks in Trench 7 extended to the base of the historical deposits. Stratigraphy was poor in this part of the section, but two white silt layers within 10 cm below the lowest historic deposit were disrupted within the fault zone. This disruption appears to be at a higher stratigraphic level than the youngest event in Trench 1. We therefore call this event 1, and refer to the youngest event in trench 1 as event 2.

Event 2 was not visible in Trench 7, but event 3 is present at the same stratigraphic level as in Trench 1. It is identified in Trench 7 based on a pronounced angular unconformity and a buried graben. Evidence for event 4 in Trench 7 consisted of a package of beds thinning against an inferred fold scarp at the same level as event 4 in T1.

Approximately fifty charcoal samples were collected from trench 7, including samples from almost every unit exposed. Seven of these have been radiocarbon dated, along with 42 samples from the other trenches. The samples from Trenches 1, 6 and 7 combined constrain the ages of the events as follows: Event 1, AD 1738-1853; Event 2, AD 1670-1828; Event 3, AD 1521-1616; Event 4, AD 1349-1445; Event 5, AD 1076-1258; Event 6, AD 807-961, Event 7, AD 579-845. The 95% confidence interval on the recurrence interval is 159-210 years. Given that the most recent earthquake was at least 158 years ago, the Claremont fault is likely approaching the end of its earthquake cycle.

Identifying undetected early aftershocks and non-volcanic tremors associated with the 12 August 1998 Mw 5.1 San Juan Bautista earthquake and slow slip event

Taka'aki Taira, Roland Bürgmann, and Robert M. Nadeau
Berkeley Seismological Laboratory, University of California, Berkeley, CA 94720, USA

Aftershocks are triggered by abrupt changes of stress induced by a larger earthquake. Detailed images of spatiotemporal changes in aftershock activity help delineate the mainshock rupture area. However, large numbers of early aftershocks are not detected because they are masked by large-amplitudes and long-duration of seismic coda waves from the mainshock and other aftershocks. Peng and Zhao [2009] have demonstrated that ~10,000 aftershocks following the 2004 M 6.0 Parkfield earthquake were undetected by the standard earthquake-detection algorithm of the Northern California Seismic Network (NCSN).

We focus on the detection of uncatalogued aftershocks following the 12 August 1998 Mw 5.1 San Juan Bautista (SJB) earthquake. This event was the largest historic earthquake in the SJB area and was associated with a large slow slip event [Uhrhammer et al., 1999]. Additionally, Nadeau and McEvilly [2004] and Templeton et al [2008] found accelerations in repeating microearthquake frequency accompanying the 1998 slow slip event.

Following Peng and Zhao [2009], we have been identifying undetected early aftershocks with a cross-correlation based approach. We use waveforms from 248 SJB earthquakes detected by the NCSN during a 10-day period spanning the 1998 SJB earthquake (9 August through 18 August, 1998) as templates to identify additional, previously undetected earthquakes. Using continuous data recorded by the closest two seismic stations to the 1998 SJB event (BK.SAO and NC.BVY; less than 4 km from the mainshock), our preliminary analysis has detected ~900 individual earthquakes, with the averaged cross-correlation threshold of 0.7 (Figure 1). We have identified four times more aftershocks than listed in the NCSN catalog (Figure 2). We also searched for small foreshocks immediately preceding the mainshock [e.g., Dodge el al., 1996; Bouchon et al., 2011], but no events were detected during the 2 minutes preceding the mainshock.

The locations of the newly detected events will be estimated by a waveform cross-correlation based double-difference relocation. We currently assign the locations of the detected events to that of the template events providing the highest cross-correlation values (Figures 2a and 2b). With the detected early aftershocks, we find that a highly productive burst of aftershocks started 17 hours after the mainshock (Figure 2c). In this aftershock episode, ~100 events occurred within a 3-hour period. These aftershocks occurred in the northwest part of the rupture area (Figure 2c). This aftershock episode may be the result of the redistribution of stress induced by the 1998 SJB earthquake. Strain and creepmeter data of the associated slow slip event do not resolve an acceleration of slip associated with this accelerated aftershock activity.

Both triggered and ambient tremors are found in the SJB region. Gomberg et al. [2007] and Peng et al. [2009] recently identified several triggered tremor events induced by the passage of teleseismic surface waves near SJB and Bitterwater, California. Our preliminary work found a number of instances of ambient tremor (i.e., tremor not triggered by the passage of surface waves) emanating from the SJB area, including the time of the 1998 slow slip event (Figure 3).

As with the Parkfield tremor, differences (i.e., moveout) in the arrival times of tremor energy over widely distributed stations are small, indicating the tremors are occurring at great depth. In addition to the examples shown in Figure 3, several other ambient tremor events were identified during our preliminary search. We suspect, therefore, that as in the Parkfield-Cholame region [Nadeau and Guilhem, 2009; Shelly, 2009], ambient tremor in the SJB region is an ongoing process that is sensitive to small stress changes and that its activity through space and time will reflect stress and deformation changes in the lower crust [e.g., Rubinstein et al., 2009; Thomas et al., 2009], possibly induced by slow slip events, the occurrence of moderate earthquakes or larger-scale tectonically driven processes.

References

Bouchon, M., H. Karabulut, M. Aktar, S. Özalaybey, J. Schmittbuhl, and M.-P. Bouin (2011), Extended nucleation of the 1999 Mw 7.6 Izmit earthquake, Science, 331, 877-880, doi:10.1126/science.1197341.

Dodge, D. A., G. C. Beroza, and W. L. Ellsworth (1996), Detailed observations of California foreshock sequences: Implications for the earthquake initiation process, J. Geophys. Res., 101(B10), 22, 371–22, 392.

Gomberg, J., J. L. Rubinstein, Z. Peng, K. C. Creager, and J. E. Vidale (2007), Widespread triggering of non-volcanic tremor in California, Science Express, doi:10.1126/science.1149164.

Peng, Z., and P. Zhao (2009), Migration of early aftershocks following the 2004 Parkfield earthquake, Nature Geosci. 28, 877-881.

Peng, Z., J. E. Vidale, A. G. Wech, R. M. Nadeau, and K. C. Creager (2009), Remote triggering of tremor along the San Andreas Fault in central California, J. Geophys. Res., 114, B00A06, doi:10.1029/2008JB006049.

Nadeau, R. M., and A. Guilhem (2009), Nonvolcanic tremor evolution and the San Simeon and Parkfield, California, earthquakes, Science, 325, 191-193.

Nadeau, R. M., and T. V. McEvilly (2004), Periodic pulsing of characteristic microearthquakes on the San Andreas Fault, Science, 303, 220-222.

Rubinstein, J., D. R. Shelly, and W. L. Ellsworth (2009), Non-volcanic tremor: A window into the roots of fault zones, in New Frontiers in Integrated Solid Earth Sciences, edited by S. Cloetingh and J. Negendank, Springer, New York.

Shelly, D. R. (2009), Possible deep fault slip preceding the 2004 Parkfield earthquake, inferred from detailed observations of tectonic tremor, Geophys. Res. Lett., 36, L17318, doi:10.1029/2009GL039589.

Templeton, D., R. M. Nadeau, and R. Bürgmann (2008), Behavior of repeating earthquake sequences in Central California and the implications for subsurface fault creep, Bull. Seismol. Soc. Am., 98, 52-65.

Thomas, A. M., R. M. Nadeau, and R. Bürgmann (2009), Tremor-tide correlations and near-lithostatic pore pressure on the deep San Andreas fault, Nature 462, 1048-1051.

Uhrhammer, R., L. S. Gee, M. Murray, D. Dreger, and B. Romanowicz (1999), The Mw 5.1 San Juan Bautista, California earthquake of 12 August 1998, Seismol. Res. Lett., 70, 10-18.
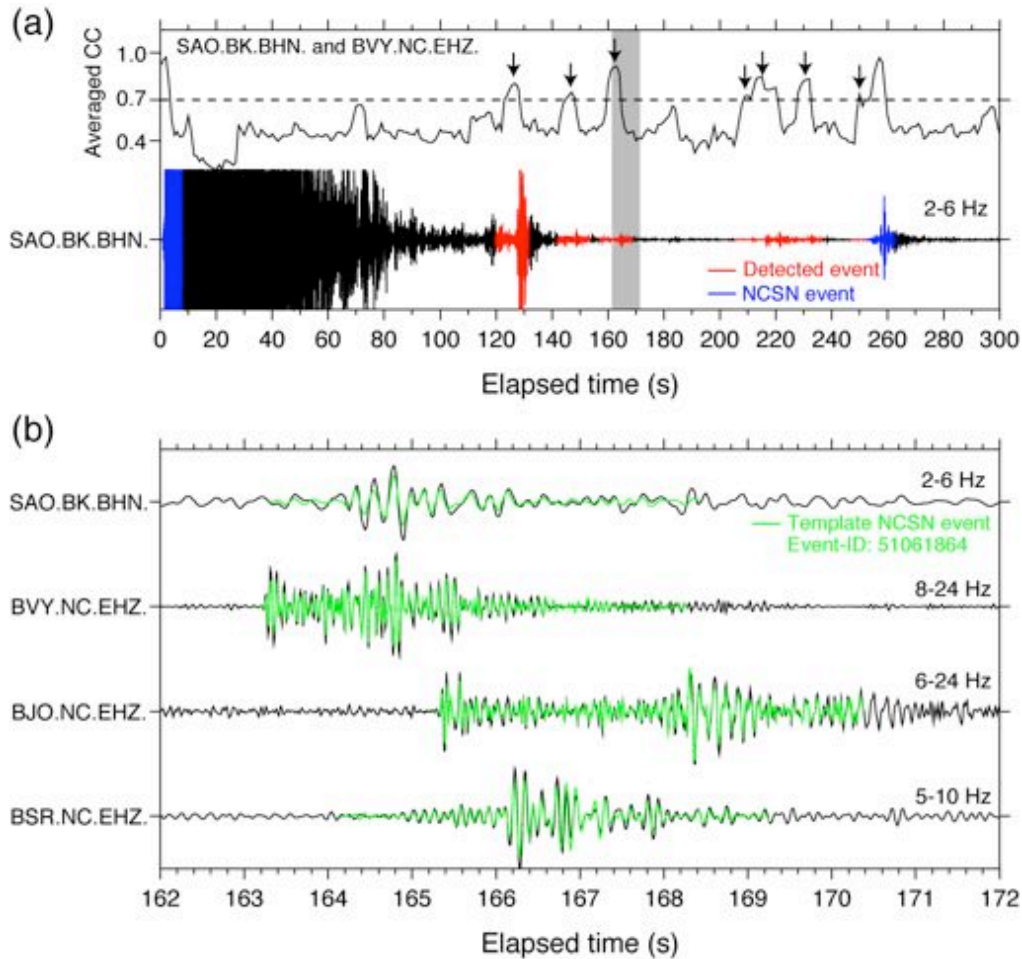
Figure 1. Identified early aftershocks following the 1998 Mw 5.1 SJB earthquake. (a) Top panel shows averaged cross-correlation functions based on SAO.BK.BHN and BVY.NC.EHZ data. Highest cross-correlation values were plotted at individual time steps from cross-correlation functions for the 248 template events. Black arrows indicate identified events using the threshold with averaged cross-correlation value of 0.7 (dashed line). Bottom panel shows observed seismograms (black) recorded at BK.SAO in the N-S component with a 2-6 Hz bandpass filter. Waveforms shown in red and blue are the newly detected events and the NCSN events (the first 10-s data). (b) Detected early aftershock at ~160 s after the mainshock shown in grey area in Figure 1a using the template event nc51061864 (M 0.85) occurring ~4 days after the mainshock. Waveforms shown in black and green are the continuous waveforms and the template waveforms.
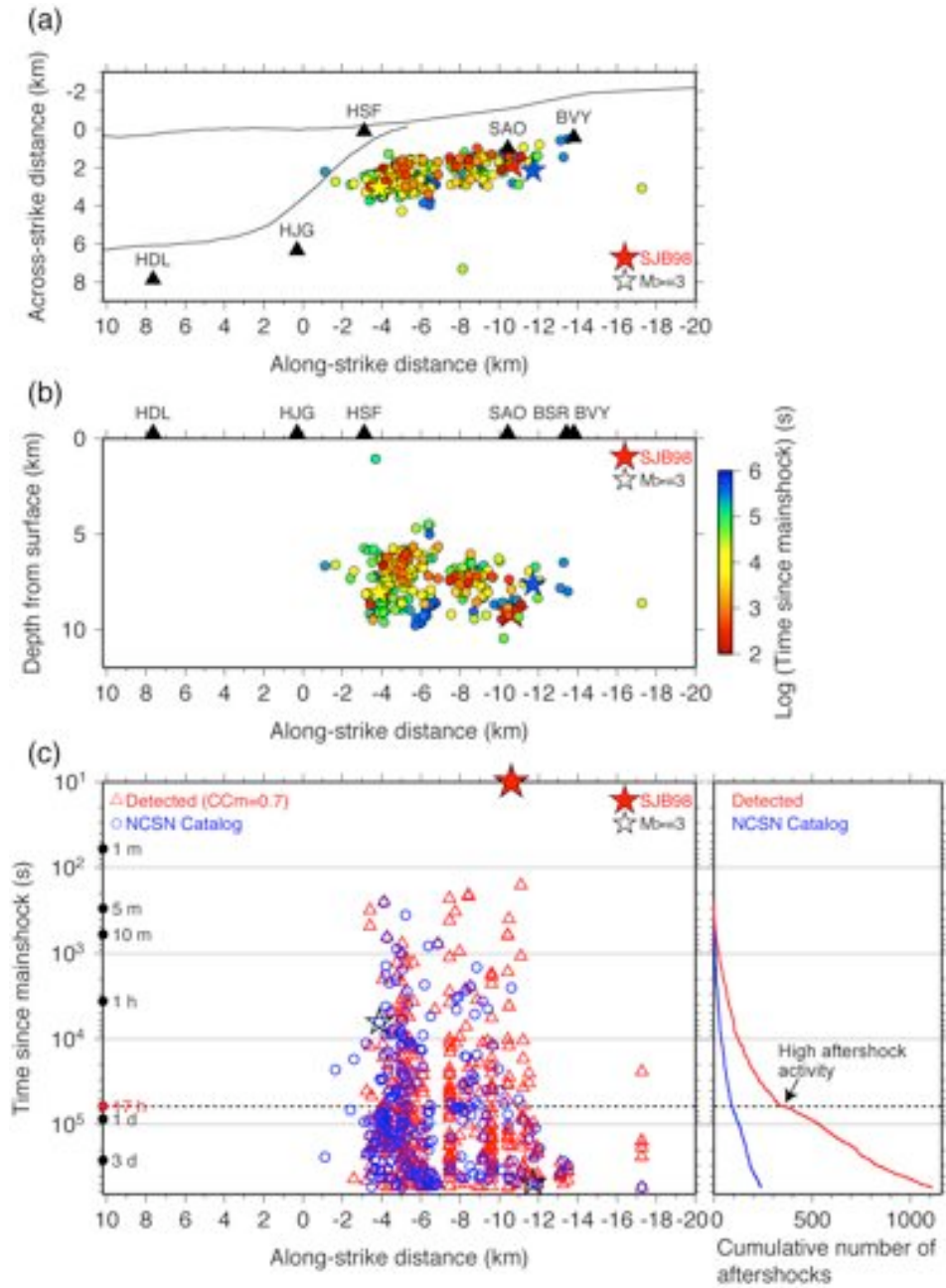
Figure 2. Aftershock seismicity following the 1998 SJB earthquake. (a) Map and (b) cross-section views of the newly detected and NCSN events along the San Andreas fault in the SJB area color-coded by the logarithmic time after the mainshock (red star). Triangles are seismic stations. (c) Left panel shows the occurrence times of aftershocks since the 1998 SJB mainshock as a function of the along-strike distances. The blue circles are the events listed in the NCSN catalog and the red triangles are newly detected events by the cross-correlation analysis. Right panel shows the cumulative numbers of aftershocks by the NCSN catalog (blue) and this study (red).
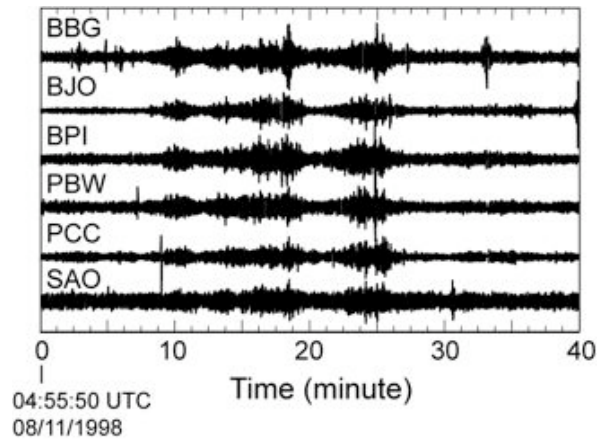
Figure 3. Ambient non-volcanic tremor (i.e., not triggered by teleseismic surface waves) associated with the 1998 slow slip event and the 1998 Mw 5.1 SJB earthquake. This tremor occurred in the ~30 hours preceding the 1998 SJB mainshock. Seismic data is bandpass filtered between 1.5 and 8 Hz.

Toward a multiscale seismic velocity model for Alaska

Carl Tape

Geophysical Institute and Department of Geology & Geophysics
University of Alaska Fairbanks, USA
EarthScope Annual Meeting, May 2011
Austin, Texas

Seismic velocity structure is a fundamental characteristic of any given region. Seismic velocity models provide a starting point for iterative seismic tomographic inversions, whereby the velocity models are improved while minimizing differences between observed and synthetic seismograms. The success of the tomographic inversion is driven by three features: (1) the availability and quality of observed data; (2) the accuracy of the forward model to compute synthetic seismograms; (3) the accuracy of the inverse model. The availability and quality of data in Alaska motivates the underlying multiscale nature of the seismic velocity model. Target structures at scales of 1 km include onshore and offshore seismic reflection and refraction surveys, as well as tidewater glacier settings (e.g., Yahtse glacier), where water, ice, sediments, and rock must be taken into account. Target structures at scales of 10 km include large sedimentary basins (e.g., Cook Inlet basin, Nenana basin) and active volcanoes (e.g., Mount Spurr, Augustine Volcano). Target structures at scales of 50 km include the continental crust, and at 100 km include the subduction system comprising slabs, crust, and upper mantle. After generating unstructured hexahedral meshes for several of these models, I perform 2D and 3D seismic wavefield simulations using the spectral-element method (SEM). The SEM simulations may be used within an adjoint-based inverse problem, as demonstrated extensively for the southern California crust. Future efforts will involve assembling all different structural and seismic data into constructing initial 3D seismic velocity models in Alaska. These 3D models will serve as a basis for iterative seismic inversion using spectral element and adjoint methods.
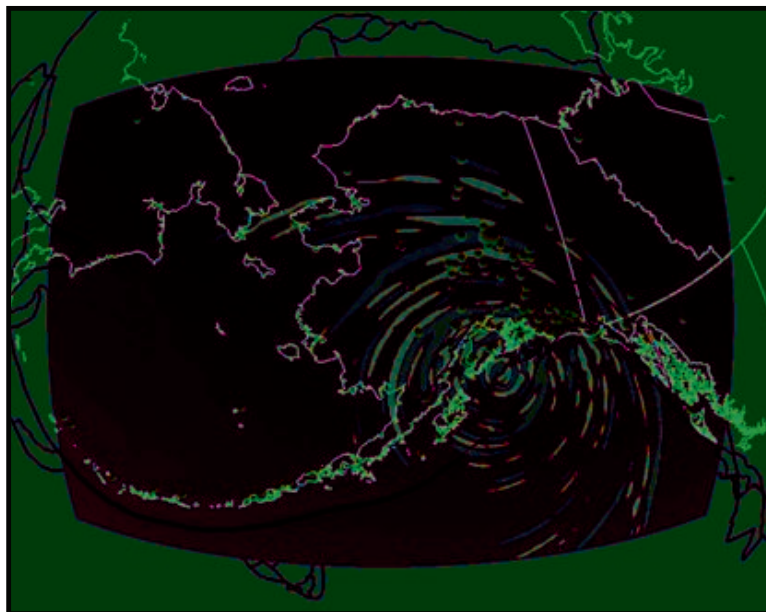
Snapshot from a wavefield simulation of a $M_\mathrm{w}\,9.2$ scenario earthquake on the Aleutian megathrust. Accurate structural models are needed to improve the predicted ground displacements for such earthquakes.

Investigating geologic and geodetic vertical motion discrepancies of the Southern San Andreas Fault System

Garrett M. Thornton and Bridget R. Smith-Konter
Department of Geological Sciences, University of Texas at El Paso, El Paso, Texas 79968
gmthornton@miners.utep.edu

An accurate characterization of the 3D spatial and temporal distribution of earthquake cycle deformation is an essential component of seismic hazard mitigation along the San Andreas Fault System (SAFS). Arrays of seismometers along the SAFS provide tight constraints on the coseismic processes of the earthquake cycle, but geodetic and geologic measurements are needed for understanding the slower processes. Furthermore, while the horizontal velocity field of the SAFS has been thoroughly examined, vertical velocity measurements are often ignored. Here we investigate the relationship between available vertical geologic data from the SCEC Vertical Motion Database (Niemi et al., 2008) and geodetic data primarily from the EarthScope Plate Boundary Observatory. The geologic dataset comprises over 1800 observations located in southern California ranging from -7 to 14 mm/yr with uncertainties on the order of 0.5 mm/yr. These data reflect the motions of rocks ranging in age from 10 Ka to 1 Ma and primarily reflect long time-scale tectonic motions, however these data are spatially limited to a 24,000 km^2 region west of the SAFS. The geodetic dataset reflects GPS vertical velocities from 1100 stations distributed throughout California, ranging from -50 to 18 mm/yr with an average uncertainty of 2.7 mm/yr. These data reflect average vertical motions over the past 20 years associated with both tectonic events and anthropogenic effects such as groundwater pumping and hydrocarbon extraction.

Initial comparison of the geologic and geodetic vertical motion data in California reveals a poor agreement (Fig. 1). The fundamental issue is that these datasets are not spatially co-located, thus we explore several different surface and triangulation techniques for optimal analysis of the data. While the number of available data points for comparison largely depends on the chosen interpolation technique, all methods suggest that the relationship between geologic and geodetic vertical data is not 1:1. In regions of subsidence, for example, the geodetic rates are often twice as fast as the geologic rates. In several locations the observations are even anticorrelated, suggesting that the respective timescales of the data play an important role. Since anthropogenic effects may contaminate some of the geodetic data signal, we also use a vertical velocity crustal deformation model of the SAFS to help identify locations where tectonic motions should dominate the data signals. We adjust the elastic plate thickness of the model to explore the sensitivity of data to this parameter and find that both datasets correlate best with a thick elastic plate. As we continue to explore the vertical motion discrepancies of the SAFS using regional tide gauge records along the California coast, we emphasize the fundamental need for future deployment of geodetic arrays in locations complimentary to existing geologic observations.
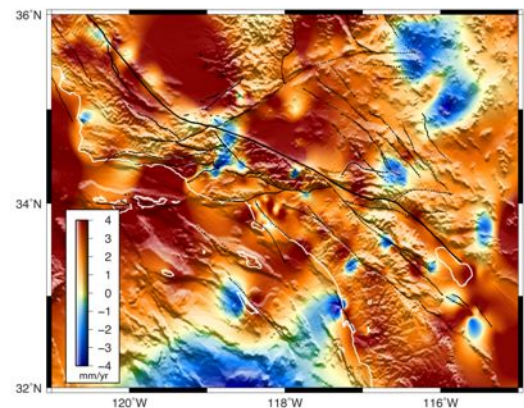
Fig. 1. Vertical motion differences between geologic and geodetic datasets. This map reveals significant variations in the two datasets (geologic-geodetic), with colors saturated at +/- 4 mm/yr. A simple blockmedian surface interpolation was used to construct this map.

The western Idaho shear zone and collision of the Insular Terrane: Tectonic interpretations of ongoing results of the IDOR project

Tikoff, B.[1], Braudy, N.[1], Gaschnig, R.[2], Vervoort, J.[2], Russo, R.[3], Hole, J.[4], Davenport, K.[4], Mocanu, V.I.[5]

1. Department of Geoscience, University of Wisconsin-Madison, Madison, WI 53706; basil@geology.wisc.edu, nbraudy@gmail.com
2. School of Earth and Environmental Sciences, 1228 Webster Physical Sciences Bldg., Washington State University, Pullman, Washington   99164
3. Department of Geological Sciences, University of Florida, 241 Williamson Hall Gainesville, FL 32611; rmrusso2010@gmail.com
4. Dept. of Geosciences, Virginia Tech, 4044 Derring Hall, Blacksburg VA, 24061; hole@vt.edu, davenport.k42@gmail.com
5. Dept. of Geophysics, University of Bucharest, 6 Traian Vuia Street, Bucharest, 70139, Romania, vi_mo@yahoo.com

The lithospheric evolution of the western edge of the North American craton is being investigated by the EarthScope IDOR (Idaho-Oregon) project. Western Idaho and easternmost Oregon contain an extremely well exposed and sharp boundary between continental and oceanic lithosphere, which were juxtaposed in the Mesozoic. The present boundary is marked by a distinct change in geology, and is reflected by an abrupt change in Sr and O values. The boundary correlates exactly with the extent of the Late Cretaceous western Idaho shear zone (WISZ) near McCall. Geochronology suggests that the western Idaho shear zone was active by ~95 Ma, inactive by ~90 Ma, and cooled to ~350° by ~80 Ma. Kinematics record dextral transpressional deformation. Deformation associated with the western Idaho shear zone extends from the Owyhee Mountains, in the southwestern corner of Idaho, to Grangeville, Idaho, where the WISZ is cut by a younger shear zone.

The Blue Mountains terranes, immediately west of the WISZ, show no evidence of any deformation at this time. Paleomagnetic data suggests that these terranes were located 1,700 km to the south with respect to the WISZ at 95 Ma. Further, there is a profound mismatch between undeformed mid Cretaceous conglomerates (Gable Creek and Goose Rock) deposited on the Blue Mountain terranes, exhibiting chert and low-grade metavolcanic rocks, relative to the high-grade metamorphic rocks exhumed from the WISZ at exactly the same time. Thus, it is unlikely that the Blue Mountain terranes were immediately outboard of North American at the latitude of western Idaho during formation of the WISZ.

To the east, the Idaho batholith is almost entirely younger than 95 Ma and composed of 83-67 Ma granites. These granites do not have a strong mantle signature and were probably produced dominantly by crustal melting. Minor roof pendants contain Precambrian and Paleozoic wallrocks. Xenocrysts of zircon indicate that the Archean zircons are limited to the southern portion of the Atlanta lobe, while Proterozoic zircons occur throughout the Bitterroot and Atlanta lobes. The youngest part of the Idaho batholith – the 66-54 Ma Bitterroot lobe – contain zircons inherited from 95-67 Ma

granites, suggesting that the 95-67 Ma batholith was emplaced along the length of the current extent of exposed granites.

Deformation of the WISZ is interpreted to have occurred in an intra-arc setting due to the collision of the Insular terrane with cratonic North America. Paleomagnetic constraints have the Insular superterrane 3000 km south of its present position at 95 Ma (Note that the relation between the Blue Mountain terranes and the Insular terrane is unknown). Reconstruction of known post-Cretaceous strike-slip faulting places the south end of the Insular terrane to a position immediately west of the entire length of the western Idaho shear zone, a position compatible with fixist models of Cordilleran deformation.

The WISZ does not mark the suture between the Insular terrane and North America. Rather, the WISZ was an intra-arc shear zone; it affects almost exclusive rocks of magmatic arc affinity with ages from ~120-95 Ma. What terrane was located immediately west of the WISZ, when ~95 Ma transpressional deformation occurred, is unknown; Either the Intermontane or Blue Mountain terrane could have occupied that structural position, depending on how much post-WISZ northward translation has occurred. Geological reconstructions place the mid-Cretaceous San Juan thrust belt (WA and southernmost British Columbia) immediately westward of the WISZ at 95 Ma; both of these features were active at this time and record major contractional deformation.

We tentatively attribute the main phase of Idaho batholith formation to crustal thickening as a result of collision (plateau formation). This model explains the position (east of the WISZ), timing (immediately post WISZ), and the geochemistry (a result of crustal melting).

a. Pre-western Idaho shear zone and pre-Idaho batholith (~110 Ma)

b. Formation of western Idaho shear zone (~95 Ma)

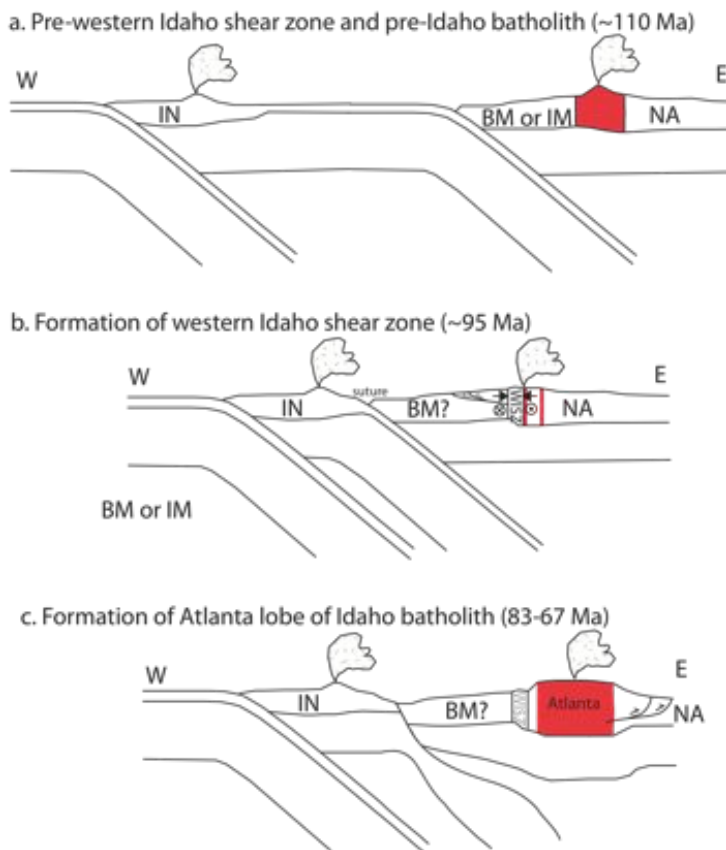c. Formation of Atlanta lobe of Idaho batholith (83-67 Ma)

Figure 1. Three EW oriented cross sections through the western edge of North America at different times in the Cretaceous. IN = Insular terrane; BM = Blue Mountain terranes; IM = Intermontaine terrane; NA = NorthAmerica; WISZ = western Idaho shear zone.

High resolution interseismic crustal velocity model of the San Andreas Fault System from GPS, InSAR, and a dislocation model

Xiaopeng Tong[1] (xitong@ucsd.edu), David T. Sandwell[1] (dsandwell@ucsd.edu), Bridget Smith-Konter[2] (brkonter@utep.edu)

1. Institution of Geophysics and Planetary Physics, Scripps Institution of Oceanography, University of California, San Diego, La Jolla, California.
2. Department of Geological Sciences, University of Texas at El Paso, El Paso, Texas.

Abstract

We recover the interseismic deformation along the entire San Andreas Fault System (SAFS) at a spatial resolution of 200 m by combining InSAR and GPS observations using a dislocation model. Previous efforts to compare 17 different GPS-derived strain rate models of the SAFS shows that GPS data alone cannot uniquely resolve the rapid velocity gradients near faults [*SCEC UCERF workshop report*, 2010], which are critical for understanding along-strike variations in stress accumulation rate and associated seismic hazards. To improve near-fault velocity resolution, we integrate new GPS observations [*T. Herring, personal communication, 2010*] with InSAR observations, initially from ALOS, using a remove/restore approach [*Wei et al.*, 2010]. The integration uses a dislocation-based

velocity model [*Smith and Sandwell*, 2009] to interpolate the line-of-sight velocity at the full resolution of the InSAR data in radar coordinates. We use GMTSAR software [*Sandwell et al.*, 2010] to process, stack, and filter hundreds of interferograms over the entire SAFS from the Mendocino Triple Junction to the Imperial fault in Mexico. Before stacking the unwrapped interferograms, we correct "phase jump" errors close to low coherence areas, which sometimes will corrupt signals near the fault. The initial results show previously unknown details in along-strike variations in surface fault creep. Moreover, the high-resolution velocity field can resolve asperities in these creeping sections that are important for calculating seismic moment accumulation rates and earthquake hazard probabilities. We find that much of the high-resolution velocity signal is related to non-tectonic processes (e.g., ground subsidence and uplift) sometimes very close to the fault zone. We mask the data from these anomalous zones to better isolate the interseismic signal. The refined model, initially based on ALOS (L-band) data, will be used to help unwrap the phase of C-band interferograms, which suffer from temporal decorrelation along most of the fault system. Multiple look directions will be needed to distinguish the horizontal and vertical motion at full spatial resolution.

Key Reference:

SCEC UCERF workshop report (2010): http://www.scec.org/workshops/2010/gps-ucerf3/FinalReport_GPS-UCERF3Workshop.pdf

Sandwell, D. T., R. J. Mellors, X. Tong, M. Wei, and P. Wessel (2010), GMTSAR Software for Rapid Assessment of Earthquakes, *EOS Trans. AGU*, Fall Meeting suppl., abstract G13A-0651.

Smith-Konter, B., and D.T. Sandwell (2009), Stress evolution of the San Andreas Fault System: Recurrence interval versus locking depth, *Geophys. Res. Lett.*, 36, doi:10.1029/2009GL037235.

Wei, M., D. T. Sandwell, and B. Smith-Konter (2010), Optimal combination of InSAR and GPS for measuring interseismic crustal deformation, *Advances in Space Research*, 46, 2, 236-249, doi: 10.1016/j.asr.2010.03.013.

Subducted Seamounts and Recent Earthquake Activity Beneath the Central Cascadia Forearc

Anne M. Tréhu[1], Richard J. Blakely[2], Mark C. Williams[1]

1. College of Oceanic and Atmospheric Sciences, Oregon State University, Corvallis OR 97330
2. U.S. Geological Survey, Menlo Park CA

Bathymetry and magnetic anomalies indicate that a seamount on the Juan de Fuca plate plowed through the central Cascadia accretionary complex over the past 750 ka. Although the indentation that likely formed as the seamount breached the deformation front has subsequently healed, passage of this seamount through the accretionary complex has resulted in a pattern of uplift followed by subsidence that has had a profound influence on slope morphology and sedimentation. Based on potential-field data and a new 3D seismic velocity model, we infer that this is the most recent of several seamounts subducted over the past several million years at Cascadia and that deeply subducted seamounts may be responsible for recent earthquake activity on the plate boundary in this region.

Target session: **Session 3: Exploration and Unexpected Discoveries**

Viability of the USArray TA Network as a Platform for Severe Weather Now-Casting and Weather Research

By Jonathan Tytell[1], Frank Vernon[1], Jennifer Eakins[1], Bob Busby[2] and Bob Woodward[2]

Barometric pressure sensors onboard the USArray Transportable Array provide a unique platform for surface weather monitoring in real-time. Pressure fluctuations observed via the internal VTI SCP1000 MEMS sensors have consistently been linked with severe thunderstorm signatures such as gust fronts and dense pockets of higher pressure. Synoptic scale features have also been observed including low-pressure centers, squall lines and even Tropical Storm Hermine as it made landfall in south Texas on September 7th 2010. Oftentimes the quality and resolution of data being sampled far exceeds that of other real-time weather networks as nothing quite matches the quantity of data recorded via the TA network, nor its sampling precision. The TA platform is also a potential resource for severe weather forecasters, particularly in rural locations where weather observations are limited. Therefore the capability of aiding now-casts and providing insight on surface influences to severe weather is a very real possibility. Furthermore, additional research opportunities are opening up with the installation of Setra 278 barometric pressure sensors and NCPA infrasound sensors onto new stations. As the TA network continues its eastward march across the country the density of stations equipped with pressure sensors is increasing as well, creating a vast network of real-time surface weather stations that is unprecedented in the meteorological community.

1 - University of California, San Diego, California
2 - Incorporated Research Institutions for Seismology (IRIS), Washington, DC

Jonathan Tytell:
jtytell@ucsd.edu
(858)534-9574

Seismic experiment to unravel details of stable Midcontinent Rift System

Suzan van der Lee, Seth Stein, Donna Jurdy, Emily Wolin, Trevor Bollmann, Jessica Lodewyk, Miguel Merino – Northwestern University
Douglas Wiens, Michael Wysession, Patrick Shore, Ghassan Al-Eqabi, Shawn Wei – Washington University in St. Louis
Justin Revenaugh, Brian Bagley, Tao Wang – University of Minnesota
Andrew Frederiksen, Taras Zaporozan – University of Manitoba
Fiona Darbyshire – University of Quebec at Montreal

The western part of the North American continent is currently being formed and deformed, as evidenced by strong relief, hot spots, earthquakes, and volcanic activity. The midcontinent region (the middle part of North America centered on the Mississippi River), completed a similar formation process by about 1 Ga with convergence along the Grenville Orogeny and extension along the contemporaneous Midcontinent Rift (MR). Enormous volumes of basalt were deposited in the MR, causing a 60+ mgal Bouguer gravity anomaly, as well as a correlated magnetic anomaly, that cuts curiously through major geologic units, including the Superior and Yavapai Provinces. Extensive normal faulting accompanied the volcanic activity, but both appear confined to the immediate vicinity of the rift rather than having formed a new ocean between Minnesota and Wisconsin. Although the MR is by far the strongest anomaly in the midcontinent, no evidence has been found for current geologic activity or correlated anomalies in the mantle lithosphere. The installation this year of the first swath of Earthscope-USArray stations east of the Mississippi River allows us to shed light on this enigmatic anomaly but specifically a new seismic field experiment named SPREE (Superior Province Rifting Earthscope Experiment) aims to uncover important details such as the depth and lateral extent of rift-related structures. SPREE is a collaboration between Canadian and US universities (see author institutions). This field experiment is in its beginning stages and includes a Flexible Array (FA) extension of the US-based Transportable Array (TA) into Ontario north of Lake Superior, as well as three lines of 10-km spaced FA stations along and across the MR west and east of the northern Mississippi. We aim to use the recorded earthquakes and ground motion noise to detect microseismicity as well as to construct a multi-scale, three-dimensional image of the seismic velocity and discontinuity structure of the study region's lithosphere and underlying mantle.

Broadband Array Studies of an Intracratonic basiN in Michigan (BASIN): An Earthscope proposal to examine the origin of intracratonic basins

Ben van der Pluijm[1], Richard Allen[2], John Oldow[3], Jeroen Ritsema[1], Peter van Keken[1]
[1]Univ of Michigan-Ann Arbor; [2]UC-Berkeley; [3]UT-Dallas
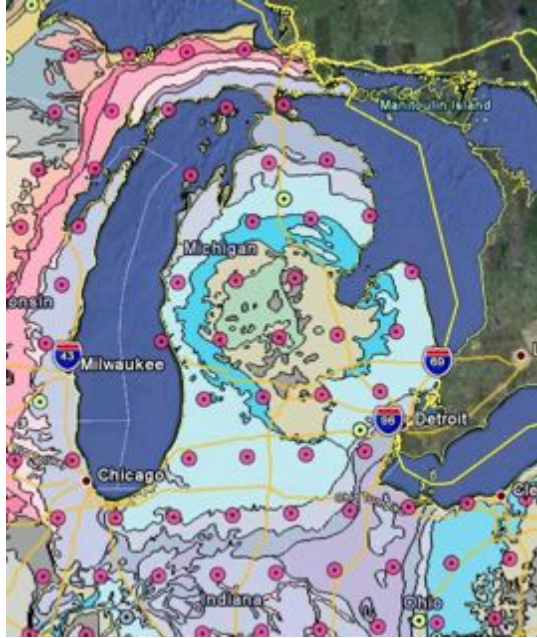
Intracratonic basins are found around the world, but their formation remains a poorly understood geologic process. These basins are located on ancient continental crust hundreds of kilometers away from plate margins; examples in North America include the Michigan, Illinois and Williston basins. The deformation associated with epeirogeny does not appear to fit well into plate tectonic theory.

The Michigan Basin (MB) is the type example of an intracratonic basin. It is characterized by a gentle depression filled with shallow water sedimentary rocks without evidence for faulting or other significant deformation. Whereas a plethora of scenarios have been proposed, the origin of the MB remains unclear because of a paucity of observations beyond its well-known ~5km basin-fill stratigraphy. Its deceptively simple basin geometry (figure) masks a highly heterogeneous Proterozoic basement, a long and episodic subsidence history, and initiation hundreds of Ma after last major tectonic activity in the region (including failed rifting). A range of hypotheses have been advanced for the origin of intracratonic basins, but they require new geophysical observations to test them. Earthscope's USArray provides an unrivaled opportunity by imaging the structure of the deep crust and upper mantle to answer fundamental questions of basin formation. Seismic and gravity data will be used to test three main hypotheses on the basin's origin: downwelling, stretching, and lithospheric architecture. Proposed imaging of the deep structure of the area will involve receiver function analysis, ambient noise tomography, shear-wave splitting and teleseismic wave analysis, toward unraveling the lithospheric architecture below the sedimentary basin. Phase 1 will focus on imaging and regional analysis and, if successful, Phase 2 would involve geodynamic modeling of intracratonic basin formation.

The proposed BASIN experiment would leverage the arrival of the Transportable Array (TA) in Michigan in 2012 (figure) by adding two high-density passive source traverses that collectively will offer a 3D view of the structure and anisotropy of the lithosphere under the basin. The project primarily targets the lower crust and upper mantle under the basin, but broad characteristics of deeper and shallower structure may be imaged as well. The basin fill sequence of the MB has been well-studied previously and is mostly outside the resolution of the BASIN experiment.

Tiny intraplate earthquakes
triggered by nearby episodic tremor and slip in Cascadia

John Vidale, Alicia Hotovec, Abhijit Ghosh, Ken Creager
University of Washington

Episodic tremor and slip (ETS) has been observed in many subduction zones, but its mechanical underpinnings as well as its potential for triggering damaging earthquakes have proven difficult to assess. Here we use a seismic array in Cascadia of unprecedented density to monitor seismicity around a moderate 16-day ETS episode.

In the four months of data we examine, we observe five tiny earthquakes within the subducting slab during the episode, and only one more in the same area, which was just before and nearby the next ETS burst. These earthquakes concentrate along the sides and updip edge of the ETS region, consistent with greater stress concentration there than near the middle and downdip edge of the tremor area. Most of the seismicity is below the megathrust, with a similar depth extent as the background intraslab seismicity. The pattern of earthquakes that we find suggests slow slip has a more continuous temporal and spatial pattern than the tremor loci, which notoriously appear in bursts, jumps, and streaks.
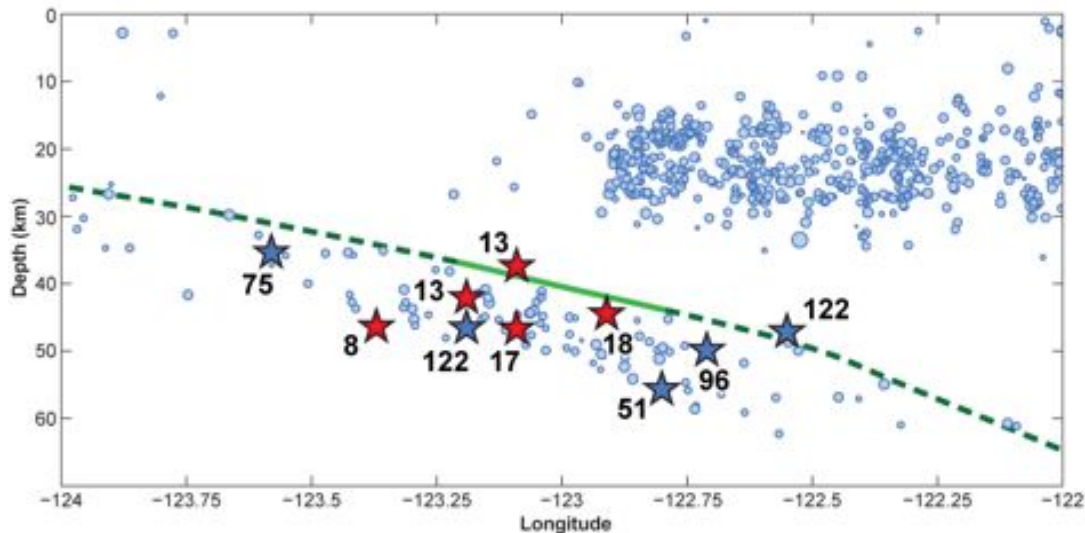
Cross-section of earthquakes between latitudes 47.75° and 48.25° N (red (lighter?) stars mark earthquakes during tremor), background earthquakes (blue circles), slab interface (green line, [*McCrory et al.*, 2004]), and tremor extent (solid portion of green line). The background seismicity is taken from the years 2000 to 2010, and located by the PNSN using the same velocity structure as we located the events with the Array of Arrays. There was also considerable seismicity detected in the crust in this experiment, but its timing was unrelated to the tremor episode, and so is omitted for simplicity.

A Year in the Life of the EarthScope Plate Boundary Observatory Southwest Region
Chris Walls, Shawn Lawrence, Andre Bassett, Doerte Mann, Chelsea Jarvis, Mike Jackson, Karl Feaux - UNAVCO

The SW region of the Plate Boundary Observatory consists of 453 continuously operating GPS stations located principally along the transform system of the San Andreas fault and Eastern California Shear Zone. In the past year network uptime exceeded an average of 97% with greater than 99% data acquisition. Communications range from CDMA modem (304), radio (92), Vsat (30), DSL/T1/other (25) to manual downloads (2). Over 600 maintenance activities were performed during 306 onsite visits out of approximately 355 engineer field days. Within the past year there have been 7 incidences of minor (attempted theft) to moderate vandalism (solar panel stolen) with no loss of receivers. Security was enhanced at these sites through fencing and more secure station configurations. In the past 12 months, 4 new stations were installed to replace removed stations or to augment the network at strategic locations.

Following the M7.2 El Mayor-Cucapah earthquake CGPS station P796, a deep-drilled braced monument, was constructed in San Luis, AZ along the border within 5 weeks of the event. In addition, UNAVCO participated in a successful University of Arizona-led RAPID proposal for the installation of six continuous GPS stations for post-seismic observations. Permitting proved to be a protracted process that delayed installations, however 5 stations are installed and being telemetered through a UNAM relay at the Sierra San Pedro Martir. The sixth and final station permit is in process and will be constructed before the end of the project in mid May. The stations will be maintained as part of the PBO network in coordination with CICESE, an Associate UNAVCO Member institution in Mexico.

UNAVCO is working with NOAA to upgrade PBO stations with WXT520 meteorological sensors and communications systems capable of streaming real-time GPS and met data. The real-time GPS and meteorological sensor data streaming support watershed and flood analyses for regional early-warning systems related to NOAA's work with California Department of Water Resources. Currently 19 stations are online and streaming with 7 more in preparation.

In 2008 PBO became the steward of 209 existing network stations of which 140 are in the SW region that included SCIGN, BARD, BARGEN stations. Due to the mix of incompatible equipment used between PBO and existing network stations a project was undertaken to standardize existing network GPS stations to PBO specifications by upgrading power systems and enclosures. To date 77 stations have been upgraded.

UNAVCO is currently funded through a USGS ARRA grant to construct 8 new GPS stations in the San Francisco Bay Area capable of streaming high rate data. At present 4 stations are built with 1 pending and 3 permits outstanding. Other projects with PGE and Edison are currently underway with 2 of 7 stations constructed. Data from these 7 stations will be integrated into PBO dataflow and available to the science community.

A shallow, offshore tremor and slow slip event at the Nicoya Peninsula, Costa Rica

Jacob I. Walter[1*], Susan Y. Schwartz[1], J. Marino Protti[2], Victor Gonzalez[2]
    [1]University of California, Santa Cruz
    [*]jwalter@ucsc.edu
    [2] Observatorio Vulcanológico y Sismológico de Costa Rica (OVSICORI)

We present evidence of a tremor and slip event occurring offshore of the Nicoya Peninsula, Costa Rica in August 2008. Tremor locations indicate that the tremor is concentrated at a region adjacent to the locked plate interface, up-dip of the seismogenic zone, and offshore. Coastal GPS station offsets suggest a slow slip event occurring offshore in the area of tremor activity. In addition, a perturbation in the pressure recorded in IODP borehole 1255 (located at the trench, near the tremor activity), is indicative of shear motion on the plate interface. The periodicity of the tremor during this event corresponds to the peak coulomb stress forced by the semi-diurnal ocean tide. This result is significant in that locations of slow slip and tremor at other subduction zones are largely limited to the down-dip frictional transition. The results may provide better insight into the transition from stable sliding to stick-slip motion, as the shallow tremor is located adjacent to and at similar depth as a zone inferred to be geodetically locked. The tidal modulation of the tremor is consistent with a coulomb friction model confirming tremor occurs as shear slip on weak faults and processes invoking fluid transport are not required. The shallow depths postulated for offshore tremor (~10 km), suggest that hydrogeology and interface heterogeneities may have important limiting roles. The discovery of offshore tremor and slip using land stations at the Nicoya Peninsula is likely only possible due to its proximity to the trench. Such discoveries at the Cascadia margin may also be possible with the installation of seafloor ocean bottom seismometer infrastructure related to the NSF Cascadia Initiative.

Web services at the IRIS Data Management Center

Bruce Weertman, Chad Trabant, Rich Karstens and Yazan Suleiman
IRIS Data Management Center

The IRIS Data Management Center (DMC) has developed a growing suite of web services. The primary goal is to provide programmatic access to data and processing services in a manner usable by and useful to the research community. The focus to date has been to provide access to the DMC's primary time series holdings and their related metadata and also simple, on-the-fly data processing capabilities. We anticipate these services being used for everything from simple command line access to integrated access from within data processing software. In addition to improving access to our data by the seismological community the web services will also make our data more accessible to other disciplines.

In this poster we introduce our existing suite of core web services for the direct access of time series and related information. The web services include **ws-bulkdataselect** for the retrieval of large volumes of miniSEED data, **ws-timeseries** for the retrieval of individual segments of time series data in a variety of formats (miniSEED, SAC, ASCII, audio WAVE, and PNG plots) with optional signal processing, **ws-station** for station metadata in StationXML format, **ws-resp** for the retrieval of instrument response in RESP format and **ws-sacpz** for the retrieval of sensor response in the SAC poles and zeros convention. The web services are relatively simple to understand and use. Based on standard Web technologies they can be accessed programmatically with a wide range of programming languages (e.g. Perl, Python, Java), command line utilities such as wget and curl or with any web browser. We also provide several client scripts written in Perl for the retrieval of waveform data and metadata.

No evidence for slow slip microearthquakes prior to 2002 Denali Fault Earthquake

Michael West
Geophysical Institute
University of Alaska Fairbanks
Fairbanks, AK 99775
mewest@alaska.edu

Recent work by Bouchon et al. [Science, 331, 877 (2011)] showed that the 1999 Izmit, Turkey earthquake was preceded by a remarkable sequence of much smaller earthquakes. Individual foreshocks are common before large earthquakes. However, these foreshocks typically lack characteristics suggestive of an imminent larger mainshock. The Izmit microearthquakes are a unique observation because their pattern, in retrospect, suggests a tractable relationship to the M_w 7.6 earthquake. The frequency of these events accelerated prior to the mainshock. They locate near the mainshock hypocenter. And they have a repeating waveform that indicates a fixed source and fault mechanism. The multiplet aspect of these earthquakes is an instructive observation, but also suggests a mechanism for identifying these types of sequences even when they elude obvious visual detection.

Based on the Izmit sequence, we revisited the 2002 M_w 7.9 Denali Fault earthquake to establish whether or not similar precursory microearthquakes might have occurred. The Denali Fault is a tectonically comparable intracontinental strike-slip fault. Based on the size of the 2002 earthquake, presence of a large foreshock and numerous continuously-recorded seismic stations in the vicinity of the hypocenter, the Izmit results suggest that the Denali Fault might also have been capable of accelerating slip prior to the 2002 earthquake. We use a cross-correlation technique to examine a 22-hour window prior to the earthquake to look for *any* signal in the record that could be identified multiple times. We scan for matching waveforms on all channels within 100 km of the hypocenter. We also include two hours after the earthquake. Since this time period is filled with hundreds of aftershocks, many with similar waveforms, it provides a control dataset to validate our approach and assess its sensitivity.

We find no repeating microearthquake activity prior to the Denali Fault earthquake. It is possible that such activity exists below our threshold of detection. If such signals exist, however, they must be significantly smaller than the ml 0.3-2.7 Izmit events. It is possible no repeating microearthquake occurred because a true foreshock a few hours prior, and a nearby earthquake two weeks earlier, inhibited the necessary conditions. It is also possible that the thrust-type mechanism at the initiation of the Denali earthquake was inappropriate to produce Izmit-like microquakes inferred to be sourced by strike-slip stresses near the brittle–dutile transition. Lastly, it is possible that the Izmit sequence was a one-time chance occurrence and not a phenomenon to be anticipated elsewhere.

Case Studies in Seismic Data Processing using EMERALD

John D. West[1], Matthew J. Fouch[1], J Ramón Arrowsmith[1]

[1]School of Earth and Space Exploration, Arizona State University, Tempe, AZ 85287
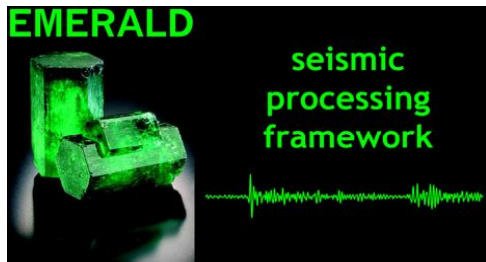
EMERALD (**E**xplore, **M**anage, **E**dit, **R**educe, & **A**nalyze **L**arge **D**atasets) is a software system for efficiently and effectively managing large amounts of seismic event data. It has been in development for 2½ years and has been in beta test since October 2010. Here we present case studies from several early users of the software, illustrating the pre-processing efficiencies and time savings possible with this system. Initial projects have been diverse, including studies of mantle transition zone heterogeneity, seismic tomography of the southwestern US, shear-wave splitting. and graduate-student homework assignments.

EMERALD is an open-source software framework for easily managing large collections of seismic waveforms and associated metadata. A typical EMERALD installation will serve an individual researcher or small workgroup; it is server-based software with an easy-to-use intuitive web browser interface. This interface allows processing of seismic data from any browser-equipped device regardless of operating system, including smart phones and tablets. Users can seamlessly move between devices without losing their place in the workflow in progress. Users new to seismic processing can began reviewing waveforms after only a few minutes of instruction, making it an ideal platform introducing new students to event-based seismology.
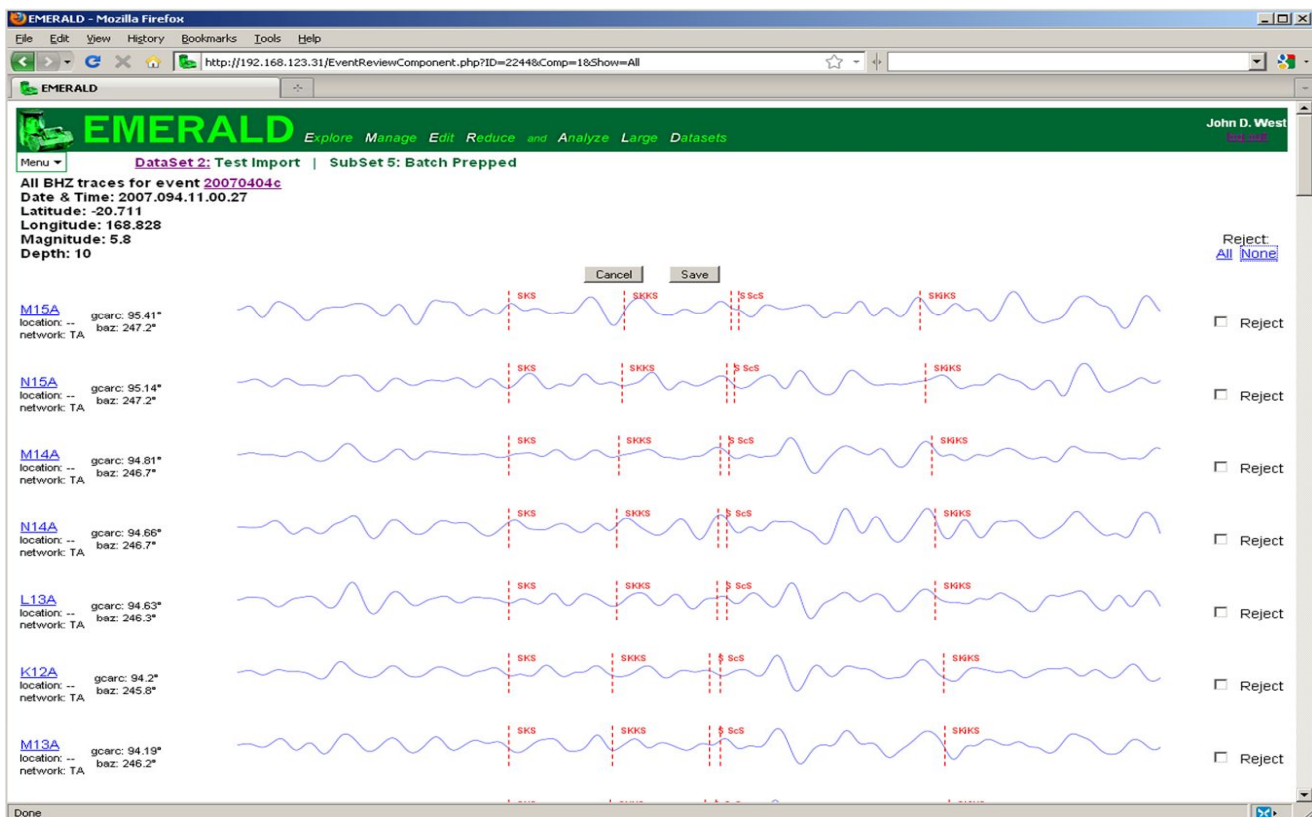
This is the EMERALD screen to review all traces for a given seismic event and component (axis). Users can quickly scroll through all traces for an event and, with the click of a mouse, reject noisy or faulty data. A similar companion screen reviews all traces for a given station and component, making it easy to switch between event-based and station-based workflows and quickly eliminate entire noisy or unsuitable stations and events.

Current pre-processing capabilities include importation of traces in Seismic Analysis Code (SAC) file format, phase arrival-time calculations (using the TauP Toolkit [seis.sc.edu/TauP]), filtering traces with user-defined filters, trimming traces to a window around a given phase, removing the mean from all traces, multiple methods of signal-to-noise calculation, rotation of north and east components to radial and transverse, and rapid review and elimination of faulty traces individually, by station, or by event. Processing and reviewing capabilities are being added frequently, often at the suggestion of the beta users.

EMERALD provides functionality to define, modify, and save workflow automation batches. An automation batch is a group of processing methods and the parameters for those methods stored for execution as a single command. This allows users to define preferred workflows for different seismic investigations and save them for future execution against different data sets.

Data pre-processed with EMERALD can be exported as sets of SAC files in user-defined file and directory naming conventions. This provides an easy path between EMERALD and the investigator's external seismic processing codes, which usually require data to be in a pre-defined naming and directory convention.

EMERALD is designed to be extensible; users are encouraged to write their own processing codes into EMERALD in any of 12 coding languages. Such add-on methods automatically become available in the EMERALD menu structure, and can be easily shared with other EMERALD users.

We are actively seeking new beta users for EMERALD. Becoming a beta user requires no commitment of hardware resources – at this stage we are hosting the EMERALD beta system on servers at Arizona State University. All that is required is an internet connection and a willingness to help guide the development of this new tool for seismic processing.

Finite element modeling of the 2011 Christchurch, New Zealand, M_W 6.3 earthquake

Charles Williams[1], Bill Fry[1], Brad Aagaard[2], John Beavan[1], Russell Robinson[1], Caroline Holden[1], Stephen Bannister[1], Martin Reyners[1], Susan Ellis[1], John Ristau[1]

[1]GNS Science, Lower Hutt, New Zealand
[2]USGS, Menlo Park, California, USA

Contact e-mail: C.Williams@gns.cri.nz

On February 22, 2011, a M_W 6.3 aftershock struck near the city of Christchurch, following a M_W 7.1 mainshock near the town of Darfield on September 4, 2010. Although much smaller than the mainshock, the aftershock caused significantly more damage to the city. Initial Coulomb stress modeling indicates that the aftershock occurred on a fault that experienced a slight Coulomb failure stress increase from the M_W 7.1 event.

To refine our understanding of the causes of this event as well as implications for future events, we are developing finite element models that make use of seismic velocity information to infer elastic material properties. Our preliminary models consist of a single fault plane using geodetically derived (GPS and InSAR) fault slip estimates for the M_W 6.3 event. The models use several different velocity structures: 1) a homogeneous model with a Poisson's ratio of 0.25, for comparison with the half-space solution used to infer fault slip; 2) a homogeneous model with properties corresponding to an average of a New Zealand-wide velocity model at 8 km depth; 3) a 1D model based on a profile at Christchurch; 4) a full 3D model. Our initial results show virtually no difference between the predicted surface deformations of the first two models, while there are significant differences between models 1 and 3, as well as models 1 and 4. There are also measurable differences (~ 20 mm in predicted InSAR line-of-sight displacement) between models 3 and 4, indicating that lateral variations in the material properties are influencing the predicted deformation field.

For each of these deformation models, we have calculated Coulomb stress changes on a target fault with the same orientation as the fault for the M_W 6.3 event, and a range of rake angles. We have also superimposed the stresses inferred for the M_W 7.1 event using an elastic dislocation model. In both cases, we find little to no correlation between elevated Coulomb stresses and the location of aftershocks following the M_W 6.3 event. Our present work focuses on improving our aftershock locations (which will refine the source fault geometry as well as the Coulomb target fault parameters) and including finer scale features in the 3D seismic velocity model. We expect that these refinements will provide a clearer picture of how stress is being redistributed in the Christchurch region.

Broadband Signal-to-Noise Near the Coast - Comparing Onshore and Offshore Seismic Stations

Mark C. Williams, Anne M. Tréhu
College of Oceanic and Atmospheric Sciences, Oregon State University

One of the major challenges to analyzing and interpreting data from an onshore/offshore passive seismic array is recognizing major differences in the background noise sources in the two environments. The chief variables controlling the noise floor on modern seismometers fall into three categories: 1) the electronic and mechanical properties of the hardware, 2) coupling of the seismometer to the ground, and 3) the environment of the installed location. While installation of land stations involves careful choice of site characteristics, burying the seismometer, separation of the sensor from the recording instrumentation, and post-installation data quality tests, logistical and cost restraints require that most ocean bottom seismometer (OBS) installations be much less controlled. Generally OBSs are deployed by allowing them to fall freely to the seafloor, where they may land on an uneven surface or in sediments with a shear modulus that is much lower than that of terrestrial sediments. If the sensor is decoupled from the recording package, it can be difficult to assess the quality of the decoupling. Protrusion of the sensor above the seafloor puts it in the path of benthic currents and fauna. This can result in significant differences in both the background noise level and in the number of transient noise sources between land and seafloor instruments. We present a summary of signal-to-noise data for selected land (FlexArray) and ocean bottom seismometers (from the OBSIP) simultaneously deployed on- and off-shore the coast of Oregon, on the forearc of the Cascadia subduction zone from 2007-2009. In addition to summaries of the background noise floor at several elevations, ocean depths, and distances from the coast, we also present properties of teleseismic and local earthquakes and transient environmental and electronic signals recorded by stations of the array at different frequency bands. We also discuss ongoing efforts to develop an automated method of classifying signals to separate earthquakes from the many transient signals resulting from benthic fauna. While the noise floor can be much higher for ocean bottom instruments, several offshore 4-component (geophone + pressure gauge) broadband stations can improve detection/location of regional and local events, given a sufficient number of coastal stations.

The NEES@UTexas Low Frequency Vibrator 'Liquidator'

A Unique Tool for Active Source Seismic Studies with US Array

Clark R. Wilson[1]

Kenneth H. Stokoe, II[2]

Ellen M. Rathje[2]

Farn-Yuh Menq[2]

1 Department of Geological Sciences, Jackson School of Geosciences

2 Geotechnical Engineering, Department of Civil and Architectural Engineering

The University of Texas at Austin, Austin TX 78712

The George E. Brown Network of Earthquake Engineering Simulation (NEES) is an NSF-sponsored earthquake engineering consortium with facilities at 14 different universities. The University of Texas at Austin NEES facility operates mobile field equipment for seismic investigations, (http://nees.utexas.edu), with 5 Vibroseis sources able to generate seismic waves over a range of frequencies and force loads. Sources are capable of both horizontal and vertical shaking. One of the sources, 'Liquidator', is a 30 ton buggy mounted vibrator which is unique in its low frequency capability, with significant output below 1 Hz. In contrast, virtually all Vibroseis sources in commercial oil and gas exploration applications are limited to about 3 Hz at the low frequency end. Thus Liquidator is a candidate for active-source seismic experiments where the goal is long offsets and deep penetration, and would be suitable for experiments where US Array broad-band seismometers are the receivers. As in conventional Vibroseis applications with a repeatable source, array synthesis and improved signal to noise ratio are achieved by stacking of repeated source 'sweeps'. Liquidator will be on display at the Earthscope meeting and is available for a live demonstration as the meeting schedule permits.

U.S.A. National Surface Rock Density Map - Interim Report

Daniel Winester
NOAA – National Geodetic Survey
325 Broadway, NGS41
Boulder, CO 80305
303-497-6132
daniel.winester@noaa.gov

A map of surface rock densities over the USA is under development by the NOAA-National Geodetic Survey (NGS) as part of its Gravity for the Redefinition of the American Vertical Datum (GRAV-D) Program. GRAV-D is part of an international effort to generate a North American gravimetric geoid for use as the vertical datum reference surface. As a part of modeling process, it is necessary to eliminate from the observed gravity data the topographic and density effects of all masses above the geoid (or above the ellipsoid, depending on particular modeling to be done). However, the long-standing tradition in geoid modeling, which is to use an average rock density (e.g. 2.67 g/cm^3), does not adequately represent the variety of lithologies in the USA.

The U.S. Geological Survey has assembled a downloadable set of surface geologic formation maps (typically 1:100,000 to 1:500, 000 scale in NAD27) in GIS format. The lithologies were assigned densities typical of their rock type and this variety of densities were then rasterized and averaged over one arc-minute areas. All were then transformed into WGS84 datum. Thin layers of alluvium and some water bodies (interpreted to be less than 40 m thick) have been ignored in deference to underlying rocks. Deep alluvial basins have not been removed, since they represent significant fraction of local mass.

For this Interim Report, the initial assumption for modeling the geoid will be that the surface rock densities extend down to the geoid. If this provides to be a significant improvement to forward-modeling, then individual formation densities will be investigated and, as possible, assigned. Also variable lithologies with depth will be included. Initial modeling will use elevations from the SRTM DEM.

A presentation of entire USA is not read- able on a poster, thus, by way of example, two states (New York and Nevada) are presented with maps of geology and density, along with a list of lithologies and densities use for CONUS.

Investigating the role of deglaciation in passive margin seismicity
Emily Wolin and Seth Stein

Continental margins like eastern North America are called "passive" margins because the continent and adjacent seafloor are part of the same plate and thus should experience no earthquakes. In reality, such margins might better be termed "passive-aggressive" due to the infrequent (but sometimes large and hazardous) earthquakes that occur along them. In 1929, a magnitude 7.2 earthquake on the Grand Banks caused a landslide and tsunami that killed 27 Canadians, and in 1933 a magnitude 7.4 earthquake rocked Baffin Bay. The cause of such earthquakes remains a matter of debate, with glacial isostatic adjustment (GIA) a favored explanation. We derive a strain field from the vertical-component GPS data of Sella et al. (2007) and examine its relationship to the distribution of moment release along the passive margin. We also consider the relationship between the strain field and moment release within the continental interior. Finally, we show that slow loading rates along the margin result in long aftershock sequences after the Grand Banks and Baffin Bay earthquakes and discuss the implications of this result for hazard assessment.

Affiliation and contact information:
Northwestern University
1850 Campus Dr.
Evanston, IL 60208
emilyw@earth.northwestern.edu

Crustal structure of the Bighorn Mountains, northern Wyoming: Results from the active-source component of the Bighorn Arch Seismic Experiment (BASE)

Lindsay L. Worthington (l.worthington@tamu.edu), *Department of Geology and Geophysics, Texas A&M University*
Kate C. Miller, *Department of Geology and Geophysics, Texas A&M University*
Steven H. Harder, *Department of Geological Sciences, University of Texas at El Paso*
Eric A. Erslev, *Department of Geology and Geophysics, University of Wyoming*
Anne F. Sheehan, *Department of Geological Sciences, University of Colorado at Boulder*
and BASE Group

While basement-involved foreland arches, such as the Bighorn Arch, are typical of Laramide-style orogenesis, details concerning the mode of arch shortening at depth remain unresolved due to lack of geophysical imaging. The Bighorn Arch Seismic Experiment (BASE) was designed to image the crust and mantle below the Bighorn Arch in north central Wyoming to determine crustal velocity and thickness and to detect large-scale structures in the crust and upper mantle using complementary active and passive seismic techniques. For the active portion of BASE, we recorded 21 seismic shots on ~1800 4.5 Hz vertical component geophones and 'Texan' dataloggers deployed in one east-west profile and one north-south profile. Here, we present 2-dimensional compressional wave velocity models of the upper crust and mantle derived from tomographic inversion of travel time picks along these two profiles.

The north-south profile lies west of the arch and crosses its southern curve. Crustal velocities on this profile are laterally continuous in the upper crust and mantle velocities (>7.8 km/s) are observed at ~50 km depth below surface elevation. The velocity model along the east-west profile, sub-parallel to the direction of contraction across the mountains, shows basin structure on either side of the arch within the upper ~5-10 km which correlates with that derived from previous geologic work. The vertical velocity gradient increases on both profiles at ~25 km depth, which we interpret as a mid-crustal transition associated with compositional changes within the crust. Above this mid-crustal transition, the model shows evidence for thickening of the upper crust across the arch. We observe mantle velocities (>7.8 km/s) at ~45-50 km depth below surface elevation beneath the arch. This observation is consistent with our Moho boundary modeled using PmP phase arrivals at source-receiver offsets of 210-250 km. Low-velocity zones emerge within the upper 20 km of the crust that may coincide with known or predicted large-scale fault zones and will be targets for future modeling and reconstruction efforts.

Thickened crust observed beneath the eastern edge of the Rio Grande Rift

Yu Xia[1], Stephen P. Grand[1] and Jay Pulliam[2]
[1]Department of Geological Sciences, Jackson School of Geoscience (The University of Texas at Austin, 1 University Station C1100, Austin, TX 78713)
[2]Department of Geology, Baylor University (One Bear Place #97354, Waco TX 76798)
Email:yu.xia@mail.utexas.edu

The Rio Grande Rift (RGR) marks the western edge of the stable North American craton in the southern United States. The La Ristra experiment (1999-2006), a linear array of seismographs deployed across the Rift, imaged a narrow high-velocity anomaly in the mantle beneath the eastern edge of the Rift (Gao, et al. 2004). Wilson et al. (2005), using receiver function analysis, found thicker crust in the region directly above the downwelling, suggesting a connection between the downwelling and the surface.

In August 2008 a 2D array of broadband seismographs (SIEDCAR) was deployed on the eastern flank of the Rift to confirm and constrain quantitatively features that might be associated with edge-driven convection at the boundary between a rift and a stable craton. SIEDCAR (Seismic Investigation of Edge Driven Convection Associated with the Rio Grande Rift) deployed a total of 71 stations interspersed with 25 Transportable Array stations. Our aim is to determine the seismic structure and thickness of the continental crust, as well as the upper mantle structure beneath the eastern edge of the Rio Grande Rift.

We present here results from P to S conversion receiver functions that enables us to address fundamental questions about the role of crustal and mantle lithospheric delamination in the evolution of the continental crust in general. Our results show variable crustal thickness through the region with an average thickness of 45 km to the east of the Rift. Particularly, the crust achieves its maximum thickness at 105W longitude, between 33.5N and 32.2N latitude. This observation confirms previous receiver function results from Wilson et al, 2005. Meanwhile, results from travel time tomography (Rockett, et al. 2011) using the same data show a mantle downwelling closely associated with the thickened crust. We believe that the thickened crust might be due to lower crustal flow associated with mantle downward flow or possibly mantle delamination.

Imaging Basin Structures with Teleseismic P Reverberation Virtual Sources

Zhaohui Yang[1], Anne Sheehan[1], William Yeck [1], Eric Erslev[2], Lindsay Worthington[3], and the BASE Seismic Team

[1]*Department of Geological Sciences and CIRES, University of Colorado, Boulder*
[2]*Department of Geology and Geophysics, University of Wyoming*
[3]*Department of Geology and Geophysics, School of Geosciences, Texas A&M University*

We demonstrate a case of using teleseisms recorded on single component high frequency geophones to image upper crustal structure. The dataset was obtained through the EarthScope FlexArray Bighorn Arch Seismic Experiment (BASE). In addition to traditional active and passive source seismic data acquisition, BASE included a 15 day continuous (passive source) deployment of 850 geophones with 'Texan' dataloggers. The geophones were deployed in three E-W lines in north-central Wyoming extending from the Powder River Basin, across the Bighorn Mountains, and across the Bighorn Basin, and two N-S lines on east and west flanks of the Bighorn Mountains. The approach used in this study is equivalent to conventional active source seismic reflection profiles except that high-frequency (up to 2.5 Hz) transmitted wave fields from distant earthquakes are used as natural sources. Our preliminary seismic profiles along the E-W line show strong reflections which we interpret as dipping basement beneath the sedimentary basins flanking the Big Horn Mountains. This study demonstrates the feasibility of using passive Texan data to image shallow crustal layers, increasing the function of EarthScope Flexible Array datasets.

Bighorn Arch Seismic Experiment (BASE) Flexible Array Preliminary Passive Seismic Analysis

Yeck, W.L.[1]; O'Rourke, C.[1]; Sheehan, A.F.[1]; Yang, Z.[1]; Stachnik, J.[1]; Schulte-Pelkum, V.[1]; Anderson, M.[2]; Erslev, E.[3]; and the BASE Seismic Team

1) Department of Geologic Science, University of Colorado at Boulder
2) Department of Geology, Colorado College
3) Department of Geology and Geophysics, University of Wyoming

We present a preliminary look into some of the passive seismic methods being applied to Bighorn Arch Seismic Experiment (BASE) data set as a means of investigating the subsurface structures controlling the Bighorn Mountains of north central Wyoming. Methods include the use of P and S receiver functions, body wave tomography and ambient noise surface wave tomography. BASE is a Flexible Array experiment integrated with Earthscope. BASE deployed over 210 three component seismic stations (38 broadband and 172 intermediate-period) with station spacing in key areas of less than 5 km. Over 1800 single-component geophones with Texan dataloggers were deployed with station spacing of 100 m – 500 m for the first phase of the active + passive experiment (3 x 6 hours) and nominally 1km spacing, with 850 Texans, for the main passive Texan deployment (15 days). All station types captured teleseismic events as well as local earthquakes and abundant mining blasts. Seismometers were placed to both densify the coeval USArray Transportable Array (TA) stations in the region as well as create 5 transects designed to probe subsurface structures associated with the Bighorn Arch and neighboring basins. The main objective of the BASE project is to better understand the tectonic processes involved in the formation of basement-cored arches. The Bighorn Mountains are an archetype of basement-involved foreland arches and therefore act as an excellent setting for the investigation of these types of structures.

Imaging Moho topography is crucial in understanding the formation of the Bighorn Mountains. The dense nature of the array should allow for a detailed Moho image through the use of receiver functions. Low velocity sedimentary basins bound the Bighorn Mountains to the east and west. Reverberations in these basins can mask the Moho signal in standard Ps receiver functions. In order to bypass these signals, Sp receiver functions are investigated as S to P conversions arrive before strong sedimentary layer reverberations and therefore are not masked.

The use of geophones with Texan dataloggers for passive source seismology is not common owing to the short battery life of the Texans (days), single-channel capability, and typically high frequency response. Our preliminary results have shown that the instruments perform very well and are capable of recording teleseismic events with high fidelity. The teleseisms can be utilized for travel time picks and for full waveform modeling. We plan to use this data to create a deep-crust/upper-mantle velocity model using teleseismic body wave tomography. This data can also be used to supplement the three-component receivers in areas of poor coverage.

Three-dimensional shear wave velocity variations are also investigated using the diffusive (ambient noise) wave field. The combination of these multiple passive seismic techniques will allow for a detailed understanding of the subsurface below the Bighorn Mountains.

Depth Dependent Azimuthal Anisotropy in the Western US Upper Mantle

Huaiyu Yuan and Barbara Romanowicz
Berkeley Seismological Laboratory, University of California-Berkeley, CA, 94720 USA

Abstract

We present the results of a joint inversion (Yuan and Romanowicz, 2010; Yuan *et al.*, 2011) of long period seismic waveforms and SKS splitting measurements for 3D lateral variations of anisotropy in the upper mantle beneath the western US, incorporating recent datasets generated by the USArray deployment as well as other temporary stations in the region. We find that shallow azimuthal anisotropy (Figure 1) closely reflects plate motion generated shear in the asthenosphere in the shallow upper mantle (70-150 km depth), whereas at depths greater than 150 km, it is dominated by northward and upward flow associated with the extension of the East-Pacific Rise under the continent, constrained to the east by the western edge of the north-American craton, and to the north, by the presence of the East-West trending subduction zone.
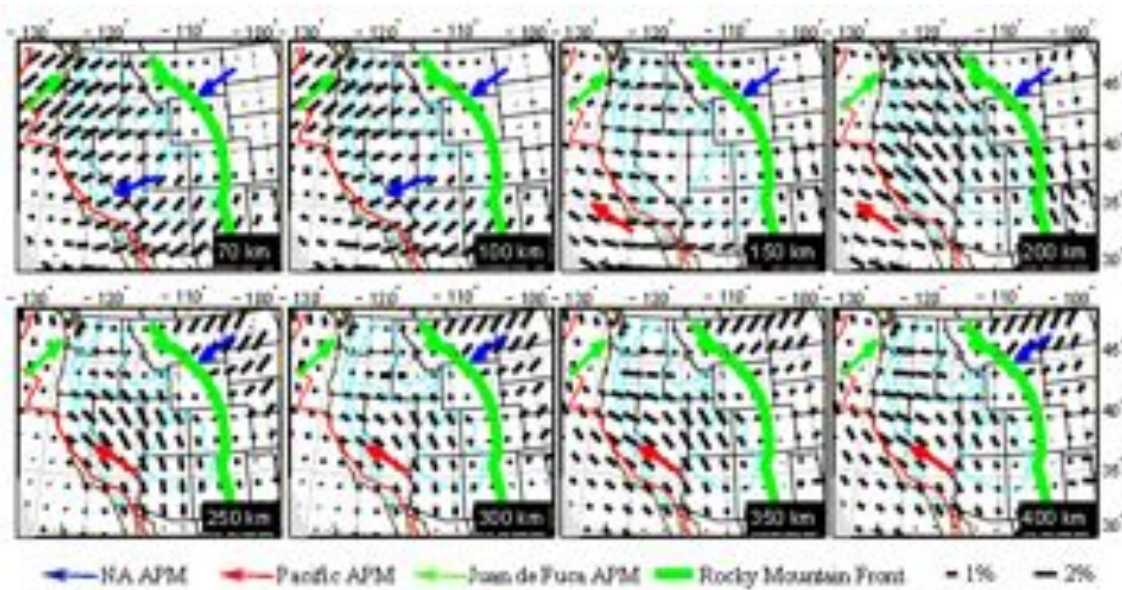
Figure 1 Azimuthal anisotropy variations with depth. Black bars indicate the fast axis direction and the bar length is proportional to the anisotropy strength. Blue, green and red arrows show the absolute plate motion (APM) directions of the North American, JdF, and the Pacific plates respectively, computed at each location using the HS3-NUVEL 1A model (Gripp and Gordon, 2002).

The depth integrated effects of the western US upper mantle anisotropy (Figure 2) explain the apparent circular pattern of SKS splitting measurements observed in Nevada without the need to invoke any local anomalous structures, e.g. ascending plumes or sinking lithospheric instabilities (Savage and Sheehan, 2000; West *et al.*, 2009); the circular pattern results from the depth-integrated effects of the lithosphere-asthenosphere coupling to the NA, Pacific and JdF plates at shallow depths, and in the depth range 200-400 km, northward flow from the EPR

channeled along the craton edge and deflected by the JdF slab, and more generally slab related anisotropy.
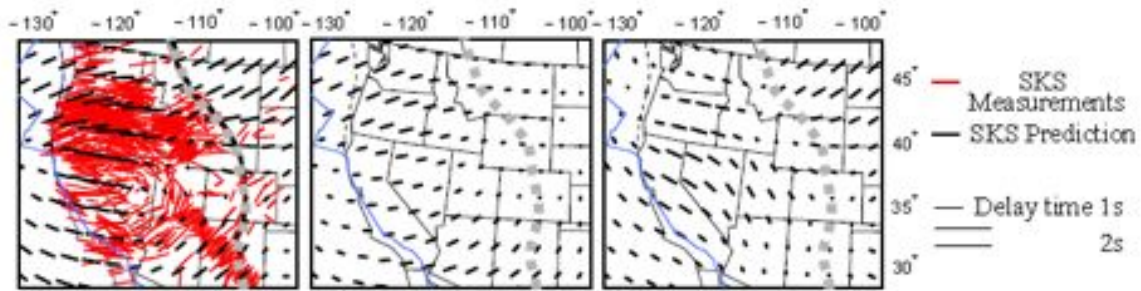

Figure 2 Comparison of observed and predicted station averaged SKS splitting direction and time. Red bars indicate observations and are shown in the left panels only, for clarity. Black bars indicate the model predictions. Predicted splitting is shown as red bars for integration of the models over, (a) the full depth range of the azimuthal anisotropy models, (b) the top 150 km of the models, and (c) the portion of the model between 150 and 500 km, respectively.

The strong lateral and vertical variations throughout the western US revealed by our azimuthal anisotropy model reflect complex past and present tectonic processes. In particular, the NA and Pacific plate shear is dominant shallower than 150 km; at 150 km east-west flow is present due to the JdF slab rollback; and at > 350 km the east-west directed anisotropy is associated with frozen-in/structural anisotropy in the stagnant/flattened JdF slab (Figure 3). With the accumulating high quality TA data, surface wave azimuthal anisotropy combined with multiple layer SKS splitting modeling (e.g., Özalaybey and Savage, 1995; Levin *et al.*, 1999; Yuan *et al.*, 2008) now make it possible to resolve complex depth dependent anisotropic domains in the North American upper mantle.
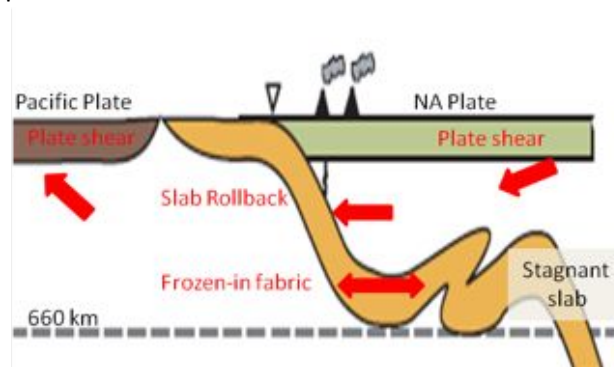

Figure 3 Schematic anisotropic domains in the western US upper mantle. Red arrows denote depth dependent anisotropy associated with the NA/Pacific plate shear, JdF slab rollback, frozen-in fabrics/mechanic anisotropy within the slab. Figure modified from (Schmid *et al.*, 2002; Fukao *et al.*, 2009).

Acknowledgements

References Cited

Fukao, Y., Obayashi, M. & Nakakuki, T., 2009. Stagnant Slab: A Review, *Annual Review of Earth and Planetary Sciences,* 37**,** 19-46**,** 10.1146/annurev.earth.36.031207.124224.

Gripp, A.E. & Gordon, R.G., 2002. Young tracks of hotspots and current plate velocities, *Geophys. J. Int.,* 150**,** 321-361

Levin, V., Menke, W. & Park, J., 1999. Shear wave splitting in the Appalachians and the Urals; a case for multilayered anisotropy, *J. Geophys. Res.,* 104**,** 17,975-917,994

Özalaybey, S. & Savage, M.K., 1995. Shear-wave splitting beneath western United States in relation to plate tectonics, *J. Geophys. Res.,* 100**,** 10.1029/95jb00715.

Savage, M.K. & Sheehan, A.F., 2000. Seismic anisotropy and mantle flow from the Great Basin to the Great Plains, western United States, *J. Geophys. Res.,* 105**,** 13,715-713,734

Schmid, C., Goes, S., van der Lee, S. & Giardini, D., 2002. Fate of the Cenozoic Farallon slab from a comparison of kinematic thermal modeling with tomographic images, *Earth Planet. Sci. Lett.,* 204**,** 17-32

West, J.D., Fouch, M.J., Roth, J.B. & Elkins-Tanton, L.T., 2009. Vertical mantle flow associated with a lithospheric drip beneath the Great Basin, *Nature Geosci,* 2**,** 439-444

Yuan, H., Dueker, K. & Schutt, D., 2008. Testing five of the simplest upper mantle anisotropic velocity parameterizations using teleseismic S and SKS data from the Billings, Montana PASSCAL array., *J. Geophys. Res,* 113**,** doi:10.1029/2007JB005092

Yuan, H. & Romanowicz, B., 2010. Lithospheric layering in the North American craton, *Nature,* 466**,** 1063-1068**,** 10.1038/nature09332.

Yuan, H., Romanowicz, B., Fischer, K.M. & Abt, D., 2011. 3-D shear wave radially and azimuthally anisotropic velocity model of the North American upper mantle, *Geophys. J. Int.,* 184**,** 1237-1260**,** 10.1111/j.1365-246X.2010.04901.x.

Explore lowermost mantle structure with reflected and diffracted waves recorded by USArray

Zhongwen Zhan, Risheng Chu, Don Helmberger

Seismological Laboratory, California Institute of Technology

1200 E. California Blvd., MS 252-21, Pasadena, California 91125-2100, zwzhan@gmail.com

Waveform modeling of the D" SH wave triplication (Scd) beyond 70 degrees are commonly used to map velocity variations in the lowermost mantle. On the other hand, travel time and amplitude decay of diffracted P and SH waves (Pdiff and SHdiff) in the shadow zone (from 90 degrees to 140 degrees) are used extensively to study large scale lowermost mantle structure. Joint inversion of these two phases proves helpful in constraining the velocity structure due to their different sensitivities, analog to body waves and surface waves in studying crustal structures. However, they are not usually jointly inverted, due to lack of overlapping coverage. USArray, with its large station density and aperture, provides an unprecedented opportunity to study both reflected waves and diffracted waves jointly and increase the resolution and accuracy. Moreover, USArray records of earthquakes occurred from Kuril, Japan Trench to Taiwan present overlapping sampling of reflected and diffracted waves in the lowermost mantle beneath northern Pacific roughly along a great circle. Initial study indicated that inaccurate earthquake focal mechanism and station side structure (upper mantle, crust and site amplification) can cause systematic bias and strong scattering. Here we obtain high-accuracy focal mechanism and depth with 30-90 degree P and SH waves for the earthquakes we use, and correct the station side effect with reference earthquakes which sample similar station site structure. In this poster, we present result from this joint inversion of lower mantle velocity structure for both P and SH waves.

GPS postseismic surface displacements of Mw 7.2 El Mayor - Cucapah earthquake, Mexico, 2010

Yang Zhang (yangzhang@unr.edu), Corné Kreemer, and Geoffrey Blewitt
Nevada Bureau of Mines and Geology, University of Nevada, Reno

The 4 April 2010, Mw7.2 El Mayor - Cucapah earthquake, occurred in northern Baja California, approximately 60 km south of the Mexico-USA border. The earthquake ruptured over 50 km of a system of faults located on the western side of the Sierra El Mayor mountains. This earthquake has induced a notable and extensive postseismic process. We are using more than 400 GPS stations, mostly from the Plate Boundary Observatory network, to characterize it. The farthest stations used in our research are about 550 km away from the rupture.

All GPS stations analyzed have data at least two year prior to the earthquake so that we can well constrain the secular and seasonal movement of each station. After subtracting the long-term preseismic movement, we do the curve fitting on the post-seismic part of time series. The GPS stations are grouped into groups according to their distance to the rupture faults. We assume that stations in each group are affected by the same afterslip process, described by $a_i \log\left(1 - t/\tau\right)$, where a_i is the amplitude of postseismic movement of each time series i and τ is the decay time, a common factor to all time series in each group. Our results show that groups within 300 km range have τ values from 25 to 300 days. There is a general increasing trend of τ with the increasing distance from the rupture. Beyond 300 km from the rupture, the τ values are either too large or too small to be realistic, which could mean that the post-seismic process is not notable in that region. We will validate this result with variance-reduction and F-test results.
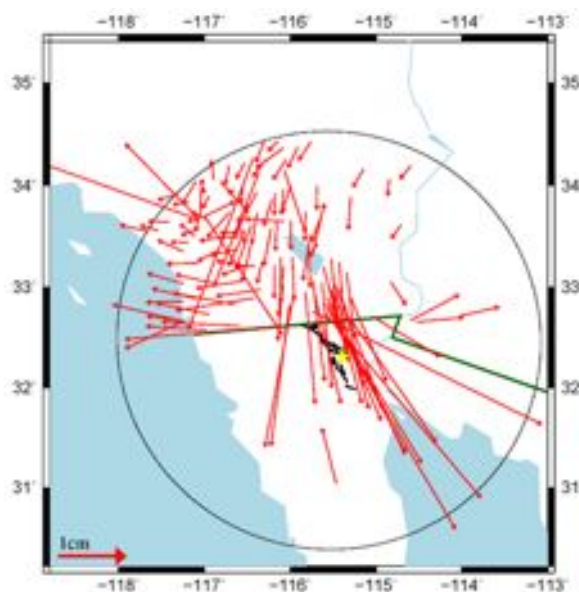

Fig. 1 Postseismic displacement until 12th February, 2011. τ is estimated using all stations within a 200km circle (shown by the black circle) around the rupturing faults. Yellow star shows the epicenter. Black lines are rupturing faults.
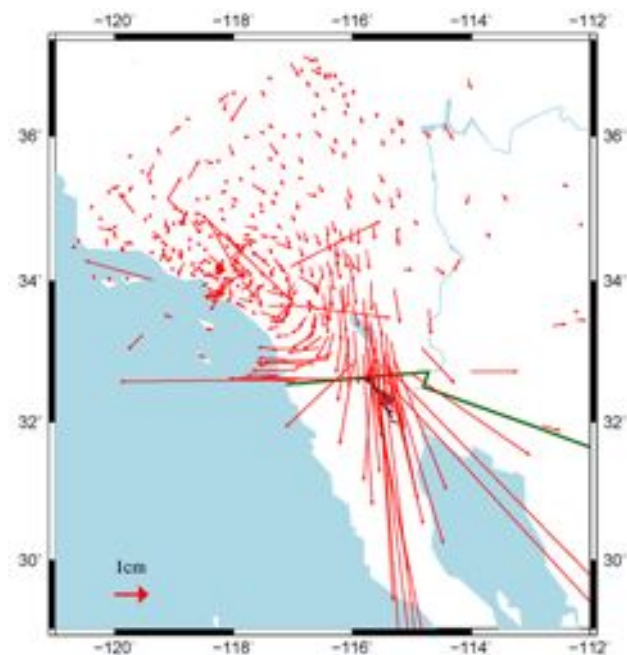

Fig. 2 Coseismic displacements of all stations

Fine-scale structure of the bottommost mantle beneath Cocos Plate

Chunpeng Zhao
zhaochp@asu.edu
School of Earth and Space Exploration, Arizona State University, Tempe, Arizona, USA

Edward Garnero
garnero@asu.edu
School of Earth and Space Exploration, Arizona State University, Tempe, Arizona, USA

Using Transportable Array (TA) data from EarthScope's USArray, we have constructed a data set of ~2000 high quality SH component seismograms to investigate the fine structure of the bottom 10's kilometers of the mantle beneath the Cocos and Caribbean plates. This region has been previously identified to have higher-than-average shear velocities, and velocity discontinuities some 100's of km above the core mantle boundary (CMB). We have developed a new ScS stacking approach that simultaneously utilizes the pre- and post-cursor wavefield to study the fine scale shear velocity structure right at the bottom of the mantle, such as ultra-low velocity zones (ULVZs), and forward and/or backward transitions across the perovskite-to-post-perovskite phase boundary. We stacked source-deconvolved ScS waveforms to extract and combine the ScS pre- and post-cursors with ScS removed – stripping ScS from recordings permits investigation of fine-scale layering near the CMB, which would otherwise be obscured by ScS. Stacking the data significantly suppresses incoherent noise while enhancing coherent features in the wavefield. Synthetic seismograms show that the time-amplitude behavior of the stacked-stripped signals are sensitive to velocity structure in the bottom 100 km of the mantle. While ULVZs are most commonly associated with low velocity, presumably warmer, provinces in the deepest mantle (owing to the partial melt hypothesis for their origin), some ULVZs have been noted in higher-than-average velocity region in deep mantle. This raises the possibility of a chemically distinct origin to some ULVZs, and we thus pursue this region with unprecedented dense sampling for boundary layer structure at the CMB. In the western portion of our study area, a previous study noted a small ULVZ, but most of the study area has not been specifically probed for ULVZ. While much of our study region appears consistent with models lacking any significant CMB heterogeneity, preliminary results show compelling evidence for both high and low

velocity layering in the bottom 10's of km in some spots, with some suggestion of geographical correlation to large-scale shear velocity heterogeneity. We will compare these results with our recent work in the central Pacific, which shows abundant evidence for ULVZ structure.

Crustal Thickness Variation in Eastern North America and Its Implications on Evolution of North American Continent

Lupei Zhu[1], Yuming Zhou[1], and Xiaodong Song[2]

1: Department of Earth and Atmospheric Sciences, Saint Louis University
2: Department of Geology, University of Illinois Urbana-Champaign

We reprocessed teleseismic P waveform recordings of 87 broadband seismic stations in eastern North America between 1995 and 2002. More than 3,000 good quality teleseismic receiver functions were obtained. For each station, crustal thickness and the average crustal V_p/V_s ratio were estimated simultaneously by H-κ stacking of receiver functions of the station. The technique uses the Moho primary P-to-S converted wave and its reverberations in the crust and provides good "point" measurement of crustal thickness. We also obtained crustal velocity models by jointly inversion of receiver function waveforms and surface wave dispersion data derived from ambient noise cross correlation. In addition, crustal structure images along two seismic profiles were constructed using Common Conversion Point (CCP) stacking of receiver functions. The results show that the crust in eastern North America is on average 42 km thick and varies from 28 to 55 km. Archean cratons and early Proterozoic juvenile crustal provinces (1.8 Ga and older) have crustal thicknesses between 34 and 42 km. Thicker crust (40 to 55 km) is found in the 1.6–1.8 Ga juvenile Central Plains Province, the 1.0–1.3 Ga imbricated crust of the Grenville Province, and the Paleozoic Appalachian orogen. The passive margins of the Atlantic and the Gulf coasts have relative thin crust of 28–35 km thick. The coincidence of thick 1.8–1.6 Ga juvenile crust and wide distribution of anorogenic magmatism in the Central Plains Province suggests an episodic crustal growth at the time.